Dissecting the genome-wide dynamic responses of the HIF transcriptional system

Min Sun
St Anne's College
University of Oxford
A thesis submitted for the degree of Doctor of Philosophy
Trinity 2018

Abstract

Hypoxia is an important stimulus for physiological processes such as development and adaptation to high altitude. It is also important in the pathology of many human diseases such as cancer, cardiovascular and diabetic disorders. The sequence-specific, heterodimeric transcription factor HIF (Hypoxia Inducible Factor) has been shown to play a key role in cellular adaptation to hypoxia. This work aimed to better understand the contribution of HIF to hypoxia-inducible gene expression through determining the range of HIF-target genes (both direct and indirect) by sequencing the whole transcriptome (RNA-seq) in HKC-8 wild type and a series of mutant cells (in which one or more components of the HIF-VHL pathway are inactivated). The work went on to examine the pan-genomic binding distribution of HIF polypeptides in response to different severity and duration of hypoxia and in cells bearing introduced mutations in the von Hippel-Lindau tumour suppressor (pVHL), the chromatin remodelling component BRG1-associated factor 180 (BAF180, encoded by *PBRM1* gene), and the HIF asparaginyl hydroxylase, FIH (Factor Inhibiting HIF). This was performed using chromatin immunoprecipitation coupled to high-throughput sequencing (ChIP-seq), and was subjected to a range of quantitative and qualitative analyses.

Analyses of hypoxic gene expression profiles demonstrated that the vast majority of hypoxia-dependent genes in HKC-8 cells were regulated by the canonical HIF pathway i.e. via dimerisation of either HIF-1α or HIF-2α with HIF-1β. There was little evidence for any HIF-independent contributions to gene expression in hypoxia under the conditions analysed. Analyses of hypoxia-dependent genes in HIF mutant cells revealed some persistent regulation by hypoxia that was less than in the wild type cells, and also a set of genes with a lipid metabolism signature that were more regulated by hypoxia in HIF-deficient cells. This observation might represent an adaptive response to enable cell survival in the absence of a functional HIF response.

Having confirmed the critical role of the canonical HIF pathway in regulating hypoxic gene expression in the wild type cells, I then went on to study the canonical HIF DNA-binding profiles across the genome in response to various physiological and pathophysiological conditions as outlined above. It was hypothesised that these conditions might alter the profile of HIF binding as a result of changes in HIF protein abundance, or transcriptional function, as well as by the potential rearrangement of chromatin accessibility. Highly stringent canonical HIF binding sites were defined in each condition, and quantitative analyses of ChIP-seq signals were performed. Overall, the HIF binding signal at any one site was broadly proportional to the total binding for that HIF protein, with HIF-1α and HIF-2α behaving largely independently of each other and showing little evidence for redistribution of HIF DNA-binding profiles in response to different severity and duration of hypoxia, or in the mutant cells.

In summary, this study demonstrates that the canonical HIF pathway is central to hypoxia-dependent gene regulation. HIF DNA-binding occurs over a quantitative continuum, which appears to be qualitatively unaltered under the conditions examined, with the applied interventions only altering the magnitude of HIF binding at the existing sites, rather than qualitatively generating new sites.

Dissecting the genome-wide dynamic responses of the HIF transcriptional system

Min Sun

St Anne's College

University of Oxford

A thesis submitted for the degree of *Doctor of Philosophy*

Trinity 2018

Declaration

This thesis is submitted to the University of Oxford in support of my application for the degree of Doctor of Philosophy in Clinical Medicine. The work described herein was performed while I was a graduate student at the Nuffield Department of Medicine, under the supervision of Professor Sir Peter Ratcliffe and Dr Norma Masson. All the work presented in this thesis is the result of my own work unless otherwise stated and has not been submitted in any previous application for any degree.

Acknowledgements

Studying towards a DPhil degree has been a very challenging and fulfilling experience of my life. The work presented in this thesis would not have been possible without the generous help and inspirations from many individuals, to all I am very grateful.

First and foremost, I would like to express my greatest gratitude to my supervisors, Professor Sir Peter Ratcliffe and Dr Norma Masson, who offered me invaluable guidance and support throughout my D.Phil study. I would especially like to thank Dr Norma Masson who has spent much time helping me with the experiment designs, troubling-shooting the results and providing feedbacks of my work. Her passion in science and conscientious attitude to research have been great inspirations for me. I would also like to express my gratitude to Professor David Mole and Dr Rafik Salama for the constructive advice on the project and on data analysis.

I must also thank Professor Colin Goding and Professor Julian Knight who were the examiners for my transfer and confirmation of status examinations. Their advice is truly appreciated.

My thanks also go to the core genomic facility at the Wellcome Trust Centre for Human Genetics. Special thanks go to Angie Green and her team for the assistance with the sequencing preparation. I would also like to thank Mary Muers for her critical comments on the thesis.

Big thanks to all my past and present colleagues, in particular Tzu-lan Yeh and Ya-Min Tian, for being incredibly helpful both in and out of the lab. I am also genuinely thankful to Catherine King, for her kind encouragement and help with keeping things running smoothly.

Thanks to all my friends outside the lab, particularly Johanna and Sanne, with whom I shared many ‘microadventures’ in the past few years. Special thanks also go to Cong, for always being there as the most trustworthy friend. I am also fortunate to have my supportive friends Yunfei, Marie, Xiao, Jingyi and Pakavarin, who enriched my time in Oxford. In addition, thank you Ian and Alejandro, for bringing me the inspirations and motivations for running and triathlon.

My deepest gratitude goes to my parents, who sometimes believe in me more than I believe in myself. Your support and encouragement make my DPhil possible.

Abstract

Hypoxia is an important stimulus for physiological processes such as development and adaptation to high altitude. It is also important in the pathology of many human diseases such as cancer, cardiovascular and diabetic disorders. The sequence-specific, heterodimeric transcription factor HIF (Hypoxia Inducible Factor) has been shown to play a key role in cellular adaptation to hypoxia. This work aimed to better understand the contribution of HIF to hypoxia-inducible gene expression through determining the range of HIF-target genes (both direct and indirect) by sequencing the whole transcriptome (RNA-seq) in HKC-8 wild type and a series of mutant cells (in which one or more components of the HIF-VHL pathway are inactivated). The work went on to examine the pan-genomic binding distribution of HIF polypeptides in response to different severity and duration of hypoxia and in cells bearing introduced mutations in the von Hippel-Lindau tumour suppressor (pVHL), the chromatin remodelling component BRG1-associated factor 180 (BAF180, encoded by *PBRM1* gene), and the HIF asparaginyl hydroxylase, FIH (Factor Inhibiting HIF). This was performed using chromatin immunoprecipitation coupled to high-throughput sequencing (ChIP-seq), and was subjected to a range of quantitative and qualitative analyses.

Analyses of hypoxic gene expression profiles demonstrated that the vast majority of hypoxia-dependent genes in HKC-8 cells were regulated by the canonical HIF pathway i.e. via dimerisation of either HIF-1α or HIF-2α with HIF-1β. There was little evidence for any HIF-independent contributions to gene expression in hypoxia under the conditions analysed. Analyses of hypoxia-dependent genes in HIF mutant cells revealed some persistent regulation by hypoxia that was less than in the wild type cells, and also a set of genes with a lipid metabolism signature that were more regulated by hypoxia in HIF-deficient cells. This observation might represent an adaptive response to enable cell survival in the absence of a functional HIF response.

Having confirmed the critical role of the canonical HIF pathway in regulating hypoxic gene expression in the wild type cells, I then went on to study the canonical HIF DNA-binding profiles across the genome in response to various physiological and pathophysiological conditions as outlined above. It was hypothesised that these conditions might alter the profile of HIF binding as a result of changes in HIF protein abundance, or transcriptional function, as well as by the potential rearrangement of chromatin accessibility. Highly stringent canonical HIF binding sites were defined in each condition, and quantitative analyses of ChIP-seq signals were performed. Overall, the HIF binding signal at any one site was broadly proportional to the total binding for that HIF protein, with HIF-1α and HIF-2α behaving largely independently of each other and showing little evidence for redistribution of HIF DNA-binding profiles in response to different severity and duration of hypoxia, or in the mutant cells.

In summary, this study demonstrates that the canonical HIF pathway is central to hypoxia-dependent gene regulation. HIF DNA-binding occurs over a quantitative continuum, which appears to be qualitatively unaltered under the conditions examined, with the applied interventions only altering the magnitude of HIF binding at the existing sites, rather than qualitatively generating new sites.

Contents

1

Introduction

1.1 Hypoxia and the transcriptional response to hypoxia

Molecular oxygen started to accumulate in the Earth's atmosphere approximately 2.5 billion years ago and since then allowed the evolution of an efficient energy production system, namely oxidative phosphorylation in the mitochondria. This process involves electron transfer from glucose derivatives in the presence of oxygen, to the high-energy phosphate bond in ATP (adenosine triphosphate) (Lane and Martin. 2010). This form of energy production by aerobic respiration is sufficient for the development and maintenance of eukaryotes, and is more efficient than the anaerobic glycolysis, which is used by most prokaryotes.

Oxygen presents in a unique manner as an external stimulus, as it can simply diffuse from the atmosphere into the organisms and initiate cellular responses. Organisms relying on oxygen-dependent energy production suffer when the oxygen level falls below the demand. Therefore when faced with low oxygen tensions (or hypoxia), cells have evolved intricate mechanisms that are necessary to regulate the cellular availability and usage of oxygen.

1. Introduction

Varying oxygen concentrations are frequently observed in both physiological and pathophysiological processes. Physiological hypoxia occurs when oxygen requirements temporarily cannot meet requirements in respect of normal cellular functions, in settings such as during embryonic development, increased altitude, wound healing, inflammation or transient vascular alterations (Elson et al., 2000). In comparison, pathophysiological hypoxia is usually a chronic state (Dvorak. 1986). An example of this is tumour hypoxia. Despite the constant hypoxic signaling in tumours and responses that include the formation of new blood vessels, some tumours are never able to fully resolve the hypoxia (Denko and Giaccia. 2001). Other settings for pathophysiological hypoxia include anaemia and ischemic diseases such as stroke and myocardial infarction.

Upon hypoxia, one of the most effective and fundamental cellular responses to restore oxygen homeostasis is through altered gene transcription, i.e. hypoxia-inducible gene expression (reviewed in Weake and Workman. 2010). The transcriptional mechanisms in response to hypoxia have been identified in both prokaryotes as well as in eukaryotes. Although both the mechanisms and the magnitudes for the gene regulation under hypoxia vary greatly between unicellular and multicellular organisms, the underlying principal goal of maintaining oxygen homeostasis when extracellular oxygen level decreases remain the same.

Single-cell prokaryotes such as *Escherichia coli* utilise FNR (fumarate and nitrate reduction regulators) as oxygen sensors. Under conditions of normal oxygen tension (or normoxia), the Fe-S cluster in the sensory domain of FNR is converted from an active form ($4[Fe\text{-}S]^{2+}$) to an inactive form ($2[Fe\text{-}S]^{2+}$) by interacting with oxygen, resulting in FNR inactivation; whereas under hypoxia, FNR remains active. It serves as a transcription factor (TF) and forms a homodimer to activate target genes (Unden and Schirawski. 1997; Green et al., 2001). In lower eukaryotes such as yeast *Saccharomyces*

cerevisiae, one mechanism in regulating hypoxic gene expression is through an active transcriptional repression system based on the heme-regulated ROX1 (RNA on the X) repressor molecule. Under normoxia, heme accumulates and activates the transcriptional activator HAP1 (Heme Activator Protein 1). This heme-HAP1 complex then transactivates *ROX1*, which in turn blocks the expression of a large set of hypoxia-responsive genes (Becerra et al., 2002). By contrast, the transcription of *ROX1* is inhibited under hypoxia due to the decrease in heme level. Therefore, the hypoxia-responsive genes are derepressed (Zitomer et al., 1997). In higher eukaryotes such as mammals, the transcriptional response to hypoxia is more complicated. Over the past decade, the identification of oxygen sensors and the transcriptional factors (TFs) responsible for the cellular adaptation to hypoxia have been extensively studied. The most profound changes in the induced gene expression are mediated by TFs known as HIFs (Hypoxia Inducible Factors).

1.2 The HIF family of transcription factors

HIFs are basic-helix-loop-helix DNA-binding proteins of the PAS (PER [period circadian protein]- AHR [aryl-hydrocarbon receptor]/ARNT [aryl-hydrocarbon-receptor nuclear translocator]-SIM [single-minded protein]) family. These TFs function as heterodimers, which consist of an oxygen-sensitive HIF-α subunit, and an oxygen-insensitive and stably expressed HIF-1β subunit (Semenza and Wang. 1992; Wang et al., 1995; Tian et al., 1997; Gu et al., 1998).

In mammals, the HIF-α subunits are encoded by three genes: *HIF1A, EPAS* (also known as *HIF2A*) and *HIF3A* (Ema et al., 1997; Gu et al., 1998; Iyer et al., 1998b). The investigation of erythropoietin (encoded by *EPO*, a glycoprotein hormone that stimulates the generation of red blood cells) in response to hypoxia led to the discovery of HIF-1α as

a factor binding to the hypoxic-dependent enhancer in the 3' region of *EPO* (Semenza and Wang. 1992). Subsequently, HIF-1α was characterised as a TF of bHLH-PAS family that dimerised with HIF-1β. HIF-2α was discovered soon after as a second oxygen-sensitive TF that also dimerised with HIF-1β under hypoxia (Ema et al., 1997; Flamme et al., 1997; Tian et al., 1997). Through homology searches for additional HIF-related proteins, HIF-3α subunits were identified (Gu et al., 1998; Makino et al., 2001). HIF-3α undergoes extensive alternative splicing and at least six HIF-3α splicing variants have been discovered so far. However, they share less structural similarity and functional characteristics with HIF-1α and HIF-2α. They also display different oxygen-sensitivities, differences in ability to dimerise with HIF-1β and different transcriptional functions (Makino et al., 2002; Maynard et al., 2003; Pasanen et al., 2010). Under hypoxia, the expression of HIF-3α variants was shown to be both up-regulated (Tanaka et al., 2009) and down-regulated (Maynard et al., 2005). One of the splicing variant, also known as IPAS (or HIF3A1), was transcriptionally induced by HIF-1α. However, it was found to interact with HIF-1α and form an inactive heterodimer, potentially acting as a negative feedback regulator of HIF-1α (Makino et al., 2001). Normoxic expression of HIF-3α is tissue and cell-type specific, and to date HIF-3α variants are only detected in a few human cancer cell lines (reviewed in Ravenna et al., 2016). With regard to the mRNA expression level of HIF-3α, it is also clear from interrogation of publically available databases e.g. the Protein Atlas and MERAV (Metabolic gEne Rapid Visualizer) that in most cells transcripts for HIF-3α are either expressed at much lower levels (or not at all) in comparison with HIF-1α and HIF-2α.

The HIF-1β subunits, which are also known as ARNT, exist in two isoforms that are encoded by *ARNT* and *ARNT2* separately (Hirose et al., 1996; Reyes et al., 1992). However while *ARNT* is ubiquitously expressed, *ARNT2* has a much more restricted

expression pattern, being most abundant in the neuronal tissues and the kidney (Hirose et al., 1996; Drutel et al., 1996).

1.3 Domain organisation of the HIF proteins

Overall, members of the HIF family share a highly conserved protein domain structure (**Figure 1**). Both HIF-α and HIF-β subunits possess an amino-terminal bHLH (basic helix-loop-helix) domain for DNA binding, as well as a PAS (Per/ARNT/Sim) domain that is responsible for protein-protein interaction and dimerisation. Within the HIF-α subunits, HIF-1α and HIF-2α shared about 85% identity in their bHLH domain, and 70% identity in their PAS domain. By contrast, the bHLH and PAS domains of most isoforms of HIF-3α only share approximately 74% and 52%-58% identity with the corresponding domains in HIF-1α/2α (Hara et al., 2001). HIF-1α and HIF-2α also carry N- and C-terminal transactivation domains (N-TAD, and C-TAD) that are required for the activation of HIF target genes.

HIF-α isoforms are subjected to an oxygen-dependent protein turnover that is mediated by the prolyl-hydroxylations in the oxygen-dependent degradation domains (ODD) (Ivan et al., 2001, Jaakkola et al., 2001). The ODD is partly overlapping with the N-TAD and contains two (in HIF-1α and HIF-2α) prolyl residues for hydroxylation (Jiang et al., 1996; Huang et al., 1998; O'Rourke et al., 1999; Lendahl et al., 2009). The C-TAD contains an asparaginyl residue implicated in oxygen-dependent target gene transcriptional activation. In comparison, the ODD in HIF-3α contains only a single prolyl residue that can be hydroxylated, and most HIF-3α splicing variants carry an N-TAD but lack of a C-TAD with some carrying a C-terminal LZIP (leucine zipper) motif of unknown function (reviewed in Ravenna et al., 2016).

Similar to HIF-α subunits, both isoforms of HIF-1β contain bHLH, PAS and a C-TAD (in this case without a regulatory asparaginyl residue). However, in contrast to the HIF-α subunits, the HIF-1β subunits are constitutively expressed under normoxia due to the lack of an ODD domain (Huang et al., 1996).

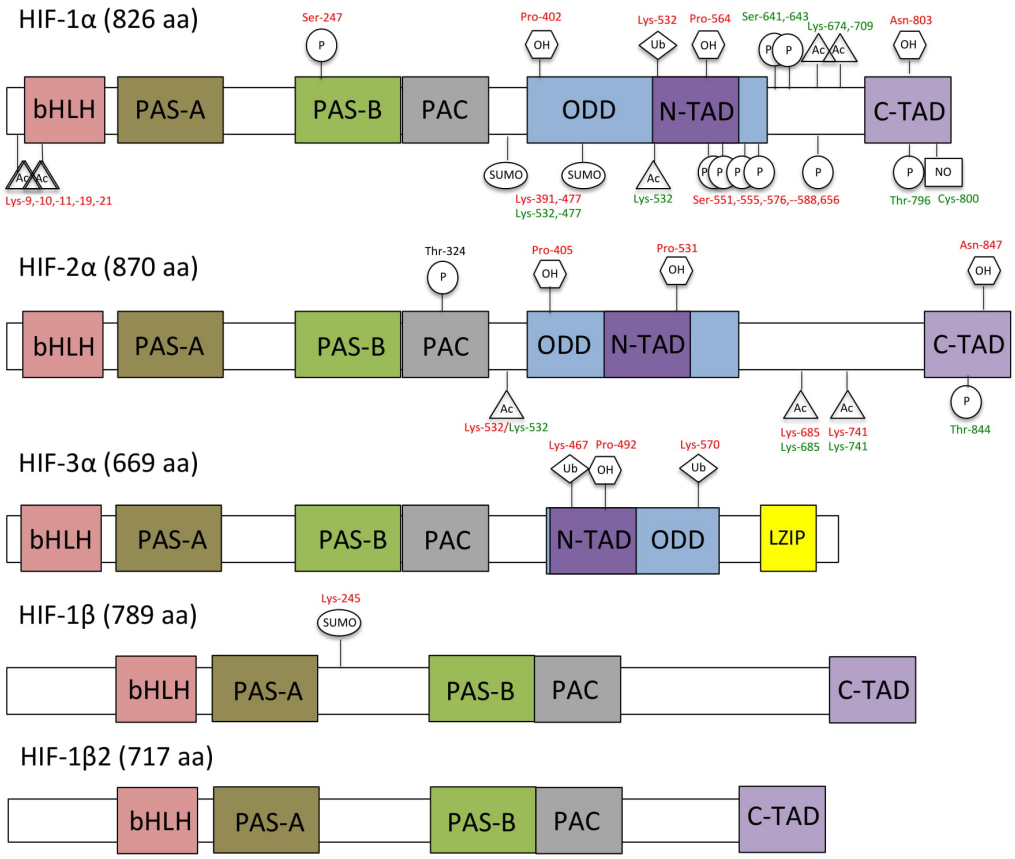

Figure 1. Schematic structure of HIF protein domains and post-translational modifications.

HIF protein consists of several conserved domains that are involved in DNA-binding (bHLH: basic-helix-loop-helix), protein-protein interaction and dimerisation (PAS: per-arnt-sim, PAS-1, PAS-B, PAC: PAS associated C-terminal domain), oxygen-dependent degradation (ODD), and transcriptional activation (NAD: N-terminal Activation Domain, CAD: c-terminal activation domain). Multiple HIF-3α isoforms have been identified with some possessing transactivation and leucine zipper (LZIP) domains while others lack transactivation domains. Numerous post-translational modifications are known to modulate HIF protein stability and transcriptional activity. Some of the modifications are shown here, together with the overall positive (green) or negative (red) effects on HIF transcriptional function. Modified from Dengler et al., 2014.

1.4 Post-translational modifications of HIF-α

1.4.1 PHD-dependent regulation of HIF

HIF regulation is primarily based on post-translational modification and protein stability. Under normoxia, a family of highly conserved oxygen-sensitive prolyl-4-hydroxylases (PHDs) hydroxylates the conserved prolyl residues in the ODD of HIF-α subunits (Jaakkola et al., 2001; Epstein et al., 2001; Berra et al., 2003; Appelhoff et al., 2004; Landazuri et al., 2006; Koivunen et al., 2007). This prolyl hydroxylation results in binding of the von Hippel–Lindau protein (pVHL), which polyubiquitinates HIF-α and leads to its degradation by the 26S proteasome pathway (Huang et al., 1998; Ohh et al., 2000; Tanimoto et al., 2000; Cockman et al., 2000).

PHDs are members of the non-heme iron-dependent dioxygenases family. They utilize ferrous iron (Fe^{2+}) to catalyze the reduction of molecular oxygen, and incorporate each oxygen atom into 2-OG (2-oxoglutarate) and the substrate polypeptides, to form succinate, CO_2, and *trans*-4-hydroxylated prolyl products (reviewed in Schofield and Ratcliffe. 2004). PHDs act as direct 'oxygen sensors' that link cellular oxygen concentrations to HIF responses. They bind loosely to oxygen with K_m values (the concentration required for half-maximal catalytic rate) in the range of 230 – 250 μM (reviewed in Schofield and Ratcliffe. 2004). Notably, the PHD hydroxylation sites exist within an LXXLAP motif in the ODDs of all 3 HIF-α subunits, however they are not equivalent for the three HIF-α subunits, i.e. Pro-402 and Pro-564 in HIF-1α, Pro-405 and Pro-531 for HIF-2α and Pro-492 for HIF-3α (Ivan et al., 2001; Jaakkola et al., 2001; Masson et al., 2001; Maynard et al., 2003).

To date, there are 4 PHD isoforms (PHD1-4) that have been identified, of which only PHD1-3 are shown to hydroxylate HIF-α (reviewed in Fandrey et al., 2006). Genetic studies have demonstrated important roles of PHD1-3 in development. For instance,

homozygous deletion of PHD2 results in embryonic lethality between embryonic day 12.5 and 14.5. A double deletion of PHD1 and PHD3 led to moderate erythrocytosis (Takeda et al., 2008) although mice with PHD1 or PHD3 alone appeared largely normal (Takeda et al., 2006). These phenotypes fit with additional work identifying that PHD2 is the most important isoform under normoxia (Berra et al., 2003). The putative PHD4, which possesses a transmembrane domain that is localised in the endoplasmic reticulum, was found to affect HIF-α function only when overexpressed (Oehme et al., 2002; Koivunen et al., 2007; reviewed in Myllyharju and Koivunen. 2013). Biochemical studies have also revealed that these enzymes have different affinities for HIF-α. PHD2 has a higher affinity for HIF-1α, whereas PHD1 and PHD3 have a higher affinity for HIF-2α (Appelhoff et al., 2004). Interestingly, both PHD2 and PHD3 are HIF transcriptional targets (Epstein et al., 2001; del Peso et al., 2003; Metzen et al., 2005). Therefore, the induction of PHDs is partly dependent on the transcriptional activity of HIF. This provides a feedback control and enables a fine balance between HIF-α synthesis and PHD-dependent degradation.

Although HIF is the most well-characterised substrate, in recent years it has been reported that PHDs have diverse and isoform-specific substrates (reviewed in Yang et al., 2014; Kim and Yang. 2015). For example, PHD1 and 3 have been reported to hydroxylate IKKβ (IκB kinase β, an inhibitor of NF-κB kinase subunit beta) in the putative LXXLAP motif, resulting in a decreased activity of the NF-κB pathway (Cummins et al., 2006; Fu et al., 2013). In addition, PHD1 and 3 have also been reported to hydroxylate the large subunit of RNA Pol2 (RNA polymerase II), Rpb1 on the P1465 residue. This hydroxylation is necessary for phosphorylation of Serine 5 within in the C-terminal domain in the Rpb1, which then leads to non-degradative ubiquitination (Mikhaylova et al., 2008; Yi et al., 2010). Furthermore, ATF-4 (the Activating

Transcription Factor-4) has also been identified as a non-HIF substrate for PHD3, and the stability of the ATF4 protein is mediated in a hydroxylase activity-dependent manner (Koditz et al., 2007). Overall, the hydroxylase activity of the PHDs is reported not to be limited to regulation of the HIF pathway, but is also necessary for regulating other signaling pathways. Since some of their substrates are TFs, it seems likely that there may also be a HIF-independent gene expression signature in hypoxia that results from altered recognition of these other cellular pathways that are PHD enzyme-dependent.

1.4.2 FIH-dependent regulations of HIF

HIF-1α and HIF-2α subunits are also substrates for an additional regulatory hydroxylation. This is mediated by another oxygen-sensitive 2-OG dependent dioxygenase enzyme FIH (Factor Inhibiting HIF), which hydroxylates an asparagine residue in the C-TAD of HIF-α (Asn-803 in HIF-1α and Asn-851 for HIF-2α) (Mahon et al., 2001; Hewitson et al., 2002; Lando et al., 2002a; Lando et al., 2002b). Only one isoform of FIH exists.

Asparaginyl hydroxylation by FIH interferes with the ability of HIF-α to recruit the co-factors p300 (Gu et al., 2001)/CBP (Ema et al., 1999) and hence prevents the full activation of its target genes. These co-factors are required due to their ability to modify the local chromatin structure via their lysine acetyl-transferase activity, as well as their ability to interact with transcription machinery (Bedford et al., 2010). It has been shown that the interaction between the C-TAD and p300/CBP requires conformational changes that bury the asparagine residue in a hydrophobic environment. This explains why hydroxylation is able to block the C-TAD and p300/CBP interaction (Dames et al., 2002; Freedman et al., 2003). Interestingly, a number of genes are still induced under hypoxia in the absence of p300 binding (Dayan et al., 2006; Kasper et al., 2005). This suggests

that certain genes can be activated with either the N-TAD, or that some unknown co-activators operate in the presence of FIH-mediated hydroxylated HIF-α.

Notably, FIH has a lower K_m value (~90 μM) for oxygen as compared with PHDs. This indicates that FIH is able to maintain its function at a lower oxygen concentration and suppress HIF transcriptional activity even when HIF escapes from degradation in moderate hypoxia (Dayan et al., 2006; Koivunen et al., 2004). In addition, FIH activity is also much more sensitive to reactive oxygen species, compared with the PHDs (Masson et al., 2012).

FIH-catalysed hydroxylation of asparagine residue is also observed in multiple ankyrin-repeats-containing proteins such as Notch, NF-κB and its inhibitor protein IκBα (Coleman et al., 2007, Zheng et al., 2008, Hardy et al., 2009). However, the functional consequences of hydroxylation on these substrates and the corresponding consequences for HIF signaling remain poorly understood.

1.4.3 Other modifications of HIF

Oxygen sensing via the HIF hydroxylases has defined a core feature of HIF-α regulation. However, other post-translational modifications of HIF-α subunits that are independent of oxygen tension have also been reported, such as acetylation, phosphorylation, and S-Nitrosylation (**Figure 1**) (reviewed in Dengler et al., 2014; Kuschel et al., 2012). These modifications of HIF-1α and HIF-2α can regulate the transcriptional outputs of HIF both positively and negatively, depending on the location and the type of the modified residue. For example, lysine K532 acetylation of HIF-1α within the ODD has been reported to enhance association with VHL and thus lead to decreased HIF-1α protein stability and reduced target gene expression (Jeong et al., 2002). Conversely, acetylation of lysines (K674 and K709) in the C-terminal region of HIF-1α resulted in decreased polyubiquitination and subsequently an increased HIF-1α protein level with enhanced

target gene expression (Lim et al., 2010; Geng et al., 2012). Similarly, phosphorylation of HIF-α subunits can lead to increased HIF stability and transactivation of its targets, by either disrupting its interaction with VHL or by increasing its affinity for recruiting transcriptional coactivators (Richard et al., 1999). On the other hand, phosphorylation at Ser-247 within the HIF-1α PAS-B domain by casein kinase 1 (CK1) blocks HIF-1α interaction with HIF-1β therefore inhibiting HIF-1α induced gene expression (Knippschild et al., 2005; Kalousi et al., 2010).

1.5 The HIF transcriptional programme

1.5.1 The hypoxia response element

The binding of TFs to specific DNA sequences is the fundamental basis for gene regulation (Davidson. 2010). The HIF-α/β heterodimer binds to a consensus sequence 5'-RCGTG-3' (R=A/G), which is known as the hypoxia responsive elements or HREs. HIF-α was found to bind the 5' half-site whereas HIF-1β binds the 3' half-site (-GTG) (Swanson et al., 2002). The core HRE sequence is highly abundant with overall $1.1x10^6$ potential sites across the genome, however less than 1% of these sites are actually bound by HIFs (Mole et al., 2009; Xia et al., 2009; Schödel et al., 2011). Analyses of HIF binding sites indicated a general preference of A over G at position 1 and T at the position immediatly upstream of the functional HRE, however no other apparent difference within the HREs of HIF targets was observed (reviewed in Wenger et al., 2005).

Interestingly, sequence analysis around the core HREs has revealed some enrichment of motifs of other TFs, such as AP-1 (Activator Protein-1), CREB (cAMP Response Element-binding Protein), CEBPB (CCAAT-enhancer binding protein), NFY (Nuclear Transcription Factor Y), and MIF (Macrophage Migration Inhibitory Factor)

(Mole et al., 2009; Villar et al., 2012). This suggests a possible functional interplay of DNA-binding between HIF and other TFs, and is supported by experimental evidence. For example, a study in HeLa (cervical cancer) cells compared HIF target gene expression levels under hypoxia when either the HRE or nearby TF binding sites were mutated (Villar et al., 2012). The authors showed that while mutating HREs completely abolished the HIF-1α hypoxic response, modification of the other neighboring TF sites (i.e. CREB, CREBPB, and AP-1) also significantly reduced the expression levels of the reporter genes *LDHA (*Lactate dehydrogenase A*), GYS1* (Glycogen synthase 1*),* and *CA9* (Carbonic anhydrase 9*),* respectively. In addition, a study in the 786-O renal cancer cell line with exogenously expressed HIF-1α or HIF-2α also revealed an enrichment of the AP-1 motif at HIF binding regions (Salama et al., 2015). In this case, the AP-1 motif appeared to be more enriched at the HIF-2α binding sites in the 786-O cells.

1.5.2 Pan-genomic profiling of the HIF DNA-binding sites

In recent years, technological advances in investigating the protein-DNA interactions, as well as the advent in computing and information processing tools, have enabled more comprehensive analyses of the HIF pathway by comprehensive profiling of direct HIF binding sites within the genome. For example, using specific HIF antibodies, multiple groups have performed chromatin immunoprecipitation coupled with tiled microarrays (ChIP-chip) to assess HIF binding across the genome (Xia et al., 2009; Mole et al., 2009). These studies have identified several hundreds of HIF binding sites in MCF-7 (breast cancer) cells, and HepG2 (hepatoma) cells. Subsequently, unbiased high-resolution analyses using ChIP followed by deep-sequencing (ChIP-seq) further revealed high-stringent HIF-1α, HIF-2α and HIF-1β binding sites in several cell backgrounds (Tanimoto et al., 2010; Schödel et al., 2011; Villar et al., 2012; Schödel et al., 2012; Salama et al., 2015; Grampp et al., 2016).

One important finding from these studies is that HIF acts as a *cis* transcriptional activator rather than repressor. By coupling the HIF binding sites detected by ChIP-seq with high confidence hypoxia regulated genes from RNA-seq data in the normoxic and hypoxic MCF-7 cells, Schödel et al., demonstrated that HIF binding sites were associated with genes that were up-regulated by hypoxia (Schödel et al., 2011). In the same study, the authors also showed that HIF binding was not restricted to promoter regions and the binding sites could locate at great distance (>100 kb) from the target genes. This suggests long-range interactions of regulatory elements and HIF binding across the genome.

Indeed, with recent advances of chromosome conformation capture technology such as 3C, 4C, 5C and Hi-C, it has been revealed that some distal enhancers are capable of binding to the promoters of their targets via chromatin looping (reviewed in Dekker et al., 2013). This is also observed in the case of HIF binding. For example, a HIF-2α specific binding site was identified in the enhancer region of *CCND1* (cyclin D1). This locus locates approximately 220 kb from the transcription start site (TSS) of the gene and is a locus of polymorphism in ccRCC identified by genome-wide association studies (GWAS). By performing 3C experiments, Schödel et al., demonstrated an RCC-specific looping of this binding site to the TSS of *CCND1* (Schödel et al., 2012). Similarly, another ccRCC polymorphism at chromosome 8q24.21 was identified in the HIF-2α binding site, and it has been shown that this HIF binding locus was linked to the nearest genes *PVT1* and *MYC* via chromatin looping (Grampp et al., 2016). In addition, a newly developed technique based on 3C coupled with oligonucleotide-enriched regions of interest and next generation sequencing (known as Capture C) has allowed identification of direct interactions between gene targets and multiple distant functional elements (Hughes et al., 2014; Davies et al., 2016). As an example, in a recent study, Platt et al.,

characterised the long-distance interactions between direct HIF targets and multiple HIF-binding sites (Platt et al., 2016).

Another important finding from the genome-wide studies of HIF binding revealed that HIF preferentially binds to permissive chromatin regions that display DNAse I hypersensitivity, RNA Pol2 enrichment, histone modifications and activates genes with basal transcriptional activity under normoxia (i.e. in the absence of HIF) (Mole et al., 2009; Xia et al., 2009; Schödel et al., 2011; Galbraith et al., 2013). This suggests that HIF binding sites may be determined by the pre-existed patterns of chromatin structure.

1.5.3 Factors influencing HIF DNA-binding

It has been proposed that the transcriptional network of any given TF is highly connected and continuous (reviewed in Biggin. 2011). Essentially, each TF binds to all available target sites over a quantitative continuum of occupancy level, rather than a yes or no distinction as to which sites it could bind to. Furthermore, it was proposed that the quantitative difference in DNA binding is directly correlated with the functional specificity, i.e. genes that are occupied with high levels of TF are more likely to have biologically significant functions. Thus, understanding the variations in TF binding is important, as it would allow us to know whether each TF regulates the expression of the same gene to different degrees, as well as whether different genes are regulated differently by a pool of the same TF.

In general, TF DNA-binding can be influenced by multiple factors, such as TF protein abundance, the intrinsic affinity of binding sites, as well as the accessibility of chromatin (Brewster et al., 2014; Zabet and Adryan. 2015; Ezer et al., 2014). As a TF, the transcriptional function of HIF might be controlled by the combinational effects of all these parameters. In addition, HIF DNA-binding may also be affected by its functional interactions with oncoproteins and tumour suppressors, as mentioned above.

Multiple mechanisms exist to alter HIF protein abundance, including the relative level and duration of hypoxia, as well as disturbances of tumour suppressor and oncogenic pathways. These stimuli can regulate HIF protein levels at multiple levels, such as HIF transcription, translation, post-transcriptional modifications, and pVHL-mediated HIF degradation (reviewed in Masson and Ratcliffe. 2014). A recent pan-genomic study of HIF binding profile by ChIP-seq showed that overexpression of HIF protein increased binding intensity at sites that are already occupied, as well as created binding at new sites (Salama et al., 2015). This suggests that the level of HIF protein may affect its DNA binding intensity. Furthermore, this study (and among other ChIP-seq studies) revealed different levels of ChIP signal at binding loci across the genome. This indicates that HIF binding may display a non-uniform affinity landscape, and also raises a question as whether HIF preferentially binds to specific sites at different conditions.

The HIF response is also dependent on an open chromatin configuration. It has been shown that epigenetic modifications may affect the HRE accessibility for HIF binding via at least two mechanisms. Firstly, HIF binding can be affected by DNA methylation. Methylation of a CpG dinucleotide in the 3' enhancer of *EPO* abolished both HIF DNA-binding and the reporter gene expression, and the expression level of Epo was inversely associated with the level of CpG methylation (Wenger et al., 1998; Rössler et al., 2004). Secondly, HIF binding can be regulated via altered chromatin structure mediated by the post-translational modification of histone tails (reviewed in Shilatifard. 2006). For example, under hypoxia there is an increased level of histones displaying H3K4me3 (histone H3 lysine 4 trimethylation, a marker for actively transcribed genes), and a decrease in H3K27me3 (histone H3 lysine 27 trimethylation, a modification associated with inactive genes) in the promoter regions of HIF targets *VEGF* and *EGR1* (reviewed in Shilatifard. 2006). These modifications of histones were also observed

across HIF binding sites as demonstrated in the genome-wide ChIP-chip and ChIP-seq studies (Xia et al., 2009; Tanimoto et al., 2010). In addition, increased H3K27ac (histone H3 lysine 27 acetylation, a marker for active enhancers) was observed at the promoter of *CA9* under hypoxia (Ledaki et al., 2015), as well as in several HIF-bound enhancers and target gene promoter regions in hypoxia (Platt et al., 2016).

1.6 The HIF regulatory network

Upon binding to the core HREs, HIF acts as a molecular switch to then activate the transcriptional outputs by a myriad of processes (**Figure 2**) The first step of these processes is likely achieved through the recruitment of general co-activators that include histone modifiers, chromatin remodelers, and the CDK8-Mediator complex. This results in increased histone acetylation, bromodomain protein binding (e.g. BRD4) and release of the transcriptionally active but paused RNA Pol2 (the main component of the basal transcriptional machinery) for productive transcriptional elongation.

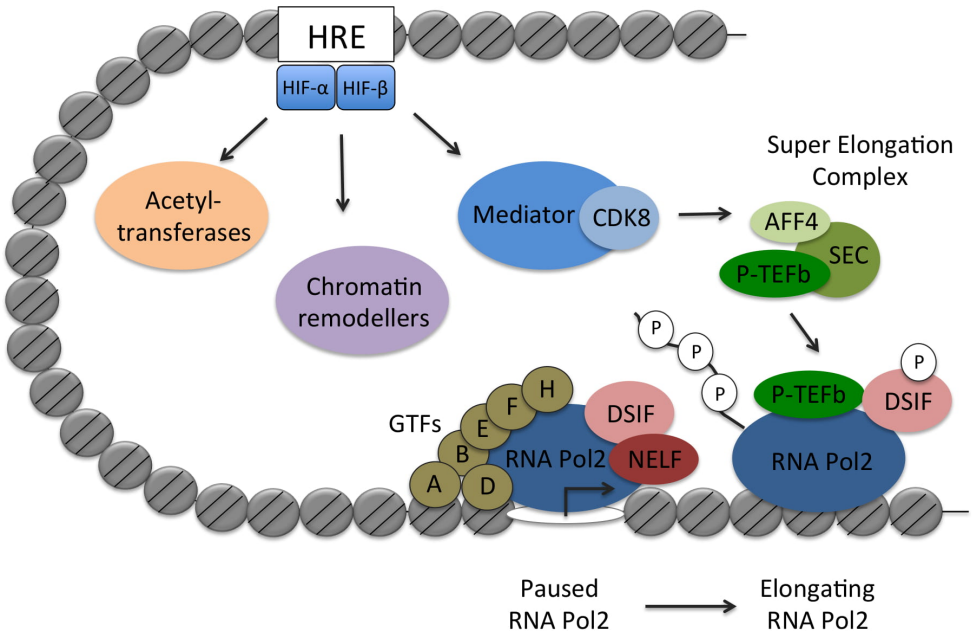

Figure 2. Schematic model of HIF-dependent transactivation.

Under normoxia, HIF targets display an open chromatin environment and harbour a transcriptionally active but paused RNA Pol2 (RNA polymerase II). Upon hypoxia, the HIF-α/β heterodimer binds to the permissive HREs (Hypoxia Responsive Elements) and recruits various co-activators, such as acetyl-transferases, chromatin remodellers, and CDK8-mediators along with the Super Elongation Complex (SEC) containing P-TEFb (the positive transcription elongation factor). These events lead to increased histone acetylation and P-TEFb triggers the release of paused RNA Pol2 into productive elongation and consequently activates the target gene expression.
AFF4: AF4/FMR2 Family Member 4. DSIF: DRB sensitivity inducing factor. NELF: negative transcription elongation factor. GTFs: General Transcription Factors. Modified from Dengler et al., 2014.

1.6.1 HIF target genes

So far, several hundred or even thousands of both primary and secondary (i.e. indirect) genes have been identified to be under the control of the HIF pathway (Wenger et al., 2005; Mole et al., 2009; Schödel et al., 2011; Salama et al., 2015). HIF target genes are involved in numerous aspects of the biology of cells and multi-cellular organisms, such as metabolism, vascular biology, cell cycle control, and even the oxygen-sensing pathway itself (reviewed in Keith and Simon. 2007; Tsai and Wu. 2012). The diversity of HIF

transcriptional targets suggests a fundamental role of the HIF pathway in the integrated physiology of oxygen homeostasis. Furthermore, analyses of HIF targets across diverse cell types indicate that the repertoire of HIF targets is highly cell-type dependent with only a small number of HIF-regulated genes conserved across all cell types (Chi et al., 2006; Ortiz-Barahona et al., 2010).

1.6.2 HIF and hypoxia-regulated gene expression

In the past decade, several genome-wide analyses of the transcriptomic response to hypoxia coupled with HIF binding have demonstrated that HIF is at the centre of hypoxia-dependent gene regulation (Mole et al., 2009; Xia et al., 2009; Schödel et al., 2011). However, some studies have also identified a number of novel and HIF-independent hypoxia-inducible genes, indicating that mechanisms other than the HIF pathway may also be involved in the regulation of gene expression under hypoxia (Elvidge et al., 2006; Ameri et al., 2004; Wellmann et al., 2004; Rong et al., 2006; Miyoshi et al., 2006).

Indeed, hypoxia can activate a number of other TFs, such as the general stress-response TFs such as AP-1, NF-κB, as well as p53 and myc (reviewed in Kenneth and Rocha. 2008; Rocha. 2007). Therefore, genes regulated by hypoxia could be a result of a coordinated response between HIF and these other pathways.

In addition to inducing changes in protein-coding RNAs, hypoxia has also been shown to regulate non-coding transcripts. Microarray-based expression profiles revealed hypoxia-induced miRNAs (microRNAs) and some of the miRNAs are directly regulated by HIF-1α (Kulshreshtha et al., 2007; Hebert et al., 2007). By sequencing of the whole transcriptome (RNA-seq) of total RNA, a recent study also demonstrated that all classes of RNA were significantly regulated by hypoxia (Choudhry et al., 2014). The authors further demonstrated that the hypoxic induction of most non-coding RNAs is directly

regulated by HIF. This further extends the hypoxic transcriptional response into the spectrum of non-coding transcripts.

The complexity of the transcriptome under hypoxia has made it difficult to dissect which hypoxia-regulated genes are direct HIF targets. Given that HIF is a TF, and its transcriptional response is evoked by binding to the DNA, the most direct measurement of HIF responses would be via the direct measurement of HIF binding across the genome.

1.6.3 The divergent roles of HIF-1α and HIF-2α

The introduction of siRNA technology has further elucidated the role of each HIF-α isoform in regulating gene expression (Sowter et al., 2003; Hu et al., 2003; Warnecke et al., 2004; Raval et al., 2005). It has been shown that HIF-1α and HIF-2α appear to regulate overlapping but distinct sets of genes. For example, some targets such as glycolytic genes are discrete to HIF-1α. Cells switch from oxidative to glycolytic metabolism by expressing genes such as *PDK1* (Pyruvate Dehydrogenase Kinase 1) and *LDHA* (Kim et al., 2006; Papandreou et al., 2006; Hu et al., 2003; Rankin et al., 2005; Wang et al., 2005), *BNIP3* (BCL2 Interacting Protein 3) (Zhang et al. 2008), and *BNIP3L* (BNIP3-like protein) (Zhang et al., 2008; Bellot et al., 2009). Furthermore, HIF-1α also mediates the switch in the subunit composition of cytochrome c oxidase (electron transport chain complex IV), to improve the efficiency of respiration under hypoxia (Fukuda et al., 2007). Other genes that act in the glucose metabolism pathway such as glucose transporters genes are regulated by both isoforms. On the other hand, genes such as *EPO* in Hep3B (hepatoma) and Kelly (neuroblastoma) cells (Warnecke et al., 2004) and *POU5F1* (which encodes Oct-4 [octamer-binding transcription factor 4], a TF involved in maintaining stem cells pluripotency)(Covello et al., 2006) are exclusively regulated by HIF-2α. In addition, even when expressed in the same cell type with both isoforms contributing to the activation of target genes, under subsequent conditions the

two isoforms can act in opposition. For instance, macrophage differentiation to the M1 phenotype is dependent on HIF-1α. By contrast, the differentiation to the M2 phenotype is regulated by HIF-2α (Takeda et al., 2010).

The divergent targets of HIF-1α and HIF-2α may potentially explain their functionally different roles *in vivo*. For instance, mice with a homozygous HIF-1α deletion die at embryonic day 10.5 with a cardiac malformations and vascular defects (Iyer et al., 1998a; Yoon et al., 2011). By contrast, the phenotypes of HIF-2α null mice vary widely depending on the genetic background. Some die at embryonic day 12.5 with vascular defects (Peng et al., 2000), bradycardia (Tian et al., 1998), or die as neonates due to impaired lung maturation (Compernolle et al., 2002). Furthermore, in embryonic stem cells, it has been shown that HIF-2α cannot functionally substitute for HIF-1α (Hu et al., 2006). This again indicates non-redundant functions of these two isoforms.

The different roles of HIF-1α and HIF-2α have also been reported in various physiological settings, such as during chondrogenesis (Schipani et al., 2001), adipocyte differentiation (Yun et al., 2002), osteogenesis (Wang et al., 2007), as well as in pathophysiological conditions, for example wound healing (mainly by HIF-1α, reviewed in Ruthenborg et al., 2014; Hong et al., 2014), angiogenesis (Hahne et al., 2018; reviewed in Hashimoto and Shibasaki. 2015), and tumorigenesis (Raval et al., 2005; reviewed in Rankin and Giaccia. 2008). Overall, the intricate balance between HIF-1α and HIF-2α activation is required to regulate the complex HIF-dependent processes.

1.7 Hypoxia, HIF and Cancer

Hypoxia is frequently encountered in solid tumours due to the high rates of proliferation of cancer cells that subsequently limits oxygen diffusion. Hypoxic stress may also be caused by perfusion defects due to the chaotic formation of structurally and functionally

abnormal vasculature in tumours (reviewed in Bertout et al., 2008). By analysing human cancer biopsies and experimental animal models, it has been demonstrated that the HIF pathway is up-regulated in many types of cancer, and increased HIF-α expression is associated with aggressive tumour behaviour and adverse prognosis (reviewed in Semenza. 2003).

However the HIF pathway may also be up-regulated by mechanisms in cancer other than hypoxia, such as altered metabolism and redox signals, which have been proposed to lead to an inhibition of hydroxylation and subsequently accumulation of HIF (reviewed in Masson and Ratcliffe. 2014). In addition, many oncogenic pathways are functionally linked with the activation of HIF pathway. For example, mutations in the PI3K/AKT pathway promote HIF transcription and translation (reviewed in Brugarolas and Kaelin. 2004). Activation of Ras results in an inhibition of HIF-1α hydroxylation due to the increased intracellular ROS (Reactive Oxygen Species)(Gerald et al., 2004). Mutations and subsequently inactivation of succinate dehydrogenase or fumarate hydratase inhibit HIF hydroxylation through the accumulation of succinate and fumarate respectively, both of which act as 2-OG analogues, therefore outcompeting the necessary cofactors (Hewitson et al., 2007; O'Flaherty et al., 2010).

It is certainly true that genes known to be responsive to HIF contribute to tumour growth. HIF regulates genes that are involved in various aspects of tumour development, including, angiogenesis (*VEGF, PDGF*), proliferation (*MYC*), DNA damage response (*GADD45A*), extracellular matrix remodeling (*LOX, MMP1*) and invasion (*CXCR4, SDF1*) (reviewed in Kaelin and Ratcliffe. 2008).

A direct role of the HIF transcriptional pathway in supporting tumourigenesis has been implied by multiple studies. For example, murine cell lines that are deficient in HIF-1α (Ryan et al., 2000) or HIF-1β (Maxwell et al., 1997) showed impaired growth in

allografted tumour formation, and expression of HIF-1α C-TAD peptides that block the interaction between HIF-1α and its co-activators p300/CBP decreased xenograft tumour growth in mice (Kung et al., 2000). However, in this latter study, it is unclear whether the observed effects on tumour growth are truly through repression of HIF transcription or whether the peptides are blocking some other critical interactions of p300/CBP.

However, there are other experiments that do not support a key role for HIF in tumourigenesis. Inactivation of specific components of the HIF pathway does not always have negative effects on tumour growth. For instance, teratoma derived from HIF-1α deficient murine embryonic stem cells did not display retarded tumour cell proliferation (Carmeliet et al., 1998). In addition, genetic inactivation of HIF-1α in transformed murine astrocytes had either positive or negative effects on orthotopic tumour growth depending on the microenvironment in which the cells are grown (Blouw et al., 2003). Furthermore, in the mouse model of kidney-specific inactivation of FH (fumarate hydratase), it has been shown that hyperplastic renal cysts formation and tumour development were HIF-independent (Adam et al., 2011). All of these evidences suggest that the effects of HIF-α on tumour growth may be context-dependent and are influenced by cell origin and tumour location.

Despite the widespread activation of the HIF system in cancer, it does not necessarily mean HIF is the driving force for cancer development. Especially, the accumulation of HIF-α protein in highly aggressive tumours may be due to their outgrowth of blood supply and consequently a more hypoxic microenvironment. In this case, HIF-α acts as a marker, rather than a cause of enhancing malignant phenotypes. In supporting this, at the molecular level to date there is little evidence for deletions or mutations in the HIF protein itself in cancers, except for activating mutations in HIF-2α in paranglioma (Fliedner et al., 2016) and a very small number of inactivating mutations

in HIF-1α found in RCC and discussed below. Thus, a simple causal association between the up-regulation of the HIF pathway and tumourigenesis cannot be derived.

In addition, the activation of the HIF transcriptional response will lead to a global activation of HIF targets in the cancer cell, regardless of whether they may be advantageous or not. This has been termed the 'co-selection' hypothesis, where certain HIF targets are selected by oncogenic or microenvironmental stimuli in favouring cancer development while the others have to be tolerated (reviewed in Ratcliffe. 2013).

1.8 HIF and Renal Cell Carcinoma

1.8.1 The VHL syndrome and renal cell carcinoma

VHL syndrome is an autosomal dominant disease that comprises a range of benign and malignant tumours, including renal cancer carcinoma (RCC), hemangioblastoma and pheochromocytoma. Individuals with the VHL syndrome are heterozygous for a germline inactivating mutation in the VHL gene, usually followed by a somatic inactivation of the remaining wild-type VHL allele, leading to a complete loss of function of pVHL and an abnormal activation of the HIF pathway (reviewed in Kaelin. 2007).

RCC is the 14th most common malignancy and the 3rd most common urological cancers (Ferlay et al., 2010). Worldwide, renal carcinoma causes over 100,000 deaths per year (Ljungberg et al., 2011). RCC can be divided into three major types based on their histology: clear cell RCC (ccRCC, 70-75%), papillary RCC (pRCC, 10-16%) and chromophobe RCC (chRCC, 5%)(Shuch et al., 2015). Approximately 90% of sporadic ccRCC also have a loss of function of pVHL (Gnarra et al., 1994; Herman et al., 1994; Cancer Genome Atlas Research Network 2013).

The pVHL tumour suppressor protein serves as the substrate recognition component of an E3 ubiquitin ligase complex that targets proteins for proteasomal

degradation (Kibel et al., 1995). Together with the other components of the E3 ligase complex, i.e. elongin B, elongin C, cullin 2, Rbx1, and the E2 ubiquitin conjugating enzyme, it directly binds to prolyl hydroxylated HIF-α subunits, ubiquitinates them and targets them for destruction (Kibel et al., 1995; Duan et al., 1995; Kishida et al., 1995). Therefore, loss of function of pVHL results in a 'pseudohypoxic' environment by impairing the polyubiquitination and degradation of HIF-α leading to its constitutive stabilisation and activation of the HIF pathway (Maxwell et al., 1999). In the kidneys of patients with VHL disease, overexpression of both isoforms of HIF-α is detected in the early precancerous lesions that arise when there is a complete loss of pVHL (Schietke et al., 2012; Mandriota et al., 2002; Raval et al., 2005). This is accompanied by an increased level of HIF targets such as *CA9* and *GLUT1* (Mandriota et al., 2002), and *CCND1* (Raval et al., 2005). In mouse models of ccRCC, re-introduction of pVHL in VHL-defective RCC xenografts was found to inhibit the tumour growth, indicating the role of pVHL as a tumour suppressor protein in the pathogenesis of RCC (Iliopoulos et al., 1995).

1.8.2 The divergent roles of HIF-1α and HIF-2α in renal cancer

HIF-1α and HIF-2α have been reported to have different roles in the development of ccRCC. Overall evidence suggests that these two isoforms have opposing effects with a more anti-tumourigenic role for HIF-1α and a more pro-tumourigenic role for HIF-2α. There are several pieces of evidence for this.

Firstly, immunohistochemistry studies examining the normal expression pattern of HIF in the kidney have shown that normal renal tubules express HIF-1α exclusively, whereas HIF-2α expression is confined to the interstitial fibroblasts and glomerular endothelial cells (Mandriota et al., 2002; Rosenberger et al., 2002). In comparison, although both isoforms were detected in the precancerous lesions found in the kidneys of

patients with VHL disease (Schietke et al., 2012; Mandriota et al., 2002; Raval et al., 2005), HIF-1α expression is frequently lost in VHL-defective cancer, whereas HIF-2α is expressed in all VHL-associated ccRCC and many do so exclusively (Mandriota et al., 2002; Gordan et al., 2008). These findings indicate an unusual bias of the HIF pathway towards HIF-2α expression, which may be of fundamental importance to RCC development.

Secondly, genetic interventions on HIF-1α and HIF-2α indicate differing function in ccRCC cell lines and on xenograft tumour models in mice. For example, overexpression of HIF-1α in ccRCC cells reduced tumour xenograft growth, whereas short hairpin RNA-mediated knockdown of HIF-1α displayed increased cell proliferation (Raval et al., 2005; Shen et al., 2011). By contrast, overexpression of HIF-2α led to an increased tumour burden in mouse xenografts (Raval et al., 2005; Kondo et al., 2002) and inhibition of HIF-2α resulted in decreased tumour mass (Kondo et al., 2003). Importantly, this effect is restricted to HIF-2α with an intact DNA-binding domain, indicating the importance of HIF-2α-dependent transcriptional activity in tumour progression. In addition, the divergent roles of HIF-1α and HIF-2α were also illustrated in a study where primary tumours were subdivided into those that expressed wild-type VHL, as well as VHL-deficient ccRCC with expression of both HIF-1α and HIF-2α, or VHL-deficient ccRCC with HIF-2α expression alone (Gordan et al., 2008). In this analysis, tumours with exclusive HIF-2α expression appeared to have bigger volumes, perhaps consistent with a role of HIF-2α in driving proliferation, although no other clinical parameters showed a significant association.

Increasing genetic evidence also supports divergent roles for HIF-1α and HIF-2α in renal cancer. Genomic analyses of RCC have revealed a common copy number reduction for a region of the chromosome 14q, which harbours the HIF-1α gene (Shen et

al., 2011; Monzon et al., 2011). In addition, a very small but significant number of inactivating mutations have also been observed in the HIF-1α gene in VHL-defective ccRCCs (Morris et al., 2009; Dalgliesh et al., 2010). Some of the mutations in the HIF-1α gene have been shown to compromise the ability of HIF-1α to inhibit proliferation of RCC cells (Morris et al., 2009; Shen et al., 2011). Collectively this suggests a potential role of HIF-1α as a tumour suppressor protein in RCC. On the other hand, an oncogenic role of HIF-2α in RCC development is indicated by recent GWAS. A polymorphism has been identified in the first intron of *EPAS1* (HIF-2α gene). This polymorphism was found to be associated with an increased occurrence of RCC, however the functional mechanism has not yet been resolved (Purdue et al., 2011; Han et al., 2012). In addition, another polymorphism at chromosome 11q13.3, which corresponds to an enhancer region of *CCND1*, was found to be protective for RCC development (Audenet et al., 2014; Su et al., 2013; Wu et al., 2012). This locus was exclusively regulated by the HIF-2α in the context of VHL-defective RCC (Schödel et al., 2012). Overall, these studies provide direct evidence for the important oncogenic role of HIF-2α in promoting RCC growth.

1.8.3 The mechanisms that account for the differential functions of HIF-1α and HIF-2α in ccRCC

The underlying mechanism of the opposing actions of HIF-1α and HIF-2α in the pathogenesis of RCC is not fully understood, however this is likely to be driven by an alteration in the balance of activated HIF targets towards a more oncogenic profile (Raval et al., 2005; Keith and Simon 2007). Expression arrays have identified a number of genes that are regulated by HIF-1α or HIF-2α or by both isoforms in renal cancer. For instance, genes encoding glycolytic enzymes (*HK1, ALDOA, PGK*) are predominantly regulated by HIF-1α, whereas genes involved in proliferation and cell cycle control such as *TGFA* and *CCND1* are exclusively regulated by HIF-2α. However, the situation is complex as not all

HIF-1α dependent genes are anti-tumourigenic and conversely not all HIF-2α dependent genes are pro-tumourigenic. A study in a renal cancer cell line utilising overexpression of either HIF-1α or HIF-2α showed that even within the HIF-1α and HIF-2α-specific transcriptional cascades, the target genes are heterogeneous in their tumour promoting or suppressing activity (Salama et al., 2015). This indicates that other factors may be involved in regulating the selection in ccRCC drive towards HIF-2α dependent gene expression. For instance, it has been demonstrated that HIF-1α and HIF-2α may have opposing functional interactions with other crucial oncoproteins and tumour suppressors such as myc and p53 (Gordan et al., 2007a; Gordan et al., 2007b; Bertout et al., 2009).

Exactly how HIF-1α and HIF-2α achieve their selectivity in target gene expression is unclear, and there are several potential explanations. First, analysing pan-genomic binding patterns of HIF-1α and HIF-2α showed that these two isoforms bind to distinct (but overlapping) sites in the genome (Schödel et al., 2011; Villar et al., 2012; Schödel et al., 2012; Salama et al., 2015; Grampp et al., 2016). In a RCC setting, this discrete isoform-specific binding was shown to activate distinct patterns of gene expression and opposite prognosis (Salama et al., 2015). Second, it has also been shown that even when HIF-1α and HIF-2α bind to the same site, they can still differentially regulate gene expression. This differential regulation requires domains other than the DNA-binding domains. Studies that performed domain-exchange and domain-deletion experiments demonstrated that C-terminal regions of HIF-α proteins determined the target gene selectivity (Hu et al., 2007; Lau et al., 2007). Specifically, Lau and colleagues showed that regions of the HIF-1α protein between amino acids 96-390, and 411-574 are necessary for the induction of the HIF-1α specific target *CA9*, whereas a region in HIF-2α between amino acids 543-870 is necessary and sufficient for the induction of the HIF-2α target gene *EGLN3* (Lau et al., 2007). Another independent study by Hu et al., also

demonstrated the expression of distinct HIF-1α specific, HIF-2α specific and HIF-1α/2α common genes was mediated by the N-TADs of the HIF-α isoforms (Hu et al., 2007). Third, differences in target selectivity may also be due to the fact that the C-terminal transactivation domains of HIF-1α and HIF-2α have different sensitivity to FIH-mediated hydroxylation, with HIF-1α more sensitive to this hydroxylation (Koivunen et al., 2004; Bracken et al., 2006). Interestingly, inhibition of FIH led to increased HIF-1α transcriptional activity and apoptosis of RCC cells (Khan et al., 2011). This indicates that FIH may play an oncogenic role in RCC development, potentially through inhibition of the anti-tumorigenic function of HIF-1α.

1.9 Therapeutic interventions on the HIF pathway – clinical interest

Considering the critical role that HIF plays in the development, physiology and disease, especially in tumourigenesis, there has been great interest in the development of inhibitors targeting this pathway in the past two decades (reviewed in Yu et al., 2017). In particular, HIF target genes have been shown to play a role in cancer progression and therapy resistance, therefore a number of HIF inhibitors are developed for treating cancers. In pre-clinical studies, inhibition of HIF-1α activity has shown marked effects on retarding tumour growth (reviewed in Semenza. 2003).

Currently available compounds with anti-HIF-α activity have been shown to act either directly, by inhibiting transactivation, HIF-α/β dimerisation, DNA-binding activity of HIF-1α, or indirectly via blocking HIF-1α translation or promoting its degradation, and some molecules target more than one mechanism (reviewed in Masoud and Li. 2015; Wigerup et al., 2016; Burroughs et al., 2013).

In addition, isoform specific inhibitors have been developed in recent years. For instance, a novel HIF-1α specific inhibitor was reported to interrupt HIF-α/β dimerisation

by binding to the PAS-B domain without affecting HIF-2α (Miranda et al.,2013). On the other hand, two compounds, TC-S7009 and PT-2385 were reported to selectively antagonise HIF-2α dimerisation and DNA-binding. The latter one has been shown to have anti-tumorigenic effects both *in vitro* and *in vivo* (Wallace et al., 2016; Chen et al., 2016; Cho et al., 2016), and is currently undergoing clinical trials for treating advanced RCC (reviewed in Martínez-Sáez et al., 2017). This is important since HIF-1α and HIF-2α often have opposite effects on tumourigenesis. For example, glioblastoma, neuroblastoma and RCC might be more responsive to HIF-2α inhibition since in these settings HIF-2α plays an oncogenic role (Bordji et al., 2014; Hamidian et al., 2015; Raval et al., 2005). Therefore, the isoform specific inhibition may be helpful depending on the cancer type.

In addition to target HIF itself, strategies have also been made to modulate the HIF downstream target. For example, monoclonal antibodies targeting HIF target VEGF, or small molecular inhibitors targeting VEGF receptor have been used to treat various advanced cancers (reviewed in Ellis and Hicklin. 2008).

Various studies have also targeted the HIF pathway via inhibition of PHDs. It is considered that the effects of PHD inhibition are mainly through the stabilisation of HIF (as opposed to other substrates) and augmenting the expression of its target genes (reviewed in Karuppagounder and Ratan. 2012). This has been shown to have therapeutic implications in treating systemic or local hypoxia-related diseases such as anaemia, ischemic disease, inflammatory diseases, and tissue injury. Currently four PHD inhibitors are in human clinical trials (Yeh et al., 2017). One significant issue with this approach is the general elevation of the HIF-α level and hence activation of multiple downstream targets. Due to the highly complex role of HIF in cancer, and the distinct roles of HIF-α

isoforms, more specific inhibition of PHDs (e.g. tissue-specific and isoform-specific PHD inhibitors) would likely be desirable

Overall, multiple levels of regulation and multiple signaling pathways may converge on the HIF pathway. This complexity of regulation has made targeting HIF for therapeutics extremely challenging. Hence, better understanding the pathway and design of inhibitors targeting its specific downstream targets may provide new avenues for therapeutics.

1.10 Aim of this study

It is well known that HIF plays an important role in cellular adaption to hypoxia. To better understand how HIF functions, this thesis aims to determine the range of target genes it binds and regulates, and how its transcriptional network changes in response to various stimuli. Answering these questions would help an understanding of the biology of HIF pathway, as well as identifying key HIF targets that might be responsible for tumourigenesis, which would ultimately help design more effective and safer therapy.

The main cell model used in this study is the human immortalised renal proximal tubule cell line HKC-8 (Racusen et al., 1997). The laboratory has a particular interest in RCC, and pVHL-associated RCC is considered likely to derive from the proximal tubular epithelium (Motzer et al., 1996). HKC-8 cells have wild type VHL and express both HIF-1α and HIF-2α. This enables a study of the endogenous HIF response in a context that is likely relevant to RCC.

The existence of multiple TFs regulated by hypoxia raises the fundamental question as to what extent HIF system is contributing to the hypoxic response. Therefore, in the first part of the study (Chapter 2), I sought to identify the contribution of the HIF pathway in the hypoxia-dependent gene expression, and explore the potential

involvement of HIF-independent mechanisms. This is assessed by RNA-seq analysis using sub-clones of HKC-8 cells that are genetically inactivated for either HIF-α, HIF-1β or VHL and FIH components.

Recent genome-wide studies have mapped hundreds of direct HIF DNA-binding sites in response to hypoxia, however the majority of these studies are qualitative and focus on one experimental condition. Thus, it is not clear whether and how the HIF DNA-binding profile would change in response to various stimuli. In the next three chapters I then analysed the genome-wide HIF DNA-binding profiles in the HKC-8 cells using the ChIP-seq technique. The direct transcriptional targets of HIF in response to the following various stimuli were examined (**Figure 3**):

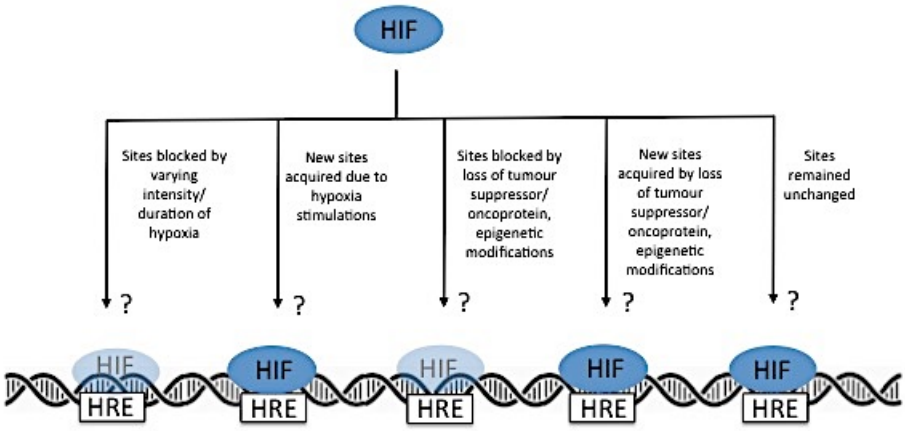

Figure 3. HIF transcriptional programmes in response to various stimuli

HIF plays an important role in physiological and pathophysiological responses to hypoxia. It is known that hypoxia can vary in both intensity and duration. This often results in different levels of HIF-α protein and may affect HIF transcriptional profiles. Likewise, in pre-cancerous cells, due to the inactivation of pVHL, HIF is stabilised. Following mutations in the key tumour suppressor or oncogenic proteins, the global HIF binding profile may change and eventually may contribute to a tumourigenic phenotype. Modified from Schödel et al., 2016.

Overall, the aims of this thesis are:

1. To assess the contribution of the canonical HIF pathway to hypoxia-dependent gene expression and to determine evidence for non-HIF hypoxia-regulated genes.

2. To understand how HIF DNA-binding genome-wide is affected by the degree and duration of hypoxia, i.e. can binding profiles (and therefore target gene output) be switched by dependent hypoxic stress?

3. To assess whether loss of ccRCC tumour suppressors and oncogenes may affect HIF binding patterns.

2

The Contribution of the HIF System to Hypoxia-dependent Gene Expression in HKC-8 cells

2.1 Introduction

Hypoxia can induce profound changes in cellular gene expression patterns. Mechanisms for the sensing of hypoxia and for the alteration of gene expression have been characterised in both prokaryotic and eukaryotic organisms (reviewed in Denko et al., 2003). In the mammalian system, several studies have used genomic approaches to identify gene expression profiles under hypoxia (Benita et al., 2009; Chi et al., 2006; Elvidge et al., 2006; reviewed in Denko et al., 2003). In general these studies have simply applied hypoxia to cells in culture, most using an atmosphere of 0-2% O_2 applied for between 1-24 hours. By extrapolating from these data, it has been proposed that approximately 1.5% of the genome is transcriptionally responsive to hypoxia, though most of these studies did not distinguish responses mediated by HIF from other pathways (reviewed in Denko et al., 2003).

Based on multiple reports that have defined HIF as the regulator of one or more specific target genes, it has been proposed that HIF is the 'master regulator' of gene expression by hypoxia. These studies mostly pre-dated the ability to perform large-scale pan-genomic studies of transcription or binding of transcription factors (TFs) to DNA. They therefore left open whether more systemic surveys could define the extent to which the concept of HIF as a 'master regulator' was true across the genome, or whether there are other pathways that contribute substantially to the hypoxia regulated transcriptome. Several lines of investigation have suggested that this might be the case.

Firstly, multiple TFs have been reported to be responsive to hypoxia. Although the best studied of these is the HIF pathway, other general stress-responsive TFs such as AP-1 (reviewed in Laderoute 2005; Cummins and Taylor 2005), NF-kB (Koong et al., 1994; reviewed in Taylor and Cummins. 2009), p53 (reviewed in Sermeus and Michiels. 2011) and the myc family (reviewed in Huang. 2008), have also been reported to play a role in regulating hypoxic gene expression. Some of the functions may involve co-operation with, or antagonism of, the HIF pathway (reviewed in Kenneth and Rocha. 2008). In general, AP-1 and NF-kB cooperate with HIF, whereas p53 appears to mostly antagonise HIF activity, and the interaction with myc depends on the isoform of HIF-α subunits. Thus, these systems might modulate the activity of HIF responsive genes or might themselves transduce transcriptional responses to hypoxia.

Secondly, in recent years, multiple alternative substrates have been described for both the HIF prolyl hydroxylases (PHDs) and the HIF asparaginyl hydroxylase (FIH). FIH has been shown to hydroxylate asparaginyl residues in the consensus ankyrin repeat of multiple ankyrin-repeat domain containing proteins. For the PHDs, in the region of 20 alternative (non-HIF) substrates have been described (reviewed in Yang et al., 2014 and Guo et al., 2016; Deschoemaeker et al., 2015; Lee et al., 2015; Luo et al., 2014; Zheng et

al., 2014; Romero-Ruiz et al., 2012; Koditz et al., 2007). Hydroxylation-dependent regulation of such substrates would be predicted to generate changes in gene expression under similar conditions as those that activate the HIF pathway, particularly as a number of the reported substrates are transcription factors. For instance, ATF-4 (Activating Transcription Factor 4) can interact with PHD3 via a zipper II domain (Koditz et al., 2007). It is degraded under normoxia due to a novel ODD (oxygen-dependent degradation) domain, and is stabilised under hypoxia (1% O_2 for 24h) or the treatment of PHD inhibitor DMOG (dimethyloxalylglycine). Hydroxylation of FOXO3a (the O subclass of the forkhead family of TFs) by PHD1 at two specific prolyl residues has been shown both *in vitro* and *in vivo*. This results in destabilisation of FOXO3a by displacing its binding to the deubiquitinase USP9x and consequently leads to increased expression of *CCND1* (Zheng et al., 2014). In addition, hydroxylation of p53 by PHD1 in colorectal cancer cell lines was shown to increase p53 phosphorylation by reinforcing its binding to p38a kinase (Deschoemaeker et al., 2015). Given the expanding number of substrates that have been identified for the PHD enzymes, it seems likely that in addition to a HIF-dependent gene expression signature under hypoxia, there may also be a complete HIF-independent gene expression that results from altered regulation of these other cellular pathways that are PHD-dependent.

Thirdly, gene expression under hypoxia can also be modulated at multiple levels other than transcription. Some of these processes might be regulated as a secondary consequence of HIF activation e.g. the hypoxic induction of certain genes (e.g. *VEGF*) as a result of increased mRNA stability (Ikeda et al., 1995); this might be mediated by an action of HIF transcription on RNA stability or by an unconnected pathway. Another possibility is raised by oxygen dependent changes in histone and DNA demethylase activity that may alter chromatin structure, with consequent effects on the accessibility of

DNA and transcriptional regulation by TFs (reviewed in Melvin and Rocha. 2012). For instance, within the dioxygenase family, the JmjC-domain containing histone lysine demethylases (JmjC-KDMs) have been shown to be involved in epigenetic regulation and function in an oxygen-sensitive manner (reviewed in Hancock et al., 2015). However it remains largely unknown whether these processes have a substantial effect on oxygen regulated gene expression. That at least some of the 60-70 known or predicted human 2-OG dioxygenases affect gene expression is supported by a comparison of gene expression profiles induced by hypoxia and by a non-specific pan-2-OG-dioxygenase inhibitor, DMOG. This identified some genes that were not regulated by the hypoxic conditions used but were regulated by DMOG (Elvidge et al., 2006). This suggests that there may be other enzymes in this family capable of regulating changes in gene expression; given that they are dioxygenases the changes in gene expression might also be regulated by oxygen under different hypoxic conditions.

In addition to a completely HIF-independent mechanism, hypoxic gene expression might be mediated by non-canonical transcriptional functions of HIF subunits. Canonical HIF function involves the heterodimeric complex of HIF-α and HIF-1β subunits to activate downstream gene expression (Jiang et al., 1996; Semenza. 2003). However several types of non-canonical function have been proposed. HIF-α and HIF-1β subunits have each been reported to bind DNA with other dimerisation partners in specific cell types or under specific circumstances.

Functional interactions with HIF-α have been described with other types of TF. For instance, under hypoxia it is reported that HIF-1α could interact with NICD (Notch Intracellular Domain), which increases NICD stability and enhances transcription of Notch target *HEY2* and *HES* in mouse cells (Gustafsson et al., 2005). A recent study also

found that STAT3 functions cooperatively with HIF-1α to recruit RNA pol2 to HIF targets such as *VEGF, CA9* and *PGK1* (Pawlus et al., 2013). In line with these experiments, HIF-2α has also been reported to function in partnership with other TFs such as USF (Pawlus et al., 2012) and SP1 (Koizume et al., 2012) at the same enhancer. HIF-α subunits might also have other HIF-β-like dimerization partners. For example, HIF-1α was shown to bind to *ARNT2*, a bHLH TF homologous to *ARNT1* with a selective expression in neurons (Drutel et al., 2000). On the other hand, HIF-1β is capable of binding to other class I bHLH proteins, most notably the AHR (*Aryl Hydrocarbon Receptor*), a TF induced by environmental stimuli (Swanson. 2002). HIF-1β is also reported to bind the neuronal PAS domain proteins, NPAS1 and NPAS3 (Wu et al., 2016). In addition, HIF-1β can homodimerise and transactivate on its own at the symmetrical CACGTG E-box element (Sogawa et al., 1995). A further possibility is of secondary changes in gene expression in response to non-canonical HIF pathways that have been proposed to regulate translation. For instance HIF-2α has been shown to mediate alternative translational initiation under hypoxia by recruiting eIF4E2 to mRNA via interaction with the RNA-binding protein RBM4 (Uniacke et al., 2012).

Taken together, these studies suggest that there are likely to be many aspects of gene expression that are regulated by hypoxia independently of HIF or through functions of HIF that are independent of its canonical action through the binding of DNA as an α/β heterodimer.

A number of studies have attempted to address this question using different technologies. Some studies have also attempted to distinguish direct from indirect responses to HIF and define HIF transcriptional targets. One early review reported that more than 70 genes had been validated as direct HIF targets in human cells using

functional evidence of a defined hypoxia response element (Wenger et al., 2005). However such studies are difficult at a pan-genomic level and are complicated by the observation that many HIF binding sites lie at large distances from the nearest promoter and appear to connect by long-distance chromatin looping (up to several hundred kb, Schödel et al., 2014; Grampp et al., 2016; Platt et al., 2016). Based on the presence or absence of an excess of HIF binding sites in the vicinity of promoters, it has been inferred that a substantial proportion of genes that are up-regulated by HIF are direct targets whereas much gene suppression by HIF is indirect.

Studies that simply measure changes in transcript abundance in response to hypoxia should identify responses that are both directly and indirectly mediated by HIF. Thus comparison of such transcript profiles in cells that are depleted for one or other component of the HIF pathway should define the numbers of genes that are directly or indirectly responsive to HIF and identify responses that are independent of HIF. For instance, microarray analysis of wild type (WT) and HIF-1α null murine fibroblasts has identified a number of hypoxia-induced genes that were regulated in a HIF-1α independent manner (Greijer et al., 2005). In addition, low levels of induction of several genes, including *VEGF*, *ANAXA-2*, and *LDHA*, were observed in HIF-1α -/- mouse embryonic stem cells (ESCs)(Hu et al., 2006). In these cases, the regulation may be mediated through HIF-2α. However, persistent regulation of gene expression was also observed in *ARNT* -/- ESCs (Hu et al., 2006). Assuming there are no other dimerisation partners for HIF-α subunits (see below), this suggests a potential for a completely HIF-independent mechanism. Comparison of gene expression in WT and HIF-1β mutant mouse hepatoma cells also found that some genes showed persistent hypoxia-regulated expression in the mutant cells (Wood et al., 1996). In other settings siRNA-mediated knockdown of HIF-α or HIF-1β subunits have defined the transcript networks that are

altered by HIF under hypoxia (Xia et al., 2009; Warnecke et al., 2008; Elvidge et al., 2006; Hu et al., 2003).

Taken together these studies have identified hundreds or even thousands of genes whose expression is regulated directly or indirectly by HIF. However incomplete inactivation of HIF using siRNA or recombinant methods that target only one component of HIF have made it difficult to assess the extent of HIF-independent activity. This question is important both in terms of understanding the basic physiology of cellular hypoxia and predicting the output of pharmaceutical approaches to modulation of the HIF pathway.

To address the problem I therefore sought to assess the contribution of the canonical HIF pathway to hypoxia-dependent gene expression, and to determine evidence for pathways that operate either through non-canonical actions of HIF or through entirely independent pathways. The development of efficient techniques for introducing targeted mutations to somatic cells by CRISPR/Cas9 technology (see **Materials and Methods**) enabled the targeting of different and even multiple components of the HIF pathway in the same cell background. I therefore combined this methodology with pan-genomic profiling of transcripts in WT and mutant cells that had been exposed to hypoxia or maintained in normoxia.

In the work described in this chapter, I aimed to answer the following questions:

1. To what extent is the HIF system is responsible for gene regulation under hypoxia?
2. Can HIF subunits regulate gene expression in a non-canonical fashion?
3. What is the extent of HIF-independent regulation of gene expression by hypoxia?

I aimed to address the above questions in two cellular contexts: HIF ‘off’ and HIF ‘on’ systems, each of which is inactivated for one or more components of the HIF-VHL

pathway. The laboratory had previously generated combined HIF-1α and HIF-2α double knockout HKC-8 cells (HIF-α DKO cells) using CRISPR/Cas9 technology. Separately I have made HIF-1β mutant cells (HIF-1β KO cells). Eliminating the expression of either the HIF-α or the HIF-1β subunits provides an opportunity to probe for the relative contributions of HIF-1α/2α or HIF-1β to the hypoxic responses, as well as an opportunity to investigate HIF-independent functions. The laboratory had also generated cells that are defective for both VHL and FIH (VHLFIH KO cells). In this setting, the HIF pathway is constitutively activated. Analysing the hypoxic gene expression profiles in these two quite different cellular settings (i.e. HIF 'off' versus HIF 'on') provided a powerful means to distinguish HIF-dependent and HIF-independent responses.

The laboratory already had RNA-seq data from HKC-8 WT and HIF-α DKO cells cultured under normoxia (21% O_2) and hypoxia (0.5% O_2) for 24h. I performed further RNA-seq experiments in HIF-1β KO cells and VHLFIH KO cells either exposed to hypoxia (0.5% O_2 or 0.1% O_2, respectively) or maintained in normoxia.

2.2 Results

2.2.1 Characterisation of mutant cell lines

2.2.1.1 Generation of HIF-1β mutant cells

HIF-1β KO cells were generated with a CRISPR/Cas9 double nickase approach (**Figure 1A**). Two pairs of guide RNAs (sgRNAs) that targeted the second exon of *ARNT* (HIF-1β gene) were designed according to the algorithms provided by the Zhang lab (http://crispr.mit.edu/). Full details of the construction of HIF-1β mutant cells can be found in the chapter of **Material and Methods**. The efficiency of the sgRNAs to mediate Cas9-dependent cleavage and introduction of insertion/deletions into *ARNT* exon 2 was first of all tested in HEK293T cells. A Surveyor nuclease digestion assay, which is an enzyme based mismatch cleavage assay to detect small insertions/deletions was used to screen the sgRNAs (**Figure 1B**). The pair of sgRNAs that was most successful at generating mutations in the HEK293T cells was chosen and transfected into the target HKC-8 WT cells.

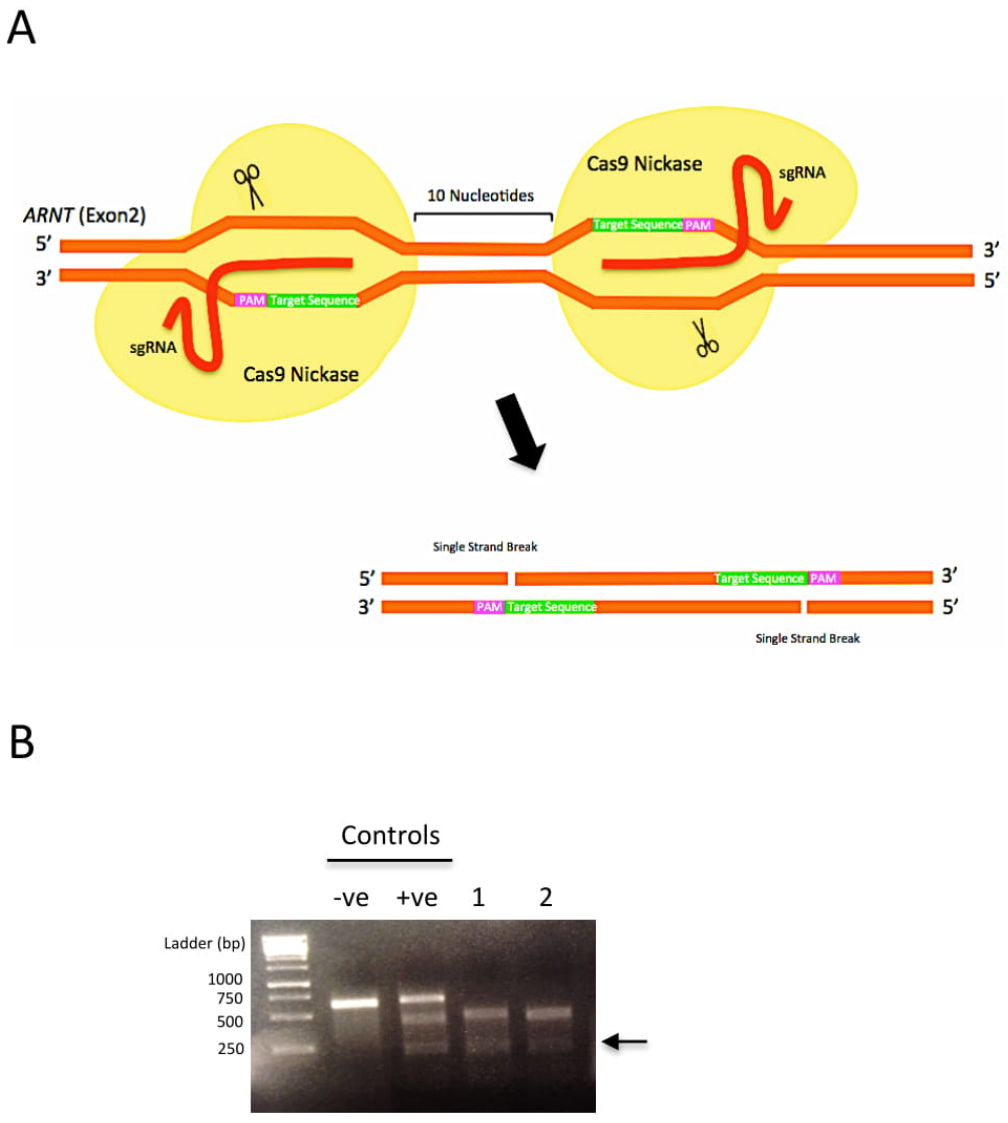

Figure 1. Generation of HIF-1β knockout cells. (A) A schematic of paired sgRNA targeting the *ARNT* (HIF-1β) gene using CRISPR/Cas9 double nickase approach. (B) Agarose gel showing the efficiency of two pairs of sgRNAs tested in HEK293T cells, using the Surveyor nuclease digestion assay as a readout. The cleaved products indicate the presence of a heteroduplex formed by a mismatch. Genomic DNA of cells transfected with different pairs of sgRNAs was extracted. A PCR product encompassing the CRISPR targeted region was amplified using specific primers. DNA products were imaged by BioRad Imaging System. Standard controls were obtained from the kit, which represent either homoduplex (negative controls, G plasmid DNA) or heteroduplex (positive control, G+C plasmid DNA). Lane 1 and 2 cleavage products were observed in the cells transfected with two different pairs of sgRNAs. Pair 1 sgRNAs were then chosen for transfecting the target HKC-8 WT cells.

HKC-8 clones were then screened by both genomic PCR (for insertions/deletions at the targeted locus) and by immunoblot (to screen for loss of HIF-1β protein). One particular clone was taken forward for more detailed characterisation. In order to verify mutation at the genomic level in the HKC-8 HIF-1β KO clone, sgRNA targeted regions from the WT and HIF-1β mutant cells were amplified by genomic PCR using two pairs of primers (P1 and P2). With both pairs of primers, smaller PCR products were observed in the HIF-1β mutant cells than in the WT cells, indicating deletions at *ARNT* exon 2 in these mutant cells (**Figure 2A**). To resolve the exact mutation on each allele in the knockout cells, the genomic DNA product from the region amplified by primer set P1 was cloned into a pcDNA3 vector and following transformation of the plasmid into bacteria, DNA from individual colonies was then sequenced. Overall from the ten colonies screened, there were six with an 11 nucleotide (nt) deletion, two with a 23 nt deletion, one clone with a 38 nt deletion and one clone with a mixed sequence that could not be interpreted (**Figure 2B, left panel**). Each of these deletions was expected to introduce a frame shift in the *ARNT* gene, and consequently a premature termination and loss of HIF-1β protein (**Figure 2B, right panel**). Loss of HIF-1β protein function was next confirmed by a ChIP-qPCR experiment (**Figure 2C**). The hypoxic DNA-binding signal for both HIF-2α and HIF-1β at the HIF HRE sites (*NDRG1* and *EGLN3*) was absent in the HIF-1β mutant cells. Overall, these results confirmed the loss of both HIF-1β protein and DNA-binding function.

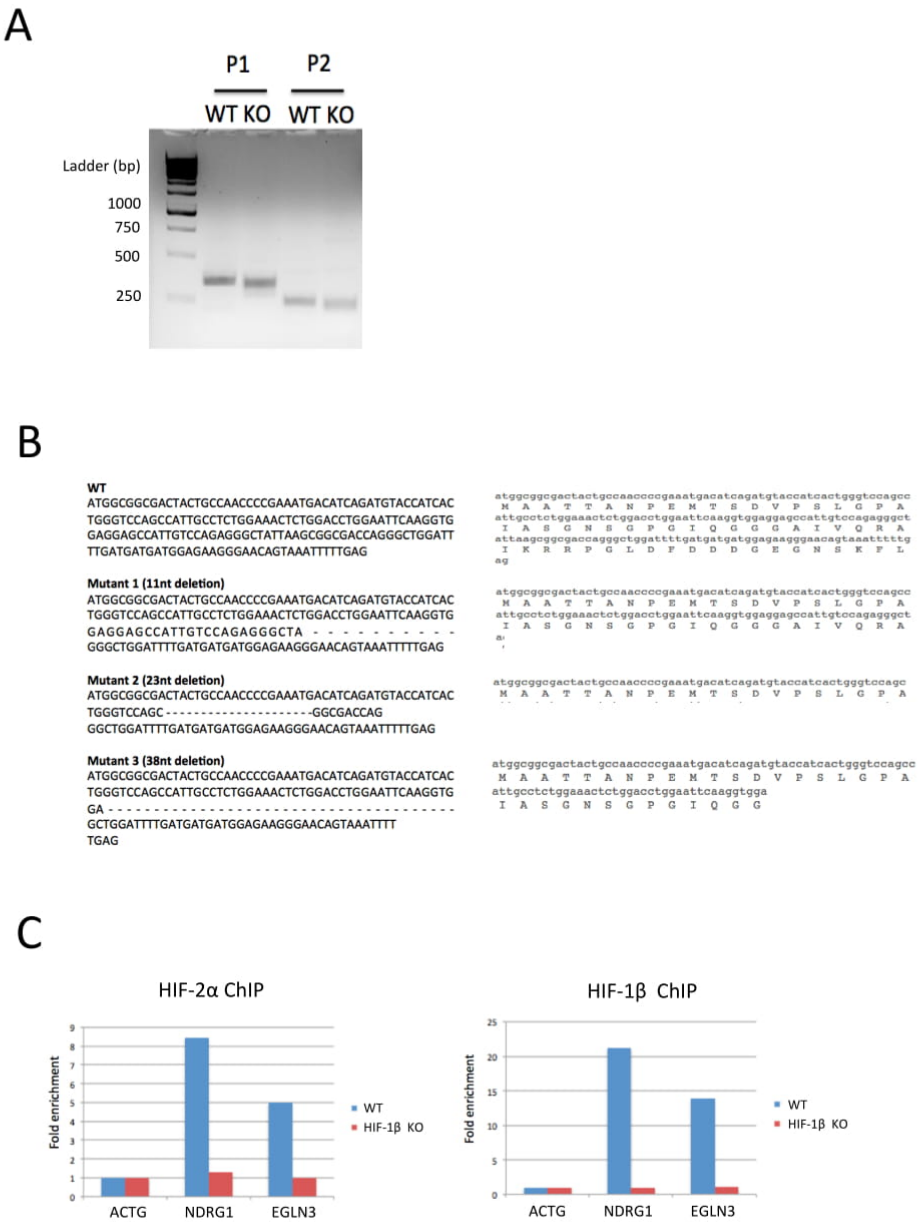

Figure 2. Characterisation of HKC-8 HIF-1β knockout cells. (A) Genomic PCR products of the CRISPR targeted region, using the purified genomic DNA from either the WT or HIF-1β mutant cells. The CRISPR targeted region was amplified with two pairs of primers (P1 and P2) to give a product of 446 bp and 246 bp respectively. With both primers, small mobility shifts were observed in the knockout cells, indicating deletions in the targeted region. (B) The PCR products generated with primer pair 1 (P1) from WT and mutant cells were cloned into a pcDNA3 vector and subjected for sequencing. Three different types of mutations were detected after screening ten clones (left panel), indicating at least 3 alleles for HIF-1β in this clone. The expected effects on the HIF-1β protein are shown on the right panel. (C) ChIP experiment of HKC-8 WT cells and HIF-1β mutant cells exposed to either normoxia (21% O_2) or hypoxia (0.5% O_2) for 16h, using anti- HIF-2α or anti- HIF-1β antibodies. Primers spanning NDRG1 and EGLN3 HRE sites, and a negative control site, ACTG, were used for qPCR analysis. The fold enrichment of each locus in normoxia and hypoxia was normalised to the values for ACTG using the delta-delta CT method. n=1 replicate was performed.

The transactivation function of HIF requires a heterodimerisation of the HIF-α and HIF-1β subunit (Jiang et al., 1996). Therefore to assess whether the loss of HIF-1β protein would have any effects on the HIF-α protein level, immunoblots of HIF-1α and HIF-2α were performed (**Figure 3A**). Interestingly, an increased level of HIF-1α protein was observed in the hypoxic HIF-1β KO cells than in the hypoxic WT cells, whereas the hypoxia-induced HIF-2α protein levels were similar in both cell types. To further assess whether the loss of HIF-1β protein would also affect the localisation of HIF-α protein, immunoblots of HIF-1α and HIF-2α were performed using the extracts from different fractions of WT and HIF-1β KO cells (**Figure 3B**). After exposure to normoxia (21% O_2) or hypoxia (0.5% O_2 for either 16h or 24h), cells were separated into cytoplasmic, nucleoplasmic and chromatin fractions prior to immunoblotting. Total HIF-1α/2α protein was observed in the whole cell extracts of both WT and HIF-1β KO cells following hypoxic exposure and the fractionation experiments indicated that this protein was chromatin-associated in both cell types. In the WT cells, the HIF-1α protein level decreased after 24h of hypoxia exposure. However, this decrease in HIF-1α protein was not observed in the HIF-1β KO cells. In addition, for both HIF-1α and HIF-2α proteins a slightly higher proportion of the protein was present in the nucleoplasm of HIF-1β KO cells at both 16h and 24h of hypoxia as compared with hypoxic WT cells (**Figure 3B**).

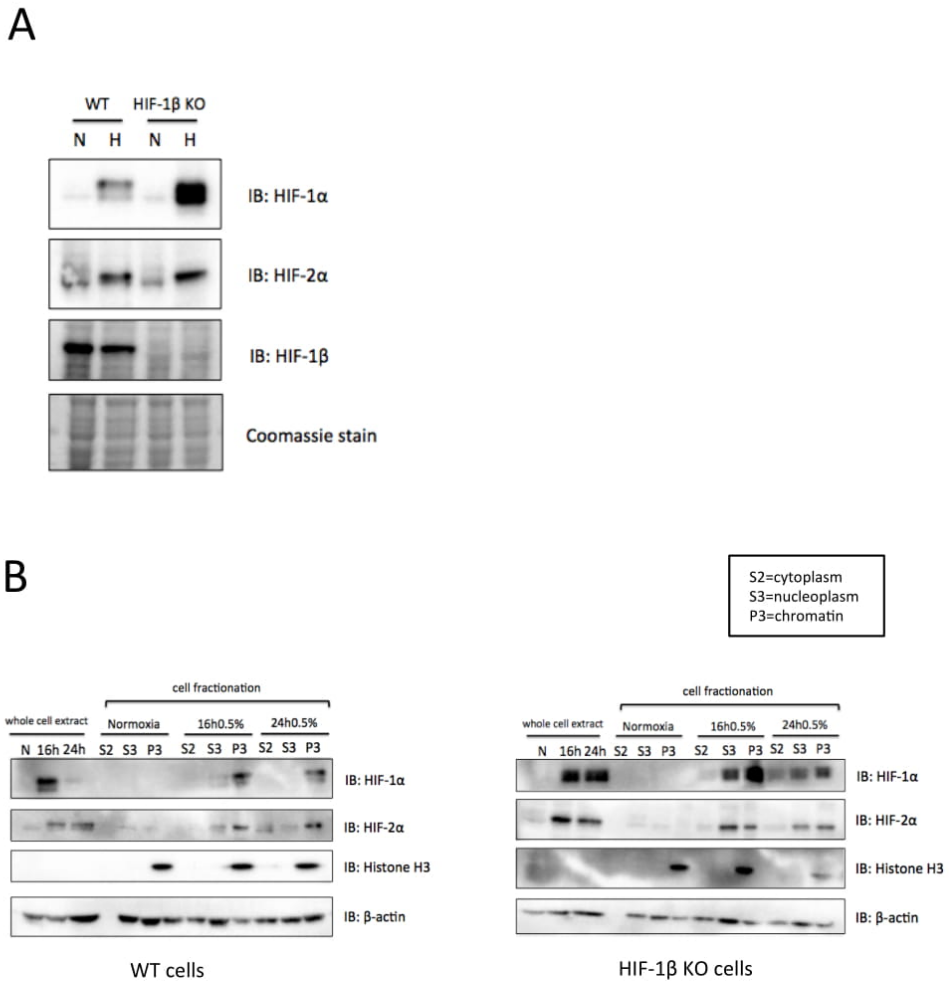

Figure 3. Examination of HIF-α protein level and subcellular localisation in HIF-1β mutant cells. (A) Immunoblot of HIF-α and HIF-1β proteins using the whole cell extracts from the WT and a clone of HIF-1β deficient cells cultured under normoxia (21% O_2) and hypoxia (0.5% O_2) for 24h. (B) Cell fractionation followed by immunoblotting of WT and HIF-1β mutant cells exposed to either normoxia or hypoxia (16h or 24h). Hypoxia induced expression of HIF-1α and HIF-2α proteins was observed in the chromatin fraction (P3) of both WT and HIF-1β KO cells, and in the whole cell extracts that were harvested in parallel. In addition, there were a significant proportion of HIF-1α and HIF-2α proteins in the nucleoplasm fraction of the hypoxic HIF-1β mutant cells but not in the WT cells. Histone H3 protein was used as a control for chromatin fraction. β-actin was used as a loading control.

2.2.1.2 Characterisation of HIF target gene expression in HIF mutant cells

To confirm the loss of HIF-α or HIF-1β proteins in the respective HIF mutant cells, immunoblots of HIF-1α/2α and HIF-1β protein were performed in the WT and HIF mutant cells that were exposed to normoxia (21% O_2) or hypoxia (0.5% O_2) for 24h. The result confirmed the loss of both HIF-1α and HIF-2α in the HIF-α DKO cells, and the loss of HIF-1β protein in the HIF-1β mutant cells (**Figure 4A**). Next, the functional consequences following the loss of HIF protein was characterised by assessing the expression levels of HIF target genes (*CA9* and *BNIP3*) under hypoxia in real time quantitative PCR (RT-qPCR) assays. In the WT cells that were cultured under 0.5% O_2 for 24h, strong induction of both genes was observed (29.8-fold for *CA9* and 2.3-fold for *BNIP3*). By contrast, the hypoxic induction of these genes was lost in both HIF-1β KO and HIF-α KO cells, although interestingly, there was some residual low level induction of both genes in the hypoxic HIF-1β mutant cells (2.3-fold for *CA9* and 1.4-fold for *BNIP3*) but not in the HIF-α mutant cells (1.0-fold for *CA9* and 0.8-fold for *BNIP3*) (**Figure 4B**).

In a separate approach to confirm the loss of function of HIF-α and HIF-1β proteins in these mutant cells, luciferase reporters containing either a minimal SV40 promoter, or a minimal promoter in combination with HIF HREs (either a *CA9* HRE promoter sequence, or a concatamerised HRE sequence of *PGK1* gene), were transiently transfected in the WT, HIF-1β KO and HIF-α DKO cells (**Figure 4C and D**). In the control WT cells, the reporter with the SV40 promoter showed no induction under normoxia or hypoxia. By contrast, both constructs of HIF HRE-reporters showed very low levels of activity under normoxia but were strongly induced under hypoxia (21-fold and 39-fold respectively in **Figure 4C**, 22-fold and 53-fold in **Figure 4D**). In the HIF-α and HIF-1β mutant cells, the hypoxic induction of these HIF HRE-luciferase reporters

was absent. This suggested that these mutant cells could not form a functional HIF transcriptional complex to activate gene expression under hypoxia. In addition, the data also suggested that there were no other proteins in these HIF mutant cells that were capable of binding and activating gene expression at the HREs (at least at these two representative HRE sequences).

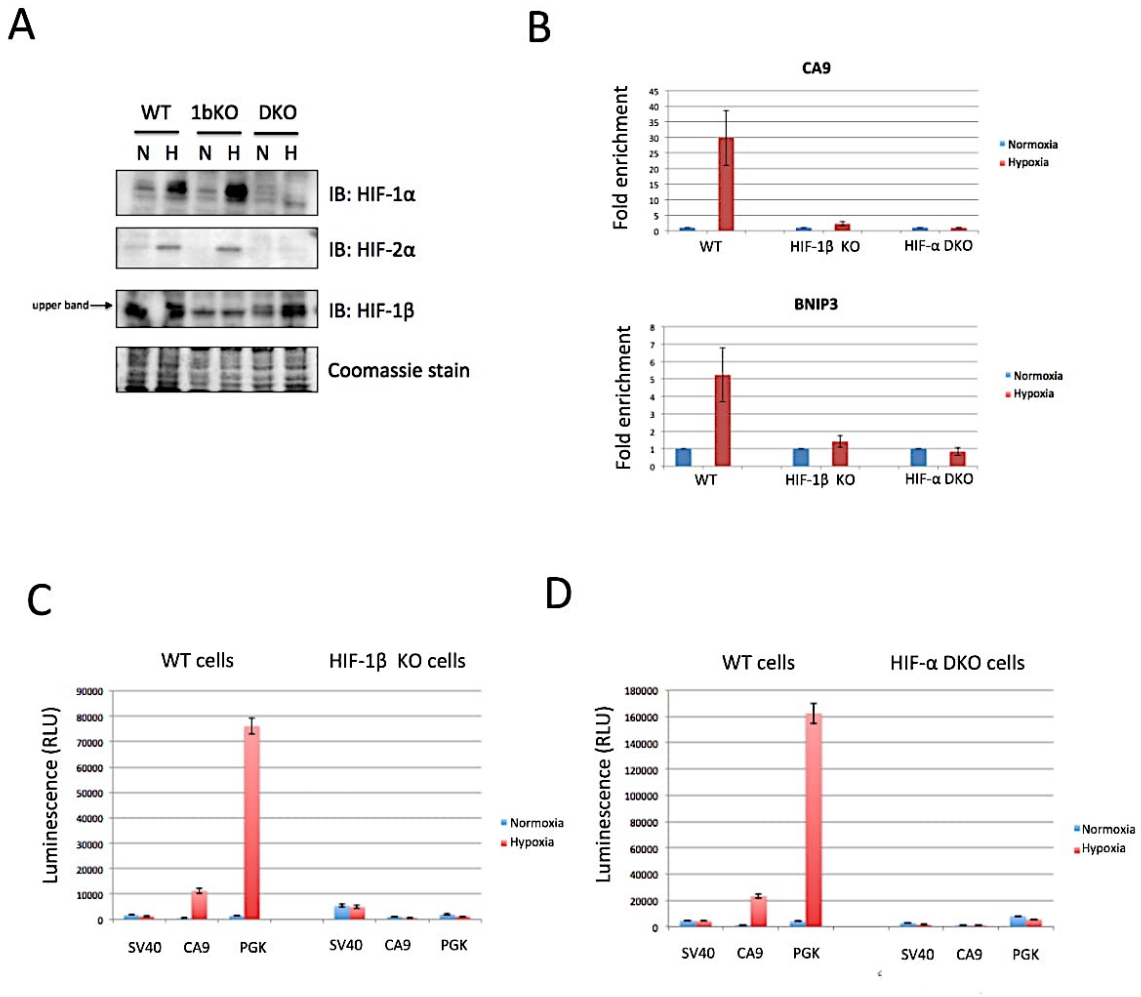

Figure 4. Loss of expression and gene activation function of HIF-α and HIF-1β proteins in the respective HIF mutant cells. (A) Immunoblot of HIF-α and HIF-1β using the whole cell extracts from the WT, HIF-1β KO or HIF-α DKO cells that were cultured under normoxia (21% O_2) or hypoxia (0.5% O_2) for 24h. (B) Expression levels of HIF target genes (*CA9* and *BNIP3*) were measured under normoxia or hypoxia (0.5% O_2 for 24h) in RT-qPCR assays. Strong induction of both genes was observed in the hypoxic WT cells. The levels were significantly reduced in the hypoxic HIF-1β KO cells, and were barely detectable in the HIF-α DKO cells. The fold enrichment of each gene was normalised to the values for the housekeeping gene *HPRT* using the delta-delta CT method. Bar shows mean ± s.d. n=4 replicates were performed. (C) Luciferase reporter assay comparing the transient expression levels of SV40 control, *CA9* HRE or *PGK* HRE-reporter in the WT cells or HIF-1β KO cells. The cells were cultured under normoxia (21% O_2) or hypoxia (0.5% O_2) for 24h. Bar shows mean ± s.d. n=3 replicates were performed. (D) The same reporters were tested in the HIF-α DKO cells. SV40, minimal promoter sequence. CA9, 5' flanking sequence of *CA9* gene. PGK, 6 copies of PGK1 gene with a TK promoter.

2.2.1.3 Characterisation of VHLFIH mutant cells

Constitutive expression of HIF-1α/2α proteins was observed in the VHLFIH KO cells and the parental VHL KO cells under normoxia (21% O_2) and hypoxia (0.5% O_2) for 24h,

indicating the loss of function of pVHL and of the HIF prolyl hydroxylation/degradation pathway (**Figure 5A**). Further immunoblots confirmed the loss of FIH protein in the VHLFIH KO cells. The levels of both HIF-1α/2α proteins were similar in the VHLFIH KO and VHL KO cells. This suggests that loss of FIH did not affect the total HIF-α protein level, at least under these conditions.

Hydroxylation of the HIF-1α protein was also examined using the specific antibodies that recognised either hydroxylated asparaginyl (N803) or prolyl (P564) residue. An absence of hydroxylated HIF-1α protein at the N803 in the normoxic and hypoxic VHLFIH KO cells further confirmed the loss of function of FIH protein. HIF-1α protein with hydroxylated P564 was clearly observed in the normoxic VHL KO cells, but was largely absent in the hypoxic cells, indicating inhibition of the PHD enzymes at 0.5% O_2 (**Figure 5A**). Interestingly, the prolyl hydroxylated HIF-1α proteins observed in the VHLFIH KO cells that were cultured under normoxia were also clearly observed following hypoxia (**Figure 5A and 5B**). This indicated that the loss of FIH might have altered the HIF prolyl hydroxylation capacity of the cells. Since it was possible that changes in the prolyl hydroxylation of HIF might affect activity of HIF (particular the internal transactivation domain that contains P564), I used a more severe level of hypoxia (i.e. 0.1% O_2 for 24h) that supressed hydroxylation effectively at this site (**Figure 5C**).

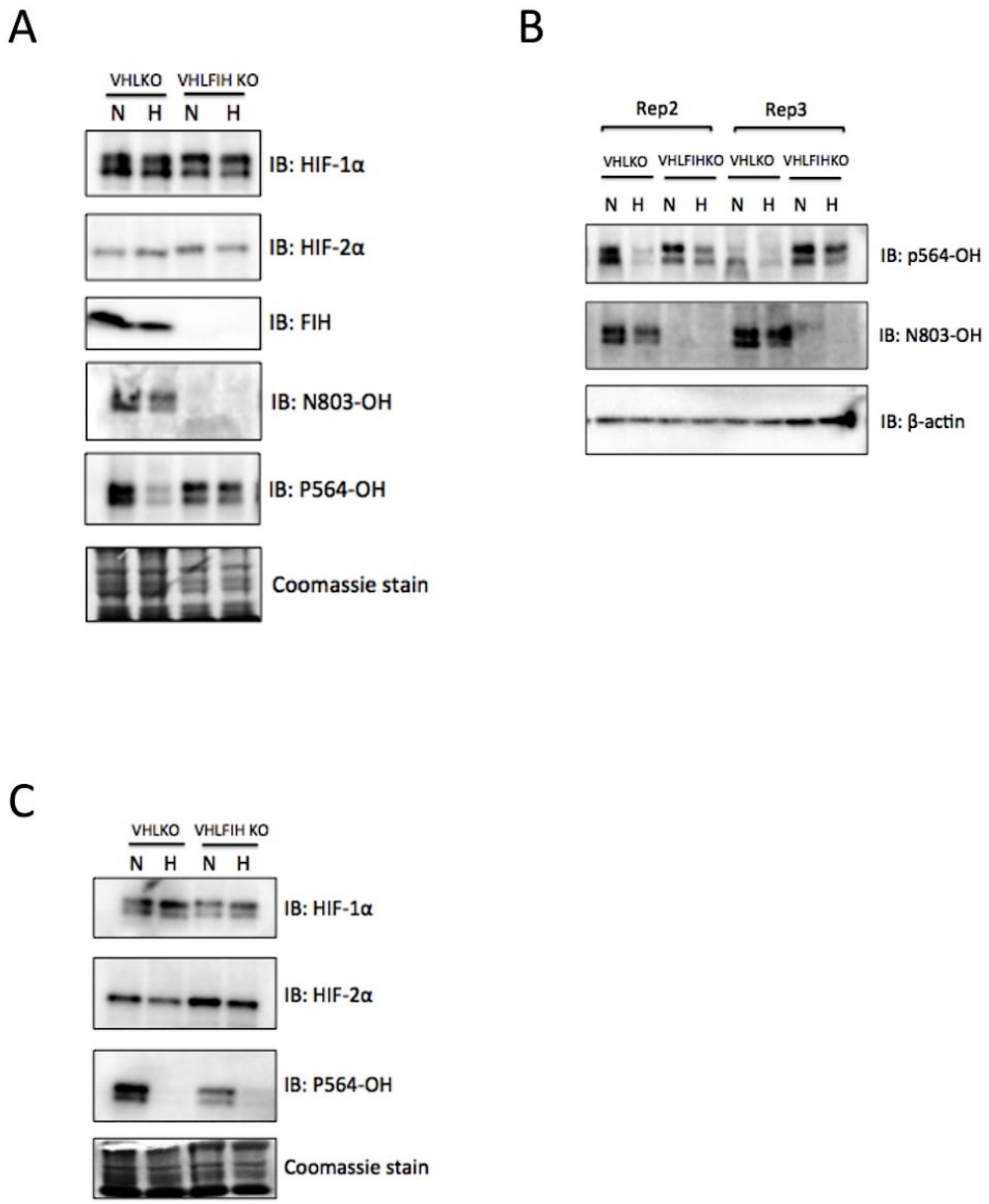

Figure 5. Characterisation of VHLFIH KO cells. (A) Constitutive expression of both HIF-1α and HIF-2α proteins was observed in the VHLFIH KO cells and its parental VHL KO cells that were cultured under normoxia (21% O_2) or hypoxia (0.5% O_2) for 24h. Immunoblots of FIH protein in the VHLFIH KO cells confirmed the ablation of FIH protein in these cells. An absence of hydroxylated HIF-1α at asparagine residue (N803) in the same extracts further confirmed the loss of function of FIH protein. However, increased hydroxylation of HIF-1α at prolyl residue (P564) was detected in the hypoxic VHLFIH KO cells, indicating PHD enzymes were more active at 0.5% O_2. (B) Another two independent replicates of immunoblot experiments. Cells were cultured under normoxia (21% O_2) or hypoxia (0.5% O_2) for 24h. Again P564 hydroxylation of HIF-1α was observed in the hypoxic VHLFIH KO cells. (C) Cells were cultured under a more severe hypoxia condition, i.e. 0.1% O_2 for 24h. Again, constitutive expression of HIF-1α and HIF-2α proteins was observed in both mutant cell lines. No prolyl hydroxylation was observed in the hypoxic VHL KO or VHLFIH KO cells, suggesting the activity of PHD enzymes was inhibited in both cell lines at 0.1% O_2. N refers to normoxia. H refers to hypoxia.

2.2.2 RNA-seq experiments

In order to examine the contribution of the HIF pathway to hypoxia-dependent gene expression, and to probe for any potential HIF-independent but hypoxia-dependent genes, a series of RNA-seq experiments was then performed in the HKC-8 WT cells and in the various mutant cells with either the HIF system switched off or having a constitutive HIF transcription activity (**Table 2.1**).

Table 2.1 RNA-seq datasets in this chapter

cell line	HIF status	condition	reps
HKC-8 HIF-1β KO	Off	21% O_2 vs 0.5% O_2 (24h)	2
HKC-8 VHLFIH KO	On	21% O_2 vs 0.1% O_2 (24h)	2
Existing RNA-seq data in the laboratory			
HKC-8 wild type (WT)		21% O_2 vs 0.5% O_2 (24h)	2
HKC-8 HIF-1α/2α double KO	Off	21% O_2 vs 0.5% O_2 (24h)	2

To verify the status of the cells from which material was prepared for transcript profiling by RNA-seq, protein extracts were prepared in parallel. Immunoblots of HIF-1β in the HIF-1β KO cells confirmed the absence of HIF-1β in the samples from both RNA-seq replicates (**Supplementary Figure 1A**). Again, an increased level of HIF-1α (but not HIF-2α) protein was observed in the hypoxic (0.5% O_2) HIF-1β KO cells compared with that in the hypoxic WT cells. In the VHLFIH KO cells, immunoblots of FIH indicated the loss of FIH protein in these cells. In addition, a constitutive expression of both HIF-1α and HIF-2α was observed (**Supplementary Figure 1B**) consistent with the loss of pVHL. Finally, a lack of hydroxylation of HIF-1α at both proline and asparagine residues in the VHLFIH KO cells under hypoxia (0.1% O_2) was confirmed.

2.2.3 Definition of hypoxia-regulated genes

Following the RNA-seq experiments, the subsequent bioinformatic analysis of the data to identify hypoxia-dependent gene expression within each WT and knockout cell genotype

was undertaken as shown in **Figure 6.** Full details can be found in the chapter of **Material and Methods**.

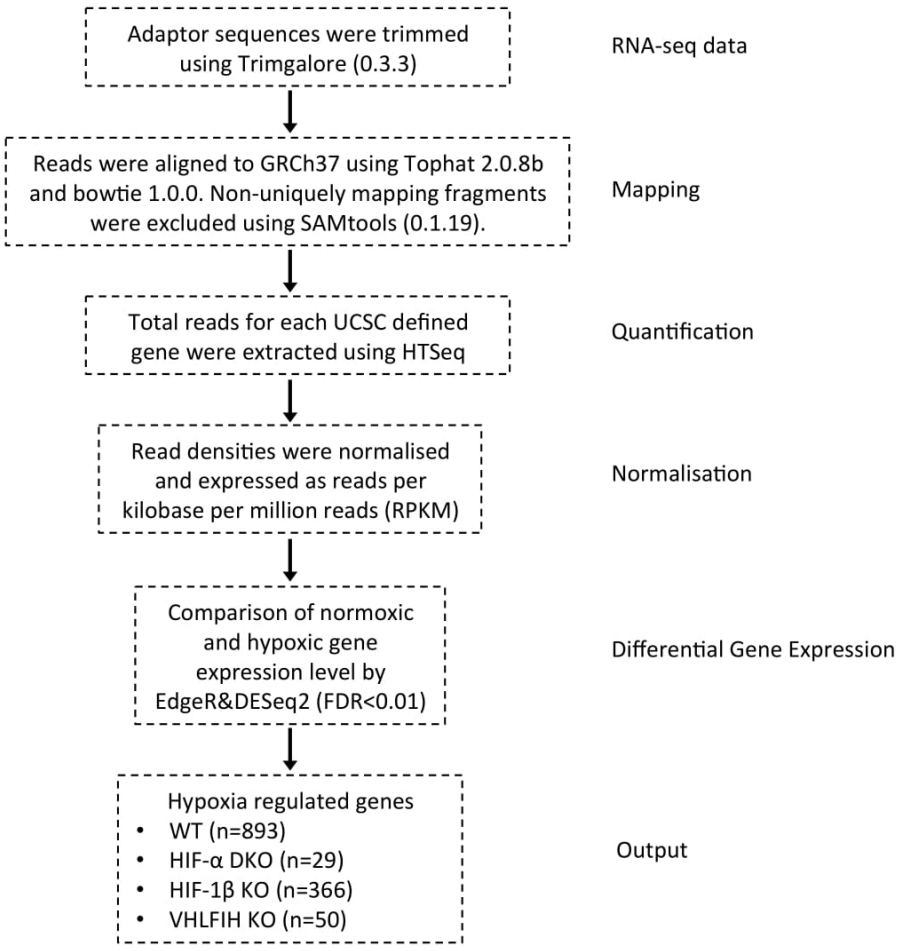

Figure 6. Workflow for RNA-seq analysis

A comparison of the normoxic and hypoxic gene expression in the WT cells detected 893 transcripts that showed statistically significant hypoxia-dependent regulation (FDR<0.01). Similarly, there were 366 transcripts in the HIF-1β KO cells, 29 in the HIF-α DKO cells and 50 in the VHLFIH KO cells that were regulated by hypoxia (**Figure 6**). The difference in expression levels between normoxia and hypoxia across all genotypes ranged from 0.22-fold to 28.6-fold, as determined by EdgeR and DESeq2 analyses.

2.2.4 Analysis of hypoxia-dependent gene expression in the WT versus mutant cells

Having established the changes in gene expression induced by hypoxia across all cellular backgrounds, I wished to examine the extent of involvement of the HIF pathway in the hypoxic gene expression response. Hypoxia-regulated genes were first of all examined in the WT cell background. The genes were separated into hypoxia up-regulated (n=536) and down-regulated genes (n=357). Full lists of genes are shown in Appendix 8.1 and 8.2. The Log_2 fold change in expression for the genes identified as significantly up-regulated (**Figure 7A**) or down-regulated (**Figure 8A**) by hypoxia in WT cells was shown in the box plots for each of the genotypes (WT, HIF-α DKO, HIF-1β KO and VHLFIH KO cells). In comparison with the expression level in the WT cells, the level of both hypoxia up- and down-regulated genes showed a significant decrease in the three mutant cell lines. Both the number of genes and the amplitude of their regulation was reduced indicating that loss of either HIF subunit or constitutive activation of the HIF pathway greatly reduced the hypoxia response. Thus, canonical HIF function (i.e. HIF-α and HIF-1β) and the presence of VHL/FIH were required for the majority of changes in gene expression under hypoxia.

To further dissect this observation at the level of individual genes, the hypoxia-dependent fold change in expression of each up-regulated gene was compared between WT cells and each of the mutant cell backgrounds (**Figure 7B**). The R-squared values describe the correlation observed in each pairwise analysis. This revealed that there was essentially no correlation between hypoxia induced gene expression in HIF-α DKO and WT or between VHLFIH KO cells and WT (R_2=0.06 in both backgrounds). However, there was some correlation between hypoxia-dependent regulation in the HIF-1β KO cells (R_2=0.39).

Taken together these results indicate that hypoxia induced expression of the majority of the genes was greatly impaired in cells with a lack of HIF-α or cells with a constitutively active HIF pathway. Many more genes in the HIF-1β mutant cells showed hypoxia inducible gene expression than in the other mutant background and these genes showed modest correlation with the amplitude of regulation in the WT cells. Although in all mutant cells, hypoxia inducible gene expression was much reduced there were examples of genes that were significantly regulated by hypoxia in each mutant background.

A similar analysis was performed for the hypoxia down-regulated genes as defined in the WT background (**Figure 8B**). Again the extent of down-regulation amongst these genes was greatly reduced in all of the mutants and in some cases genes that were down-regulated in WT cells were even up-regulated in some of the mutant cells. No correlation of hypoxia dependent regulation was observed in the HIF-1β KO cells (R_2=0.07) and in the VHLFIH KO cells (R_2=0.04) when compared with that in the WT cells. However there was a modest correlation between genes that were down-regulated by hypoxia in HIF-α DKO cells and WT cells (R_2=0.28).

Overall, these results revealed that hypoxia-dependent regulation of the majority of genes is dependent on HIF and requires the presence of both HIF-α and HIF-1β subunits. Since hypoxia-dependent gene expression was observed in each of HIF-α HIF-1β mutant cells and VHL/FIH mutant cells, it was hypothesised there might also be HIF-independent mechanisms of regulation and/or non-canonical HIF dependent regulation.

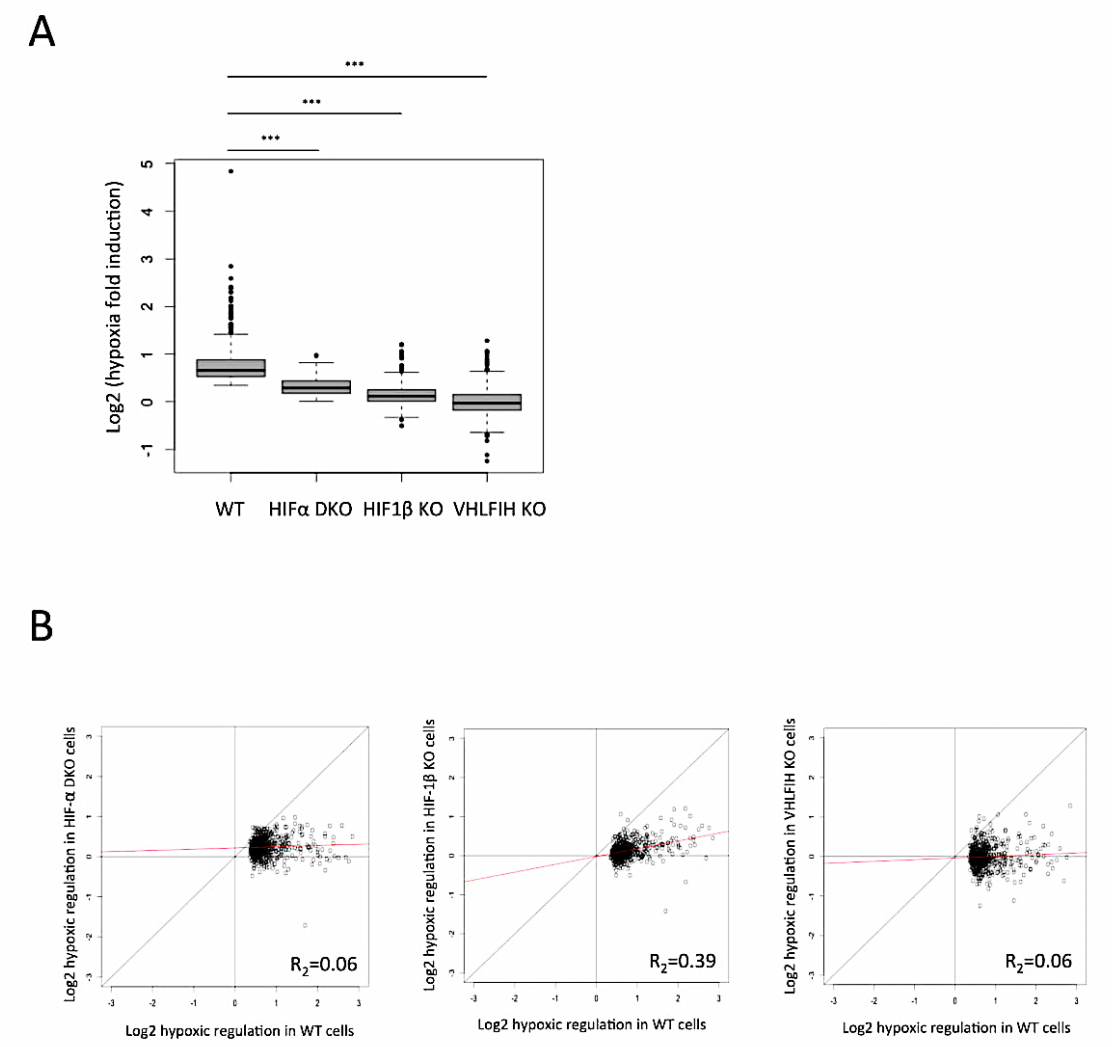

Figure 7. Comparing the amplitude of hypoxia-dependent regulation (Log2 fold changes) across multiple cellular backgrounds using the hypoxia up-regulated genes that were identified in the WT cells (n=536). (A) Box plot representing the total hypoxic regulation of these genes across all four cellular backgrounds. (B) Scatter plots comparing the amplitude of hypoxia-dependent regulation of individual genes in the WT cells with that in each of the mutant cell backgrounds on a Log2 scale. The correlation is shown by the regression line (highlighted in red) and by the R-squared value. *** indicates *p*-values ≤ 0.001.

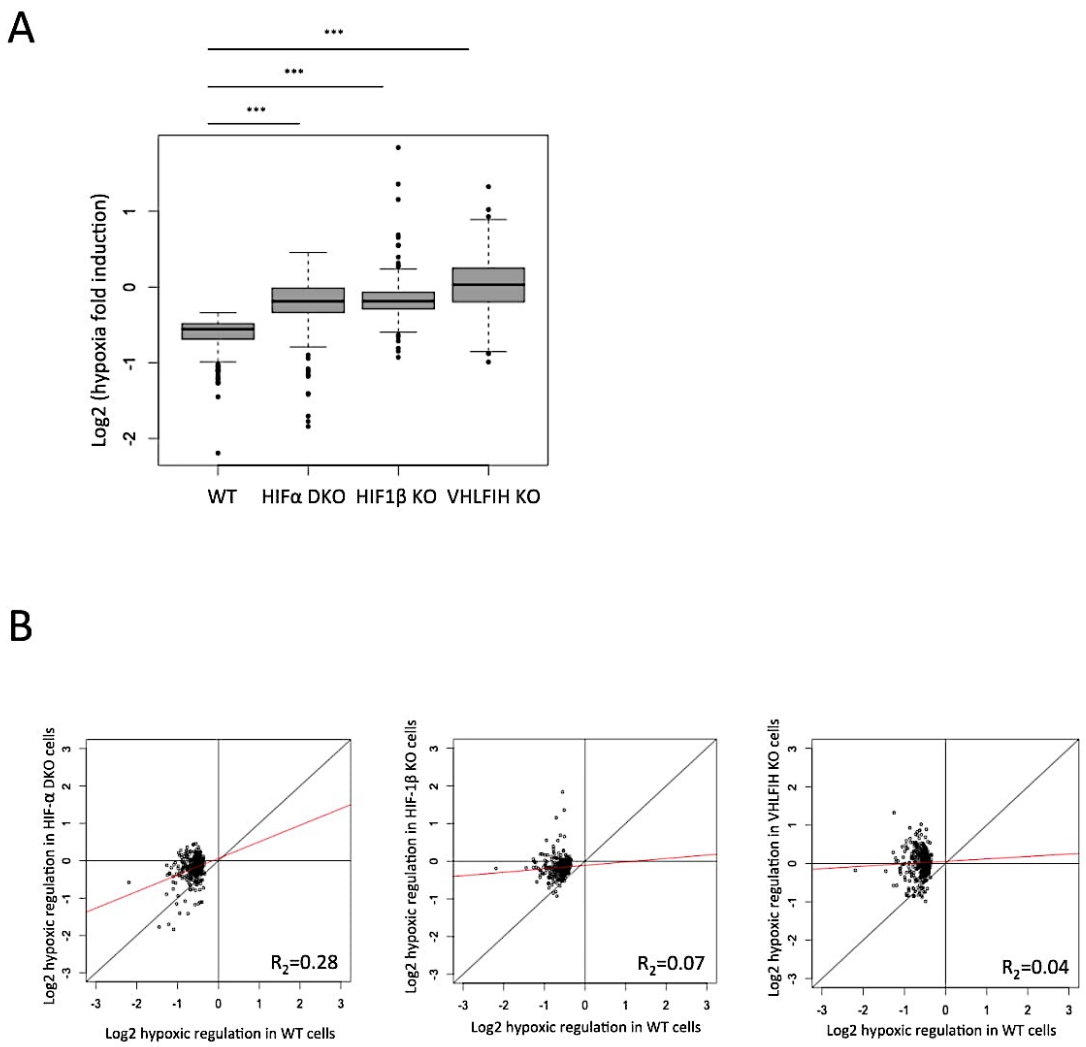

Figure 8. Comparing the amplitude of hypoxia-dependent regulation (Log2 fold changes) across multiple cellular backgrounds using the hypoxia down-regulated genes that were identified in the WT cells (n=357). (A) Box plot representing the total hypoxic regulation of these genes across all four cellular backgrounds. (B) Scatter plots comparing the amplitude of hypoxia-dependent regulation of individual genes in the WT cells with that in each of the mutant cell backgrounds on a Log2 scale. The correlation is shown by the regression line (highlighted in red) and by the R-squared value. *** indicates *p*-values ≤ 0.001.

2.2.5 Analyses probing for HIF-independent but hypoxia-dependent gene expression

Having shown that there were some genes with persistent hypoxia-dependent regulation in the mutant cells, I next sought to assess candidates for HIF-independent, but hypoxia-dependent regulation. It was argued that a pathway that was operating wholly independently of HIF ought to do so across all of the cell backgrounds, and be reflected in genes that continued to be regulated by hypoxia to a similar degree across all the cells tested. On the other hand genes that were apparently regulated in one cell background but not the others might present a non-canonical function of the components of the pathway that remained intact in those cells, or simply represent random variation or noise in a given dataset. Several different analytical methods were applied that aimed to distinguish these possibilities.

Firstly, a stringent statistical analysis was performed using the transcripts that appeared in the WT, HIF-α DKO and HIF-1β KO cells (**Figure 9A left panel**). If a gene is truly HIF-independent, its RNA level in hypoxia (and in normoxia) should not be affected by HIF status. Therefore, the analysis grouped all the hypoxic RNA-seq data from WT and mutant cells to define the transcripts with the smallest variance in read counts (FDR<0.01), which might therefore be considered to be independent of HIF. A similar grouping analysis was performed with all of the normoxic RNA-seq data. Genes that were selected by these criteria, but which showed statistically significant regulation by hypoxia (FDR<0.01) were then defined as hypoxia-regulated HIF-independent genes. Overall, there was only 1 gene, *LOC100506548* (an uncharacterised non-coding RNA), that fulfilled this stringent definition of a completely HIF-independent gene (**Figure 9A right panel**).

In the second method, a qualitative analysis was performed to compare the overlap of hypoxia-regulated genes that were defined in each of the WT and the HIF

mutant cells (**Figure 9B left panel**). The Venn diagram showed that only one candidate, *TXNIP* (Thioredoxin Interacting Protein) was regulated by hypoxia in all three cellular backgrounds. However, this gene was actually up-regulated by hypoxia in the WT cells but down-regulated in both HIF mutant cells (**Figure 9B right panel**). This discordant regulation by hypoxia across the multiple cell types indicated that differences in expression were unlikely to be related to hypoxia itself and therefore that *TXNIP* is not in fact a genuine hypoxia-regulated HIF-independent transcript.

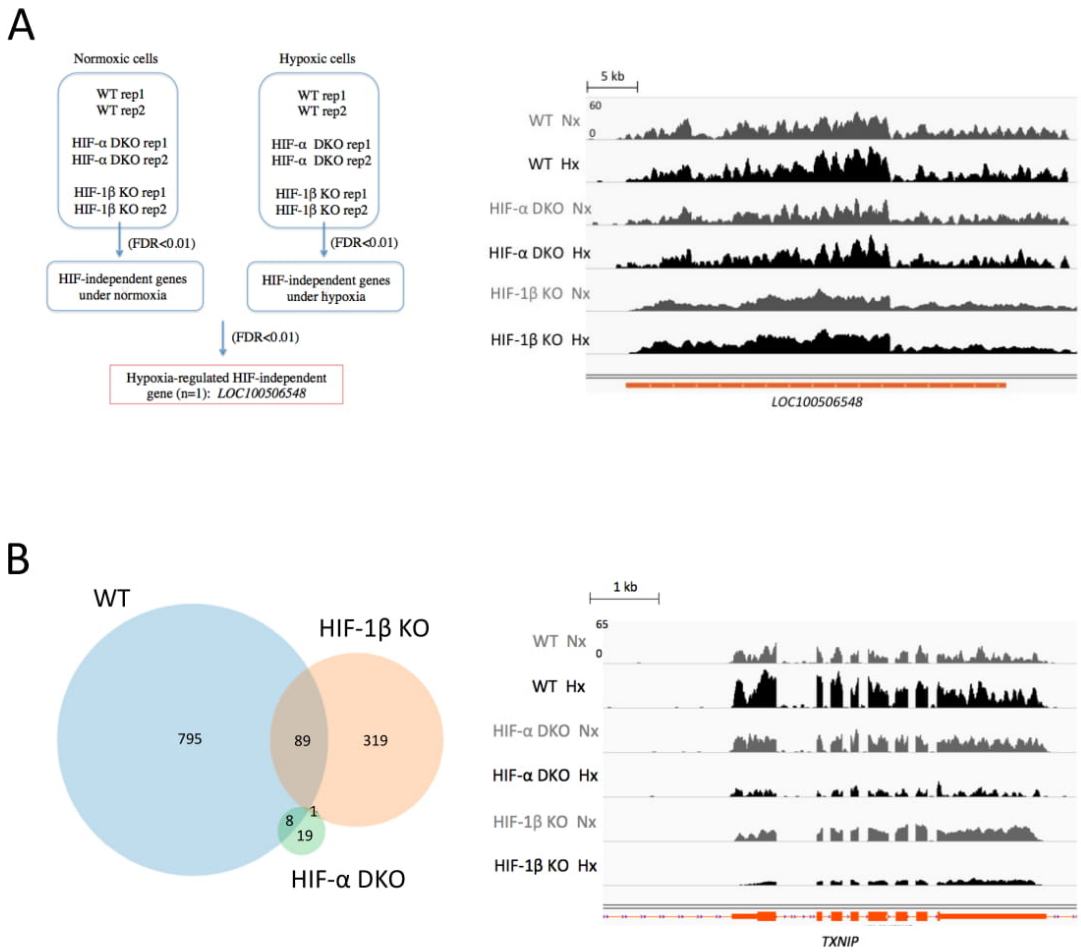

Figure 9. Quantitative and qualitative approaches used to probe for HIF-independent genes. (A) Statistical analysis comparing the genes with the least variance in read counts between all six normoxic RNA-seq samples, versus the genes with the least variance in read counts between all six hypoxic samples. This method identified one candidate HIF-independent gene (*LOC100506548*) that was significantly regulated by hypoxia. The RNA-seq tracks for this gene as seen on the Integrative Genomics Viewers (IGV) was shown on the right panel. (B) Venn diagram comparing hypoxia regulated genes defined in the WT, HIF-1β KO, and HIF-α DKO cell backgrounds. One candidate gene, *TXNIP*, showed persistent hypoxia regulation in all three cellular backgrounds. However, the hypoxia regulation of this gene was inconsistent, i.e. it was up-regulated by hypoxia in the WT cells, but appeared to be down-regulated in the HIF mutant cells. An IGV track image of the RNA-seq data at this locus is shown on the right. This indicated that this candidate was not a genuine HIF-independent gene. *LOC100506548* refers to an uncharacterised long non-coding RNA. *TXNIP* refers to Thioredoxin Interacting Protein.

The above quantitative and qualitative analyses were also performed with an incorporation of hypoxia-regulated genes defined in the VHLFIH KO cells. In these analyses, activation of HIF in normoxia would be predicted to exclude genes that were regulated by HIF from appearing in the low variance group, whereas in hypoxia, HIF

target genes might be predicted to show little variance across WT and VHLFIH KO cells. Again, no candidate HIF-independent genes were identified. Taken together, these analyses did not support the existence of a statistically significant prevalence of HIF-independent hypoxia inducible genes, under the conditions examined.

Given the importance of the question, and the possibility that the hypoxia-dependent regulation of HIF-independent genes might be infrequent or low in amplitude and may therefore have been missed by these stringent statistical thresholds, several other analyses were performed on the data.

Following the argument that truly HIF-independent regulation by hypoxia should be present in all cells including the WT cells, these analyses were performed on genes whose regulation by hypoxia was defined as significant in WT cells. To avoid falsely identifying genes that are regulated in different directions by hypoxia, analyses were performed separately on genes that were up-regulated or down-regulated by hypoxia in the WT cells. Analyses were then performed to compare the amplitude of regulation by hypoxia in WT and mutant cells. If such genes were regulated independently of HIF, then I argued that they should display similar regulation by hypoxia in the mutant cells lines. On the other hand, if regulation by hypoxia in the mutant cells was due to incomplete activation of HIF, or the persistence of non-canonical oxygen-dependent functions, then a correlation between regulation by hypoxia in the WT cells and mutant cells might be expected.

To assess this, a frequency plot was first used to examine the relative amplitude (fold change, FC) of regulation in the WT versus that in each mutant cell background. The x-axis represents the ratio of these amplitudes (i.e. the ratio of hypoxia-dependent regulation (as fold change) in the WT to that of hypoxia-dependent regulation in each KO cell background) on a Log_2 scale. If there were genes with a similar regulation by

hypoxia in the two cellular backgrounds, then it was argued that a bimodal distribution or a separate frequency peak should be discernible around x=0 (i.e. equal hypoxia regulation in both backgrounds). However, for both hypoxia up- and down-regulated genes, unimodal distributions with an averaged FC ratio above x=0 were observed in all three comparisons. There was no evidence of a grouping of transcript around x=0. (**Figure 10A and B**). This indicated that the majority of the hypoxia-dependent regulation was indeed greater in the WT cells than in any of the mutant cells, and suggested that it was not truly independent of HIF.

Despite the absence of a bimodal distribution, I was concerned that there might still be a very small number of genes that had persistent regulation by hypoxia across all genotypes i.e. that the number of genes was too small to create a signal in the above frequency distribution. Therefore, to address this, the data was further interrogated by manual examination for rare genes for which the amplitude of induction by hypoxia (fold change in expression) was closely similar across the genotypes. To do this I selected 3 arbitrary thresholds for the ratio of amplitudes of hypoxic regulation between WT and mutant genotypes (**Figure 10C**); FC ratio<1 i.e. the same or lower hypoxia regulation in the WT than in each mutant cell background; FC ratio <1.15-fold (i.e. less than Log_2=0.2 greater in the WT than in each of the mutant cell backgrounds); FC ratio <1.32-fold (i.e.Log_2= 0.4 greater in the WT than in each mutant cell background). In this way it was possible to examine in detail for individual transcripts that might have retained regulation by hypoxia in the mutant cell background, but might have failed to reach significance.

A

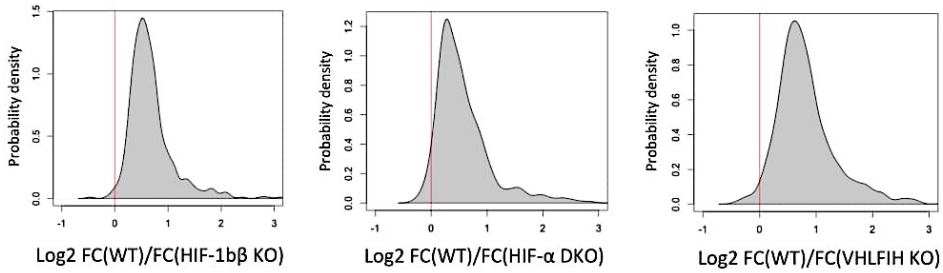

B

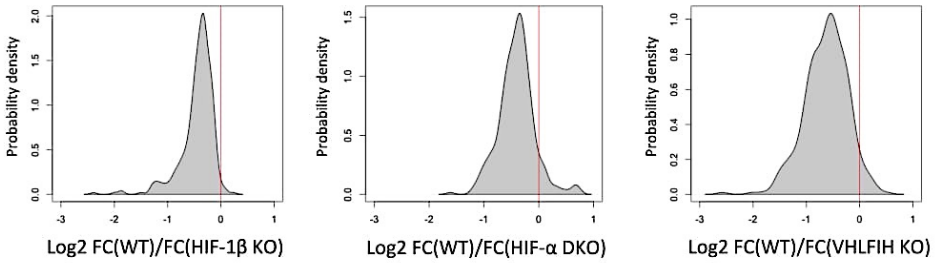

C

Hypoxia up-regulated genes	Hypoxia down-regulated genes
Calculate FC ratio of each gene: 1) FC (WT)/FC (HIF-1β KO) 2) FC (WT)/FC (HIF-α DKO) 3) FC (WT)/FC (VHLFIH KO)	Calculate FC ratio of each gene: 1) FC (WT)/FC (HIF-1β KO) 2) FC (WT)/FC (HIF-α DKO) 3) FC (WT)/FC (VHLFIH KO)
The FC ratio of all three comparisons <1, n=1 <1.15, n=3 <1.32, n=24	The FC ratio of all three comparisons <1, n=0 <1.15, n=5 <1.32, n=50

Figure 10. Probing for HIF-independent hypoxia-regulated genes with manually imposed arbitrary cut-off values. Hypoxia-regulated genes were defined in the WT cell background and were separated into hypoxia up- and down-regulated ones. Frequency plots comparing the total fold change (FC) ratios of (A) hypoxia up-regulated genes, and (B) hypoxia down-regulated genes, between the WT cells and each of the mutant cells. Genes with a FC ratio around 'x=0' (i.e. Log2=1) would be the candidates for HIF-independent regulation since they showed concordant regulation by hypoxia regardless of the cell type. (C) Cut-off values with different stringency were applied to each group of genes to select candidates for HIF-independent hypoxia-dependent regulation.

Results are shown in **Table 2.2** and **2.3**. As indicated earlier, all these genes that had met a criterion of significant up-regulation by hypoxia in WT cells. Using the most stringent cut-off, i.e. FC ratio<1, only a single gene, *S100A2*, was identified. When the cut-off was relaxed to consider genes that were only slightly (up to 1.15-fold), more strongly regulated in WT than any of the mutant cells, two further genes were identified. Finally, when the FC ratio was relaxed to consider genes that were up to 1.32 fold more strongly regulated, 21 further genes (24 in total) were identified (**Table 2.2**). Within the hypoxia down-regulated genes, overall no genes were identified with an FC ratio<1 (i.e. less down-regulated by hypoxia in WT cells than mutant cells), five genes were found for whom down-regulation was only slightly less than WT (FC ratio<1.15), and a total of 50 genes were identified with an FC ratio<1.32 (**Table 2.3**).

Table 2.2 Hypoxia up-regulated genes with hypoxia-dependent regulation in the WT and in all three mutant cell backgrounds

The fold changes (FC) between normoxic and hypoxic conditions in each cell background are shown in the 2nd-5th columns. The FC ratios between WT cells and each of the mutant cell backgrounds are shown in the next 3 columns.

	WT	HIF1β KO	HIF-α DKO	VHLFIH KO	WT/1βKO	WT/DKO	WT/VHLFIH KO	Description
FC(WT)/FC(KO)<1								
S100A2	1.51	2.09	1.60	2.02	0.72	0.94	0.75	S100 Calcium Binding Protein A2
FC(WT)/FC(KO)<1.15								
LOC100506548	1.45	1.38	1.30	1.36	1.04	1.12	1.07	Uncharacterized RNA Gene
KIAA1804	1.42	1.24	1.25	1.24	1.14	1.14	1.15	Mixed Lineage Kinase 4
FC(WT)/FC(KO)<1.32								
GRB10	1.62	1.51	1.41	1.27	1.08	1.15	1.28	Growth Factor Receptor Bound Protein 10
KLF11	1.62	1.47	1.32	1.26	1.10	1.23	1.28	Kruppel-Like Factor 11
PGLS	1.58	1.26	1.28	1.25	1.26	1.24	1.27	6-Phosphogluconolactonase
ARHGEF10	1.51	1.21	1.28	1.20	1.24	1.18	1.25	Rho Guanine Nucleotide Exchange Factor 10
FGFR1	1.47	1.19	1.45	1.15	1.24	1.02	1.28	Fibroblast Growth Factor Receptor 1
SGPL1	1.46	1.16	1.16	1.17	1.25	1.26	1.24	Sphingosine-1-Phosphate Lyase 1
ZBTB44	1.42	1.18	1.16	1.10	1.20	1.23	1.30	Zinc Finger And BTB Domain Containing 44
PAPD7	1.42	1.15	1.27	1.34	1.23	1.12	1.06	PAP Associated Domain Containing 7
SUN1	1.39	1.14	1.16	1.08	1.22	1.20	1.29	Sad1 And UNC84 Domain Containing 1
KDM5C	1.37	1.04	1.18	1.08	1.32	1.16	1.27	Lysine Demethylase 5C
EIF4G3	1.36	1.03	1.19	1.07	1.32	1.14	1.27	Eukaryotic Translation Initiation Factor 4 Gamma 3
CCDC6	1.36	1.16	1.20	1.22	1.18	1.14	1.11	Coiled-Coil Domain Containing 6
PHF17	1.35	1.15	1.12	1.23	1.18	1.20	1.10	Jade Family PHD Finger 1
SLC38A1	1.33	1.08	1.22	1.17	1.24	1.10	1.14	Solute Carrier Family 38 Member 1
VPS35	1.32	1.06	1.04	1.04	1.25	1.27	1.27	VPS35 Retromer Complex Component
TP53	1.32	1.06	1.20	1.19	1.25	1.11	1.11	Tumor Protein P53
MCM6	1.32	1.05	1.29	1.08	1.26	1.03	1.22	Minichromosome Maintenance Complex Component 6
LRPPRC	1.31	1.08	1.12	1.14	1.22	1.17	1.15	Leucine Rich Pentatricopeptide Repeat Containing
MCM3	1.30	1.09	1.19	1.07	1.19	1.09	1.21	Minichromosome Maintenance Complex Component 3
NOTCH2	1.30	0.99	1.29	0.99	1.32	1.01	1.31	Notch 2
ADAM9	1.30	1.04	1.15	1.21	1.25	1.14	1.07	ADAM Metallopeptidase Domain 9

Table 2.3 Hypoxia down-regulated genes with hypoxia-dependent regulation in the WT and in all three mutant cell backgrounds

The fold changes (FC) between normoxic and hypoxic conditions in each cell background are shown in the 2nd-5th columns. The FC ratios between WT cells and each of the mutant cell backgrounds are shown in the next 3 columns.

Gene	WT	HIF1β KO	HIF-α DKO	VHLFIH KO	WT/1β KO	WT/DKO	WT/VHLFIH KO	Description
FC(WT)/FC(KO)<1.15								
NQO1	0.68	0.75	0.68	0.64	0.91	1.00	1.06	NAD(P)H Quinone Dehydrogenase 1
ACOX1	0.69	0.76	0.75	0.71	0.90	0.91	0.96	Acyl-CoA Oxidase 1
KIAA1586	0.70	0.75	0.65	0.72	0.93	1.08	0.97	E3 SUMO-protein ligase
PSMC2	0.73	0.81	0.81	0.83	0.91	0.90	0.89	Proteasome 26S Subunit, ATPase 2
MRPL51	0.75	0.85	0.81	0.85	0.88	0.93	0.88	Mitochondrial Ribosomal Protein L51
FC(WT)/FC(KO)<1.32								
ARHGAP18	0.58	0.69	0.70	0.63	0.85	0.83	0.92	Rho GTPase Activating Protein 18
HTATSF1P2	0.60	0.68	0.77	0.60	0.88	0.78	0.99	HIV-1 Tat Specific Factor 1 Pseudogene 2
ENTPD7	0.60	0.78	0.68	0.72	0.78	0.88	0.83	Ectonucleoside Triphosphate Diphosphohydrolase 7
LOC100506305	0.62	0.53	0.59	0.73	1.18	1.06	0.85	Uncharacterized RNA Gene
PCYT1A	0.65	0.79	0.81	0.67	0.82	0.80	0.96	Phosphate Cytidylyltransferase 1, Choline, Alpha
SEC22B	0.66	0.81	0.85	0.78	0.82	0.78	0.84	SEC22 Homolog B, Vesicle Trafficking Protein
DNAJB11	0.67	0.78	0.84	0.86	0.86	0.79	0.77	DnaJ Heat Shock Protein Family (Hsp40) Member B11
DCDC2	0.67	0.77	0.78	0.64	0.87	0.85	1.05	Doublecortin Domain Containing 2
FASTKD1	0.67	0.85	0.83	0.85	0.79	0.81	0.79	FAST Kinase Domains 1
LOC401397	0.67	0.76	0.65	0.78	0.89	1.04	0.86	Uncharacterized RNA Gene
MSRB1	0.67	0.71	0.88	0.54	0.95	0.77	1.24	Methionine Sulfoxide Reductase B1
CISD1	0.68	0.83	0.86	0.89	0.82	0.79	0.77	CDGSH Iron Sulfur Domain 1
AASS	0.68	0.84	0.88	0.64	0.81	0.78	1.07	Aminoadipate-Semialdehyde Synthase
BPNT1	0.69	0.87	0.83	0.81	0.79	0.82	0.84	3'(2'), 5'-Bisphosphate Nucleotidase 1
GNG11	0.69	0.88	0.64	0.60	0.79	1.08	1.16	G Protein Subunit Gamma 11
PSMC6	0.70	0.79	0.83	0.80	0.88	0.84	0.87	Proteasome 26S Subunit, ATPase 6
UGDH	0.70	0.87	0.82	0.81	0.80	0.85	0.86	UDP-Glucose 6-Dehydrogenase
TMCO1	0.70	0.80	0.77	0.87	0.87	0.91	0.81	Transmembrane And Coiled-Coil Domains 1
TPMT	0.71	0.80	0.92	0.80	0.88	0.77	0.88	Thiopurine S-Methyltransferase
CDKN2C	0.71	0.85	0.85	0.60	0.83	0.83	1.19	Cyclin Dependent Kinase Inhibitor 2C
MPHOSPH10	0.72	0.81	0.92	0.90	0.88	0.78	0.79	M-Phase Phosphoprotein 10
SKP2	0.72	0.73	0.93	0.80	0.97	0.77	0.89	S-Phase Kinase Associated Protein 2
GPX8	0.72	0.89	0.83	0.87	0.81	0.86	0.83	Glutathione Peroxidase 8 (Putative)
HRSP12	0.72	0.82	0.84	0.85	0.87	0.86	0.85	Reactive Intermediate Imine Deaminase A Homolog
MED30	0.72	0.83	0.68	0.83	0.86	1.05	0.87	Mediator Complex Subunit 30
DYNLL1	0.72	0.91	0.83	1.03	0.79	0.87	0.70	Dynein Light Chain LC8-Type 1
SNHG3	0.72	0.88	0.86	0.80	0.82	0.84	0.91	Small Nucleolar RNA Host Gene 3
IMPA1	0.73	0.91	0.79	0.91	0.80	0.93	0.81	Inositol Monophosphatase 1
KNSTRN	0.73	0.91	0.81	0.85	0.80	0.90	0.86	Kinetochore Localized Astrin/SPAG5 Binding Protein
RARS	0.74	0.87	0.78	0.89	0.85	0.95	0.83	Arginyl-TRNA Synthetase
DDX47	0.74	0.83	0.81	0.93	0.90	0.91	0.80	DEAD-Box Helicase 47
EPT1	0.74	0.87	0.82	0.96	0.86	0.91	0.78	Selenoprotein I
TRMT112	0.74	0.86	0.90	0.95	0.87	0.83	0.78	TRNA Methyltransferase Subunit 11-2
H3F3B	0.74	0.90	0.84	0.88	0.83	0.89	0.84	H3 Histone Family Member 3B
USP16	0.75	0.81	0.70	0.96	0.92	1.07	0.78	Ubiquitin Specific Peptidase 16
TMEM184C	0.75	0.82	0.91	0.90	0.91	0.82	0.83	Transmembrane Protein 184C
SDHD	0.75	0.94	0.81	0.84	0.80	0.92	0.88	Succinate Dehydrogenase Complex Subunit D
PPP2R1B	0.75	0.80	0.98	0.86	0.94	0.77	0.88	Protein Phosphatase 2 Scaffold Subunit Abeta
UBB	0.75	0.91	0.83	0.90	0.83	0.91	0.84	Ubiquitin B
PPP2CA	0.75	0.84	0.88	0.96	0.90	0.85	0.78	Protein Phosphatase 2 Catalytic Subunit Alpha
CFL2	0.76	0.82	0.80	0.88	0.92	0.95	0.86	Cofilin 2
SRSF1	0.76	0.81	0.90	0.86	0.93	0.84	0.88	Serine And Arginine Rich Splicing Factor 1
NBN	0.76	0.87	0.70	1.00	0.88	1.09	0.76	Nibrin
SKA2	0.77	0.97	0.98	0.92	0.79	0.78	0.83	Spindle And Kinetochore Associated Complex Subunit 2
CALM2	0.78	1.00	0.81	1.02	0.78	0.96	0.76	Calmodulin 2

Genes within each sub-category were ranked based on their hypoxic regulation in the WT cells. The tables illustrate that none of the genes identified in this way manifest high amplitude of induction or suppression by hypoxia. Furthermore, no genes showed persistent regulation across WT and mutant cells that were statistically significant. They therefore corroborated the analyses described in **Figure 9** and **Figures 10A and B**.

Finally, I wished to test whether even amongst these genes manifesting relatively low levels of induction by hypoxia, there were examples in which reproducible low amplitude regulation was preserved across the panel of mutant cells. To this end, the genes manifesting the largest regulation by hypoxia were selected for testing by independent RT-qPCR assays, using WT, HIF-1β KO and HIF-α DKO cells, which were cultured under similar conditions to those used in the RNA-seq experiments, i.e. normoxia (21% O_2) or hypoxia (0.5% O_2) for 24h. The expression of known HIF targets (*CA9* and *BNIP3*) was used as an internal comparator; their high amplitude induction in the hypoxic WT cells and their lack of induction in the HIF-α DKO and HIF-1β KO cells, confirming the quality of mRNA and the application of an effective hypoxic stimulus (**Figure 11A**). Three apparently HIF-independent, hypoxia up-regulated candidates, with the biggest hypoxia regulation across the cells (*S100A2*, *LOC100506548* and *GRB10*) were examined. Hypoxia-induced expression of *S100A2* and *LOC100506548* was observed by RT-qPCR in the WT cells. However, no consistent hypoxia-dependent regulation was seen across the HIF-α DKO and HIF-1β KO cells. For *GRB10*, no apparent hypoxia regulation was observed in the WT and HIF-α DKO cells, although some weak regulation was seen in the HIF-1β KO cells (**Figure 11B right panels**). Similarly, three candidates for HIF-independent hypoxia down-regulated genes (*PSMC2, ACOX1, MRPL51*) were chosen for analysis by RT-qPCR testing. However the low amplitude regulation that had been observed in the RNA-seq experiments was not

reproduced in WT or HIF-1β KO cells and these genes were not analysed further (**Figure 12**).

In summary, despite extensive analyses, no clear evidence was obtained for hypoxia inducible responses that were fully independent of HIF in HKC-8 cells, cultured under these conditions.

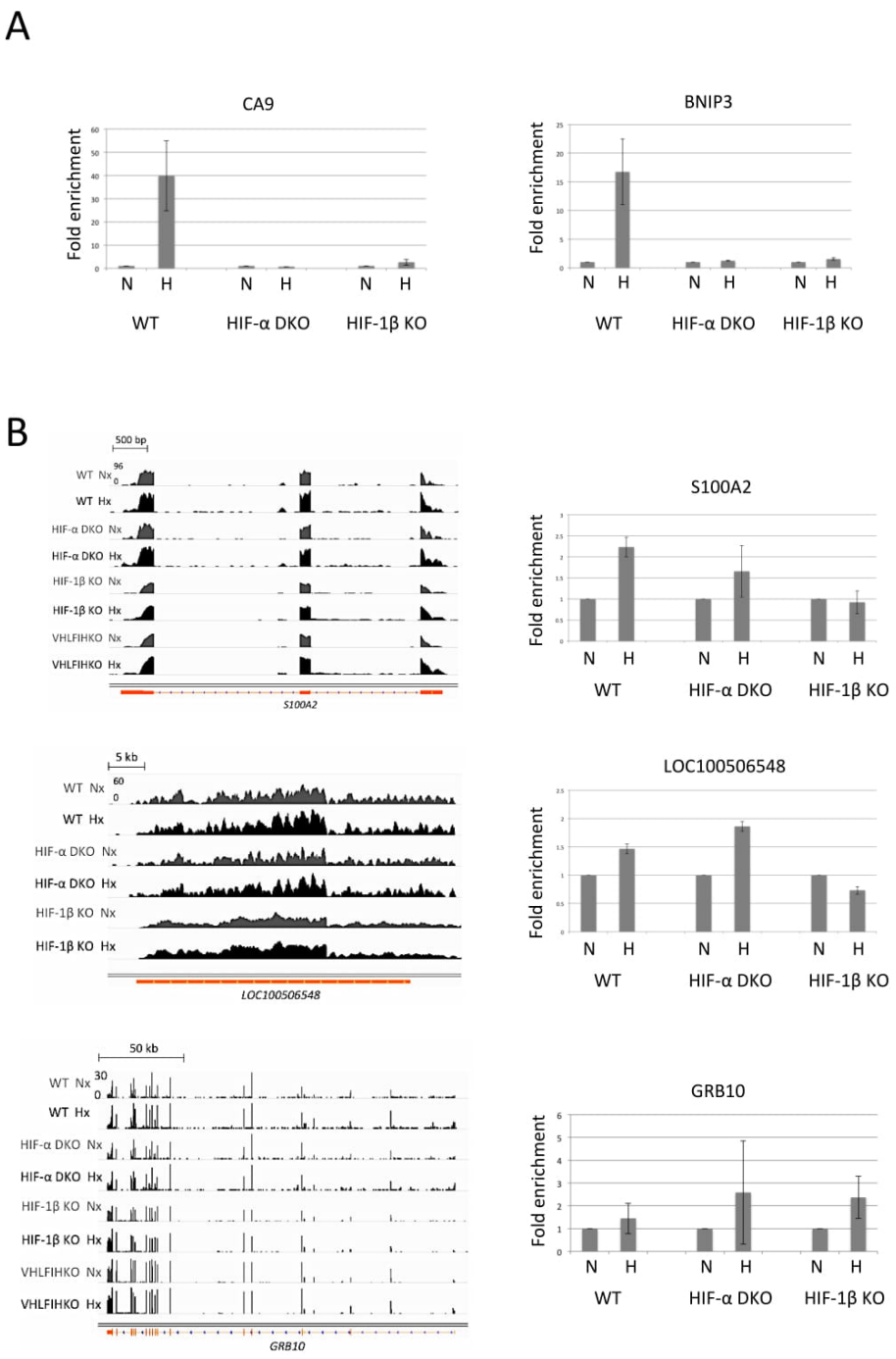

Figure 11. Examination of candidate HIF-independent hypoxia up-regulated genes in the WT, HIF-α DKO and HIF-1β KO cells by RT-qPCR assays. Cells were cultured under normoxia (21% O_2) or hypoxia (0.5% O_2) for 24h. (A) HIF targets genes *CA9* and *BNIP3* were used as internal controls. Strong hypoxic induction of both genes was observed in the hypoxic WT cells but not in the mutant cells. (B) Three candidates for HIF-independent hypoxia up-regulated genes were tested by RT-qPCR. The IGV tracks of these genes are shown on the left panels. Gene expression analysis is shown on the right panels. The fold enrichment of each gene was normarlised to the value for the housekeeping gene *HPRT* using the delta-delta CT method. Bar shows mean ± s.d. n=3 biological replicates were performed. N refers to normoxia. H refers to hypoxia.

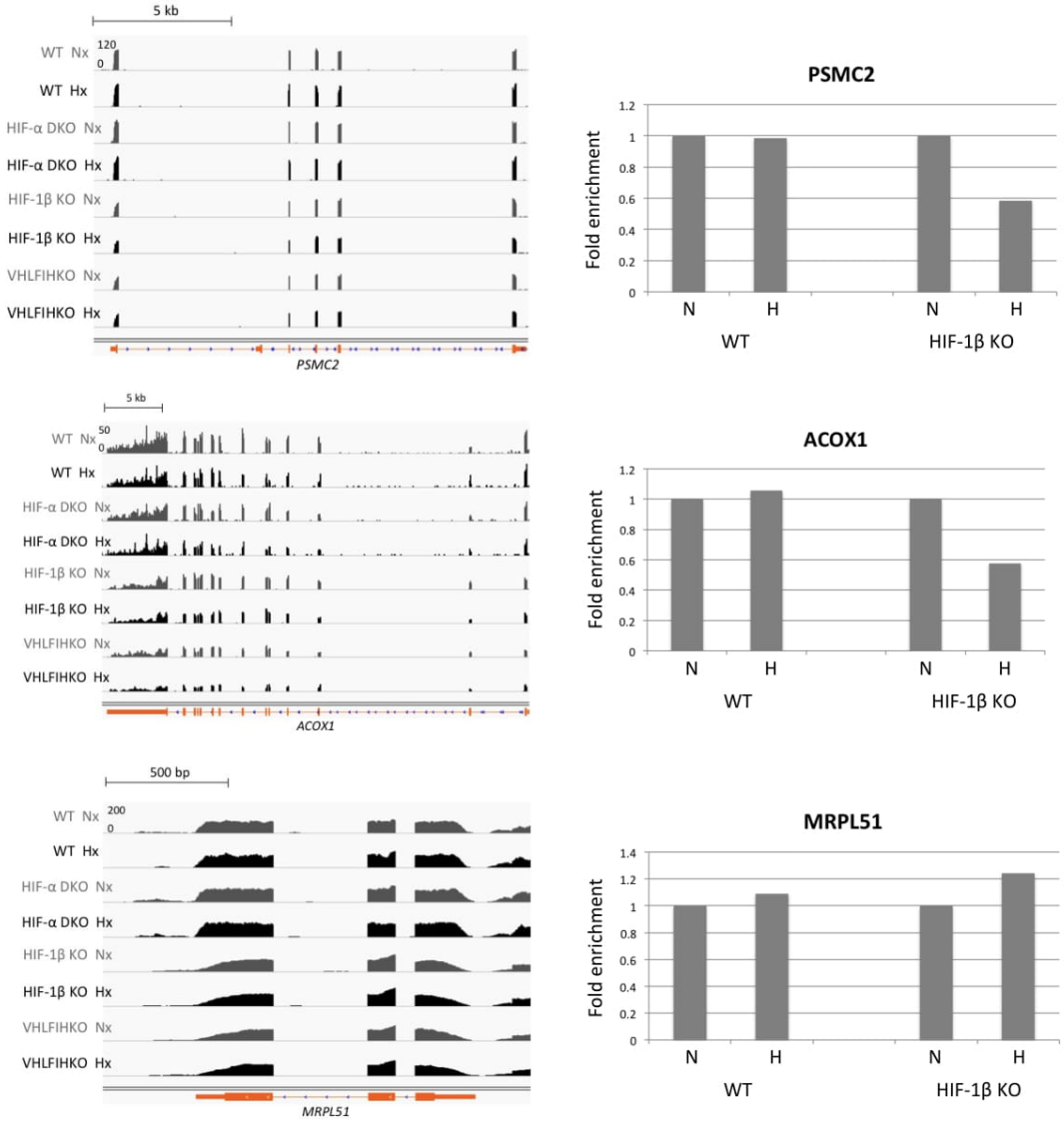

Figure 12. Examination of candidate HIF-independent hypoxia down-regulated genes in the WT, HIF-α DKO and HIF-1β KO cells by RT-qPCR assays. Cells were cultured under normoxia (21% O_2) or hypoxia (0.5% O_2) for 24h. Three candidates for HIF-independent hypoxia down-regulated genes were tested by RT-qPCR. IGV tracks for these genes are shown on the left panels. Gene expression analysis is shown on the right panels. The fold enrichment of each gene was normarlised to the values for the housekeeping gene *HPRT* using the delta-delta CT method. n=1 replicate was performed. N refers to normoxia. H refers to hypoxia.

2.2.6 Analyses probing for non-canonical dependence of hypoxia gene regulation on the HIF system

Having found no clear evidence of HIF-independent gene regulation by hypoxia, I next sought to interrogate the data for the existence of non-canonical actions of HIF on hypoxic gene regulation. Evidence that this might be present was seen in analyses of hypoxic gene regulation of individual mutant cells, which revealed examples of persistent regulation by hypoxia, albeit of different genes in the different cell types.

In these analyses, the same strategy was used as in section 2.5 i.e. the amplitude of regulation (fold-change) of induction or repression by hypoxia in a given mutant cell was compared with that in the WT cell to test different hypotheses as to the existence or otherwise of non-canonical functions of the HIF pathway. I defined 'non-canonical' as any function of HIF other than that mediated by α/β heterodimeric binding between either of HIF-1α or HIF-2α, and HIF-1β. For example, hypoxia-regulated genes that appeared in the HIF-1β KO, but not HIF-α DKO cells may represent a non-canonical HIF-α function. Likewise, genes regulated in the HIF-α DKO cells, but not HIF-1β KO cells, might potentially suggest a non-canonical HIF-1β function. The VHLFIH KO cells were also included in these analyses. Although the principal purpose of including these cells was to examine for hypoxia-inducible gene expression that was wholly independent of HIF, it was also considered possible that they might reveal non-canonical functions of HIF. For instance, as demonstrated in **Figure 5B**, hypoxia reduced HIF hydroxylation at P564 in human HIF-α; since this residue resides in one of two transactivation domains in the polypeptide its hydroxylation status might affect expression of a class of genes irrespective of VHL-dependent degradation.

In order to probe for hypoxia-dependent gene regulation that is mediated by non-canonical function of HIF, in the next three sections, the hypoxia-regulated genes are

defined by statistically significant regulation in the given mutant cell lines (HIF-1β KO, HIF-α DKO and VHLFIH KO). After fulfilling this criterion, their regulation by hypoxia was compared with that in the WT cells.

2.2.7 Hypoxia-regulated genes in the HIF-1β deficient cells

First I compared HIF-β KO and WT cells. In total there were 366 hypoxia-regulated genes identified in the HIF-1β KO cells. These genes were divided into hypoxia up-regulated and down-regulated genes (n=198 and n=168 respectively) and were analysed separately.

The levels of hypoxia-dependent regulation in the HIF-1β KO cells were then compared with those in the WT cells. In these analysis I also wished to consider the possibility that non-canonical functions of HIF might be revealed specifically in the mutant cells i.e. inactivation of the canonical dimerisation partner might uncover a non-canonical function that was otherwise difficult to identify. Thus, the comparison of regulation by hypoxia between WT and HIF-1β mutant cells aimed to distinguish three categories of behaviour: genes with larger hypoxia-dependent regulation in the WT than mutant; genes with a similar regulation in the WT and HIF-1β mutant cells, and genes with a larger hypoxic regulation in the HIF-1β mutant cells.

To define these categories, regulation by hypoxia in each cell type was defined as the fold-change (FC) in expression between hypoxia and normoxia. FC ratios were then calculated to compare WT and mutant cells. An arbitrary cut-off of 1.2-fold was applied to the FC ratio, i.e. FC(WT)/FC(HIF-1β KO). Thus, the genes that were categorised as more regulated by hypoxia in WT than mutant, i.e. FC(WT)/FC(HIF-1β KO)>1.2, n=49; similarly regulated in WT versus mutant, i.e. FC(WT)/FC(HIF-1β KO) is between 0.8 and 1.2, n=68; or more regulated in the mutant than the WT, i.e. FC(WT)/FC(HIF-1β KO)<0.8, n=81.

Similar analyses were also performed using the hypoxia down-regulated genes, again as defined in the HIF-1β KO cells (n=168). 25 of these genes actually showed an up-regulation by hypoxia in the WT cells. These genes could not be rationally categorised according the hypotheses outlined above and may represent clonal variation unrelated to HIF genotype. Their behaviour in relation to HIF status was therefore not analysed further. This left a total of 143 hypoxia down-regulated genes in the HIF-1β mutant cells. Of these genes, 111 showed similar regulation by hypoxia as was observed in WT cells i.e. the FC(WT)/FC(HIF-1β KO) was between 0.8 and 1.2, whereas six showed greater suppression by hypoxia in WT cells than mutant cells and 26 showed greater suppression by hypoxia in mutant than WT cells.

The findings for genes that were up-regulated or down-regulated in HIF-1β mutant cells are summarised in **Figure 13** and detailed in full in Appendix 8.3 and 8.4. Since one aim of these analyses was to determine the existence or otherwise of physiological pathways that might be responding to non-canonical actions of HIF-α, Gene Ontology pathway analysis was applied to groups of genes defined as above.

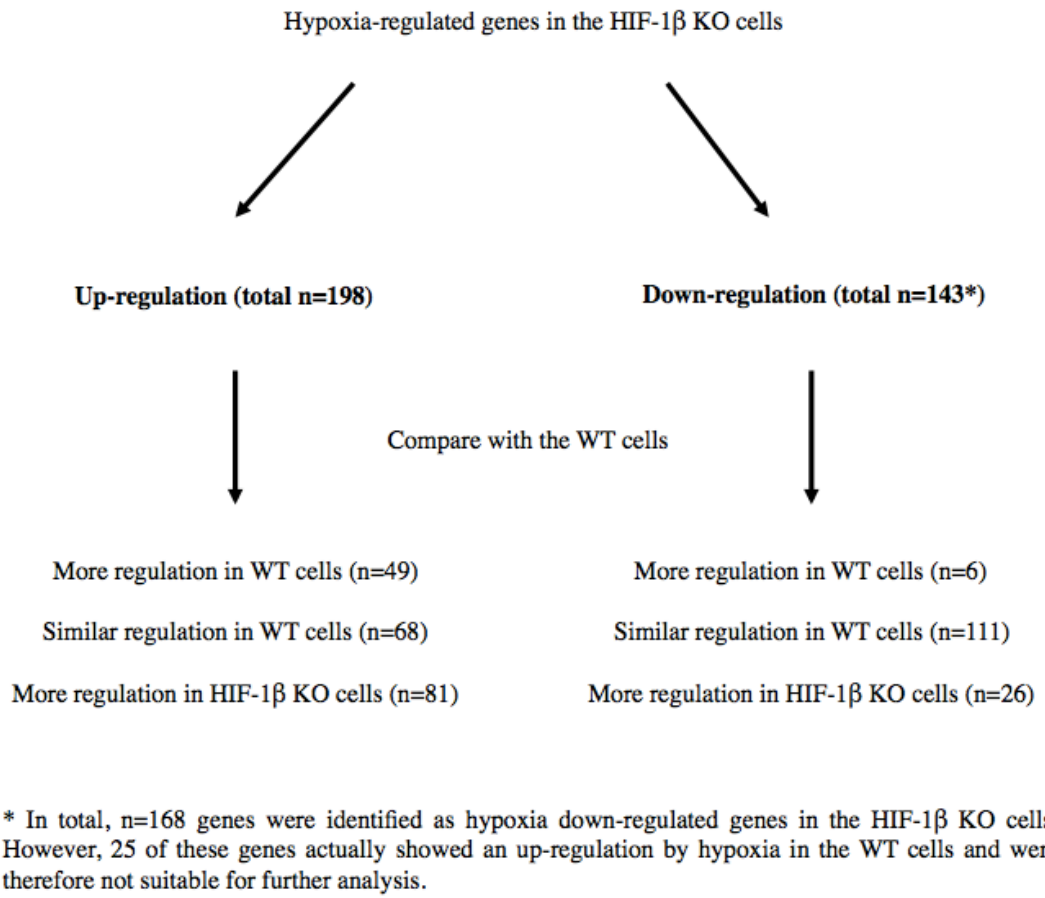

Figure 13. A summary of genes that are regulated by hypoxia in HIF-1β KO cells.

I first considered genes that were up-regulated by hypoxia in the HIF-1β mutant cells (n=198). Gene Ontology (GO) pathway analysis was performed separately for genes within each category (**Figure 14**). In the first category in which genes manifest greater hypoxia-dependence in the WT cells than in the HIF-1β mutant cells, the analysis revealed a strong signature of response to hypoxia, as well as glycolysis and collagen fibril organisation (**Figure 14A**). This, together with the observation that regulation by hypoxia in mutant cells showed some, albeit weak, correlation with that in WT cells suggests that the persistent regulation in HIF-β mutant cells was in some way related to the wild-type HIF pathway, for instance through the use of an alternative HIF-β dimerisation partner. Inspection of data for individual genes showed that most of them

only have a low amplitude regulation by hypoxia in the HIF-1β mutant cells (i.e. FC is between 1.2 to 2.3-fold) (Appendix 8.3.1).

In the second category in which genes manifest a similar hypoxia-dependent regulation in the WT and HIF-1β mutant cells, although GO analysis revealed some physiological pathways that reached a lower level of statistical significance, no common physiological functions was apparent amongst these pathways (**Figure 14B**). In addition, genes in this category also only manifested a small induction by hypoxia (i.e. FC was between 1.2 to 2.1-fold) (Appendix 8.3.2).

In the last category, genes that displayed a greater hypoxia-dependence in the mutant than in the WT cells, some showed moderately high amplitude (>2-fold) of hypoxia regulation in the mutant cells but not WT cells (Appendix 8.3.3). Interestingly, GO analysis revealed a strong signature for involvement in lipid/cholesterol metabolism. The top five statistically over-represented pathways in the hypoxia up-regulated genes were all associated with lipid/cholesterol synthesis (**Figure 14C**). Furthermore, of the top 30 genes within this group, 70% are involved in lipid/cholesterol metabolism (highlighted in blue in **Table 2.4)**. A further characterisation of some of these genes is performed later in this chapter (**section 2.2.10**).

A

Hypoxia up-regulation: WT>HIF-1β KO (n=49)

	Genes	p-value
cellular response to hypoxia	BNIP3L; MYC; BNIP3; PGK1; NDRG1; VEGFA	5.79E-09
collagen fibril organization	COL5A1; COL4A2; COL4A1; SERPINE1; ITGB8; ITGA5; LOXL2	9.17E-08
glycolytic process through fructose-6-phosphate	LDHA; HKDC1; PGK1; ALDOA	2.25E-07
extracellular matrix organization	COL5A1; COL4A2; COL4A1; SERPINE1; ITGB8; ITGA5	0.000001306
positive regulation of sprouting angiogenesis	BTG1; SERPINE1; ITGA5; RHOB; VEGFA	0.000001695

B

Hypoxia up-regulation: WT=HIF-1β KO (n=68)

	Genes	p-value
regulation of cellular response to oxidative stress by transcription from RNA polymerase II promoter	KLF11; PINK1; CEBPB; KLF13; MAFF; DVL2; HIVEP2	0.00002854
ERAD pathway	CEBPB; PMAIP1; PDIA5; HERPUD1	0.0001591
peptidyl-serine autophosphorylation	PINK1; LATS2; DAPK1; MINK1; MASTL	0.0001649
peptidyl-threonine dephosphorylation	PTPRS; DUSP1; CTDSP2; PTPN12	0.0002401
positive regulation of cysteine-type endopeptidase activity involved in apoptotic process	DUSP1; DAPK1; PMAIP1	0.0002437

C

Hypoxia up-regulation: WT<HIF-1β KO (n=81)

	Genes	p-value
cholesterol biosynthetic process	IDI1; FDPS; MVK; HMGCS1; CYP51A1; MSMO1; HMGCR; LSS; ACAT2; ACLY; SQLE; EBP; NSDHL; MVD; DHCR7; FDFT1	1.04E-25
isoprenoid biosynthetic process	ACLY; MVK; ACSS2; ACSL1; MVD; HMGCR	6.53E-11
steroid biosynthetic process	ACLY; ACSS2; ACSL1; CYP51A1; MSMO1; LSS; FDFT1	3.49E-09
regulation of lipid metabolic process	ALAS1; HMGCS1; ACSL1; ID2; HMGCR; FADS1; FDFT1	3.44E-08
regulation of lipid kinase activity	ALAS1; HMGCS1; ACSL1; ID2; HMGCR; FADS1; FDFT1	6.18E-08

Figure 14. GO pathway analysis was performed for genes that up-regulated by hypoxia in the HIF-1β mutant cells using the EnrichR software (Chen et al., 2013). The top five statistically over-represented pathways, together with the genes involved in that pathway and the *p*-values are shown in the table.

Table 2.4 Hypoxia up-regulated genes with greater regulation in the HIF-1β mutant cells

The hypoxia up-regulated genes were defined in the HIF-1β mutant cells. The ratios of hypoxic fold regulations (fold change, FC) between WT cells and HIF-1β KO cells, i.e. FC(WT)/FC(1β KO), are shown in the 2nd column. Genes with larger hypoxic regulation in the HIF-1β KO cells (i.e. FC ratio<0.8) were selected and ranked by their hypoxia regulation in HIF-1β mutant cells (3rd column). The top 30 candidates are listed in the table. Genes involved in lipid metabolism pathways are highlighted in blue. A full list of genes can be found in Appendix 8.3.3.

Gene	WT/1β KO	1β KO	WT	DKO	VHLFIH KO	Description
INSIG1	0.28	3.92	1.09	1.28	1.02	Insulin Induced Gene 1
HMGCS1	0.19	3.58	0.68	1.00	1.25	3-Hydroxy-3-Methylglutaryl-CoA Synthase 1
ACSS2	0.43	2.89	1.24	1.30	1.38	Acyl-CoA Synthetase Short-Chain Family Member 2
MSMO1	0.27	2.56	0.70	1.03	1.15	Methylsterol Monooxygenase 1
SCD	0.57	2.26	1.30	1.40	1.50	Stearoyl-CoA Desaturase
LPIN1	0.43	2.25	0.96	1.30	1.82	Lipin 1
TNFSF9	0.34	2.24	0.77	0.85	0.82	Tumor Necrosis Factor Superfamily Member 9
IDI1	0.28	2.22	0.61	0.99	1.23	Isopentenyl-Diphosphate Delta Isomerase 1
ZC3H6	0.62	2.13	1.32	1.28	0.79	Zinc Finger CCCH-Type Containing 6
LDLR	0.49	2.11	1.04	1.27	1.19	Low Density Lipoprotein Receptor
S100A2	0.72	2.09	1.51	1.60	2.02	S100 Calcium Binding Protein A2
MVD	0.40	2.07	0.82	1.30	1.08	Mevalonate Diphosphate Decarboxylase
DHCR7	0.40	2.04	0.81	1.18	1.27	7-Dehydrocholesterol Reductase
CYP51A1	0.42	1.99	0.84	0.90	1.33	Cytochrome P450 Family 51 Subfamily A Member 1
LSS	0.48	1.98	0.94	1.52	1.30	Lanosterol Synthase (2,3-Oxidosqualene-Lanosterol Cyclase)
SQLE	0.42	1.98	0.83	0.93	1.24	Squalene Epoxidase
SPP1	0.31	1.96	0.61	0.69	0.60	Secreted Phosphoprotein
FADS2	0.62	1.85	1.15	1.17	1.35	Fatty Acid Desaturase 2
FDFT1	0.46	1.83	0.83	1.04	1.24	Farnesyl-Diphosphate Farnesyltransferase 1
MVK	0.40	1.78	0.72	1.15	1.09	Mevalonate Kinase
STARD4	0.58	1.72	1.01	0.90	1.17	StAR Related Lipid Transfer Domain Containing 4
JUND	0.64	1.72	1.10	1.17	1.48	JunD Proto-Oncogene, AP-1 Transcription Factor Subunit
ITM2B	0.72	1.69	1.22	1.12	0.87	Integral Membrane Protei
FASN	0.72	1.66	1.19	1.42	1.12	Fatty Acid Synthase
ACSL1	0.58	1.65	0.96	0.99	1.50	Acyl-CoA Synthetase Long-Chain Family Member 1
TFRC	0.68	1.64	1.12	1.23	0.94	Transferrin Receptor
TACSTD2	0.41	1.61	0.66	1.35	0.96	Tumor Associated Calcium Signal Transducer 2
HMGCR	0.45	1.57	0.70	0.85	1.05	3-Hydroxy-3-Methylglutaryl-CoA Reductase
CREBRF	0.72	1.56	1.13	1.05	1.13	CREB3 Regulatory Factor
ACSL3	0.71	1.56	1.10	1.07	1.44	Acyl-CoA Synthetase Long-Chain Family Member 3

Next, genes that were down-regulated by hypoxia in the HIF-1β mutant cells were analysed by GO (**Figure 15**). Only six genes (*PLK2, NXPE3, ASF1A, CHPF2, SLC5A6, SRSF2*) showed a greater down-regulation in the WT cells than in the mutant cells, and GO analysis found no evidence of a common pathway. 111 genes were found to be negatively regulated by hypoxia and the regulations were similar in the WT and HIF-1β mutant cells. Several genes in this category encode for 26S proteasome subunits (**Figure 15A**). However, the top 5 statistically over-represented pathways that analysed by GO analysis did not reveal any significant pattern of a common pathway. Within the genes that have more down-regulation in the mutant than WT cells (n=26), interestingly GO analysis revealed a specific signature of protein translation process (**Figure 15B**).

Overall, the amplitude of down-regulation by hypoxia in the genes defined in the HIF-1β cells was again generally small (i.e. between 0.99 to 0.52-fold) compared with that in the hypoxia up-regulated genes.

A

Hypoxia down-regulation: WT=HIF-1β KO (n=111)

	Genes	p-value
positive regulation of cellular amino acid metabolic process	NQO1; PSMD12; PSMD6; PSMC6; PSMB2; PSME3; PSMC2; ODC1; PSMD3	1.083e-11
mitotic cytokinesis checkpoint	PSMD12; PSMD6; PSMC6; PSMB2; PSME3; PSMC2; PSMD3; AURKA	7.937e-10
maturation of LSU-rRNA	LTV1; NOP16; PNO1; NIP7; DDX56; NOP2; RRS1; UTP20; WDR46; DCAF13; RRP9; NOL6	1.413e-9
NF-kB signaling	PSMD12; PSMD6; PSMC6; PSMB2; PSME3; PSMC2; PSMD3	6.414e-8
protein linear polyubiquitination	RNF145; PSMD6; PSMD12; PSMC6; PSMB2; PSME3; PSMC2; PSMD3; SKP2	0.000003056

B

Hypoxia down-regulation: WT<HIF-1β KO (n=26)

	Genes	p-value
mature ribosome assembly	DDX3X; EIF6	0.0001064
positive regulation of translational initiation	DDX3X; EIF6; POLR2G	0.0001096
transcription elongation from RNA polymerase I promoter	POLR1A; CCNH	0.0007869
positive regulation of tumor necrosis factor-mediated signaling pathway	AXL; SPPL2A	0.001292
cleavage involved in rRNA processing	PDCD11; DKC1; DIS3L	0.001704

Figure 15. GO pathway analysis was performed for genes that were down-regulated by hypoxia in the HIF-1β mutant cells using the EnrichR software (Chen et al., 2013). The top five statistically over-represented pathways, together with the genes involved in that pathway and the *p*-values are shown in the table.

2.2.8 Hypoxia-regulated genes in the HIF-α deficient cells

In contrast with the results in HIF-1β mutant cells, comparison of gene expression profiles of the normoxic and hypoxic HIF-α DKO cells only identified 29 differentially expressed genes.

As before, these genes were further divided into hypoxia up-regulated (n=8) and hypoxia down-regulated (n=21) ones. Similar to the analysis performed in the HIF-1β

mutant cells, the genes were stratified into 3 sub-categories based on their hypoxia-dependent regulation in the DKO cells compared to that in the WT cells. A summary is shown in **Figure 16.** The full list of genes together with their regulations in the WT and HIF-α DKO cells can be found in Appendix 8.5 and 8.6.

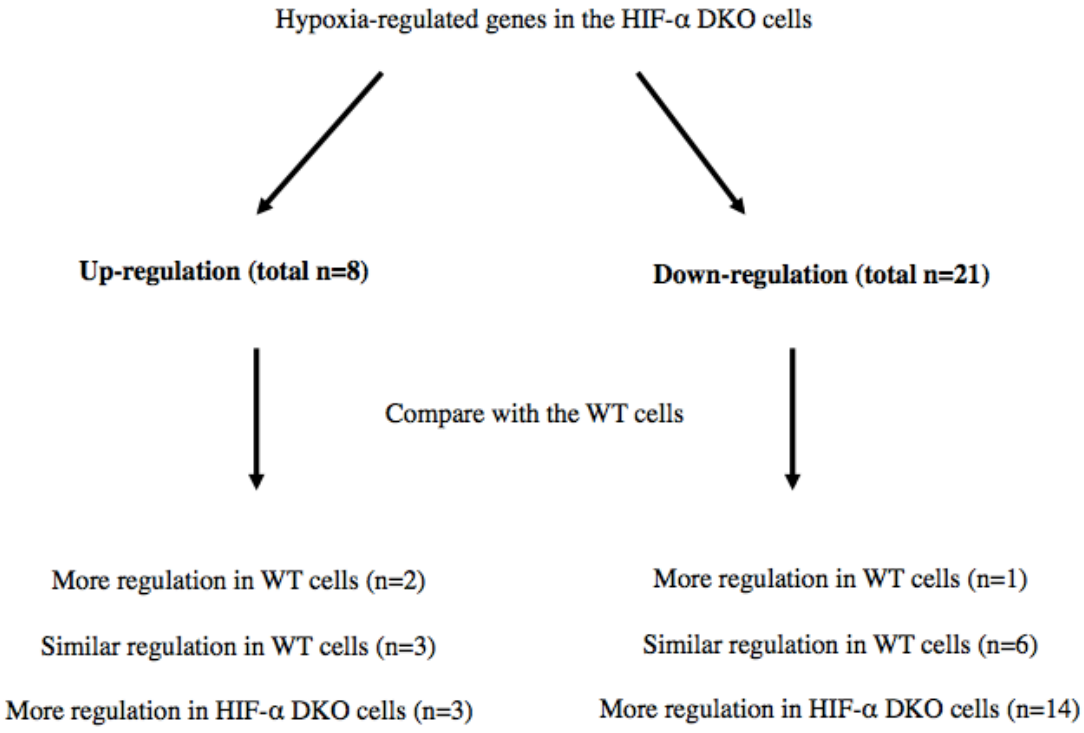

Figure 16. A summary of genes that are regulated by hypoxia in HIF-α DKO cells.

Amongst the 8 genes that were up-regulated by hypoxia, overall the amplitude of hypoxia regulation of these genes was again small (i.e. FC is between 1.60 to 2.36-fold). On the other hand, within the hypoxia down-regulated genes, the amplitude of hypoxia regulation (i.e. FC) was also small, i.e. FC is between 0.62 to 0.28-fold. Since observation earlier in this chapter indicates a modest correlation between genes down-regulated by hypoxia in the HIF-α DKO and WT cells, I therefore performed GO analyses on these hypoxia up and down-regulated genes. Due to the small number of genes identified in these mutant cells, GO analyses were performed for the total up or

down-regulated genes (**Figure 17**). The *p*-values associated with each pathway were generally small, and furthermore the analyses did not reveal any clear signature of alignment with specific common pathway.

A

Hypoxia up-regulation: (n=8)

	Genes	p-value
bone development	TRAPPC2; GNAS	0.0009443
cardiac endothelial cell differentiation	LAMA5	0.003595
L-serine biosynthetic process	PSAT1	0.003994
lymphatic endothelial cell differentiation	LAMA5	0.005189
endothelial cell development	LAMA5	0.002797

B

Hypoxia down-regulation: (n=21)

	Genes	p-value
negative regulation of translational initiation	RBM4; NCBP2	0.003315
negative regulation by virus of host cell division	TXNIP	0.006284
glutamine biosynthetic process	GLUD1	0.006284
positive regulation of mRNA polyadenylation	NCBP2	0.007328
nuclear-transcribed mRNA catabolic process, nonsense-mediated decay	NCBP2; RPL17	0.007529

Figure 17. GO pathway analyses were performed for the hypoxia up or down-regulated genes in HIF-α mutant cells using the EnrichR software (Chen et al., 2013). The top five statistically over-represented pathways, together with the genes involved in that pathway and the *p*-values are shown in the table.

2.2.9 Hypoxia-regulated genes in the VHLFIH deficient cells

In this mutant cell background, as a consequence of loss of both VHL and FIH proteins, the HIF pathway is constitutively stabilised with maximum transcription activity. As shown in the previous analyses, hypoxia-regulated gene expression was almost completely abolished in these cells both at the global level and at individual gene level (**Figure 7 and 8**). This indicates that the presence of VHL/FIH is essential for at least the large majority of the regulation of gene expression by hypoxia. Nevertheless, a small number of genes (n=50) passed the statistical thresholds and were defined as hypoxia regulated genes in these cells. Regulation of these genes may be due to a complete HIF-independent function irrespective of VHL-dependent degradation, but this was not supported by the analyses in section 2.2.5. It may also be due to a non-canonical function of HIF, mediated by the effect of reduced hydroxylation at P564 as shown in **Figure 5C**.

Within these genes, 27 were induced and 23 were suppressed by hypoxia. Full list of genes are in Appendix 8.7 and 8.8. Since no correlation of hypoxia regulation with the WT cells, these genes were not further divided into sub-categories. GO analyses were again performed for the total up or down-regulated genes by hypoxia in the mutant cells (**Figure 18**). However, the analyses did not reveal any strong evidence of a common physiological function.

A

Hypoxia up-regulation: (n=27)

	Genes	p-value
positive regulation of pseudopodium assembly	CDC42EP3; CDC42EP1	0.0001149
ribosomal large subunit biogenesis	RRS1; URB2	0.0008490
mitochondrion organization	ALAS1; PPRC1	0.003360
positive regulation of hh target transcription factor activity	CEBBG; PPRC1	0.006817
regulation of keratinocyte differentiation	ERRFI1	0.008074

B

Hypoxia down-regulation: (n=23)

	Genes	p-value
negative regulation of epidermal growth factor-activated receptor activity	SHC1; MVP	0.001440
intrinsic apoptotic signaling pathway in response to endoplasmic reticulum stress	CD24; HSP90B1	0.004973
immune response-inhibiting cell surface receptor signaling pathway	CD24	0.006881
interkinetic nuclear migration	SYNE2	0.007328
positive regulation of MAP kinase activity	SHC1; CD24	0.008053

Figure 18. GO pathway analysis was performed for the hypoxia up or down-regulated genes in the VHLFIH KO cells using the EnrichR software (Chen et al., 2013). The top 5 statistically over-represented pathways, together with the genes involved in that pathway and the *p*-values are shown in the table.

2.2.10 Characterisation of hypoxia up-regulated genes that only appeared in the HIF- 1β deficient cells

Analysis of hypoxia up-regulated genes in the HIF-1β KO cells has revealed a set of genes that were regulated by hypoxia in HIF-1β KO and not in the WT, HIF-α DKO or VHLFIH KO cells, and these genes had a striking signature of lipid metabolism pathways (**Figure 14C and Table 2.4**). This raised the possibility that a potential non-canonical

HIF-α mechanism might play a role in regulating the expression of these lipid metabolism genes when the HIF-1β subunit was absent.

To further characterise the signature of these hypoxia-regulated genes that were specific to the HIF-1β deficient cells, the upstream regulators that are associated with these genes were examined by Ingenuity Pathways Analysis software tool (Version IPA 8.8-3204) (**Figure 19**). The top 3 of these regulators (*SREBF2, SCAP, SREBF1*) that were predicted by IPA are directly involved in lipid metabolism (Hughes et al., 2005; reviewed in Osborne and Espenshade 2009). *TP53* has also previously been identified as a novel regulator of lipid metabolism pathways in cancer (reviewed in Parrales and Iwakuma, 2016). Overall, this result indicated a clear signature of lipid metabolism regulation within this sub-group of hypoxia-induced genes.

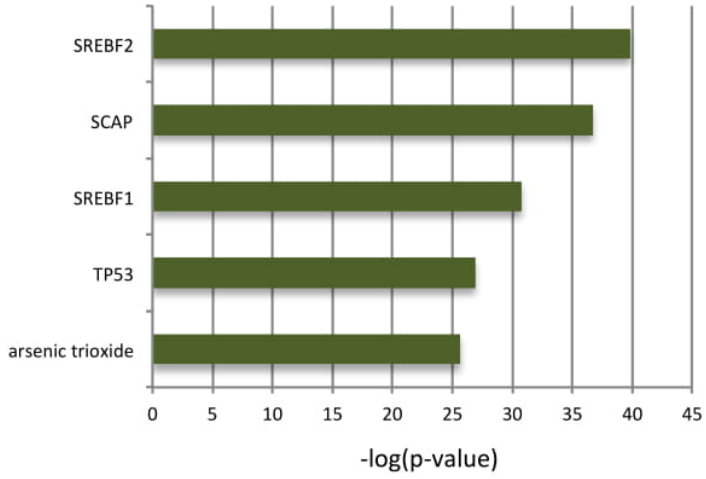

Figure 19. Downstream analysis of hypoxia up-regulated genes that specifically regulated in the HIF-1β mutant cells using Ingenuity Pathway Analysis (IPA). The top 5 upstream regulators identified by IPA are displayed and are ranked by the –log10(*p*-value). –log10(*p*-value)>1.3 denotes a level of significance.

The top 3 candidates (*INSIG1, ACSS2, HMGCS1*) with the largest hypoxia induction levels in the HIF-1β KO cells were selected for validation in the RT-qPCR assays (**Figure 20**). The expression levels of these lipid genes were examined across multiple biological replicates (n=5) in the WT, HIF-1β mutant and HIF-α mutant cells that were cultured under normoxia (21% O_2) or hypoxia (0.5% O_2) for 24h. The gene expression levels were also measured in cells that were cultured up to 48h in hypoxia, since the further accumulation of transcripts over time might enable more confident assessment of any signal.

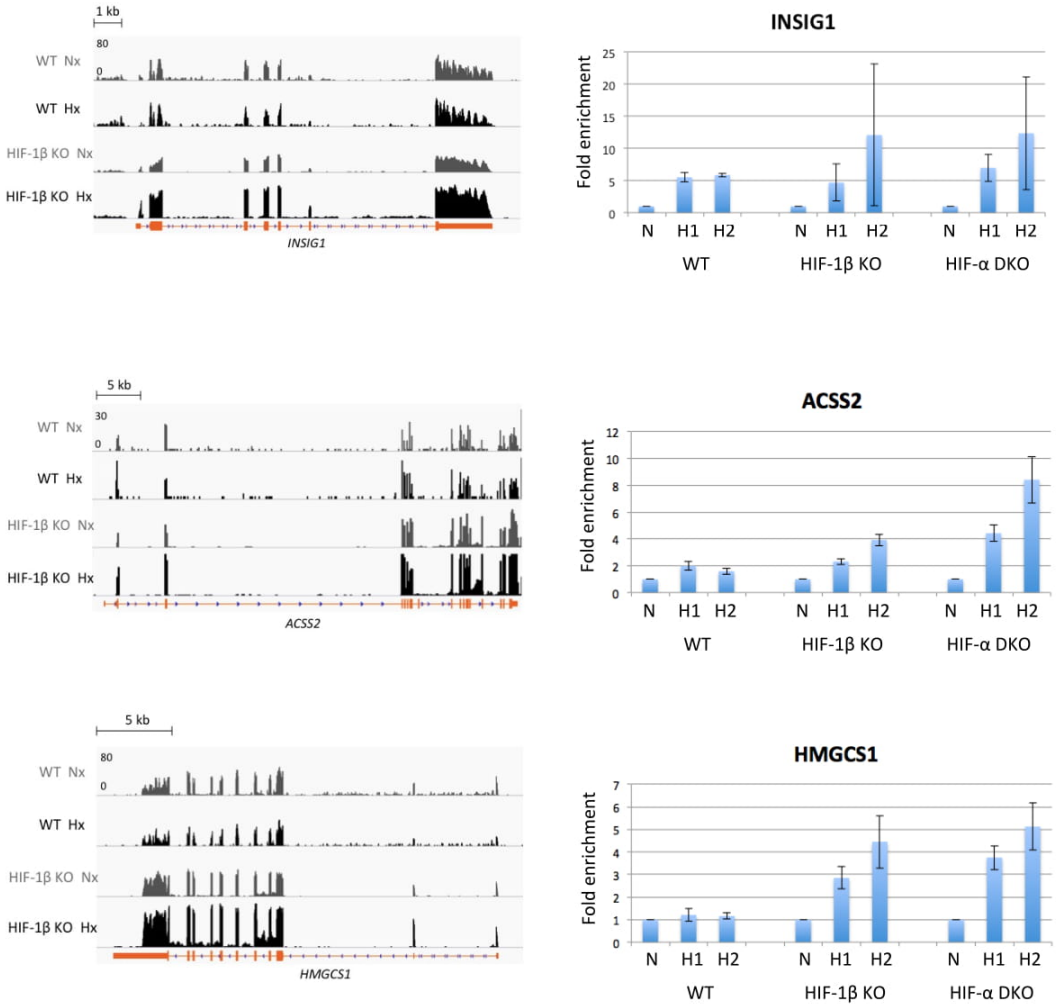

Figure 20. Analysis of candidate genes with the largest hypoxia-dependent regulation in the HIF-1β mutant cells using RT-qPCR assays. WT, HIF-1β KO and HIF-α DKO cells were cultured under normoxia (N) or hypoxia (0.5% O_2, H1=24h, H2=48h). Hypoxic induction of *INSIG1* and *ACSS2* (but not *HMGCS1*) was observed in the WT cells cultured for 24h and 48h. Hypoxic induction of *ACSS2* and *HMGCS1* were observed in the HIF-1β mutant cells, but there was no significant induction of *INSIG1*. For all three genes tested, there were significant hypoxic inductions in the HIF-α DKO cells after both 24h and 48h culture. The fold enrichment of each gene was normarlised to the values for the housekeeping gene *HPRT* in each condition using the delta-delta CT method. Bar shows mean ± s.d. n=5 biological replicates were performed. *INSIG1* represents Insulin Induced Gene 1. *ACSS2* represents Acyl-CoA Synthetase Short Chain Family Member 2. *HMGCS1* represents 3-Hydroxy-3-Methylglutaryl-CoA Synthase 1.

Induction of *INSIG1* and *ACSS2* but not *HMGCS1* was observed in the WT cells at both 24h and 48h of hypoxia. All three genes showed a small but significant hypoxia induction in the HIF-1β KO cells at 24h. For *ACSS2* and *HMGCS1*, the levels of induction at 24h of hypoxia in the mutant cells were higher than those in the WT cells, and the levels increased further at 48h. However in contradiction to the RNA-seq data, which revealed no statistically significant hypoxia induction of these genes in the HIF-α DKO cells, a robust up-regulation of gene expression was observed at both 24h and 48h hypoxia in these cells. A closer inspection of the RNA-seq data indicated that one of the replicate had a lower read count, therefore the hypoxia up-regulation of these lipid genes was observed in only one replicate but not the other. This could potentially explain why the lipid genes signature was missed in the RNA-seq analyses. However the lack of lipid signatuere in one RNA-seq replicate could also be variation in a stress response.

In order to test whether the increase in mRNA level was followed by an increase at the protein level, immunoblots of HMGCS1 protein were undertaken using the whole cell extracts that had been prepared in parallel with RNA harvested for the RT-qPCR experiments (**Figure 21**). HMGCS1 protein appeared to be slightly down-regulated by hypoxia in the WT cells at both 24h and 48h in both replicates, but was either unaffected or induced by 48h of hypoxia in both HIF-1β KO and HIF-α DKO cells.

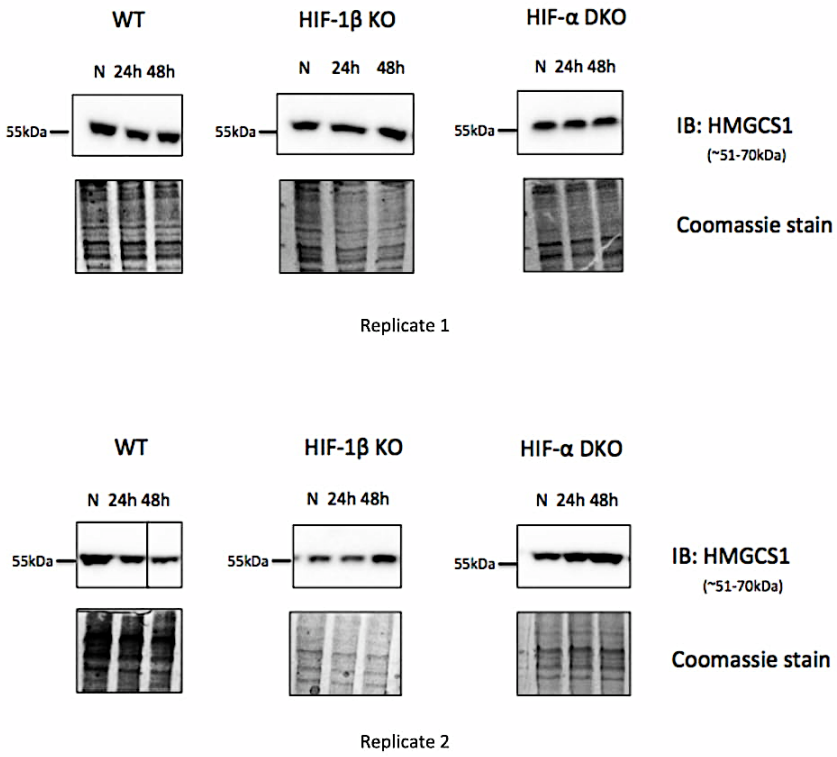

Figure 21. Two representative immunoblots of HMGCS1 protein using the whole cell extracts from WT, HIF-1β mutant or HIF-α mutant cells. The cells were cultured under normoxia (N) or hypoxia (0.5% O_2 for 24h or 48h). HMGCS1 protein was down-regulated by hypoxia (24h and 48h) in the WT cells but showed an induction by hypoxia (48h) in both the HIF-1β KO and HIF-α DKO cells.

2.3 Discussion

In this chapter, extensive analyses of RNA-seq data were performed to examine the contribution of the HIF pathway to the regulation of hypoxia-dependent gene expression.

By comparing the normoxic and hypoxic gene expression profiles in the HKC-8 WT cells, I identified 536 genes that showed significant up-regulation, and 357 genes that showed significant down-regulation by hypoxia. Thus, as has been observed in previous studies almost as many genes were down-regulated as up-regulated by hypoxia. HIF is known to be a transcriptional activator rather than a repressor of gene transcription under hypoxia, by the direct interaction with promoters of its targets (Schödel et al., 2011; Xia et al., 2009; Mole et al., 2009). However it has been proposed that hypoxia down-

regulated genes are regulated through indirect mechanisms that connect the HIF pathway with repressive functions and thus that both up-regulation and down-regulation of gene expression may be HIF dependent.

By comparing the expression of hypoxia-regulated genes in the WT cells and across the range mutant cells (i.e. HIF-α DKO, HIF-1β KO and VHLFIH KO cells), the data suggests that at the global level, loss of the HIF pathway, as well as a constitutively activated HIF pathway, greatly reduces or ablates the hypoxic responses of a very large number of genes (**Figure 7A and 8A**). Furthermore, the loss of HIF-1β protein generally had broadly similar effects to the loss of HIF-α on the amplitude of regulation by hypoxia, indicating that HIF-α, and HIF-1β subunits are both important for hypoxia-dependent gene regulation. This implies that the hypoxia response is mainly mediated by a functional HIF pathway that requires canonical heterodimerisation of HIF-α, and HIF-1β subunits. Similarly, hypoxia-dependent regulation across the majority of genes was greatly reduced in the HIF-α mutant and in the VHLFIH KO cells. Taken together, these findings demonstrate the quantitative importance of the HIF pathway in regulating gene expression under hypoxia.

2.3.1 Potential HIF-independent hypoxia-dependent gene expression

The availability of RNA-seq data across WT and the different mutant cells provided a powerful means to identify hypoxia inducible pathways that were completely independent of HIF. In particular, it was argued that regulation by hypoxia that was independent of HIF ought to be present in WT cells and persist at the same level in each of the mutant cell lines. Thus by examining data from all, as opposed to just one cell line, it ought to be possible to distinguish between errors arising from random variation in assays of gene expression and signals that were genuinely produced by HIF-independent mechanisms.

To probe for potential HIF-independent genes in the HKC-8 cells, both statistical and manually imposed thresholds were applied to select genes with persistent hypoxia-dependent regulation across multiple cellular backgrounds. In the statistical analysis comparing hypoxic gene-regulation across all of the WT and HIF mutant cells, only one candidate gene (*LOC100506548*) was identified. This gene also appeared in additional analyses designed to determine if there was regulation by hypoxia which was reproducible but which has failed to reach significance across all cell lines in the statistically defined analysis. However, the amplitude of regulation of this potential HIF-independent hypoxia regulated gene (and another two candidates for HIF-independent hypoxia up-regulation) was low and did not show consistent hypoxia-dependent up-regulation across all of the WT and mutant cells when tested in independent RT-qPCR experiments (**Figure 11**). Similarly, no hypoxia-dependent regulation of the candidate HIF-independent hypoxia down-regulated genes was observed in the independent RT-qPCR experiments (**Figure 12**). One potential explanation for the inconsistency between RT-qPCR experiments and the RNA-seq data could be that the hypoxia regulation of these genes was of low amplitude based on the RNA-seq data for the WT cells, i.e. the averaged hypoxia regulation was 1.91-fold for the up-regulated genes, and was 0.66-fold for the down-regulated genes. Therefore, it is possible that this signal may be missed in the RT-qPCR assays due to a lack of sensitivity, or that the original assignment of relativity small numbers of genes whose regulation by hypoxia was of low amplitude represented 'noise' in the RNA-seq analyses. Overall, in these analyses, there was therefore no strong evidence of persistent hypoxia-dependent regulation that was truly independent of HIF. Although HIF has been previously described as the master regulator of gene expression by hypoxia, this result was somewhat surprising, in view of the many

systems that have been proposed to generate hypoxia-dependent changes in gene expression independently of HIF as outlined in the introduction to this chapter.

It is possible that some of these pathways do not operate in HKC-8 cells, or only operate under different hypoxic conditions. For instance, HIF-independent hypoxia-dependent regulation of certain genes has been proposed to be regulated by p53 (reviewed in Sermeus and Michiels. 2011). However, HKC-8 cells do not express WT p53 therefore the pathway does not operate in this cellular setting. Furthermore, hypoxic gene expression can be regulated by members of 2-OG oxygenases other than PHDs and FIH, e.g. through the JmjC-domain containing histone lysine demethylases (JmjC-KDMs) (reviewed in Hancock et al., 2015). The activity of JmjC-KDMs has been shown to be affected by changing O_2 concentration, at least *in vitro* (Sanchez-Fernandez et al., 2013). However the severity of hypoxia or time-course of any change might be different from the conditions used in these experiments. As outlined above in introduction, the HIF prolyl hydroxylase (PHD) enzymes have been reported to catalyse prolyl hydroxylation on many other substrates, including transcription factors such as FOXO3a, signal pathway intermediates such as Akt, and components of the transcriptional apparatus such as RNA Pol2. It is difficult to understand how the conditions of the current experiments would affect prolyl hydroxylation of HIF and not that of these other substrates. Therefore it would appear that if these reactions are occurring, they have little effect on gene expression.

In summary, this work clearly demonstrates that the large majority of changes in gene expression induced under these conditions are mediated by the canonical function of HIF-α/β. It revealed no evidence for high amplitude HIF-independent regulation of gene expression by hypoxia. It remains possible that some low amplitude regulation of gene expression by hypoxia occurs that is independent of HIF, but proof of this would require

substantially more sequencing depth and or experimental repetition to provide the necessary evidence.

2.3.2 Potential non-canonical HIF-α function of hypoxia-dependent gene expression observed in the HIF-1β KO cells

In contrast with the absence of consistent regulation by hypoxia across all cell lines, analyses of each three mutant cell line revealed some evidence for regulation of gene expression by hypoxia in that particular cell line. In both HIF-α DKO cells and VHL FIH KO cells such regulation was low in amplitude, affected only small numbers of genes, bore no clear relation to regulation by hypoxia in WT cells and did not appear to be focused on any specific physiological pathway.

However in HIF-1β KO cells, persistent regulation by hypoxia was more evident. Many more genes were significant regulated by hypoxia in this mutant background as opposed to the HIF-α DKO and VHLFIH KO cells. Moreover amongst the genes that were up-regulated by hypoxia in the HIF-1β KO cells, there was a significant, albeit weak, correlation with the extent of regulation in WT cells. In keeping with this, these genes manifest a signature of the hypoxia and HIF pathways in GO analyses that have been derived from published studies in HIF competent cells.

These findings are consistent with the possibility of some non-canonical functions of HIF-α as unlike in the other cell backgrounds, HIF-α subunits remained strongly regulated by hypoxia in the HIF-1β KO background. Indeed an increased accumulation of HIF-1α protein was observed in the hypoxic HIF-1β KO cells as compared with WT cells. At the protein level, this could be due to the loss of negative feedback loops provided by the PHD enzymes, which are regulated by HIF and normally accumulate during hypoxia to reduce HIF-α proteins (mainly HIF-1α) through increased prolyl hydroxylation (Ginouve et al., 2008). At the transcript level, it might be due to the

absence of the negative effects mediated by the HIF-dependent antisense HIF-1α (aHIF), therefore resulting in an increased level of HIF-1α transcript (Uchida et al., 2004). In addition, there was a significant accumulation of HIF-1α and HIF-2α proteins in the nucleoplasm of HIF-1β mutant but not in the WT cells (**Figure 3**). This suggests that the loss of HIF-1β protein may affect the sub-nuclear localisation of HIF-α subunits, although the function of these nucleoplasmic HIF-α proteins is unknown. Alternatively, this could be due to the increased total amount of HIF-α protein in the mutant cells hence an increased amount of HIF was observed in the nucleoplasm. Further experiments would be required to explore this observation. However the current work clearly demonstrated enhanced hypoxia regulation of HIF-α by oxygen in HIF-1β deficient cells, raising questions to the whether it might be responsible for regulation of gene expression by non-canonical mechanisms.

There are several possibilities that might underlie such non-canonical function of HIF-α. First of all, action of HIF-α through association with other TFs (such as USF and SP-1) has been reported elsewhere (Pawlus et al., 2012; Koizume et al., 2012). Secondly, HIF-α (particularly HIF-2α) may have indirect consequences on the translation of certain genes (Uniacke et al., 2012). Thirdly, HIF-α might also form a complex with other HIF-β isoforms. The human genome encodes two HIF-1β genes (*ARNT, ARNT2*) and additional two related bHLH-PAS proteins (*ARNTL* and *ARNTL*). The RNA levels of *ARNT2, ARNTL* and *ARNTL2* in HKC-8 cells are very low compared to *ARNT* and it is unclear how this translates to protein level. Finally it is possible that despite the demonstration of absent induction of specific HIF target genes and HRE-linked reporter genes in the HIF-β deficient cells, a small level of HIF-1β persists in these cells that is below the limit of detection, but yet able to mediate HIF activity on certain targets. Further experiments such as suppression of the HIF-α subunit and of each of the HIF-1β isoforms by siRNA

might elucidate this potential non-canonical HIF-α function in the HIF-1β mutant cells, but might be restricted by the lack of high sensitivity anti- HIF-β antibodies to monitor the interventions.

2.3.3 Increased hypoxic regulation of genes encoding lipid metabolism pathways in HIF deficient cells

Unexpectedly, HIF-1β defective cells were also observed to manifest regulation of certain genes that were not regulated by hypoxia in WT cells. For those genes that were specifically down-regulated by hypoxia in the HIF-1β mutant cells, a signature of protein translation process was observed (**Figure 15**). Interestingly, negative regulation of translational initiation was also observed (albeit weak) in the hypoxia-regulated genes that appeared in the HIF-α mutant cells (**Figure 17**). It has been well-characterised that hypoxia stress induces a global down-regulation of oxygen consumption and protein synthesis (Hochachka et al., 1996; Pettersen et al., 1986). Therefore, the observations of hypoxia down-regulation of the protein synthesis genes in these mutant cells are in keeping with the existing literature, and suggest that these mutant cells may manifest a greater energy defect.

Interestingly analysis of those genes that were up-regulated by hypoxia revealed a striking signature of lipid metabolism pathways and upstream regulators, including the sterol regulatory-element binding protein (SREBP) (**Figure 20**).

SREBP is the major TF involved in regulating lipid metabolism by stimulating *de novo* fatty acid and cholesterol biosynthesis (reviewed in Osborne and Espenshade 2009). Early work in yeast (*S. pombe*) and *C.elegans* indicated that SREBP mRNA was up-regulated by hypoxia and was required for the expression of lipogenesis genes (Todd et al., 2006; Taghibiglou et al., 2009). However, the oxygen-dependent regulation of SREBP in mammalian cells is poorly understood. This is partly because in addition to *de*

novo lipid synthesis, mammalian cells can also receive lipid from endocytic receptor-mediated pathways, which might also be regulated by oxygen, therefore complicating analysis of the SREBP response pathway to oxygen. Several studies have reported a role of the HIF pathway in regulating SREBP and lipogenesis. It has been shown that hypoxia can up-regulate the expression of SREBP and enhance its binding to the SREBP-binding site on the promoter of the fatty acid synthase (FAS) gene in a HIF-1α dependent manner (Furuta et al., 2008). In another study, inactivation of VHL in the mouse liver also resulted in an increased expression of SREBP-1c (an isoform of mammalian SREBP protein) in a HIF-2α but not HIF-1α dependent manner (Rankin et al., 2009). In contradistinction to these observations, a study reported an inhibitory effect of the HIF pathway on the mRNA and protein level of SREBP, via up-regulation of the transcriptional repressor DEC1 (Differentiated Embryo Chondrocyte 1) and its isoform DEC2 (Choi et al., 2008). Furthermore, a hepatocyte-specific deletion of HIF-1α in mice led to increased expression of SREBP-1c and an increased fatty acid synthesis (Nishiyama et al., 2012). In addition, mice with liver-specific HIF-1β ablation also showed increased mRNA and protein levels of SREBP-1c (Wang et al., 2009). Overall, the interaction between HIF and the SREBP pathway is complex, and whether SREBP is also capable of regulating lipogenesis under hypoxia in a HIF-independent manner remains unclear.

Other previous work has focused on lipid metabolism genes themselves. Interestingly, several of genes defined in the current work (*INSIG1, ACSS2, HMGCS1*) were observed to be up-regulated by hypoxia (or hypoxia-mimic treatment) in other cell lines, but dependence on HIF was inconsistent. In some studies the regulation was proposed to be HIF-dependent (Nguyen et al., 2007; Schug et al., 2015; Lin et al., 2014).

However, the hypoxia-dependent up-regulation of ACSS2 gene was found to persist even in the cells with a silenced HIF-1β (Schug et al., 2015).

In the current work, increased regulation by hypoxia in the absence of HIF-1β, strongly supports the existent of regulation a pathway that is independent of canonical HIF function. Though initial analyses of the RNA-seq suggested that regulation was not observed in HIF-α DKO this was not borne out by further RT-PCR analyses in these mutant cells. Instead it appeared that regulation by hypoxia was observed in both HIF-1β mutant cells and HIF-α DKO, but that this was somewhat inconsistent. These finding indicated that the response was unlikely to be a non-canonical function of HIF-α that was revealed by inactivation of HIF-1β. A more likely possibility is that the changes are in response to metabolic stress that is enhanced in cells that are defective in the HIF transcriptional response to hypoxia. Lipid synthesis is an energy and oxygen consuming process. Cells that are defective in different components of the HIF system have been reported to have a reduced capacity to maintain ATP levels in hypoxia (Fukuda et al., 2007; reviewed in Semenza. 2010), and to be prone to oxidative stress in hypoxia (Schipani et al., 2001). Moreover oxidative stress has been associated with changes in lipid metabolism. Defining whether these processes are involved in the findings revealed by the current work will require further investigation.

2.4 Conclusion

An extensive analysis of hypoxia-dependent gene expression has been performed in HKC-8 WT cells and in a series of mutant cells with different genetic defects in the HIF pathway. The data suggests the majority of changes in gene expression following hypoxia exposure in HKC-8 cells are mediated through the HIF pathway, and require both HIF-α and HIF-1β subunits to be intact, and the presence of VHL/FIH. Little evidence has been

found for completely HIF-independent mechanisms of gene regulation under hypoxia. However, an up-regulation of genes involved in lipid metabolism was observed in the HIF-1β mutant cells under hypoxia, which may be mediated by an alternative pathway such as SREBP, and/or could be a stress response to hypoxia due to the deficiency of an effective HIF system.

Interestingly, within the hypoxia-regulated genes identified in the WT cells, a small number of genes showed persistent hypoxia up-regulation in the HIF-1β mutant cells. The regulation of these genes by hypoxia correlated moderately with that in the WT cells. Since neither these genes nor any such correlation was observed in HIF-α mutant or VHLFIH mutant cells, these genes may represent a non-canonical HIF-α function. Whether this might be due to use of alternative HIF-β subunit, or a function that is completely independent of HIF-β is unclear. However the observed correlation with responses to hypoxia in WT cells indicates that whatever the mechanism it is focused on genes that are also induced by the canonical HIF-α/β pathway.

Overall however, given the number of proposed mechanisms for HIF-independent responses the hypoxia, the most surprising finding was the strength of evidence at a pan-genomic level for the importance of HIF in essentially all high amplitude responses to hypoxia.

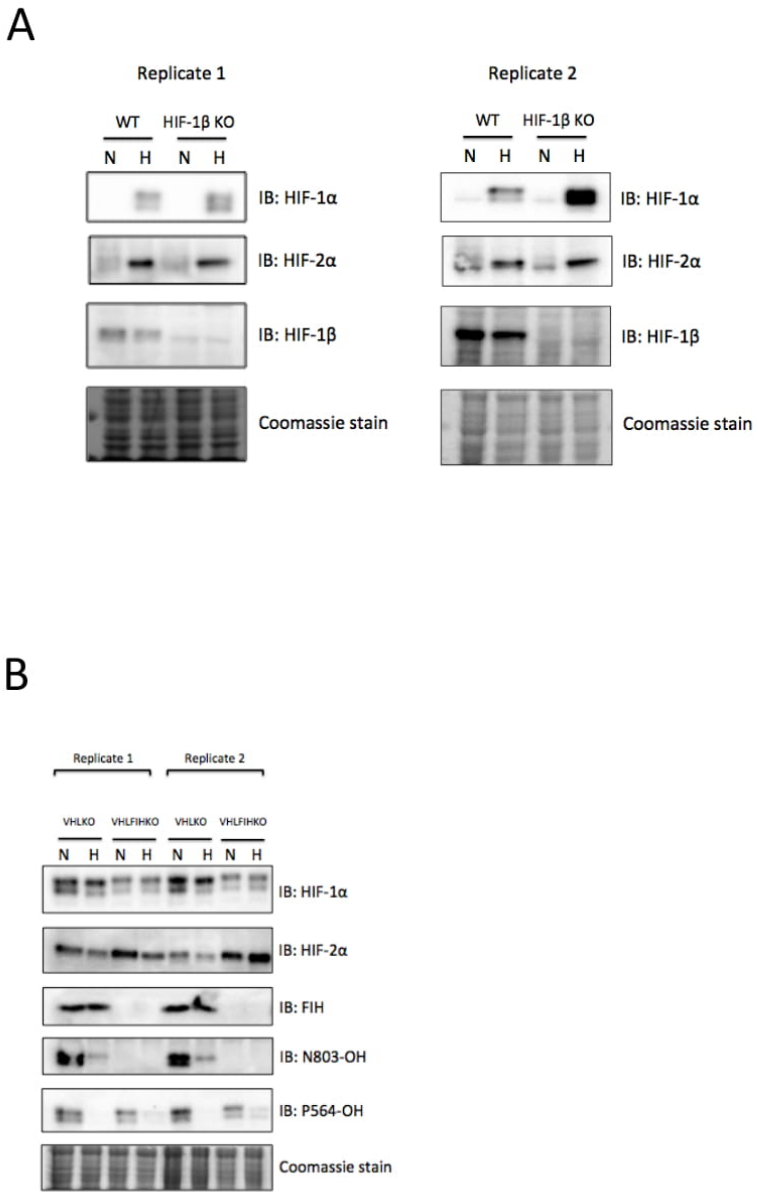

Supplementary Figure 1. Immunoblots using the whole cell extracts that were harvested in parallel with samples submitted for RNA-seq. (A) Two replicates of cell lysates from the WT and HIF-1β KO cells confirmed the absence of HIF-1β protein in the mutant cells, as well as the stabilisation of HIF-1α and HIF-2α proteins under hypoxia (0.5% O_2 for 24h). (B) Constitutive expression of both HIF-1α and HIF-2α proteins was observed in the VHLFIH KO and VHL KO cells that were cultured under normoxia or hypoxia (0.1% O_2 for 24h). There was no FIH protein or hydroxylation of HIF-1α at asparagine residue (N803) in the VHLFIH KO cells, confirming the loss of FIH protein and its function. An absence of hydroxylation of HIF-1α protein at proline residue (P564) in the hypoxic VHLFIH KO and VHL KO cells indicated a lack of function of PHD enzymes at 0.1% O_2. N refers to normoxia. H refers to hypoxia.

3

The Effects of (Acute) Graded Hypoxia on HIF Binding Genome-wide

3.1 Introduction

The range of oxygen concentrations experienced by cells *in vivo* under physiological and pathophysiological conditions can vary greatly, depending on the oxygen supply and consumption in specific tissues and cells (reviewed in De Santis et al., 2015). In healthy tissue, the oxygen tension is generally 20-70 mmHg (equivalent to 2.5-9% O_2), whereas in areas where oxygen demand exceeds oxygen supply, hypoxia exists as 8-10 mmHg (~1% O_2) (Nizet and Johnson. 2009). Markedly lower levels of oxygen tension (<1% O_2) have been described in pathological conditions such as wounds and sites of infection, and hypoxia is often associated with adverse outcomes in diseases such as cancer (Höckel and Vaupel. 2001), cardiovascular (Giordano. 2005) and diabetic disorders (Norouzirad et al., 2017). On the other hand, in tissue culture hypoxia is generally defined as levels equivalent to between 0.5% and 3% O_2 by volume in the air that is in equilibrium with

the growth medium (Nizet and Johnson. 2009). Thus, hypoxia is not a simple presence-absence dichotomy and may vary greatly in intensity.

Hypoxia is a common feature of the microenvironment of solid tumours due to the dysregulated proliferation of cancer cells in the absence of a sufficient and functional vascular bed and therefore inadequate oxygen delivery. As a result, a solid tumour often contains areas with different levels of hypoxia. Hypoxia subsequently activates a hypoxic response via the HIF system. This has been demonstrated in tumours *in vivo* and is associated with a poor clinical outcome (Brizel et al., 1996; Höckel et al., 1991).

The level of endogenous HIF-α protein is tightly regulated by cellular oxygen concentrations. This has been shown both *in vitro* by immunoblot (Huang et al., 1996) and *in vivo* by immunohistochemical staining (Rosenberger et al., 2002). Observations in multiple tissue culture cell lines suggest that HIF-α protein levels are inversely related to oxygen concentration (Jiang et al., 1996; Bracken et al., 2006; Uchida et al., 2004; Nguyen et al., 2013). In these studies, cells were exposed to ambient gas mixtures containing intermediate oxygen concentrations between 0% and 21%, and HIF-α expression as measured by immunoblotting increased as oxygen concentrations went down. Jiang et al., demonstrated that in HeLa cells HIF-1α protein showed a half maximal response between 1.5 and 2% O_2 and a maximal response at <1% O_2 (Jiang et al., 1996). The stabilisation of HIF-α protein in response to graded hypoxia is primarily due to the progressive reduction in activity of prolyl hydroxylases. This was first shown where using VHL capture assays, the hydroxylation of HIF-α peptides was shown to be sensitive to graded levels of hypoxia (Epstein et al., 2001).

HIF-1α and HIF-2α protein levels have also been directly compared in response to varying oxygen concentrations in multiple cell lines (Bracken et al., 2006; Uchida et al., 2004). In general the stabilisation of HIF-1α and HIF-2α proteins occurred under similar

O_2 levels and both isoforms showed a maximal induction at <1% O_2. However, in some cases such as in neuroblastoma cell lines (Holmquist-Mengelbier et al., 2006) and in HeLa cells (Wiesener et al., 1998), HIF-2α can be stabilised at 5% O_2, whereas HIF-1α protein was hardly detectable in that oxygen concentration.

Since HIF-α protein is expressed at different levels in response to different degrees of hypoxia, an important question to ask is whether this results in differences in the activation of HIF target genes and downstream responses. In general terms, both the cellular abundance and genomic binding pattern of transcription factors (TFs) are important determinants of the repertoire of genes expressed. For several TFs, differential expression levels are known to have different functional outcomes. For instance, low levels of MITF (Microphthalmia-associated Transcription Factor) protein can give cells an invasive and stem-like phenotype. By contrast, high levels of MITF can result in a differentiated state by expressing differentiation-associated genes such as *MART1* (Melan-A) and *TYR* (Tyrosinase), or a proliferating state by expressing genes involved in proliferation and survival such as *CDK2* (Cyclin Dependent Kinase 2) and *BCL2* (BCL2, Apoptosis Regulator) (reviewed in Hoek and Goding. 2010). However, so far the link between differential expression of TFs and their functional outputs is not well understood.

'High' and 'low' affinity TF binding sites have also been described (reviewed in Biggin. 2011). Genomic regions manifesting high levels of TF occupancy (i.e. high affinity sites) were thought more likely to exert a biologically significant function than regions bound by only a few TFs. This was demonstrated by chromatin immunoprecipitation followed by microarray assays in *Drosophila* (MacArthur et al., 2009) and by chromatin interaction analysis in human MCF-7 cells (Fullwood et al., 2009). However, it has also been shown that 'weak' binding sites can sometimes be

critical in promoting gene expression at certain stages of development. For instance, binding at low-affinity sites located in the enhancers of certain genes are required for shaping morphogen responses in *Drosophila* (Ramos et al., 2013); TF binding at two phylogenetically conserved low-affinity sites in mouse *pax6* gene enhancer is important in regulating lens formation (Rowan et al., 2010). Overall the existence of different amounts of TFs, and sites with different affinities provide the potential for differential loading of TFs across the genome.

In the context of HIF, it remains unknown whether there are differences in the repertoire of binding sites occupied when there are high or low levels of HIF expression. Several pan-genomic analyses of HIF DNA-binding have been performed to date (Mole and Blancher et al., 2009; Schödel et al., 2011; Xia et al., 2009). However, these have been largely qualitative and have focused on high-stringency sites at a single oxygen concentration. Identifying potential differences in the effects of HIF across oxygen concentrations is important both in terms of basic biology and in allowing more focused future searches for new therapeutic targets that activate specific downstream components of the HIF pathway.

As well as potential differences in binding that are associated with HIF level, we would also like to distinguish binding of the major HIF isoforms. Existing studies suggest HIF-1α and HIF-2α subunits regulate overlapping but distinct target gene repertoires (Hu et al., 2003; Warnecke et al., 2004; Raval et al., 2005; Shen et al., 2011) and this is likely due to the divergent binding profiles of the two subunits (Salama et al., 2015).

An important challenge of analysis at the transcriptomic level is its complexity. Cross-regulation between TFs and redundant regulation are prevalent in animal regulatory networks (Reviewed in Davidson. 2010). This makes it difficult to

unambiguously distinguish genes that are directly regulated by a specific TF or are secondary or tertiary targets. Given that transcriptional regulation by HIF is directly evoked by HIF-binding, I therefore decided to use pan-genomic measurement of HIF binding by chromatin immunoprecipitation coupled with deep sequencing (ChIP-seq). It was anticipated that this technology would provide sufficient power to accurately and directly measure the HIF binding profile in response to hypoxia gradient, and to assess the two HIF isoforms.

In summary, the major focus of this chapter is to perform quantitative analyses to examine HIF DNA-binding in response to various oxygen concentrations in the HKC-8 cells, aiming to address the following mechanistic questions:

1. Does the level of HIF DNA-binding correlate with the HIF protein level?
2. Is the level of HIF DNA-binding similar across potential binding sites, or do some sites 'load' preferentially and/or redistribute their bound HIF as the hypoxic stimulation becomes more severe?
3. Do HIF-1α and HIF-2α exhibit different DNA-binding profiles in response to graded hypoxia?

3.2 Results

3.2.1 Effect of graded oxygen concentrations on patterns of HIF protein

Three different oxygen concentrations were studied for effects on HIF protein level and HIF DNA-binding i.e. atmospheric conditions (21% O_2), mild hypoxia (3% O_2), and more severe hypoxia (0.5% O_2). A time course observation in HKC-8 cells showed that the induction of HIF-α protein was greater after 6h of hypoxic incubation than at 16h or 48h (data is shown in Chapter 4). Therefore a period of 6h hypoxic incubation was chosen for this study.

HKC-8 cells were incubated in normoxia or at either 3% or 0.5% O_2 for 6h. In the immunoblot from a pilot experiment, more severe hypoxia led to higher levels of HIF-1α and HIF-2α protein being detected in whole cell extracts (**Figure 1A**). The antibodies used initially for HIF-α detection and experimental planning were mouse monoclonal antibodies. Similar results were obtained using the independent rabbit polyclonal antibodies that will be used for ChIP-seq (**Figure 1B**).

3.2.2 ChIP and ChIP-seq for HIF subunits

Having established that there was a significant increase in both HIF-1α and HIF-2α protein level between 21% and 3% O_2, and between 3% and 0.5% O_2, these conditions were then used to analyse HIF DNA-binding genome-wide.

ChIP-seq experiments were performed using antibodies directed against HIF-1α, HIF-2α and HIF-1β to measure HIF-binding, as illustrated in **Table 3.1**.

Table 3.1. An outline of ChIP-seq experiments performed in this chapter

cell line	condition	ChIP	reps
HKC-8 wild type (WT)	Normoxia 21% O_2	HIF-1α, HIF-2α, HIF-1β	1
HKC-8 wild type (WT)	6h 0.5% O_2	HIF-1α, HIF-2α, HIF-1β	2
HKC-8 wild type (WT)	6h 3% O_2	HIF-1α, HIF-2α, HIF-1β	2
HKC-8 HIF1/2α double KO	Normoxia 21% O_2	HIF-1α, HIF-2α, HIF-1β	1
HKC-8 HIF-1β KO	Normoxia 21% O_2	HIF-1α, HIF-2α, HIF-1β	1

Briefly, HIF proteins were cross-linked with DNA and subsequently sheared by sonication to 250-300 bp fragments. Three antibodies previously validated for ChIP-seq experiments in our laboratory were used to immunoprecipiate fragments bound by HIF-1α, HIF-2α and HIF-1β. (Schödel et al., 2011; Mole and Blancher et al., 2009) HIF-captured DNA fragments were submitted for sequencing to the Oxford Genomic Centre at the Wellcome Trust Centre. 75 bp reads were mapped to the human genome (Human Genome 19). Detailed methods for sample preparation, peak calling and subsequent assessment are described in the Materials and Methods Chapter.

In addition to the cells harvested for ChIP-seq, whole cell extracts were prepared in parallel for analysis of HIF protein levels by immunoblots. This aimed to enable quantification of the fold change in protein level between the different ChIP-seq conditions. As expected, an increase in hypoxic HIF-α protein level was seen between 21% and 3% O_2, and a bigger contrast was observed between 3% and 0.5% O_2 **(Figure 1C)**. On average across two ChIP-seq experiments and an additional independent replicate, there was a 4.7-fold increase of HIF-1α between 21% and 3%, and around a 26.6-fold increase from 3% to 0.5% O_2. For HIF-2α, there was 1.6-fold more protein at 3% than at 21% O_2, and 3.0-fold more protein at 0.5% O_2 than at 3% O_2. HIF-1β protein level was unchanged across the three hypoxic conditions (**Figure 1D**).

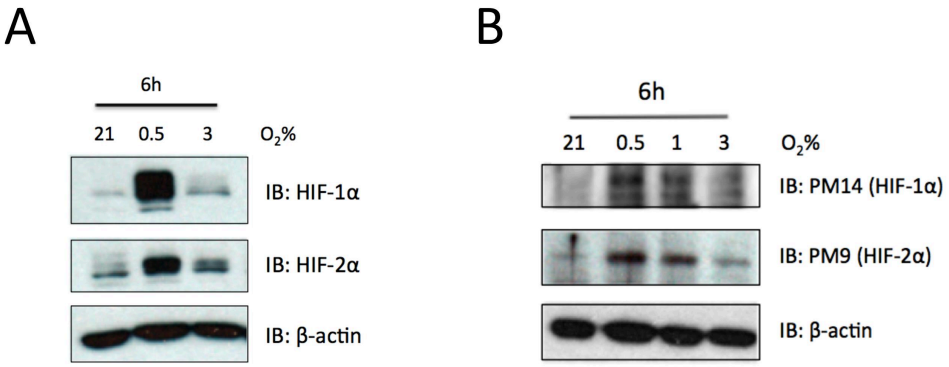
A
6h
21 0.5 3 O_2%
IB: HIF-1α
IB: HIF-2α
IB: β-actin
B
6h
21 0.5 1 3 O_2%
IB: PM14 (HIF-1α)
IB: PM9 (HIF-2α)
IB: β-actin

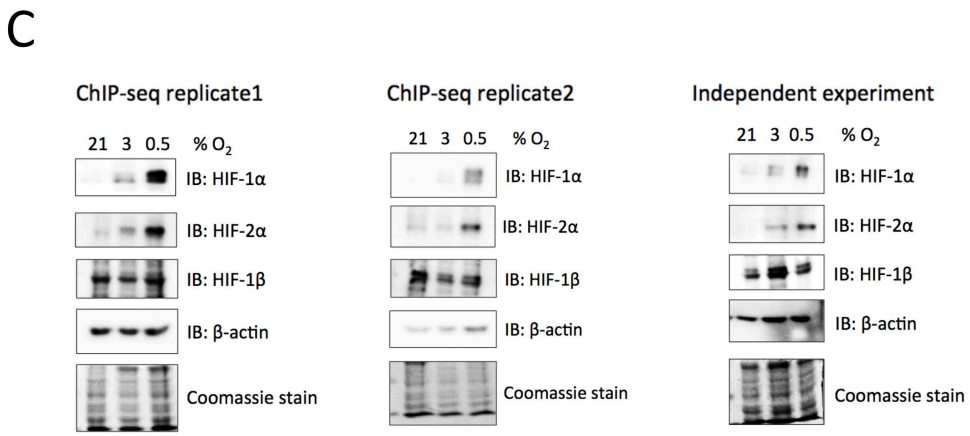
C
ChIP-seq replicate1
ChIP-seq replicate2
Independent experiment
21 3 0.5 % O_2
IB: HIF-1α
IB: HIF-2α
IB: HIF-1β
IB: β-actin
Coomassie stain

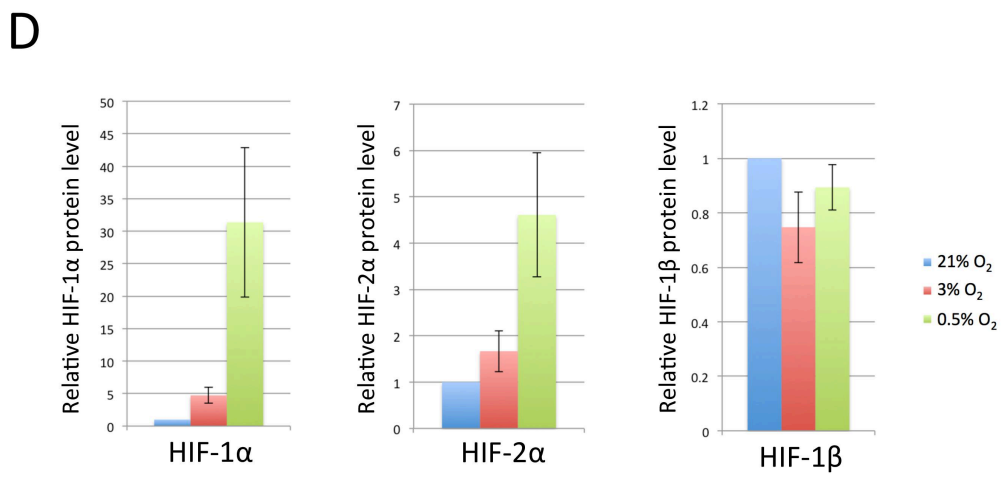
D
Relative HIF-1α protein level
HIF-1α
Relative HIF-2α protein level
HIF-2α
Relative HIF-1β protein level
HIF-1β
21% O_2
3% O_2
0.5% O_2

Figure 1. Immunoblots and quantitation of HIF protein levels in HKC-8 cells exposed to graded hypoxia. (A) Immunoblot of whole cell extracts from cells incubated at different oxygen concentrations for 6h, imaged with x-ray film. The result shows that both HIF-1α and HIF-2α protein levels are higher at 0.5% O_2 than at 3% O_2 (and also higher at 3% than at 21% O_2). The antibodies used for HIF-α immunoblotting were mouse monoclonals raised against epitopes in human HIF-1α or human HIF-2α. (B) Independent rabbit polyclonal antibodies, PM14 (HIF-1α) and PM9 (HIF-2α) confirmed the increase in HIF-α protein level with hypoxia grade. (C) Immunoblots of whole cell extracts harvested in parallel with ChIP samples, for quantitation of protein levels and as an assurance of materials submitted for sequencing. In addition, a third replicate was prepared independently for quantitation analysis. (D) Densitometry based quantitation of the relative fold difference in HIF-1α, HIF-2α and HIF-1β protein level following graded hypoxia. Immunoblot band density is quantified using the BioRad ChemiDoc MP imaging software. The immunoblot signal detected for each HIF isoform is normalised to its respective b-actin loading control signal under each condition. The fold change is then calculated by dividing each hypoxic signal by the respective normoxic signal. Data is shown as mean±SEM, n=3.

3.2.3 Genome-wide HIF binding

The ChIP-seq signal generated with anti-HIF antibodies may be a mixture of both specific and non-specific signal due to antibody cross-reactivity. Therefore, in order to assign 'true' HIF DNA-binding signals, HIF-α ChIP-seq experiments were performed in a HIF-1α/HIF-2α double knockout sub-line (HIF-α DKO) and HIF-1β ChIP-seq was performed in a HIF-1β knockout sub-line (HIF-1β KO) under normoxia conditions. Signals obtained from these ChIP experiments were used as controls for calling peaks in the respective HIF ChIP experiments from the HKC-8 WT cells. ChIP enriched regions were identified using two peak callers, MACS (Model-based analysis of ChIP-seq) (Feng et al., 2012) and TPIC (Tree shape Peak Identification for ChIP-seq) (Hower et al., 2011). To define HIF-1α and HIF-2α binding sites in the WT cells, peaks detected by both peak callers were filtered quantitatively using the total read counts under the peak to include regions that have significant enrichment over the respective regions in the HIF-1α/HIF-2α double knockout cells ($p<0.0001$). HIF-1β peaks were identified with the same approach, using the HIF-1β ChIP-seq from the HIF-1β knockout cells as a control.

Read counts at each binding site were then normalised for sequencing depth and fragment length, and were expressed as RPKM (reads per kilobase per million mapped

reads) (Mortazavi et al., 2008). The aim was to essentially adjust for biases due to the higher probability of reads falling into longer fragments and allow comparison within and between samples. Since only a small fraction of total reads falls within called binding sites, this approximates to normalising to background regions.

To assure the reproducibility of HIF ChIP-seq signals between two replicates, the Pearson correlation coefficient of the RPKM at HIF binding sites was assessed for each HIF ChIP (**Figure 2**). Total HIF-α or HIF-1β binding sites appearing in either replicate was assessed first (**Figure 2 left panels**). The correlation between replicates was suboptimal, i.e. R_2 values were below 0.5 (Bailey et al., 2013), indicating that a substantial amount of the variation came from noise rather than the true dependent variables. The level of noise was higher in the sites with low counts, and this variability could result from technical variation in the ChIP experiments. Therefore, more stringent definitions of HIF DNA-binding sites were considered. Canonical HIF transactivation function requires a heterodimerisation of HIF-α and HIF-1β subunits (Jiang et al., 1996). Therefore, signals at canonical sites binding both HIF-α and HIF-1β are more likely to represent the true HIF binding signals. However such canonical HIF binding sites can be defined using various criteria. With a less stringent definition, sites could be defined by the presence of both HIF-1α (or HIF-2α) and HIF-1β with detection of each isoform in at least one replicate. The correlation between replicates as shown by the R-squared values was observed to improve for all the datasets when this definition was applied (**Figure 2 middle panels**). Using a more stringent definition of canonical binding sites, i.e. sites with both HIF-1α (or HIF-2α) and HIF-1β binding defined in both replicates, slightly tighter correlations were observed (**Figure 2 right panels**). However, the number of binding sites defined by this more stringent definition of canonical sites was then substantially lower especially for HIF ChIP experiments performed under 3% O_2. To

enable a sufficient number of HIF binding sites for the downstream functional analysis, whilst maintain good signal-to-noise, the less stringent definition of canonical sites was chosen for the analyses described in this chapter. This identified a total of 450 HIF-1α canonical binding sites (i.e. all sites that bound HIF-1α at either 0.5% O_2, 3% O_2 or both), 403 HIF-2α and 679 HIF-1β sites (HIF-1α and HIF-2α sites combined, i.e. all HIF sites).

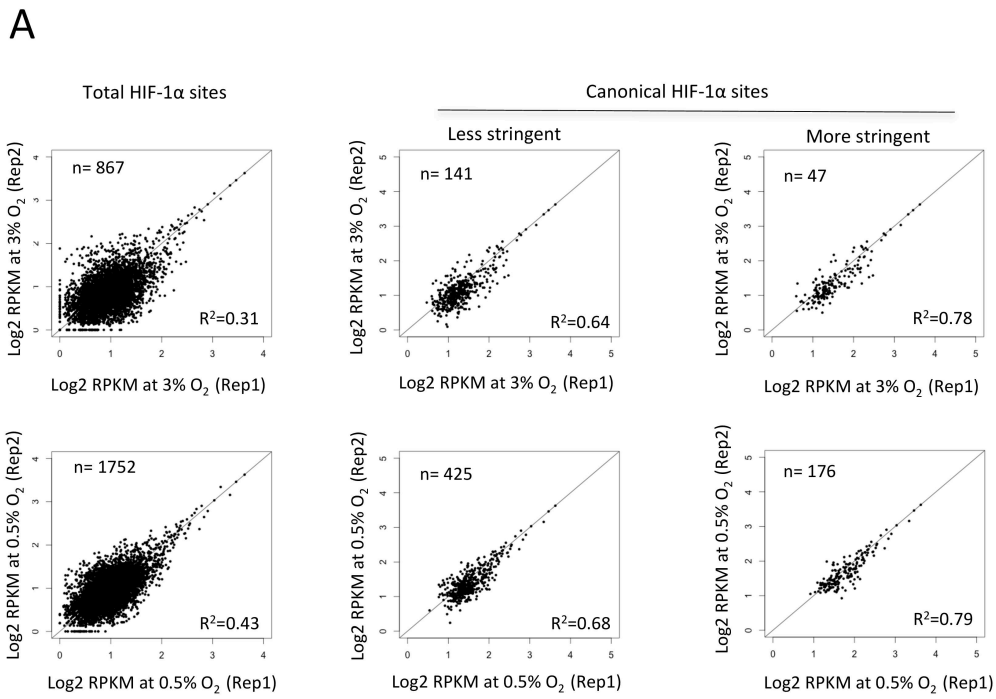
A
Total HIF-1α sites
Canonical HIF-1α sites
Less stringent
More stringent
n= 867
R²=0.31
n= 141
R²=0.64
n= 47
R²=0.78
n= 1752
R²=0.43
n= 425
R²=0.68
n= 176
R²=0.79
Log2 RPKM at 3% O2 (Rep2)
Log2 RPKM at 3% O2 (Rep1)
Log2 RPKM at 0.5% O2 (Rep2)
Log2 RPKM at 0.5% O2 (Rep1)

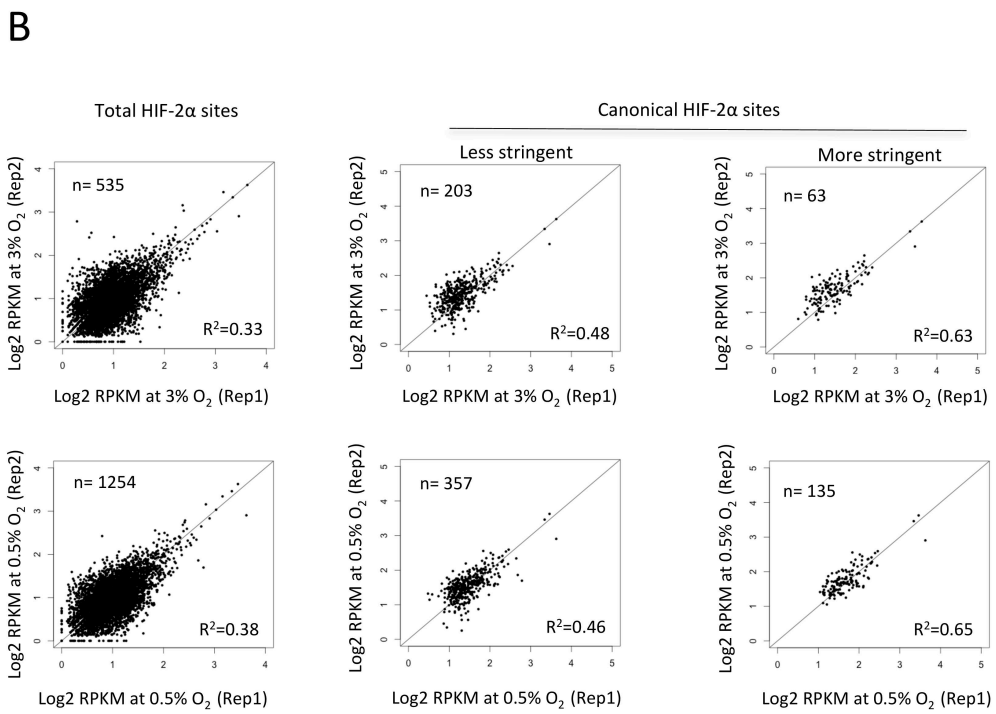
B
Total HIF-2α sites
Canonical HIF-2α sites
Less stringent
More stringent
n= 535
R²=0.33
n= 203
R²=0.48
n= 63
R²=0.63
n= 1254
R²=0.38
n= 357
R²=0.46
n= 135
R²=0.65
Log2 RPKM at 3% O2 (Rep2)
Log2 RPKM at 3% O2 (Rep1)
Log2 RPKM at 0.5% O2 (Rep2)
Log2 RPKM at 0.5% O2 (Rep1)

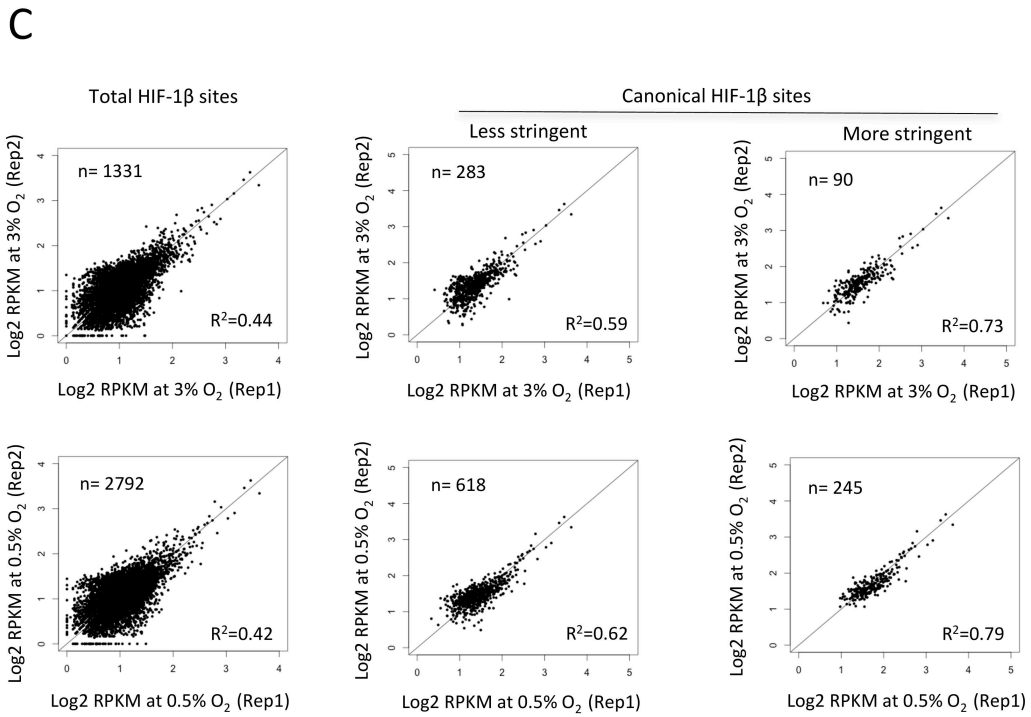

Figure 2. Assessment of the reproducibility between the two HIF ChIP-seq replicates using normalised read counts at HIF binding sites defined by three different methods. (A) Total HIF-1α sites are defined as sites that appeared in either replicate. Less stringent canonical HIF-1α sites are defined by the presence of both HIF-1α and HIF-1β with detection of each isoform in at least one replicate. More stringent HIF-1α sites are defined by the presence of both HIF-1α and HIF-1β with detection of each isoform in both replicates. Similar definitions were applied for (B) HIF-2α binding sites. (C) HIF-1β sites (i.e. all HIF sites) are defined as a combination of HIF-1α and HIF-2α sites by each method. The normalised read counts (expressed as RPKM) of each binding site are plotted using a Log2 scale. The ChIP-seq data from replicate 1 is represented on the horizontal axis, and data from replicate 2 is on the vertical axis. The number of qualified binding sites and the correlation coefficient values R^2 are indicated.

Next, the RPKM for each canonical HIF binding site across the two hypoxic replicates was averaged and this data was used in the subsequent analyses. Together with the RPKM from the single normoxic ChIP dataset, these reads were displayed in the hierarchical clustering analysis and in the heatmap (**Figure 3**). Both analyses showed clustering of the ChIP experiments performed under hypoxic conditions, which distinguished them all from the normoxic ChIP experiments. This indicated that HIF binding at these canonical sites was indeed hypoxia-responsive. Moreover, these two analyses also indicated that the major variance was between ChIP experiments using

different anti-HIFα antibodies, rather than the hypoxia conditions, i.e. the antibody conditions grouped together first and not the oxygen concentrations. This suggests that HIF-1α and HIF-2α have largely distinct binding profiles with fewer differences between oxygen concentrations than between HIF-1α and HIF-2α. Within the hypoxic ChIP experiments, a tighter correlation was observed between HIF-1α and HIF-1β, than between HIF-2α and HIF-1β.

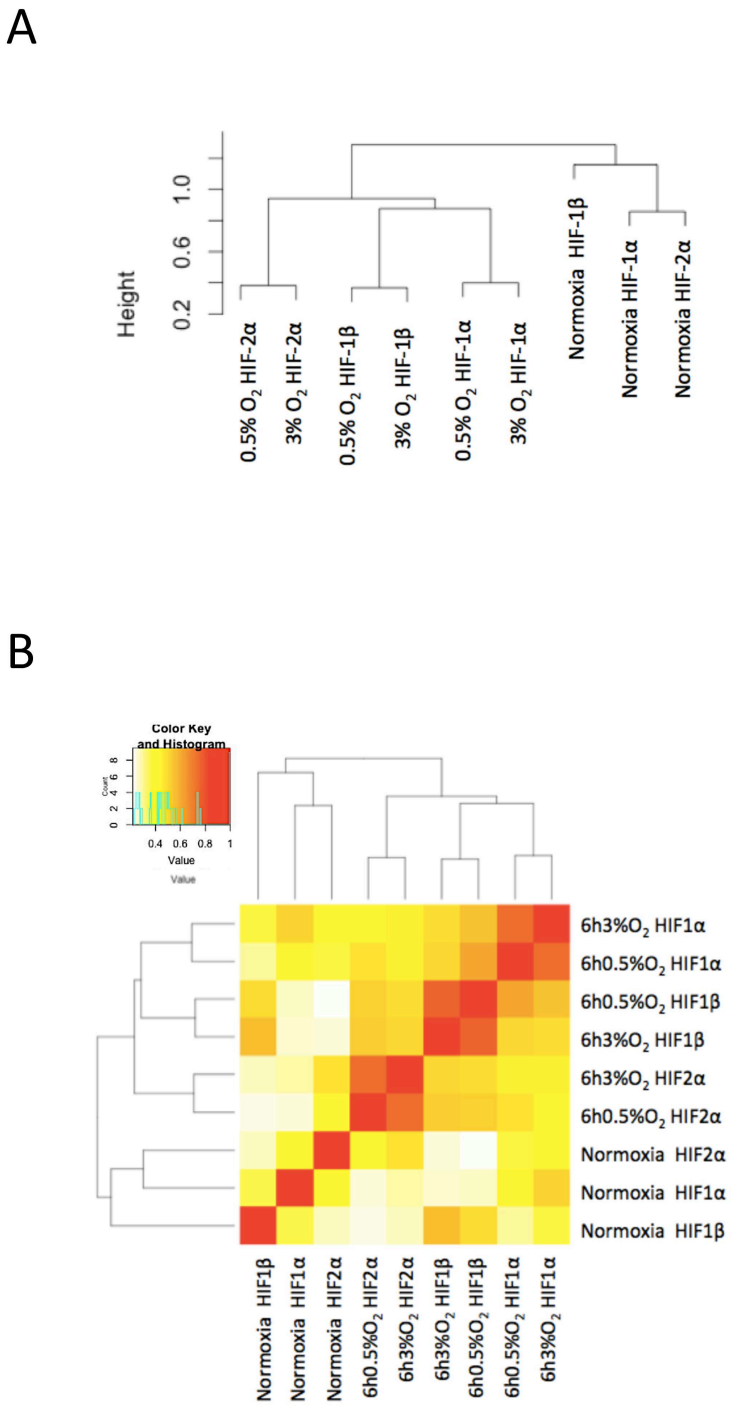

Figure 3. Quantitative comparison of HIF ChIP signals at canonical HIF binding sites (n=679) across graded hypoxia conditions (21%, 3% and 0.5% O_2 for 6h). The set of sites is defined as all HIF-α canonical sites that appeared at 0.5%, 3% O_2 or both. For each HIF binding site, this analysis uses the averaged RPKM from the two hypoxic ChIP replicates and the RPKM from the single normoxic ChIP dataset. (A) Cluster dendrogram is performed to compare the total RPKM values of each ChIP dataset. The height (distance) between the clusters displayed in the dendrogram refers to the similarity of each of the HIF ChIP samples. (B) Data is also displayed in the heatmap format. The colour in the heatmap matrix refers to the correlation between each ChIP sample. The higher the correlation, the more intense the colour is.

3.2.4 Binding at canonical sites increases in response to graded hypoxia

To understand how HIF DNA-binding responds to graded O_2 concentrations, the raw reads under canonical HIF-1α, HIF-2α and HIF-1β peaks at 21%, 3% and 0.5% O_2 were compared (**Figure 4A**). For all HIF isoforms, i.e. HIF-1α, HIF-2α and HIF-1β, the proportion of reads under canonical HIF sites was found to increase between 21% and 3% O_2, and also to increase between 3% and 0.5% O_2. Overall the pattern of changes in HIF-α binding matched that of protein expression, i.e. both increased HIF-α binding and HIF-α protein were observed along with increasing severity of hypoxia. HIF-1β binding also increased with the hypoxia grade despite the total protein level remaining unchanged.

Even though at the global level, binding at the canonical sites increased with the hypoxia severity, the question remained as to whether some sites were preferentially bound under each hypoxic condition. To address this, binding at 0.5% and at 3% O_2 was compared using two different approaches. In the first approach, signal intensity (i.e. RPKM) at each HIF-1α canonical site (n= 450) at 0.5% O_2 was plotted against the RPKM at the same sites at 3% O_2 (**Figure 4B**). The same approach was used for canonical HIF-2α (n=403) and HIF-1β (n=679) binding sites. For all three HIF subunits, binding at the vast majority of defined canonical sites increased between 3% and 0.5% O_2, as shown by most points being scattered above the identity line**.** In the second approach, to focus on the hypoxia inducibility of binding at the canonical binding sites, the ratio of binding intensity between hypoxia and normoxia ChIP experiments was assessed. Reads at each canonical HIF-1α site at 0.5% O_2 were divided by the respective reads in the normoxia condition, and then they were plotted against the reads at 3% O_2 divided by the reads in the normoxia dataset. The same approach was used for HIF-2α and HIF-1β canonical sites. The plots indicate that the signals were indeed induced by hypoxia since most sites

locate above 0 (i.e. higher in hypoxia than in normoxia) (**Figure 4C**). Interestingly, there were a few binding sites identified below the horizontal and vertical axes, suggesting signals at some sites may already exist under normoxia condition. However, the relatively low read counts at these sites suggest the binding here could be due to background noise.

Importantly, for all three HIF subunits, signal intensity at 0.5% O_2 correlates strongly with that observed at 3% O_2, suggesting that binding at the majority of the canonical sites (HIF-1α, HIF-2α and HIF-1β) increased with severity of hypoxia. However, there were no completely new sites that were only capable of binding at mild or more severe hypoxia. The results indicate that the canonical HIF binding pattern was pre-ordained regardless of the oxygen concentrations.

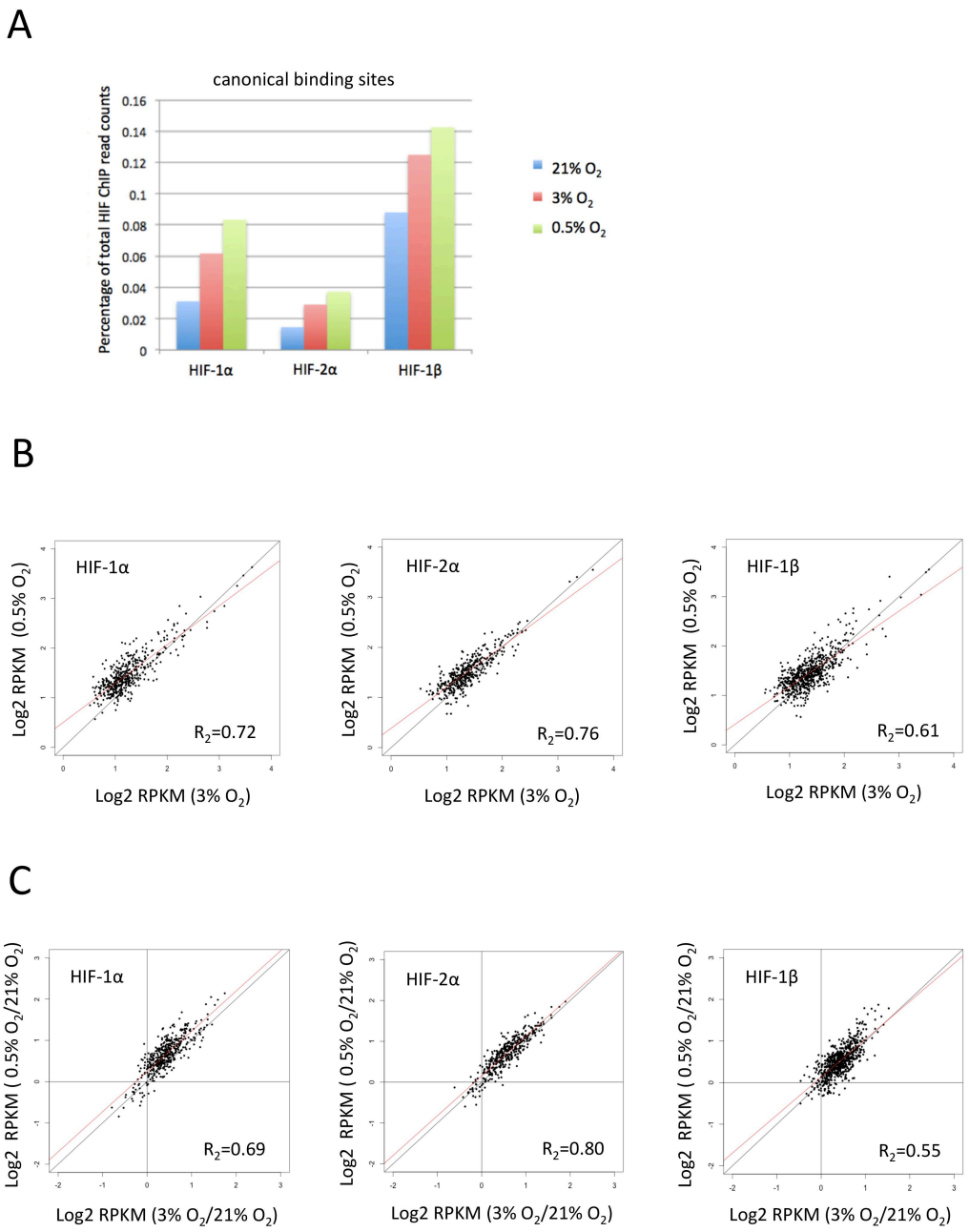

Figure 4. Binding at canonical HIF sites increased in response to graded hypoxia. (A) Raw reads in the HIF binding sites are expressed as a percentage of the total read counts in each ChIP. The figure shows that the binding for all three HIF isoforms increased between 21% and 3% O_2, and between 3% and 0.5% O_2. HIF-1α (or HIF-2α) sites are defined as all canonical sites that bound HIF-1α (or HIF-2α) at either 0.5%, 3% O_2 or both. HIF-1β sites are HIF-1α and HIF-2α sites combined. (B) For each HIF isoform, normalised reads (i.e. RPKM) of individual sites at 0.5% O_2 are plotted against the RPKM at 3% O_2. The correlation between the two variables is shown by the regression line (highlighted in red) and by the R-squared value. (C) To examine the hypoxia inducibility of binding at the canonical sites, hypoxic HIF signals (i.e. RPKM) at 0.5% O_2 are divided by the respective signal in normoxia, and plotted against the hypoxic signal at 3% divided by the signal in normoxia. Again the correlation between the two variables is shown by the regression line (highlighted in red) and by the R-squared value.

3.2.5 The effects of oxygen concentration on canonical HIF-1α sites

Although binding at all canonical HIF-1α sites increased as hypoxia became more severe, it is conceivable that the distribution of loading at individual loci is uneven, i.e. some sites were more fully loaded at less severe hypoxia than others. To test this hypothesis, the difference in binding occupancy, i.e. RPKM at individual canonical HIF-1α sites between 3% and 0.5% O_2, was assessed.

3.2.5.1 Progressive-loading sites versus early-saturated sites

First, a frequency distribution of canonical HIF-1α sites based on their occupancy between 3% and 0.5% O_2 was plotted (**Figure 5A**). Overall, this plot revealed a unimodal distribution with the mean difference above 0, i.e. binding at the majority of the sites increased with hypoxia severity without clear evidence of categorical distinctions between sites that were more or less fully loaded in milder hypoxia.

To further examine whether individual sites respond differently to graded hypoxia in a more quantitative manner, the difference between RPKM at 3% and at 0.5% O_2 (that reflects differential binding occupancy) was plotted against the averaged RPKM at 3% and 0.5% O_2 (that reflects the overall binding affinity) on a MA plot (**Figure 5B**). A spread of HIF-1α binding sites was observed. The sites were further stratified into three groups based on the difference on the vertical axis. The top one third of binding sites (n=150, coloured blue) represented a group of sites with more progressively loading behaviour, and the bottom one third (n=151, coloured green) of sites showed the least response to hypoxia gradient suggesting they were likely saturated early under mild hypoxia. A Mann-Whitney U test was used to quantitatively examine the RPKM within the two groups of sites, and a p-value<2.2e-16 indicated a statistically significant separation between these manually divided sites.

This observation of potentially two types of loading behaviour at HIF-1α canonical sites might represent true difference along a biological continuum of loading behaviour or might arise from artificial separation of groups that simply lie at different places on a statistical continuum generated by noise in the assay methods. Therefore, to distinguish these possibilities, the two types of loading behaviour at HIF-1α canonical sites were further assessed using HIF-1β ChIP-seq dataset. Since all canonical sites were defined by the presence of HIF-α and HIF-1β, the HIF-1β ChIP can therefore be used as an independent dataset for validation. If the signal is genuine, this loading behaviour should be recapitulated by the HIF-1β signal, whereas if it is noise, this should not be observed in the HIF-1β dataset. In **Figure 5C**, the two groups of sites defined in the HIF-1α dataset (i.e. progressive-loading and early-saturated) were segregated in a manner that was statistically significant (*p*-value=1.702e-10) based on their respective HIF-1β signals**.** The data was also displayed in the boxplot (**Figure 5D**). Overall the signal within the HIF-1β dataset was supportive of biological difference in loading behaviour within the HIF-1α canonical sites.

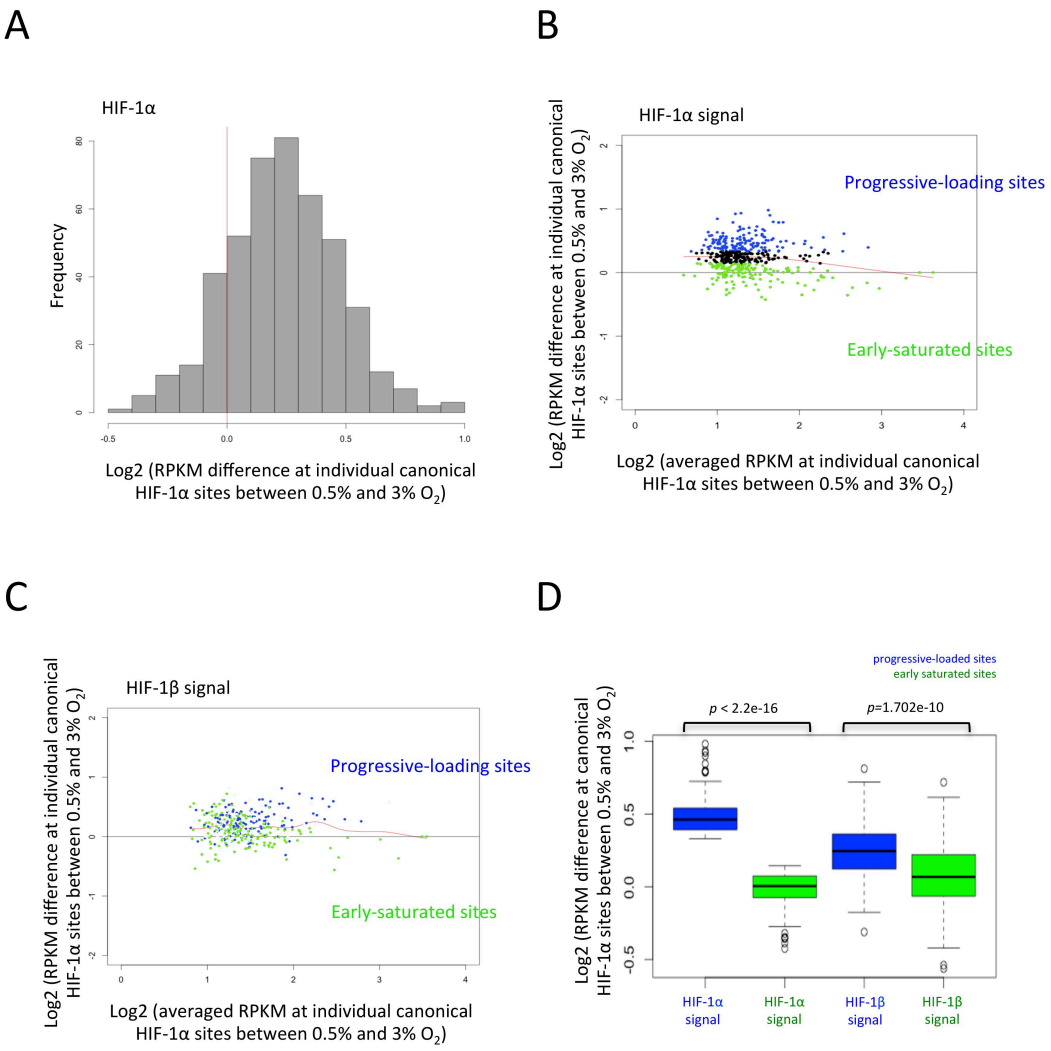

Figure 5. Quantitative analysis of HIF-1α canonical binding sites. (A) Histogram showing the frequency distribution of HIF-1α sites according to the Log2 difference of RPKM at 0.5% versus at 3% O_2. The mean difference is above 0, indicating that the overall behaviour is for progressive-loading (B) MA plot is used to display the RPKM difference at individual canonical site between 0.5% and 3% O_2 (i.e. the occupancy, vertical axis) versus the averaged RPKM between 0.5% and 3% O_2 (i.e. the affinity, horizontal axis). The binding sites are divided into those with progressive-loading (top one-third, coloured blue, n=150) and early saturated (bottom one-third, coloured green, n=151) based on the difference in occupancy on the vertical axis. A smooth spline line is highlighted in red to show the best-fit expected trend. (C) MA plot displaying the HIF-1β signals at the previously defined HIF-1α progressive-loading sites (coloured blue) and early-saturated sites (coloured green). The middle group, which was shown as black dots in B, was omitted in this plot for the reason of simplicity. (D) Boxplot representing RPKM for each group of sites. The difference observed between progressive-loading and early-saturated sites is significant in both HIF-1α ChIP data and the HIF-1β ChIP data according to Mann-Whitney U test.

3.2.5.2 Characterisation of the two groups of sites

Having found that the distribution of binding at canonical HIF-1α sites was uneven, with some sites potentially being progressively loaded as the severity of hypoxia increased and some being saturated under mild hypoxia, it was of interest to test whether this differential loading behaviour might be linked to any difference in the downstream functions of the two groups of HIF-1α sites.

Analysis of the pan-genomic distribution of binding sites from both groups showed a strong enrichment close to transcriptional start sites (TSS) (**Figure 6A**). 54% of the progressive-loading sites and 41% of the early-saturated sites clustered within a 5 kb window around TSS, and the difference in distribution was significant between the two groups of sites (p=0.0004). To determine the associated biological processes, the sites within each group were annotated to the nearest genes and pathways were examined using the Ingenuity Pathways Analysis software tool (IPA Version 01-06)**.** The top 5 statistically over-represented pathways in the groups of progressive-loading and early-saturated sites were significantly different (**Figure 6B**). However given that only a small number of genes were identified in each pathway and that some of the same genes appeared multiple times in different pathways, differences observed in the biological processes associated with the two groups of sites are not predictable of their loading behaviours.

The minimal *cis*-regulatory element required for HIF DNA-binding is the RCGTG (R=A/G) motif. To determine whether there was any sequence preference 5' or 3' to the core RCGTG motif, the flanking region (10 bp up and downstream) of each site within the two groups was examined. No significant difference in base composition between the progressive-loading and early-saturated sites was observed at any position (**Figure 6C**). The relative abundance of the RCGTG motif within the two groups of sites was also

examined. Interestingly the progressive-loading sites have on average a slightly higher occurrence of RCGTG motifs (p=0.35) (**Figure 6D**). This may in part contribute to the increased HIF binding in severe hypoxia when there is more HIF protein present.

In summary, binding at HIF-1α canonical sites increased in response to graded hypoxia. However, it has been possible to subcategorise the sites into two groups. The group of sites that showed greatest response to graded hypoxia (i.e. progressive-loading sites) had a higher average number of RCGTG motifs per site, and were located more proximally to the TSS. On the other hand, sites that showed least response (i.e. saturated at mild hypoxia) had a lower average number of RCGTG motif in each site and the sites were clustered less closely to the TSS. However, the differences between the two groups of sites were only subtle and these features were not predictive for a progressive-loading site versus an early-saturated site.

A

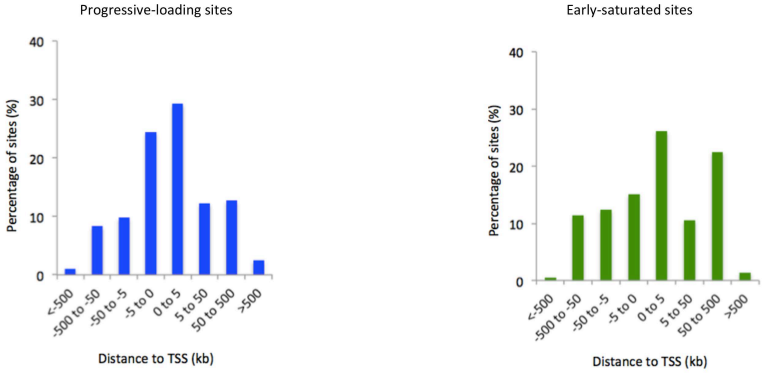
Progressive-loading sites
Percentage of sites (%)
Distance to TSS (kb)
<-500
-500 to -50
-50 to -5
-5 to 0
0 to 5
5 to 50
50 to 500
>500
Early-saturated sites
Percentage of sites (%)
Distance to TSS (kb)

B

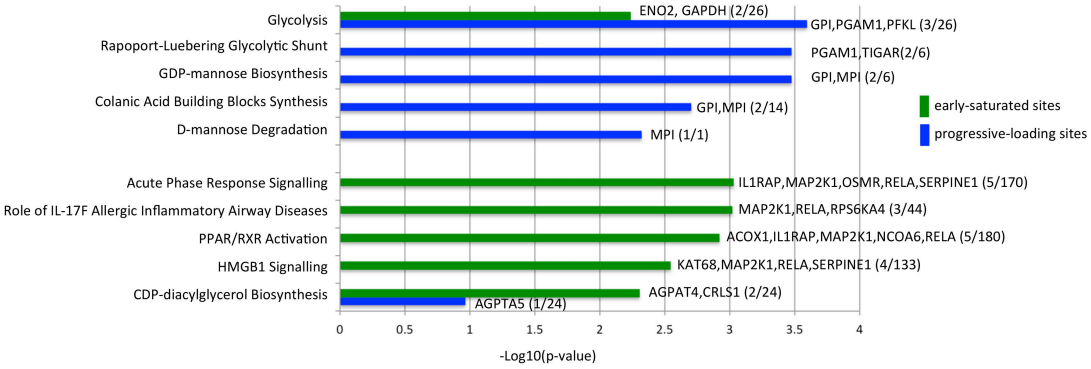
Glycolysis
Rapoport-Luebering Glycolytic Shunt
GDP-mannose Biosynthesis
Colanic Acid Building Blocks Synthesis
D-mannose Degradation
Acute Phase Response Signalling
Role of IL-17F Allergic Inflammatory Airway Diseases
PPAR/RXR Activation
HMGB1 Signalling
CDP-diacylglycerol Biosynthesis
ENO2, GAPDH (2/26)
GPI,PGAM1,PFKL (3/26)
PGAM1,TIGAR(2/6)
GPI,MPI (2/6)
GPI,MPI (2/14)
MPI (1/1)
IL1RAP,MAP2K1,OSMR,RELA,SERPINE1 (5/170)
MAP2K1,RELA,RPS6KA4 (3/44)
ACOX1,IL1RAP,MAP2K1,NCOA6,RELA (5/180)
KAT68,MAP2K1,RELA,SERPINE1 (4/133)
AGPAT4,CRLS1 (2/24)
AGPTA5 (1/24)
early-saturated sites
progressive-loading sites
-Log10(p-value)

C


Progressive-loading sites
Early-saturated sites

D

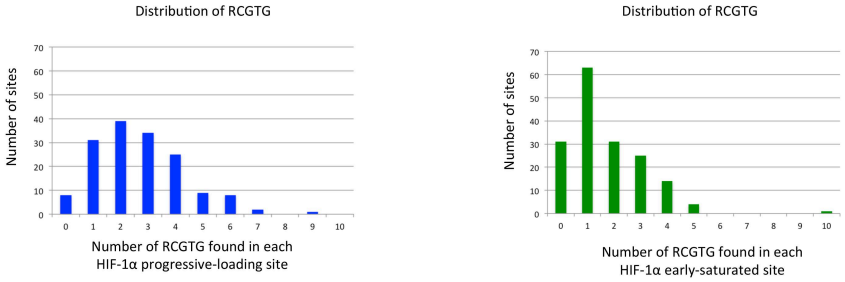
Distribution of RCGTG
Number of sites
Number of RCGTG found in each HIF-1α progressive-loading site
Distribution of RCGTG
Number of sites
Number of RCGTG found in each HIF-1α early-saturated site

Figure 6. Downstream analysis of HIF-1α binding sites that varied most (progressive-loading) and least (early-saturated) between 3% and 0.5% O_2. (A) Histogram showing the percentage of binding sites according to the distance ±500 kb from the nearest transcriptional start site (TSS). The analysis is computed by Genomic Regions Enrichment of Annotations Tool (GREAT). (B) Analysis of biological pathways based on the annotated nearest gene using Ingenuity Pathway Analysis (IPA). For the progressive-loading group of sites, 116 annotated genes were identified. For the early-saturated group of sites, there were 128 annotated genes. The pathways are ranked by the –log10(*p*-value), and top 5 most enriched pathways from each group are displayed. –log10(*p*-value)>1.3 denotes the level of significance. For each pathway, the names of the genes responsible for the signal are listed, and the overlap with total genes involved that pathway is shown in the bracket. (C) Flanking sequence ±10 bp up and downstream of RCGTG motif is scanned using the online tool WebLogo (http://weblogo.berkeley.edu/) The height of each letter was proportionate to its frequency. (D) Histogram showing the distribution of the occurrence of RCGTG core motif within each site. On average there is 2.71 RCGTG in each progressive-loading site, and 1.69 per early saturated site.

3.2.6 The effects of oxygen concentration on canonical HIF-2α sites

Similar analyses were performed for the HIF-2α canonical sites. Compared to HIF-1α binding sites, HIF-2α sites showed a broadly similar unimodal distribution in response to graded hypoxia (**Figure 7A**). An uneven binding profile was also observed, i.e. the signal intensity at HIF-2α canonical sites displayed a range of values (**Figure 7B**). HIF-2α binding sites were then artificially stratified based on the difference in the occupancy between 0.5% and 3% O_2 into an upper tertile in which HIF-2α signal loaded progressively (n=134) and a lower tertile, in which HIF-2α signal was more saturated (n=135). HIF-1β dataset was again used as an independent control to verify whether this observation of two types of loading behaviour is genuine for HIF-2α canonical binding sites (**Figure 7C**). Mann-Whitney U tests indicated that HIF-1β signal indeed mirrored HIF-2α signal, i.e. the progressive-loading and early-saturated sites were separated based on their HIF-1β signal in a statistically significant manner (**Figure 7D**). Interestingly the two groups of sites were less segregated (*p*-value=3.444e-05) compared with the similar analysis performed on the HIF-1α sites (*p*-value=1.702e-10). This was consistent with HIF-2α being in general induced in more modest hypoxia.

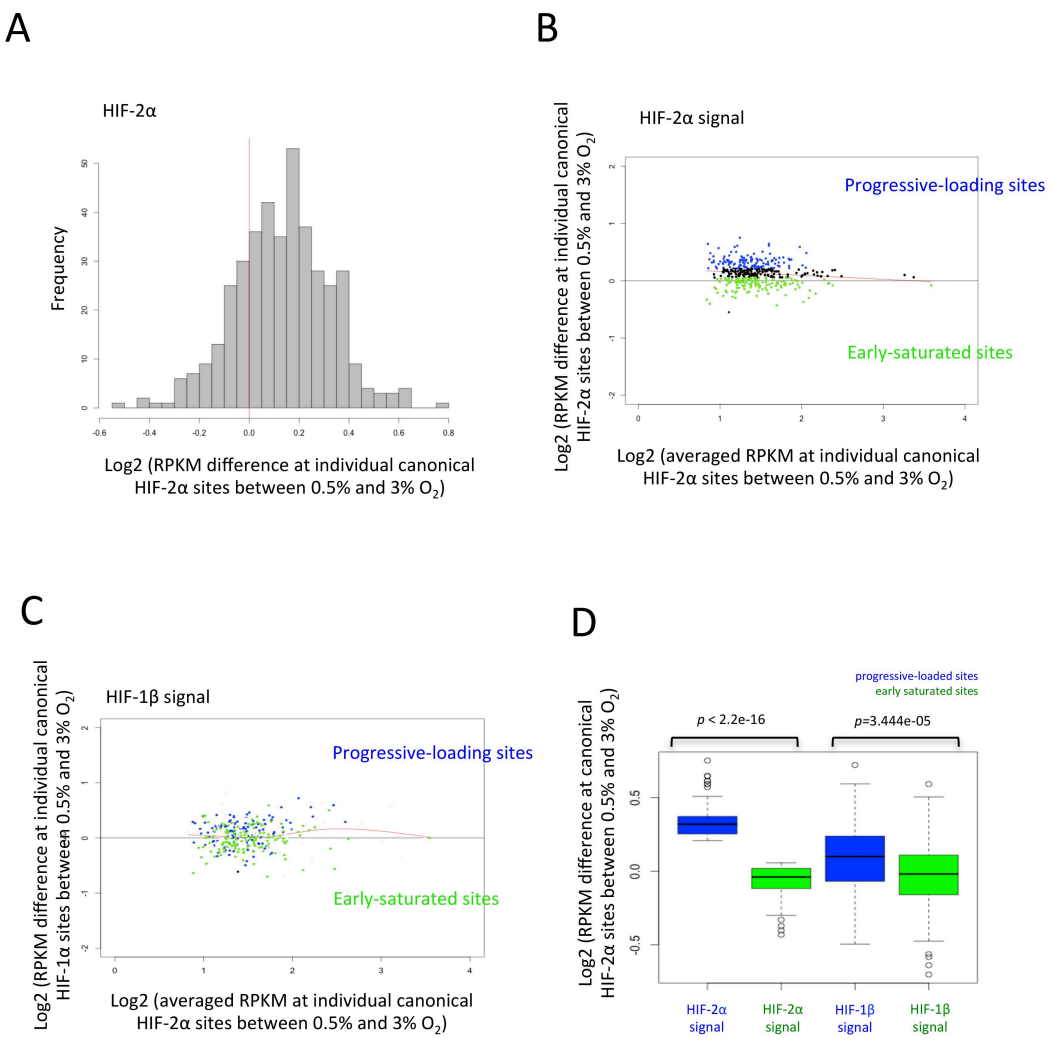

Figure 7. Quantitative analyses of HIF-2α canonical binding sites. (A) Frequency distribution of HIF-2α sites according to the Log2 difference of RPKM at 0.5% versus at 3% O_2 indicates a general progressive-loading behaviour (B) HIF-2α binding sites are divided into those with progressive-loading (top one-third, coloured blue, n=134) and early saturated (bottom one-third, coloured green, n=135) based on the difference in occupancy on the vertical axis. A smooth spline line is highlighted in red to show the best-fit expected trend. (C) HIF-1β signals at the previously defined HIF-2α progressive-loading sites (coloured blue) and HIF-2α early-saturated sites (coloured green). The middle group, which was shown as black dots in B, was omitted in this plot for the reason of simplicity. (D) Boxplot representing RPKM for each group of sites. The difference observed between progressive-loading and early-saturated sites in both the HIF-2α ChIP data and HIF-1β ChIP data is significant.

To examine potential functional differences between the two groups of sites, the distribution of binding sites around the TSS was plotted (**Figure 8A**). In contrast to HIF-1α sites (**Figure 6A**), HIF-2α sites displayed a remarkably promoter-distal distribution, with 72% of the progressive-loading sites and 88% of the early-saturated sites located greater than 5 kb from the nearest TSS. The distributions of the HIF-2α progressive-loading and early-saturated sites were also statistically different (p=2.41e-09). IPA indicated that the biological pathways associated with these two groups of sites were largely non-overlapping (**Figure 8B**). However, again no clear predictive signature can be confirmed, as only few genes were responsible for the signal of each pathway.

When the sequence preference in the regions ± 10 bp of the RCGTG core motif was examined, the two groups of sites displayed a similar motif profile (**Figure 8C**). HIF-2α progressive-loading sites were also found to have slightly more RCGTG motif per peak compared to early-saturated sites, however this was not statistically significant (p=0.85) (**Figure 8D**).

A

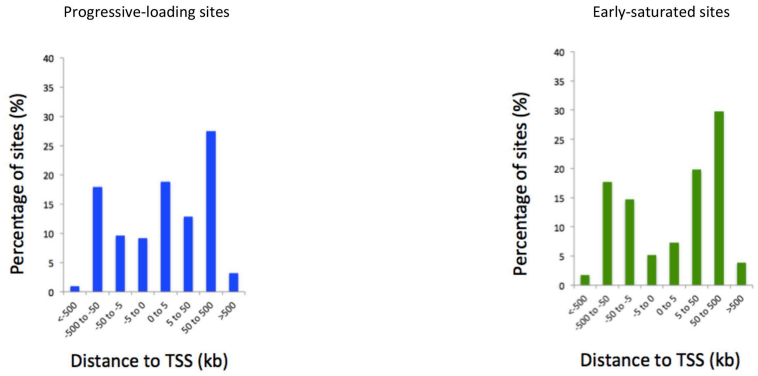
Progressive-loading sites
Percentage of sites (%)
Distance to TSS (kb)
Early-saturated sites
Percentage of sites (%)
Distance to TSS (kb)

B

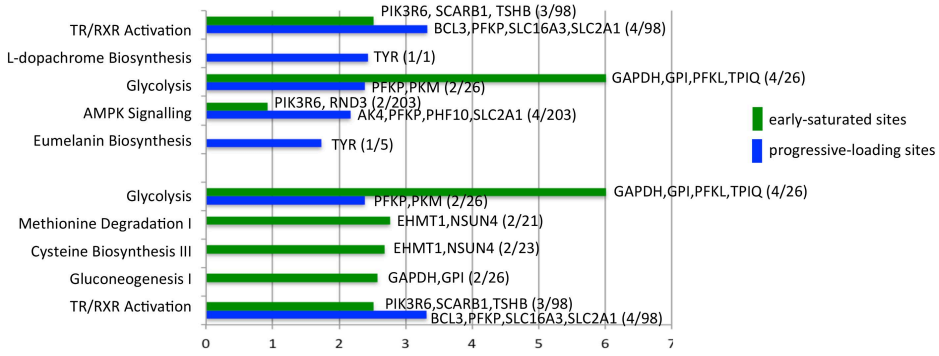
PIK3R6, SCARB1, TSHB (3/98)
TR/RXR Activation
BCL3,PFKP,SLC16A3,SLC2A1 (4/98)
L-dopachrome Biosynthesis
TYR (1/1)
Glycolysis
GAPDH,GPI,PFKL,TPIQ (4/26)
PFKP,PKM (2/26)
AMPK Signalling
PIK3R6, RND3 (2/203)
AK4,PFKP,PHF10,SLC2A1 (4/203)
Eumelanin Biosynthesis
TYR (1/5)
early-saturated sites
progressive-loading sites
Glycolysis
GAPDH,GPI,PFKL,TPIQ (4/26)
PFKP,PKM (2/26)
Methionine Degradation I
EHMT1,NSUN4 (2/21)
Cysteine Biosynthesis III
EHMT1,NSUN4 (2/23)
Gluconeogenesis I
GAPDH,GPI (2/26)
TR/RXR Activation
PIK3R6,SCARB1,TSHB (3/98)
BCL3,PFKP,SLC16A3,SLC2A1 (4/98)
0 1 2 3 4 5 6 7

C


Progressive-loading sites
Early-saturated sites

D

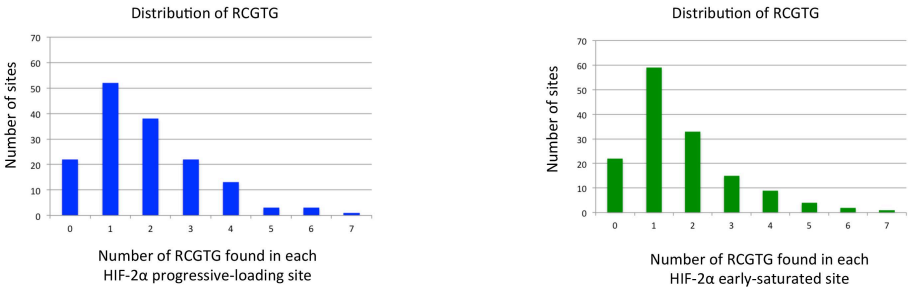
Distribution of RCGTG
Number of sites
Number of RCGTG found in each
HIF-2α progressive-loading site
Distribution of RCGTG
Number of sites
Number of RCGTG found in each
HIF-2α early-saturated site

Figure 8. Downstream analysis of HIF-2α binding sites that varied most (progressive-loading) and least (early-saturated) between 3% and 0.5% O_2. (A) Histogram showing the percentage of HIF-2α binding sites according to the distance ±500 kb from the nearest transcriptional start site (TSS). The analysis was computed by Genomic Regions Enrichment of Annotations Tool (GREAT). (B) Analysis of biological processes based on the annotated nearest gene (95 genes mapped for progressive-loading sites; 89 genes mapped for early-saturated sites) and ranked by the –log10(*p*-value) using Ingenuity Pathway Analysis (IPA). Top 5 most enriched pathways from each group were displayed. –log10(*p*-value)>1.3 denotes the level of significance. For each pathway, the names of the genes responsible for the signal are listed, and the overlap with total genes in the pathway is shown in the bracket. (C) Flanking sequence ±10 bp up and downstream of RCGTG motif was scanned using the online tool WebLogo (http://weblogo.berkeley.edu/). The height of each letter was proportionate to its frequency. (D) Histogram showing the distribution of the occurrence of RCGTG core motif within each site. On average there are 1.85 RCGTG in each progressive-loading site, and 1.68 per early-saturated site.

3.2.7 Strong binding sites versus weak binding sites

For both HIF-1α and HIF-2α sites, a distributed binding pattern was also observed across the horizontal axis, indicating HIF-α binding sites with different strengths (i.e. affinities) respond differently to hypoxia (**Figure 5B and 7B**). To investigate the downstream functions of sites with different binding strengths, HIF-1α sites were stratified into three groups of equal size according to the binding affinity (i.e. horizontal axis) (**Figure 9A**). The one third of sites (n=150) towards the right of the axis represented a group of sites with higher binding affinity (i.e. 'strong' sites), and one third of sites (n=151) towards the left of the axis were the 'weak' binding sites. *P*-value<2.2e-16 confirmed that there was a statistical difference in the binding between these two groups of sites.

When the distribution around TSS was examined, sites from both groups showed a similar promoter-proximal binding profile (*p*=0.16) (**Figure 9B**). The top 5 biological processes associated with the two groups of sites were different according to IPA, with the caveat that the signal was based on a small number of genes from each group and the same genes were involved in multiple pathways (**Figure 9C**). The sites were also examined for their RCGTG flanking sequence preferences and motif frequency, however no significant differences were observed (**Figure 9D and E**). The analyses were

performed for HIF-2α 'strong' (n=134) and 'weak' (n=135) sites. Again no differences were identified (data shown in **Supplementary Figure 1**).

A

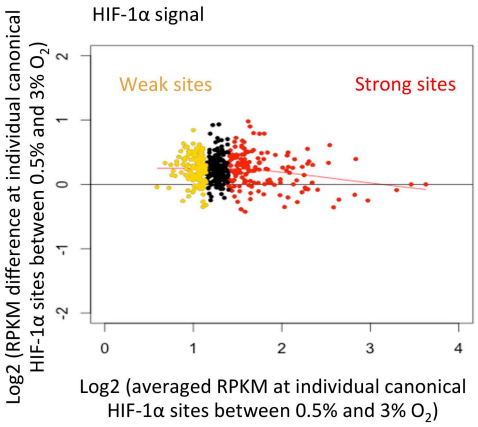

B

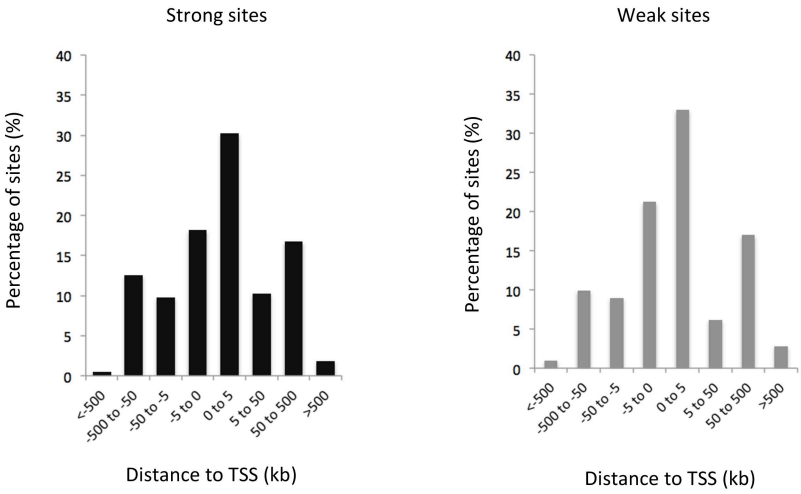

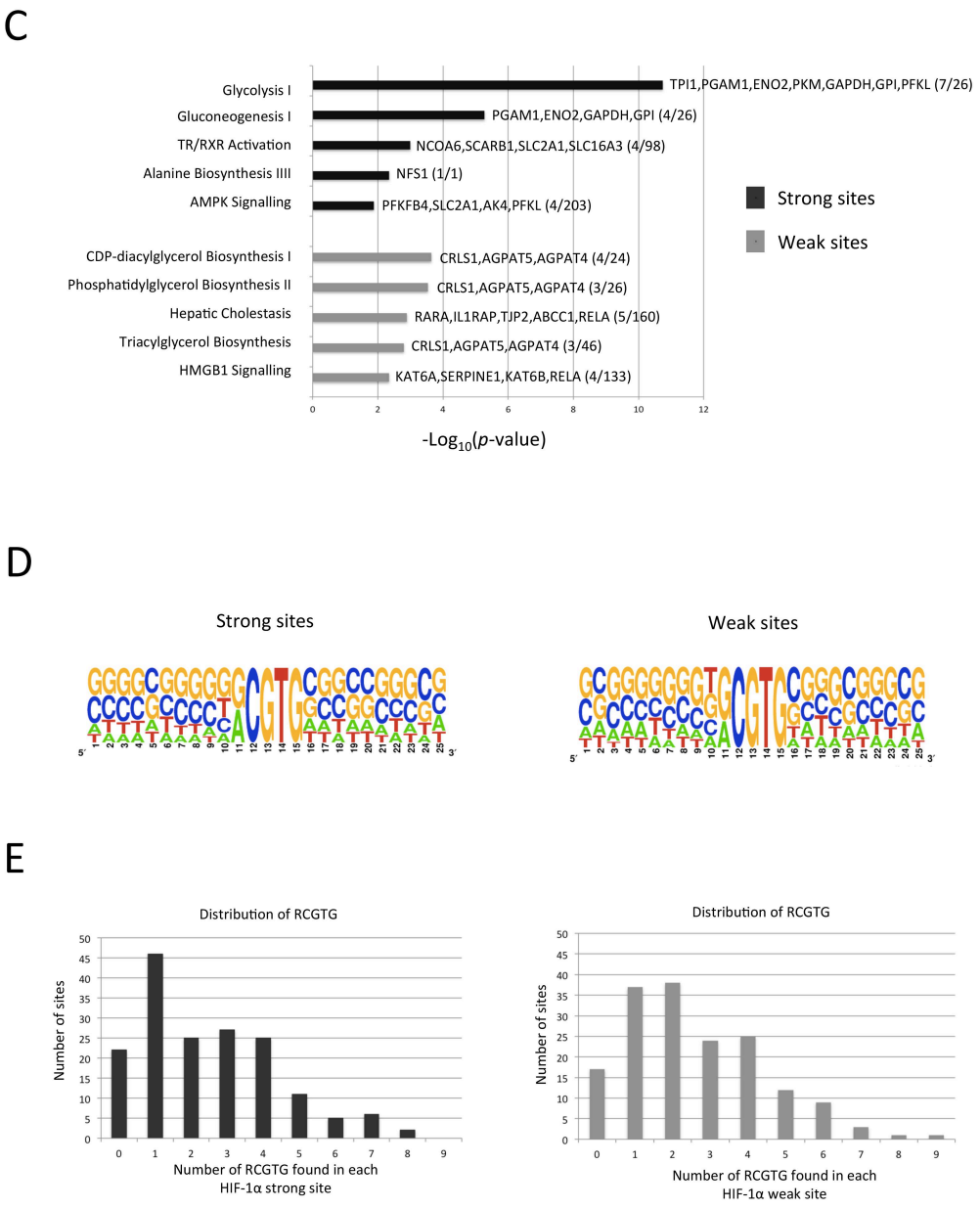

Figure 9. Downstream analysis of HIF-1α binding sites that are divided based on the binding strength. (A) The sites are stratified into 'strong' (n=150 , coloured red) and 'weak' (n=151, coloured yellow) sites according to the averaged RPKM between 0.5% and 3% O_2 on the horizontal axis. (B) Histogram showing the percentage of binding sites according to the distance ±500 kb from the nearest transcriptional start site (TSS). (C) Analysis of biological pathways for the annotated genes within each group. In this analysis, 124 genes annotated in the group of 'strong' sites and 119 genes are annotated in the group of 'weak' sites by IPA. The pathways are ranked by –log10(*p*-value). –log10(*p*-value)>1.3 was statistically significant. For each pathway, the names of the genes responsible for the signal are listed, and the overlap with total genes in the pathway is shown in the bracket. (D) Flanking sequence ±10 bp up and downstream of RCGTG motif is scanned using the online tool WebLogo (http://weblogo.berkeley.edu/) The height of each letter was proportionate to its frequency. (E) Histogram showing the distribution of the occurrence of RCGTG core motif within either HIF-1α 'strong' or 'weak' sites. On average there is 2.80 RCGTG per strong site, and 2.78 per weak site.

3.2.8 Characterisation of normoxic signal for HIF-α and HIF-1β

Although binding at the majority of HIF-α and HIF-1β sites were hypoxia inducible, some weak signals were detected in the normoxic ChIP experiments for all three HIF isoforms when the raw reads were displayed as a percentage of the total HIF ChIP signal (**Figure 4A**). Several other studies have also reported expression and binding of HIF-1α and HIF-2α under normoxic conditions (Stroka et al., 2001; Mimura et al., 2012). In order to examine whether the DNA-binding signal present in the normoxic HKC-8 cells was genuine, a quantitative analysis based on the RPKM and a qualitative analysis based on the motif signature at the normoxic binding sites were performed.

The RPKM at previously defined canonical HIF-1α, HIF-2α and HIF-1β sites were compared between normoxic and hypoxia HIF ChIP datasets in the WT cells. In addition, the RPKM from normoxic ChIP performed in the HIF-1α/2α double knockout (HIF-α DKO) cells were plotted as a negative control (**Figure 10A**). For HIF-1α and HIF-2α in the WT cells, the RPKM signal under normoxia condition was very much lower than the signal under hypoxia conditions. The normoxic signal in the WT cells was only slightly higher than that observed in the HIF-α DKO cell, indicating that this normoxic signal was largely non-specific. Interestingly, HIF-1β signal present in the normoxic WT cells was not observed in the normoxic HIF-1β knockout cells. In summary, using canonical sites defined under hypoxic conditions, we therefore have little evidence of HIF-α binding under normoxic condition, but some evidence for limited HIF-1β binding.

To further examine the potential signal observed in normoxia, we have also looked at the DNA-binding sites defined in the normoxia ChIP experiments. As before, only sites with read counts that were significantly enriched compared to the respective regions in the HIF KO cells were considered. In this analysis, a significant number of

binding sites were called in the normoxic ChIP experiments, i.e. 1614 HIF-1α, 622 HIF-2α and 1031 HIF-1β sites. This could potentially be due to the fact that only one ChIP-seq experiment was performed in normoxia, therefore it was unable to apply the more stringent definitions used in the hypoxia analyses. In order to assess whether there are any detectable HIF HREs or other motifs within those sites, a *de novo* motif search was performed (**Figure 10B**). No HRE motifs were detected. Although there were some motifs found in normoxic HIF-1α and HIF-1β binding sites, they were not significant and were not centrally enriched around the summit of the binding sites. Overall, this suggests the sites identified in the single replicate of normoxic ChIP experiments were likely to be false positives.

A

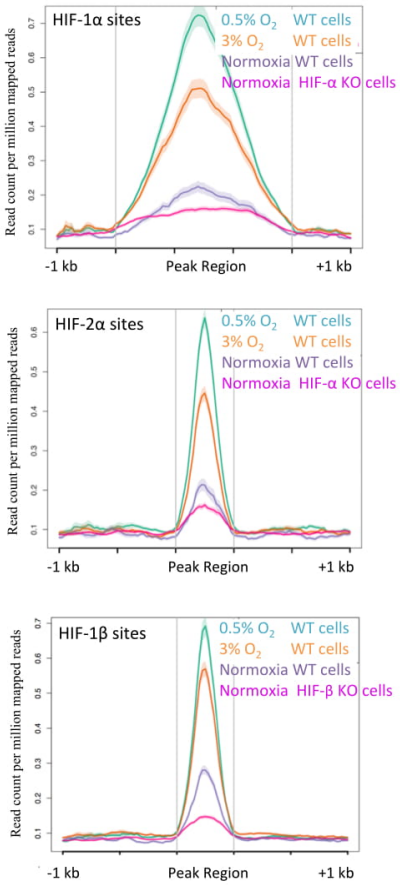

B

	Motif Found	*p*-value	Distribution
HIF-1α (n=1614)		1.2e-002	Not Centrally Enriched
		1.8e-002	Not Centrally Enriched
		2.3e-002	Not Centrally Enriched
HIF-2α (n=622)	No motif found		
HIF-1β (n=1031)		1.0e-003	Not Centrally Enriched

Figure 10. Characterisation of the specificity of normoxic HIF ChIP-seq signal. (A) RPKM of ±1 kb flanking regions around canonical HIF-1α, HIF-2α and HIF-1β binding sites are plotted, using the HIF ChIP datasets of wild-type (WT) cells at 0.5% O_2 (green), 3% O_2 (orange) and normoxia (purple). In addition, RPKM from the HIF-1α/2α double knockout (HIF-α DKO) cells at normoxica (pink) are plotted as baseline controls. (B) A *de novo* motif analysis is produced by MEME-ChIP using a ±150 bp window around the summit of HIF binding sites. Result are based on binding sites identified in the normoxic HIF-1α (n=1614), HIF-2α (n=622) and HIF-1β (n=1031) ChIP dataset. *p*-value refers to the significance of the motif. Distribution indicates the position of the discovered motif within the binding sites.

3.3 Discussion

Differential gene expression is controlled by the functional interactions between transcriptional factors (TFs) and the DNA (Simicevic et al., 2013). The cellular abundance of inducible TFs is an important determinant of their regulatory activities. However currently there has been little detailed investigation into the potential consequences that differing protein levels of inducible TF may have on genome-wide DNA binding patterns.

This chapter investigated the binding of HIF-1α, HIF-2α, and HIF-1β at canonical sites in response to graded oxygen concentrations (21%, 3% and 0.5% O_2) in HKC-8 cells. The abundance of the HIF protein was measured by immunoblots, and the actual occupancy was measured by ChIP-seq, which allowed an unbiased pan-genomic coverage of HIF DNA-binding sites.

Using stringent criteria that required detection of the site with both HIF-α and HIF-1β in at least one replicate, a total of 679 canonical sites were defined in the HKC-8 cells. This number was comparable to the number of sites previous identified in MCF-7 cells (Schödel et al., 2011). However, it was less than most other endogenous TFs which were detected bound to several thousand genomic regions, such as mammalian estrogen receptor (over five thousands sites found in Carroll et al., 2006) or myc and E2F1 (20,000 to 30,000 sites identified in Bieda et al., 2006). This suggests that there is somewhat smaller number of genes that are directly regulated by HIF as opposed to these responses.

3.3.1 Increased HIF-α protein is translated into increased DNA-binding

The parallel analysis of HIF-α protein level and genome-wide DNA binding has confirmed that the increase in HIF-α protein (by immunoblot) with increased severity of hypoxia is reflected in an increase in DNA-binding. However the fold increase in HIF-α protein level with hypoxia grade did not exactly match the fold increase in DNA-binding.

There could be many reasons for this. In the case of ChIP, the antibodies are detecting HIF-α proteins in the context of non-denatured protein-DNA complexes. It is possible that some epitopes could be masked, whereas with immunoblotting the detection is of largely denatured HIF-α protein. It is therefore not surprising that greater fold-changes are detected with immunoblotting. Other considerations are antibody specificity, as the antibodies used for immunoblot and for ChIP experiments were different, i.e. monoclonal antibodies were used for the immunoblot.

Furthermore, the immunoblot quantification was based on the HIF level using a whole cell extract procedure, whereas ChIP experiments were specifically measuring the chromatin-bound HIF. In any case we find that increases observed in HIF-α protein level are broadly paralelled by increased DNA-binding. Although not the remit of this investigation if we wished to obtain the absolute copy number quantification of a TF, newly emerged approaches with higher sensitivity and dynamic range can be considered. For example, combined SRM (selected reaction monitoring) and high-resolution mass spectrometry are able to detect between 5,000 and 50,000 HARS protein (histidyl-tRNA synthase) per cell (Simicevic et al., 2013). In addition, microfluid-based technology with a fluorescence based 'detect and bleach' strategy, can detect <30 EGFP protein (Burgin et al., 2014).

HIF-1β protein level was found to be unchanged across all three oxygen concentrations, however its DNA-binding increased with hypoxia severity, i.e. it correlates with HIF-α binding. This indicated that HIF-1β DNA-binding was hypoxia inducible, consistent with its binding to the DNA following heterodimerisation with a HIF-α subunit.

Overall, the analyses revealed that increased HIF-α DNA-binding was in accordance with increased HIF-α protein level. However, this is not always the case for

other TF such as RXRα (Retinoid X Receptor Alpha) and PPAR-γ (Peroxisome proliferator-activated receptor gamma). Simicevic et al., described a discrepancy between the protein level of TF and the level of its DNA binding during the terminal differentiation stage of mouse 3T3-L1 pre-adipocytes. The binding (measured by ChIP-seq) of these two TFs substantially increased, even though the TF protein has reached the maximal level and remained unchanged (measured by SRM-based mass spectrometry) (Simicevic et al., 2013). The authors reasoned that this was potentially due to the chromatin remodelling events at this stage such that more medium- to high-affinity sites become available for DNA-binding.

3.3.2 Increased binding occurred at the same canonical sites

The analyses in this chapter support a continuum model for HIF-α binding in response to acute (6h) hypoxia of graded severity, where essentially binding at all pre-existing sites increased, i.e. there were no unique canonical sites only detectable at either mild or severe hypoxia (**Figure 4B**). This is different to observations with other TFs, such as MITF, where high and low expression levels result in different target gene repertoires and phenotypes, possibly through the post-translational modification of MITF and its interaction with other co-factors.

It is worth noting that the analyses in this chapter are based on a particular definition of canonical sites (i.e. sites defined by the presence of both HIF-α and HIF-1β with detection of each isoform in at least one replicate). It is possible that because of the noise between the replicates for individual ChIP experiments, the current study might not be sensitive enough to investigate the binding at the weak binding sites. More replicates and/or more sequencing depth could be considered to improve the analysis.

Because of the pre-determined patterns of canonical HIF binding, by extrapolation the HIF transcriptional response to graded hypoxia will therefore be a progressive

induction of mRNAs. This is supported by existing observations, e.g. exponential increases in *EPO* mRNA levels were demonstrated in Hep3B cells as the oxygen concentration decreased (Fandrey et al., 1993); microarray analysis comparing gene expression at 1% and 5% O_2 also confirmed that the genes closely following the HIF stabilisation patterns at these two conditions (Holmquist-Mengelbier et al., 2006).

3.3.3 There is an uneven distribution of binding across the canonical HIF–α binding sites

Even though the data indicates a unimodal distribution of HIF-α binding in response to graded hypoxia, a biological continuum of loading behaviours were detected by analysing the extremes of the binding distribution (**Figure 5B and Figure 7B**). In an attempt to explore whether there were differences between sites that varied most or least with graded hypoxia, HIF-1α (or HIF-2α) sites were artificially separated in a bimodal manner into progressive-loading sites and early-saturated sites. Analyses on the two groups showed weak but significant differences in their distribution to the TSS, and associated biological pathways. There was also a subtle difference in the average number of RCGTG per binding site within the two groups of sites, which could potentially explain the observation that those progressive-loading sites were more responsive to acute graded hypoxia due to their higher number of RCGTG in each site.

Even though some weak differences between the two manually separated sites exist, they were not strong enough to predict a progressive-loading versus an early-saturated behaviour. More replicates of these graded ChIP experiments would be required to verify this potential finding of modestly differential loading behaviour.

HIF-α binding sites were also separated into ‘strong’ and ‘weak’ sites, based on their binding strength. However, again there were few significant differences in terms of the distribution around TSS, associated biological pathways and motif signatures.

3.3.4 HIF-1α and HIF-2α display distinct hypoxic binding profiles

Within the total 679 canonical sites, there were 450 HIF-1α sites and 403 HIF-2α sites, indicating the two isoforms bound largely overlapping but not identical group of sites. This was consistent with previously published analysis of HIF-1α and HIF-2α binding sites (Mole and Blancher et al., 2009; Schödel et al., 2011). HIF-1α binding sites were found to bind closer to the TSS, whereas HIF-2α bound more distantly from the promoters, which is in accordance with recent findings in 786-O cells (Salama et al., 2015).

Although the DNA-binding of both isoforms increased in response to graded hypoxia, their pan-genomic binding profiles remained quantitatively different to each other and this signature was not affected by changes in hypoxia severity (**Figure 3**). This suggests that the differential binding of HIF-1α and HIF-2α is not a function of O_2 gradient i.e. a HIF-1α profile cannot be converted to a HIF-2α profile by changing the O_2 concentration or vice versa. Our data also indicates that HIF-1β may be more associated with HIF-1α, as HIF-1β ChIP always clustered with HIF-1α rather than HIF-2α ChIP datasets (**Figure 3**). Furthermore, on the MA plot trying to separate two groups of sites, HIF-1β signal was better in recapitulating HIF-1α signal at canonical sites than that of HIF-2α sites (**Figure 5D and Figure 7D**). This could be either due to technical reasons that HIF-2α dataset has less read counts (i.e. due to the high variation between the HIF-2α ChIP replicates as shown by the correlation coefficient R_2), or it could be a true biological signal that there is less HIF-2α binding at the canonical sites.

Notably it was not possible to distinguish HIF-1α from HIF-2α binding motif preferences, even for residues outside the RCGTG consensus. This suggests that the specificity of HIF isoform binding does not depend on the core HRE composition, but rather on the cooperation with other transcription factors or the chromatin architecture.

3.3.5 HIF protein and DNA-binding in normoxic HKC-8 cells

In the present study we have very little evidence of normoxic HIF-α binding in our ChIP analysis, since the normoxic binding in the WT cells largely overlapped with the binding in the HIF-α knockout cells. The cross-reactivity of the antibody, or amplification of background DNA in the library presentation step most likely accounted for the majority of the normoxia signal. Existing studies have reported normoxic HIF-α binding in other cell lines. For example, study in a lung epithelial cell line BEAS-2B has indicated a constitutive expression of HIF-2α and an enrichment of HIF-2α binding across the genome were found under normoxia (Lee et al., 2016). Mimura and colleagues observed binding of HIF-1α at *SLC2A3* locus under normoxia in HUVEC cells and the signal was assigned by HIF-1α siRNA (Mimura et al., 2012). Normoxic HIF-α binding may therefore be restricted to only certain cell types.

Some HIF-1β binding in normoxia was detected in the WT cells, but not in the HIF-1β knockout cells. However the level was low compared to the binding in hypoxia. The nature of this normoxic HIF-1β signal in the WT cells is unclear. There was no strong evidence for enrichment of the RCGTG motif in the HIF-1β binding sites identified under normoxia condition, nor for enrichment of other motifs, such as AHR/ARNT binding motif 5'-GCGTG-3', the Xenobiotic Responsive Element (XRE), which is the motif that HIF-1β and its other most notable heterodimersation partner AHR bound to (Swanson. 2002). AHR is expressed in the HKC-8 cells, however in this study its DNA-binding would not have been induced under normoxia. Overall the results indicate that the signals that arose in the normoxia HIF-1β ChIP experiments were likely to be noise.

Rather surprisingly, I also observed some binding signals at the HIF canonical sites in the HIF KO cells. It is possible that HIF sites present at the open chromatin

regions therefore they are more likely to be bound by antibodies due to cross-reactivity, or these sites might bind other TFs (e.g. ARNT2) that might cross-react with HIF.

3.4 Conclusion

The current quantitative analysis of ChIP-seq datasets reveals that in response to increased hypoxia severity, there is an increased HIF binding at the pre-ordained and essentially the same canonical sites, which correlates with the increased HIF protein levels. Hypoxia severity fine-tunes the magnitude of binding signal at the intrinsically defined sites. There is an uneven distribution of binding signals observed across those sites. Sites with higher numbers of RCGTG motifs or located closer to the TSS tend to load more when the hypoxia condition becomes more severe. However, these features are not strongly distinguishing and therefore are not able to predict the behaviour of a given locus in response to graded hypoxia. In this study, distinct HIF-1α and HIF-2α binding patterns are observed and they are maintained across a range of hypoxic conditions, indicating the differential binding profiles between HIF-α subunits are not a function of oxygen gradient.

A

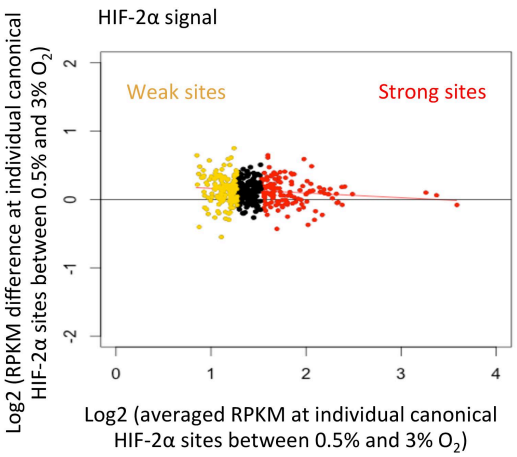
HIF-2α signal
Weak sites
Strong sites
Log2 (RPKM difference at individual canonical HIF-2α sites between 0.5% and 3% O2)
Log2 (averaged RPKM at individual canonical HIF-2α sites between 0.5% and 3% O2)

B

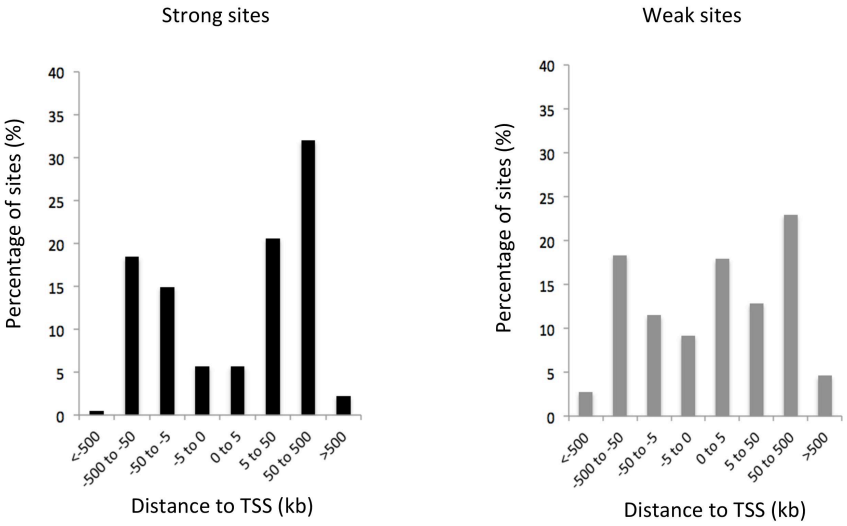
Strong sites
Weak sites
Percentage of sites (%)
<-500
-500 to -50
-50 to -5
-5 to 0
0 to 5
5 to 50
50 to 500
>500
Distance to TSS (kb)

C

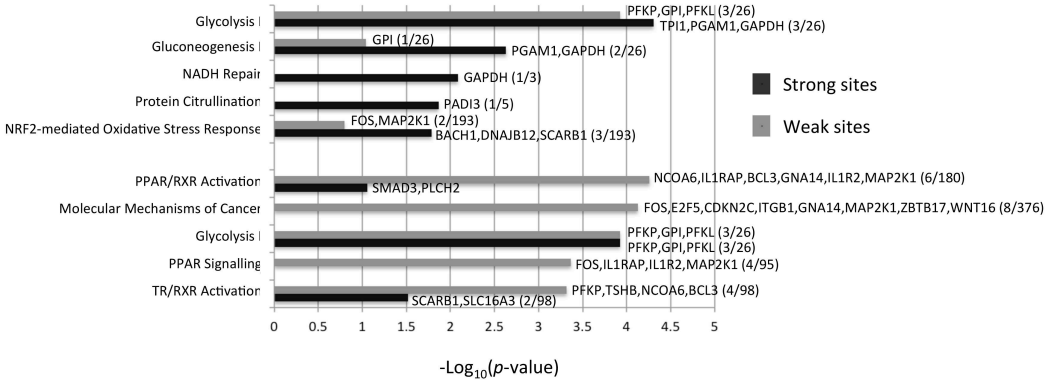

D

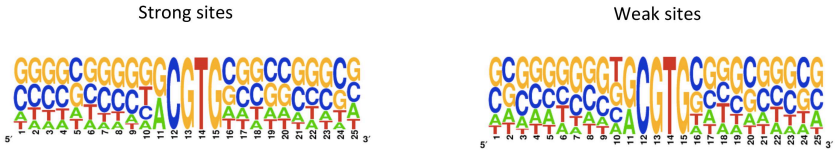

E

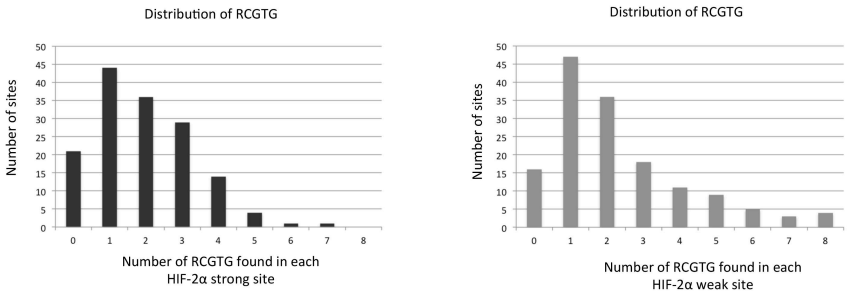

Supplementary Figure 1. Downstream analysis of HIF-2α binding sites that are divided based on the binding strength. (A) HIF-2α 'strong' and 'weak' binding sites are coloured as red and yellow respectively on the MA plot. (B) Histogram showing the percentage of binding sites according to the distance ±500 kb from the nearest transcriptional start site (TSS). (C) Analysis of the biological pathways for the annotated genes within each group (88 genes identified for the strong sites and 94 genes identified for the weak sites). The pathways are ranked by the –log10(*p*-value). The analysis is performed by Ingenuity Pathway Analysis (IPA). –log10(*p*-value)>1.3 is statistically significant. (D) Flanking sequence ±10 bp up and downstream of RCGTG motif is scanned using the online tool WebLogo (http://weblogo.berkeley.edu/) The height of each letter was proportionate to its frequency. (E) Histogram showing the distribution of the occurrence of RCGTG core motif within the peaks. On average there is 2.18 RCGTG per strong site, and 2.56 per weak binding site.

4

The Effects of Hypoxia Time-course on HIF DNA-binding Genome-wide

4.1 Introduction

External stimuli can contribute significantly to changes in gene expression. Several large-scale studies have analysed the dynamics of gene expression over the course of various developmental and environmental stimuli and showed changes in the mRNA levels of thousands of genes (Hamatani et al., 2004; Berry and Gasch. 2008). Regulation of the expression of these genes may be executed by various different mechanisms. One possible mechanism is through the direct regulation of transcription factor (TF) dynamics, such as TF protein expression, nuclear localisation and site-specific binding to DNA (reviewed in Hager et al., 2009). Stimuli can have a range of effects on TF dynamics and result in diverse gene expression profiles. For instance, γ -irradiation can result in pulses of p53 protein expression, whereas UV radiation induces sustained p53 activation (Purvis et al., 2012). In the same study, the authors showed that p53 pulses selectively activated target genes involved in transient responses to DNA damage,

whereas prolonged p53 activation resulted in the expression of senescence genes. Another example is that in the presence of stress stimuli, the yeast stress response TF Msn2 is dephosphorylated and rapidly enters the nucleus. Different stresses lead to distinct dynamics of Msn2 nuclear translocation and elicit different gene expression profiles (Hao and O'Shea et al., 2011). Several studies have also examined the TF DNA-binding profiles. Analysis of the salt stress response TFs Yap4 and Sko1 in yeast has identified multiple temporal classes of binding patterns for each of the TF, and this correlated with different gene expression profiles (Ni et al., 2009). In addition, genome-wide mapping of 38 TFs during the differentiation of mouse ESCs (embryonic stem cells) showed that the same factors could display a very different binding spectrum across different lineages (Tsankov et al., 2015). Overall, these results suggest that an individual TF may exhibit altered expression levels, localisation and binding patterns in response to different stimuli in order to differentially regulate gene expression and determine cell fates.

In the normal physiology, cells will not only be exposed to varying amplitude of oxygen level, but also to different durations of hypoxia, as well as periods of hypoxia and reoxygenation (reviewed in Michiels 2004; Bayer et al., 2011). Differing duration of hypoxia is also frequently observed in pathophysiological conditions, e.g. in solid tumours, due to the abnormal vascular geometry, limited diffusion of oxygen, and distribution of red blood cells (reviewed in Dewhirst et al., 2008). Furthermore, the presence of tumour hypoxia is generally associated with aggressive malignancy and resistance to radiation therapy and chemotherapy (reviewed in Brown et al., 2004).

It has been shown in multiple studies that the duration of hypoxia can result in dynamic changes in expression patterns of the HIF-α proteins. In general, this cellular response to hypoxia occurs rapidly. Exposure of mice to 6% oxygen resulted in

accumulation of HIF-1α protein in several organs in less than 1 hour (Stroka et al., 2001). HeLaS3 cells exposed to anoxia or hypoxia (0% or 0.5% O_2) showed nuclear induction of HIF-1α as assessed by western blots and DNA-binding by EMSA (electrophoretic mobility shift assay) in less than 2 min (Jewell et al., 2001). These observations suggest the HIF response to hypoxia is very rapid. However, the stability of HIF-1α and HIF-2α proteins can be differentially regulated by acute and chronic hypoxia. For example, using live single cell imaging and mathematical modelling, Bagnall et al., demonstrated that continuous hypoxia (1% O_2) in HeLa cells resulted in a rapid induction of HIF-1α and HIF-2α expression at 3h, however by 24h HIF-1α protein level had decayed whereas the HIF-2α protein level was more sustained (Bagnall et al., 2014). This dynamic of endogenous HIF-α expression in response to different durations of hypoxia was also in agreement with previous studies across a large range of O_2 levels and cell types (Lin et al., 2011; Ginouves et al., 2008; Moroz et al., 2009). Overall, the cell culture studies suggest a well-conserved phenomenon that HIF-1α protein rapidly increased within a few hours of hypoxia, but decreased to a lower base-line expression level after a longer period of hypoxia culture. By contrast, the hypoxic induction of HIF-2α protein remained high and stable throughout the period of hypoxia.

This differing dynamic of HIF-α protein expression in response to hypoxia time-course, raises the question as to whether varying HIF-α protein levels may elicit qualitatively different patterns of DNA-binding and consequent gene expression profiles, and whether it may provide for functionally distinct physiological responses to different durations of hypoxia. Several studies are consistent with this. For example, by studying the temporal expression profile of hypoxia-responsive genes in HUVEC (human endothelial) cells using microarray, Mimura et al., found that those early hypoxia inducible genes (i.e. up-regulated after 1,2,4 and 8h of hypoxia) were functionally

associated with response to oxygen level and glycolysis, whereas the late hypoxia regulated genes (i.e. genes up-regulated after 12h and 24h of incubation) showed a signature of angiogenesis and blood vessel development (Mimura et al., 2012). Another study by Baranova et al., showed that HIF-1α played different roles under acute and chronic ischemia, which is a condition due to insufficient blood flow and oxygen delivery (Baranova et al., 2007). In their *in vivo* mouse brain model, there was a biphasic increase of HIF-1α protein levels. In the first stage, until 12h after injury, HIF-1α protein peaked around 6h and this was correlated with up-regulation of mRNA and protein levels of pro-death genes (*BNIP3, NOXA, BNIP3L* and *DDIT4*). In the second phase, after a transient decline at day 1, HIF-1α protein expression increased again and remained elevated until at least day 8. During this period, none of these pro-death genes remained elevated. Instead mRNA levels of genes implicated in angiogenesis (*VEGF, FLT1, PAI-1, ANG-2*) were substantially higher. On the other hand, HIF-2α dependent gene expression is thought to be more critical in chronic hypoxia by mediating proliferation and survival advantages (Brahimi-Horn et al., 2007). Functionally, the sustained level of HIF-2α might indicate a necessity for keeping HIF-2α protein available to ensure sufficient regulation of HIF-2α target genes.

Overall, these results suggest that varying HIF protein expression in response to various durations of hypoxia can influence gene expression and cell fate decisions. However, these studies did not assess whether these genes with altered expression are direct targets of HIF, and therefore the exact mechanism of gene regulation cannot be easily deduced due to the complexity of effects arising from secondary transcriptional cascades, regulatory RNA networks and other indirect actions of induced genes. Furthermore, the mRNA level of HIF targets may be dependent on multiple factors affecting its processing and stability. Hypoxia can either accelerate mRNA decay or

increase mRNA stability by regulating RNA-binding proteins and microRNAs, therefore the levels of mRNA present in the cells may vary dramatically in response to hypoxia, sometimes in the absence of transcriptional changes (reviewed in Gorospe et al., 2011). In addition, variation in the mRNA levels of HIF targets may also result from the indirect effects of cross talk between HIF and other signalling pathways or secondary cascades under hypoxia, e.g. NF-κB (reviewed in Morais et al., 2011), PI3K/AKT pathway (Zhong et al., 2000) and reactive oxygen species (reviewed in Klimova and Chandel 2008),

Therefore in order to reveal how HIF responds to the variable duration of hypoxia, I again chose to measure its direct DNA-binding profiles. In the previous chapter, I showed that increases in HIF-1α and HIF-2α protein levels in response to acute hypoxia (6h) in HKC-8 cells are paralleled by increases in DNA-binding detected by ChIP-seq. A set of stringent canonical HIF binding sites were defined and HIF binding profiles were examined at 21%, 3% and 0.5% O_2. Overall the results suggested that the degree of hypoxia led to quantitative changes in both HIF-α protein expression and DNA-binding, but did not generate qualitatively new binding sites, or block existing sites. However it remains quite possible that HIF DNA-binding profiles may change qualitatively over a time-course of hypoxia exposure.

Hypoxia can have profound effects on the epigenetic landscape (reviewed in Perez-Perri et al., 2011; Tsai and Wu. 2014). For example, prolonged hypoxia culture (72h) led to increased global levels of DNA methylation and H3K9 histone acetylation in prostate cancer cells (Watson et al., 2009). It is known that HIF DNA-binding is dependent on an open chromatin configuration and is sensitive to CpG methylation (Wenger et al., 1998; Rössler et al., 2004). Therefore, the HIF response may be superimposed upon a background of epigenetic changes induced by different durations of hypoxia, and as a result the binding profiles of HIF proteins may change.

It was hypothesised that understanding the relationship between HIF protein levels and DNA-binding profiles over different periods of hypoxia might provide new insights for manipulating them in a controlled way. In addition, this may have important implications when considering new therapeutic strategies and designing of selective targets for diseases associated with chronic hypoxia such as ischaemia and cancer.

Therefore, study HIF DNA-binding in response to different durations of hypoxia, I applied ChIP-seq experiments in HKC-8 cells and mapped the direct HIF canonical binding sites in acute (6h, 16h) and chronic (48h) hypoxia; 0.5% O_2 was chosen for these ChIP-seq experiments as it was anticipated to give the highest level of HIF-α protein (as shown in chapter 2). Overall, I sought to explore and address the following key questions:

1. Is HIF-α binding profile in acute hypoxia the same as in chronic hypoxia?
2. Are some targets preferentially bound by HIF-α at certain hypoxia time point?
3. For each HIF-α isoform, how does the level of protein over time relate to the binding to the targets?
4. Is there a differential utilization of either HIF-1α or HIF-2α protein in acute versus chronic hypoxia?

I measured the HIF protein levels qualitatively by immunoblot, and also analysed HIF binding signals from ChIP-seq datasets in a quantitative manner.

4.2 Results

4.2.1 Effect of different durations of hypoxia on patterns of HIF proteins

Previous published studies have described different HIF-1α and HIF-2α protein induction patterns in response to hypoxia time-course (Lin et al., 2011; Ginouves et al., 2008; Moroz et al., 2009). In order to examine the HIF protein response in HKC-8 cells, cells were cultured at 0.5%, 1% and 3% O_2 for 0h, 3h, 6h, 16h, 24h and 48h. Whole cell extracts were prepared and the levels of HIF-1α and HIF-2α protein were examined by immunoblot and quantified by densitometry (**Figure 1A**). In all three oxygen concentrations tested, HIF-1α protein increased rapidly in response to hypoxia exposure with a maximum induction between 3h and 6h, and then gradually decreased. HIF-2α protein was also quickly induced by hypoxia but, in contrast to HIF-1α, the level appeared to be more sustained over time. A similar result was also seen by immunoblot of the same cell extracts using independent HIF-α antibodies (**Figure 1B**). In addition, the level of induction of HIF-1α was substantially higher than that of HIF-2α.

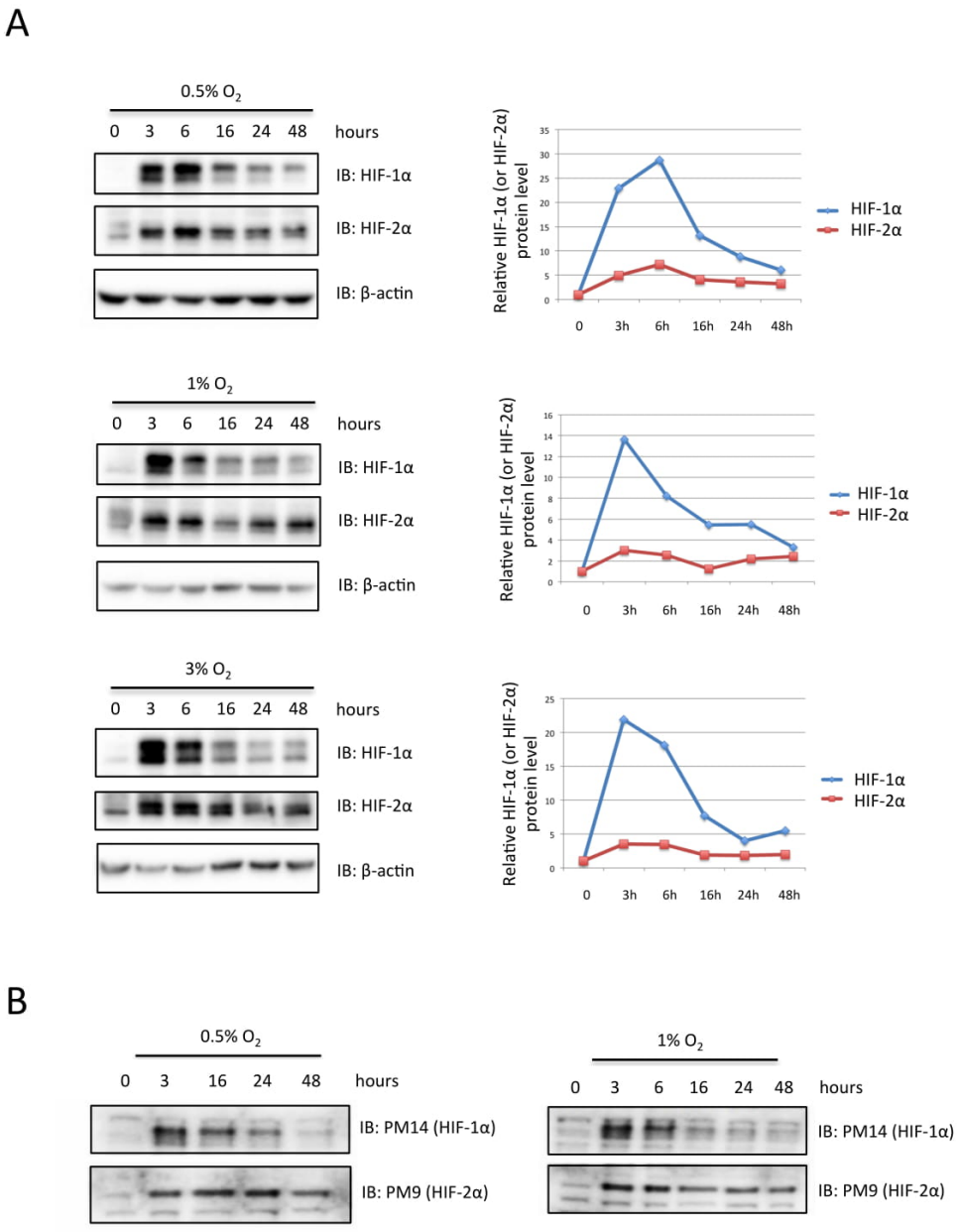

Figure 1. Immunoblot and quantitation analysis of HIF-α protein levels in HKC-8 cells in response to different durations of hypoxia. (A) HIF-1α and HIF-2α protein levels are examined by immunoblotting using whole cell extracts from cells incubated after 0h, 3h, 6h, 16h, 24h and 48h at either 0.5%, 1% or 3% O_2. The antibodies used for HIF-α immunoblotting were mouse monoclonals raised against epitopes in human HIF-1α or human HIF-2α. The signal intensity is quantified by BioRad ChemiDoc MP imaging software. The HIF-α signal at each time point is normalised to its respective b-actin loading control signal, and then expressed as a relative fold change to the normoxic (i.e. 0h) signal. (B) Independent rabbit polyclonal antibodies PM14 (HIF-1α) and PM9 (HIF-2α) are used to blot the same extracts. Immunoblots with both sets of independent antibodies gave a similar expression pattern of HIF-α protein, i.e. HIF-1α protein showed a rapid induction under hypoxia and the level decreased quickly, whereas HIF-2α protein level was less induced under hypoxia but appeared to be more sustained throughout the period of hypoxia exposure.

4.2.2 ChIP-seq experiment for HIF-1α, HIF-2α and HIF-1β

Given that the patterns of HIF-1α and HIF-2α protein induction following the hypoxia time-course were similar at 0.5%, 1% and 3% O_2 (**Figure 1**), one oxygen concentration, 0.5% O_2, was chosen for ChIP-seq analysis. ChIP-seq experiments using antibodies against HIF-1α, HIF-2α and HIF-1β were performed in HKC-8 cells incubated at 0.5% O_2 for 0h, 6h, 16h and 48h as illustrated in **Table 4.1**. The same antibodies and ChIP protocol from the previous chapter were used.

Table 4.1. An overview of ChIP-seq experiments studied in this chapter

cell line	condition	ChIP	reps
HKC-8 WT	Normoxia	HIF-1α, HIF-2α, HIF-1β	1
HKC-8 WT	6h 0.5% O_2	HIF-1α, HIF-2α, HIF-1β	2
HKC-8 WT	16h 0.5% O_2	HIF-1α, HIF-2α, HIF-1β	2
HKC-8 WT	24h 0.5% O_2	HIF-1α, HIF-2α, HIF-1β	2
HKC-8 HIF-1/2α double KO	Normoxia	HIF-1α, HIF-2α, HIF-1β	1
HKC-8 HIF-1β KO	Normoxia	HIF-1α, HIF-2α, HIF-1β	1

Whole cell extracts were harvested in parallel with the ChIP-seq experiments to enable immunoblotting and quantitation of HIF protein levels under the ChIP-seq experimental conditions. This showed that both HIF-1α and HIF-2α protein levels increased rapidly in hypoxia (**Figure 2A**). For both isoforms, HIF protein levels were highest at 6h of hypoxia incubation. HIF-1α protein showed a marked decline between 6h and 16h (and between 6h and 48h) of hypoxia exposure, whereas HIF-2α protein appeared to be more sustained. This pattern was observed clearly in ChIP-seq replicate 1 and in an independent immunoblot experiment, as well as in the pilot test experiment in **Figure 1A**. Immunoblots of the ChIP-seq replicate 2 revealed a similar pattern, but HIF-2α protein level appeared to be less stable over time. In all these comparisons, the HIF-1β level remained unchanged.

Immunoblot band densities from the two ChIP-seq experiments, together with the independent immunoblot experiment were quantified (**Figure 2B**). There was a 14.5-fold hypoxic induction of HIF-1α protein at 6h, followed by 0.43-fold decrease between 6h and 16h, or a 0.48-fold decrease between 6h and 48h. These differences in HIF-α protein level between 6h and 16h, and between 6h and 48h were significant. By contrast, the hypoxia induction of HIF-2α protein was much less compared to HIF-1α. There was only a 3.8-fold increase at 6h, and the differences in quantitation of HIF-2α protein level were not significant between 6h and 16h, and between 6h and 48h. Overall, the quantitation revealed that HIF-1α and HIF-2α protein levels both declined after prolonged hypoxia culture. However, HIF-2α protein appeared to be less hypoxia inducible and more sustained.

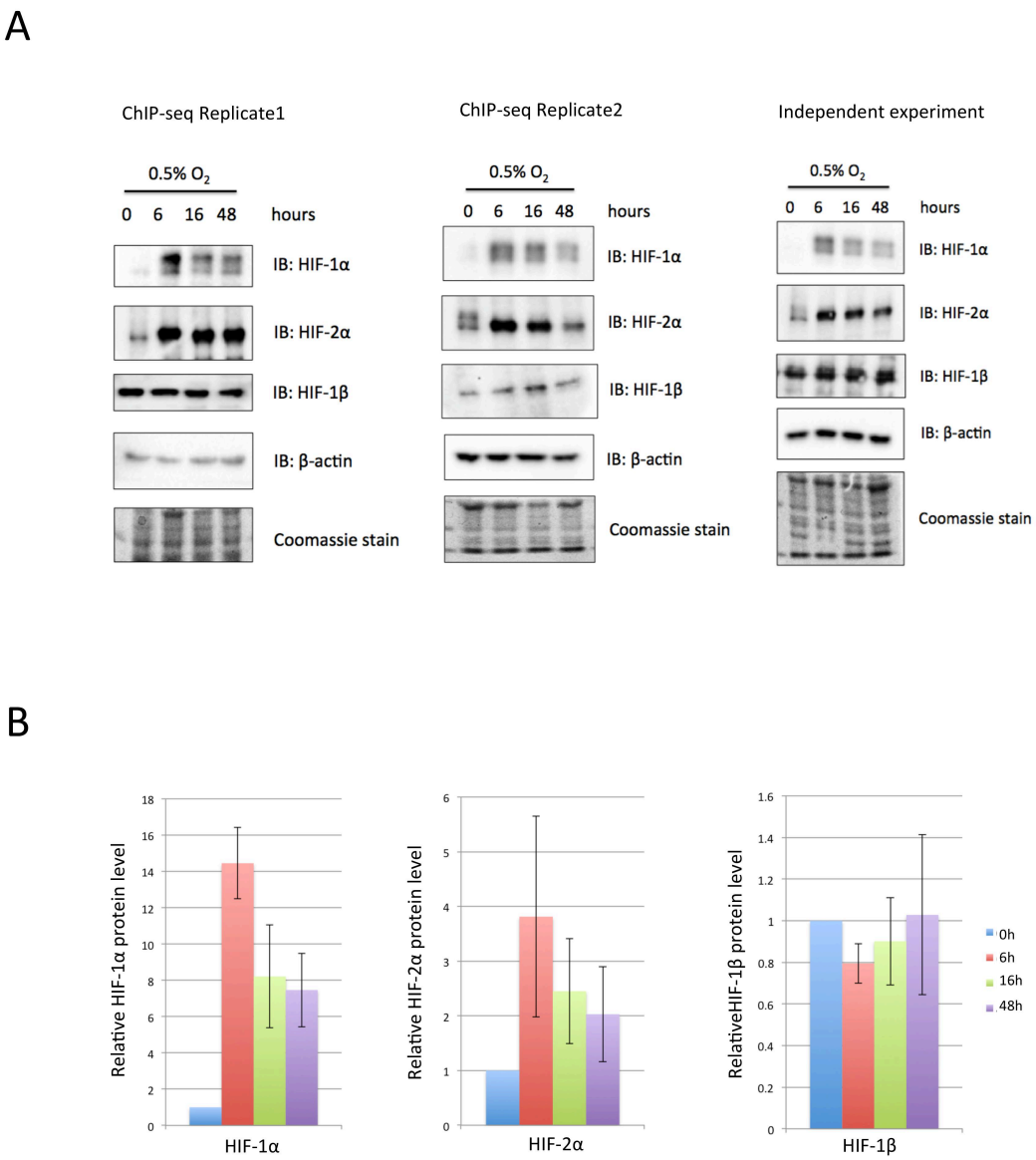

Figure 2. (A) Immunoblots of HIF subunits using whole cell extracts that were harvested in parallel with ChIP-seq samples, for quantitation of protein levels and as an assurance of materials submitted for sequencing. In addition, a third replicate of immunoblot was prepared independently for quantitation analysis. (B) Densitometry analysis of the relative fold difference for each HIF subunit. Immunoblot band intensities were first normalised to the respective b-actin signal in each condition, and were then displayed as a relative ratio to its respective normoxic (i.e. 0h) signal. Data is shown as mean ± SEM, n=3.

4.2.3 Genome-wide HIF binding

Having quantified the effect of various durations of hypoxia on HIF-1α and HIF-2α protein level, the effect on genome-wide HIF binding was next assessed. To be consistent with the analysis in the previous chapter, peak calling was also performed using HIF ChIP-seq data from HIF knockout cells as controls, i.e. HIF-α peaks in the WT cells were called as regions with significant enrichment of read counts over the respective regions in the HIF-1α/2α double knockout cells ($p<0.0001$), and HIF-1β peaks were called with the same criteria, using the HIF-1β knockout cells as controls. Signals under the peaks were then expressed as RPKM.

The analyses in this chapter (as in Chapter 3) were performed using canonical HIF binding sites (i.e. sites with both HIF-α and HIF-1β binding) since gene expression analyses in WT versus HIF mutant cells (Chapter 2) indicate these sites are more likely to represent functional HIF binding profiles. As in the previous chapter, the canonical binding sites were defined using two different criteria. In the first and most stringent approach, HIF-1α (or HIF-2α) sites were defined qualitatively in each condition by the presence of both HIF-1α (or HIF-2α) and HIF-1β in each of the two replicates. However, for some conditions this resulted in a very low number of binding sites (**Supplementary Figure 1**). In order to generate a sufficient number of sites for downstream analysis, a less stringent criterion, which was also used in the previous chapter, was considered. In the second approach, canonical binding sites at each condition were defined by the detection of both HIF-1α (or HIF-2α) and HIF-1β in at least one replicate. In total this approach gave 1398 canonical HIF-α sites that were detected at either 6h, 16h or 48h of hypoxia, of which 926 were bound by HIF-1α, and 803 were bound by HIF-2α. The reproducibility of ChIP signals was assessed by comparing the binding signal at canonical HIF binding sites defined in each condition, between the two replicates (**Figure**

3). In most cases (and as expected), the correlation between the replicates was lower than when the canonical HIF binding sites that were more stringently defined. This analysis also indicated that HIF-2α ChIP samples in particular were sub-optimal, i.e. R_2 is smaller than 0.5 (especially the HIF-2α ChIP performed at 48h 0.5% O_2). In order to minimise the level of signal variation, the RPKM values of the two replicates were averaged and this averaged RPKM value was then used in the following analyses.

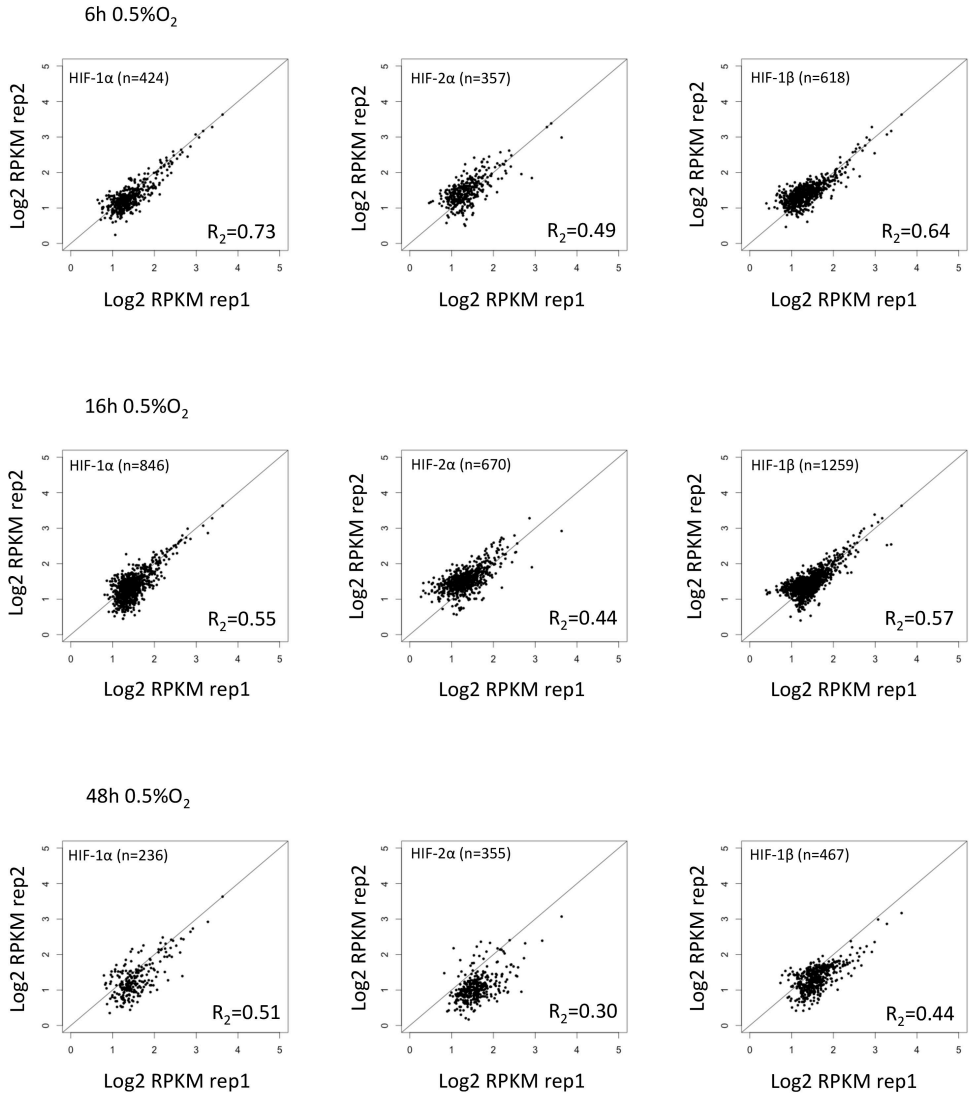

Figure 3. Reproducibility between ChIP-seq replicates at canonical HIF binding sites. HIF-α sites are defined at each condition by the presence of both HIF-1α (or HIF-2α) and HIF-1β with detection of each isoform in at least one replicate. HIF-1β sites are HIF-1α and HIF-2α sites combined. The number of qualified binding sites is shown on each plot. For each binding site, the normalised binding signal (i.e. RPKM) from replicate 1 (horizontal axis) is plotted against the signal from replicate 2 (vertical axis) in a Log2 scale. The correlation of signal between two replicates is shown by the R-squared values.

To assess the similarity between HIF-1α, HIF-2α and HIF-1β ChIP samples performed at the different hypoxia time points, the total RPKM value of the HIF-α canonical binding sites (n=1398) in each ChIP sample were compared with each other.

Both the Hierarchical Clustering Analysis and the Heatmap showed a clustering of ChIP experiments performed using the same antibody irrespective of the hypoxia time point (**Figure 4A and 4B**). This suggests that a HIF-1α profile cannot be converted to a HIF-2α profile as a result of different durations of hypoxia (and vice versa). Furthermore, ChIP experiments with HIF-1α and HIF-1β antibody were clustered more closely to each other, indicating that there is a higher similarity between the binding signals of these two subunits. By contrast, HIF-2α ChIP experiments performed at all hypoxia time points were clustered separately.

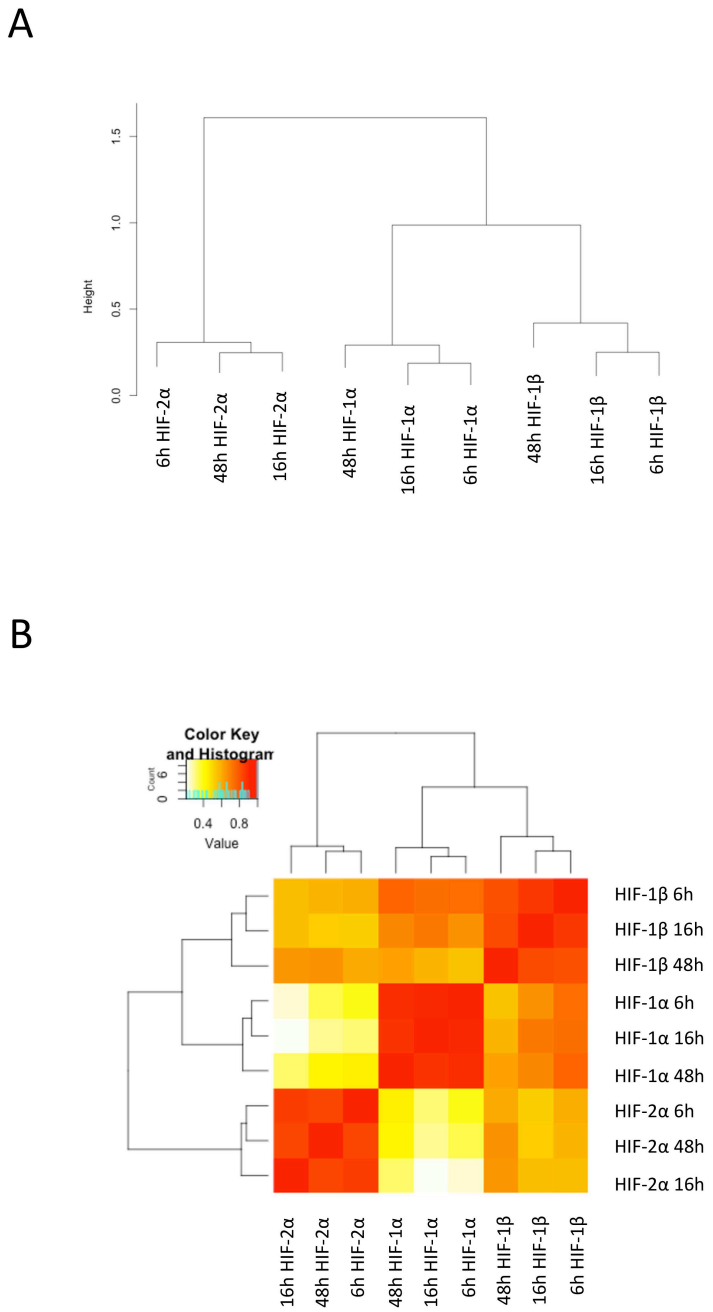

Figure 4. Quantitative analysis comparing HIF ChIP signal at previously defined canonical sites across multiple hypoxia conditions. HIF-1α and HIF-2α canonical binding sites that appeared at 6h, 16h or 48h of hypoxia are combined to give a total of 1398 sites. For each site, the analysis uses the averaged RPKM from the two replicates. (A) Cluster dendrogram is performed to compare the total RPKM values of each ChIP dataset. The height (distance) between the clusters displayed in the dendrogram refers to the similarity of each of the HIF ChIP samples. (B) Data is also displayed in the Heatmap format. The colour in the heatmap matrix refers to the correlation between each ChIP sample. The higher the correlation, the more intense the colour is.

4.2.4 Binding at canonical sites does not match the total protein level

To understand how the DNA-binding profile of individual HIF subunits is affected by the duration of hypoxia, the relative proportions of raw reads at HIF-1α, HIF-2α and HIF-1β canonical binding sites at 0h, 6h, 16h and 48h of hypoxia were compared (**Figure 5**). In contradistinction to the observations made at the protein level, where both HIF-α isoforms showed a maximal induction at 6h, HIF-1α and HIF-2α DNA-binding was found to be highest at 16h. This discrepancy potentially represents a delay between HIF-α protein induction and DNA-binding. In addition and also in contrast to the protein level, the DNA-binding signals observed at 6h and 48h for either HIF-1α or HIF-2α were found to be comparable.

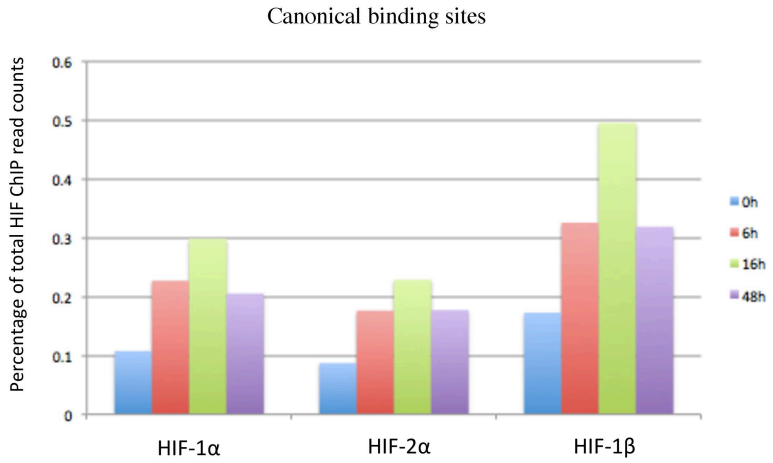

Figure 5. Binding signal at HIF canonical binding sites in response to different durations of hypoxia. For each HIF subunit (i.e. HIF-1α, HIF-2α and HIF-1β), the sites are a combination of canonical sites that appeared in the HIF ChIP performed under either 6h, 16h or 48h of hypoxia. This gives a total of 926 HIF-1α sites, 803 HIF-2α sites, and 1398 HIF-1β sites. Raw reads in the HIF binding sites at each hypoxia time point are expressed as a percentage of the total reads in that ChIP. The figure shows that for all HIF subunits, the total binding at canonical sites increased under hypoxia and peaked at 16h, then decreased from 16h to 48h.

In a hypoxic environment, HIF-α escapes degradation and dimerises with HIF-1β, and binds to HREs in the regulatory regions of hypoxia-inducible genes (Semenza, 1998). Therefore one explanation of this discrepancy between HIF protein induction and DNA-binding could be that immunoblots from whole cell extracts may not accurately represent

the abundance of HIF-α protein either in the nucleus, or on the chromatin. In order to detect HIF protein levels in individual cell fractions, after incubating cells for 6h or 16h at 0.5% O_2, extracts were separated into cytoplasmic, nucleoplasmic and chromatin fractions prior to immunoblotting for HIF (**Figure 6A**). Consistent with canonical (i.e. heterodimeric) HIF-α binding, HIF-1β protein showed more association with chromatin under hypoxia (6h and 16h) than under normoxia. For HIF-α, the result suggested that the majority of HIF-α protein present in the cell at both 6h and 16h of hypoxia was indeed chromatin bound. It also confirmed a discrepancy between the maximal chromatin-association of HIF-α protein at 6h and the maximal DNA-binding signal (assessed by ChIP-seq) at 16h.

Another possible explanation for this discrepancy is that the HIF-α protein level detected by immunoblot (i.e. the denatured protein) may not reflect the HIF-α protein level 'visible' by immunoprecipitation (i.e. non-denatured protein). Therefore, to more closely resemble the ChIP experiment, HIF-1α immunoprecipitation was also performed at 6h or 16h of hypoxia using the ChIP grade antibody (PM14). The immunoprecipitation samples were then immunoblotted for HIF-1α (**Figure 6B**). The results indicated that there was no difference in the efficiency of HIF-1α immunoprecipitation from extracts prepared after 6h and 16h of hypoxia, and provided further evidence that HIF-1α protein was indeed more abundant at 6h than at 16h of hypoxia.

In summary, all measurements of HIF-α protein levels indicate a higher level of HIF-α protein at 6h of hypoxia compared to 16h. Because all ChIP samples were processed in the same way, it is therefore unlikely that the discrepancy comes from a bias in the bioinformatics analysis. This raised the possibility as whether the discrepancy might be a bias in the sequencing of the ChIP experiment. To address this, HIF DNA-binding in response to timed hypoxia was examined by ChIP-qPCR experiments. Using

the two DNA samples submitted for ChIP-seq and a third independent ChIP experiment, the enrichment of HIF-1α, HIF-2α, and HIF-1β binding at the NDRG1 HRE was measured (**Figure 6C**). Consistent with the ChIP-seq data, the binding of all three HIF subunits at the *NDRG1* HRE was maximal at 16h of hypoxia.

Overall, a discrepancy between HIF protein level and DNA-binding in response to different durations of hypoxia was observed. Even though HIF-α protein reached the maximum level at 6h, the DNA-binding peaked later at 16h.

A

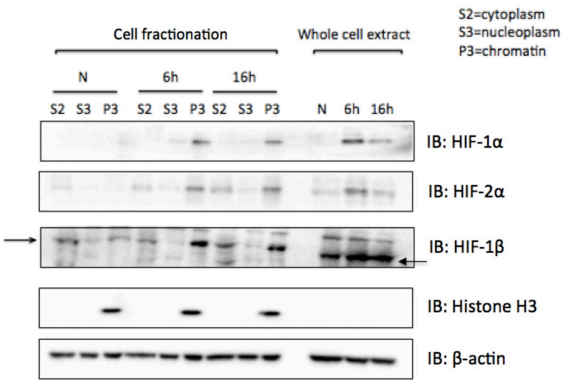
Cell fractionation
Whole cell extract
S2=cytoplasm
S3=nucleoplasm
P3=chromatin
N
6h
16h
S2 S3 P3 S2 S3 P3 S2 S3 P3 N 6h 16h
IB: HIF-1α
IB: HIF-2α
IB: HIF-1β
IB: Histone H3
IB: β-actin

B

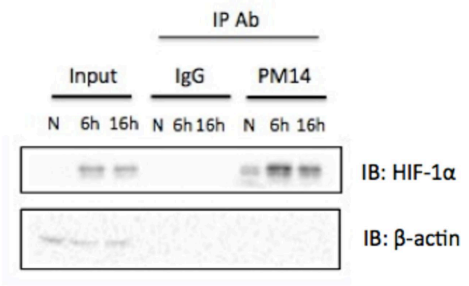
IP Ab
Input
IgG
PM14
N 6h 16h N 6h 16h N 6h 16h
IB: HIF-1α
IB: β-actin

C

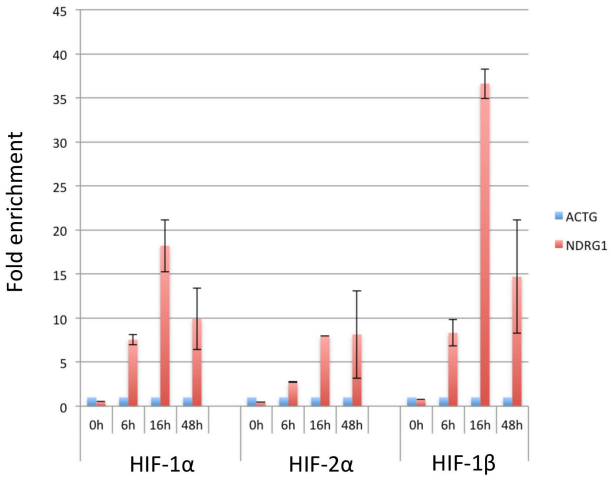
Fold enrichment
45
40
35
30
25
20
15
10
5
0
0h 6h 16h 48h
0h 6h 16h 48h
0h 6h 16h 48h
HIF-1α
HIF-2α
HIF-1β
ACTG
NDRG1

Figure 6. Investigating the discrepancy between the maximal HIF binding signal (16h) and the maximal HIF-α protein level (6h). (A) Subcellular fractionation experiments in HKC-8 cells cultured at 0h, 6h and 16h under 0.5% O_2. The extracts were separated into cytoplasm (S2), nucleoplasm (S3) and chromatin (P3) fractions. Immunoblots of HIF-α (with mouse monoclonal antibodies), HIF-1β and Histone H3 were performed using extracts from each fraction, as well as using whole cell extracts prepared in parallel. H3 was used as a control for the chromatin fraction, and b-actin was used as a loading control for all samples. (B) Immunoprecipitation of HIF-1α was followed by immunoblot. Cells were harvested after 0h, 6h and 16h under 0.5% O_2. PM14 (HIF-1α antibody used for ChIP-seq) was used for immunoprecipitation, and the mouse monoclonal antibody was used for immunoblot. The result showed that there was more HIF-1α protein being precipitated by the PM14 antibody under 6h hypoxia than under 16h hypoxia. (C) ChIP-qPCR signals of HIF-1α, HIF-2α and HIF-1β binding at *ACTG* (g-actin, an intergenic region used as a negative control) and *NDRG1* HRE (a HIF-binding enhancer) in response to hypoxia time-course. Fold enrichment was calculated as delta-delta CT value, and was normalised to the enrichment at the *ACTG* locus. Samples were from the two replicates of ChIP-seq experiments and an independent ChIP experiment. Data is shown as mean ± SEM (n=3).

4.2.5 Qualitatively, HIF subunits display different binding profiles under timed hypoxia

Mimura et al., previously identified temporal differences in hypoxic gene expression in HUVECs cultured up to 48h at 1% O_2 (Mimura et al., 2012). To examine whether a temporal response also presents at the level of HIF DNA-binding in HKC-8 cells, canonical HIF binding sites that appeared at 6h, 16h and 48h of hypoxia were compared by Venn diagrams (**Figure 7**). Overall, at least at the qualitative level, all three HIF subunits bind to somewhat different loci at different hypoxia time points, however the binding patterns at these time points are largely similar.

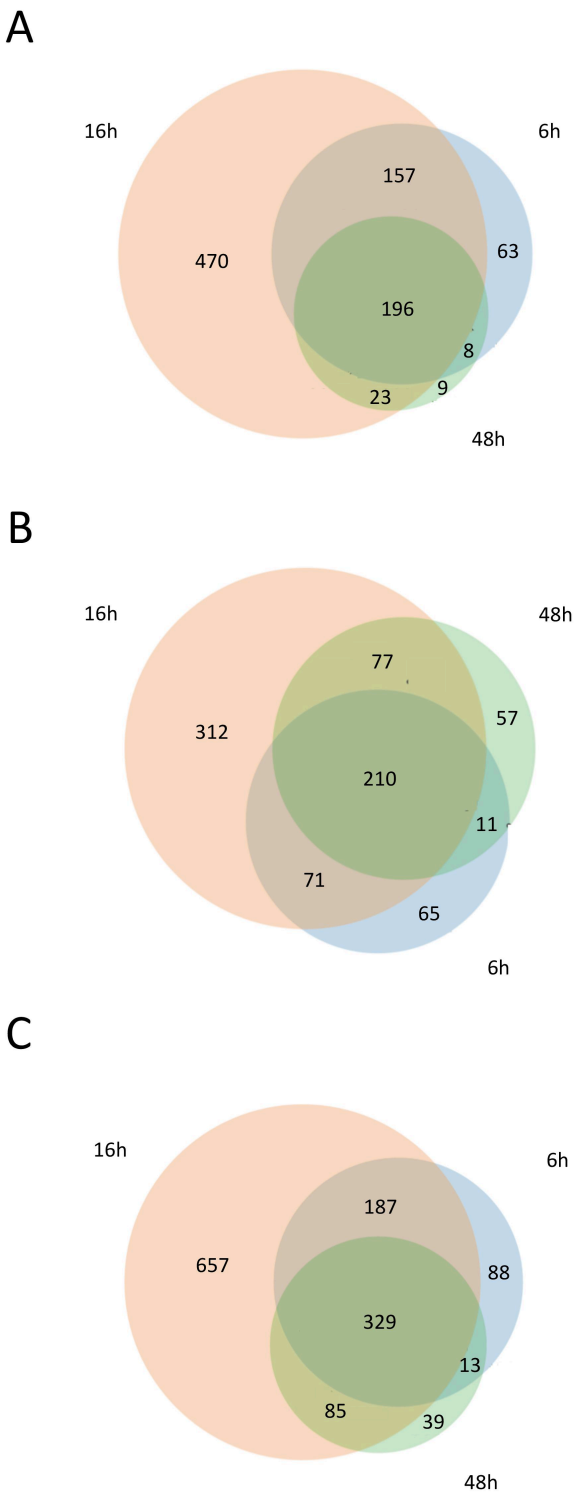

Figure 7. Venn diagrams showing the overlap of (A) HIF-1α, (B) HIF-2α and (C) HIF-1β canonical binding sites that were defined at 6h, 16h, and 48h hypoxia.

In order to characterise the properties associated with these temporally defined binding sites, and to compare these properties between HIF-1α and HIF-2α, further analyses of motif enrichment, distribution around the transcriptional start site (TSS), downstream gene class and ontology pathways, were performed.

One mechanism to allow distinct patterns of DNA-binding by different TFs is mediated via binding site sequence preferences. A functional core HRE might contain neighbouring DNA-binding sites for additional TFs that may either promote or interfere with HIF binding at the HRE. For instance, ATF-1 and CREB-1 have been shown to cooperate with HIF-1α to transcriptionally activate the *LDHA* gene (Ebert et al., 1998; Firth et al., 1995). Another mechanism to alter patterns of DNA-binding is through binding site competition. HIF is one of the major phylogenetic groups of bHLH-proteins that bind to the palindromic E-box motifs (CANNTG) (Massari and Murre, 2000). It has been shown that some of the known HRE are in fact E-boxes (reviewed in Wenger et al., 2005). Other TFs that are capable of binding this motif include Myc, USF1/2, MITF, MyoD, ADD1 and SREBP. There is a possibility that competition by these TFs to recognise the E-box motifs might reduce their availability to bind HIF.

In order to investigate the sequence preferences within the HIF-binding regions and to examine whether there is any enrichment of other TFs over time, an unbiased and pan-genomic motif analysis was performed by MEME-ChIP. HIF-1α or HIF-2α canonical binding sites were defined at each hypoxia time point. A 300 bp window around the peak summit was generated and examined for common *de novo* motifs (**Figure 8**). As expected, the most enriched motif identified within both HIF-1α and HIF-2α binding sites at all three hypoxic time-points was the RCGTG motif. A number of other motifs with statistical significance were also identified as shown in **Figure 8**. However, none of them represented the E-box motifs bound by the aforementioned TFs

such as myc and MITF. Furthermore, the enrichments (*p*-value) of these motifs were much lower compared with those of HRE motifs. Interestingly, in addition to RCGTG motif, a sequence of CCTCC was showing a higher than expected enrichment within HIF-1α binding sites at 6h and 16h of hypoxia (**Figure 8A**), and a consistent enrichment of AP-1 motif (5'-TGAG/CTCA-3') (Angel et al., 1987) were observed within HIF-2α binding sites at all three hypoxia time points (**Figure 8B**).

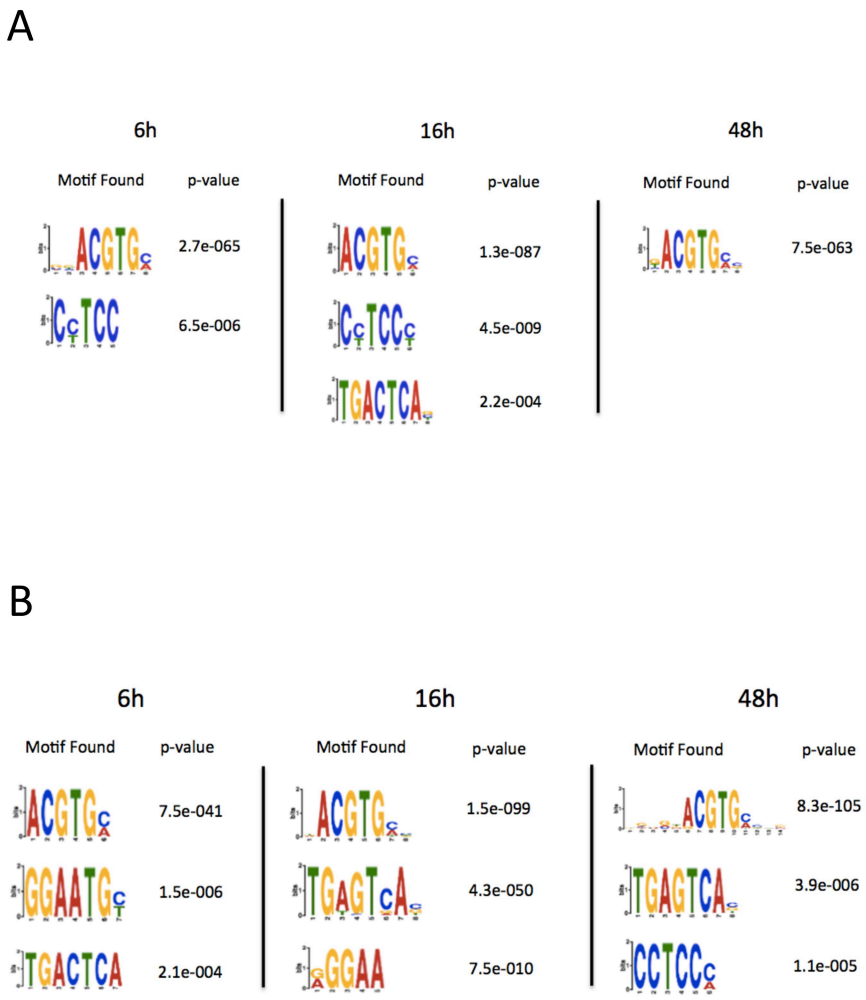

Figure 8. *De novo* motifs enriched within (A) HIF-1α and (B) HIF-2α canonical binding sites at each hypoxia time point. Within each condition, a 300 bp window is generated around the summit of each binding site. Novel motif analysis is produced by MEME-ChIP. *p*-value refers to the significance of the motif in the peak region.

Analysis from the previous chapter suggests a different distribution of HIF-1α and HIF-2α binding sites with respect of distance to the TSS at acute hypoxia (0.5% O_2 for 6h). To test whether this was affected by the duration of hypoxia, the frequency distributions of HIF-1α and HIF-2α binding sites around the nearest TSS at each hypoxia time point were compared (**Figure 9**). Using 500 kb windows, we observed a promoter-centric profile of HIF-1α sites, and a promoter-distal profile of HIF-2α sites at all three hypoxia time points. However, for each HIF subunit, the patterns of distribution looked remarkably similar across the hypoxia time-course.

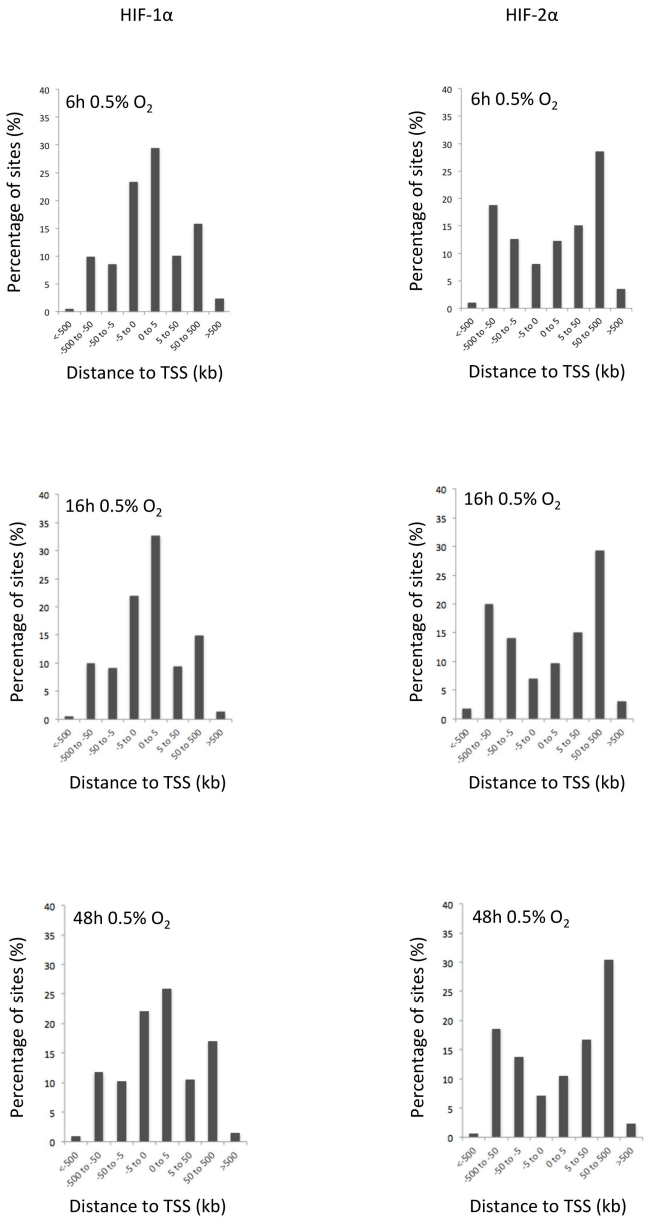

HIF-1a sites	p-value
6h vs 16h	0.063
6h vs 48h	0.100
16h vs 48h	0.001

HIF-2a sites	p-value
6h vs 16h	0.084
6h vs 48h	0.748
16h vs 48h	0.151

Figure 9. Histograms showing the percentage of HIF-1α (left panels) and HIF-2α (right panels) canonical binding sites at each hypoxia time point, according to the distance ±500 kb from the nearest transcriptional start site (TSS). The analysis is computed by Genomic Regions Enrichment of Annotations Tool (GREAT). For each HIF isoform, the frequency distribution between two hypoxia time points is compared by Fisher's exact test and is displayed in the tables.

To incorporate HIF DNA-binding profiles with associated gene functions, HIF-α canonical binding sites were annotated to the nearest gene and stratified into protein-coding, miRNA, lincRNA, antisense and others categories (**Figure 10**). The majority of both HIF-1α and HIF-2α binding sites were associated with protein-coding genes, with HIF-1α sites showing a higher proportion. For both isoforms, the signature of gene function remained largely unchanged across the period of hypoxia exposure.

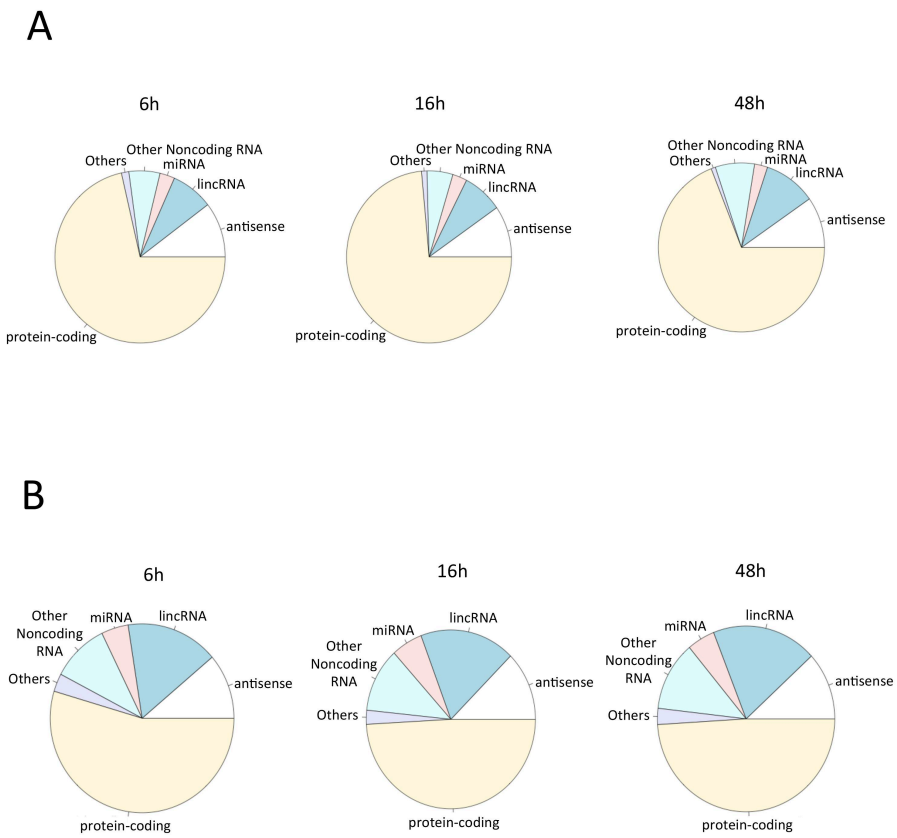

Figure 10. Distribution of (A) HIF-1α and (B) HIF-2α canonical binding sites with respect to gene function. The distribution is stratified into protein-coding, antisense, lincRNA (long intergenic noncoding RNA), miRNA (microRNA), other noncoding RNA, and others, according to the class (Ensemble) of the nearest gene. The relative frequency of each class is shown in the pie chart.

HIF-1α and HIF-2α target genes have been shown to have divergent functions in kidney cancer, with anti-tumorigenic effects of HIF-1α targets and pro-tumorigenic effects of HIF-2α targets (Warnecke et al., 2004; Raval et al., 2005; Shen et al., 2011).

Furthermore, HIF-α isoform specific binding sites were reported to confer opposing prognosis in RCC, with HIF-1α binding sites and genes specifying good prognosis and HIF-2α sites and genes specifying poor prognosis (Salama et al., 2015). In order to assess whether there is a correlation between HIF-α isoform binding and gene ontology pathways, and if so whether it is affected by hypoxia duration, HIF-1α (or HIF-2α) binding sites were annotated to the nearest genes. The expression of these genes was then examined for their enrichments in Cancer and RCC associated pathways (**Figure 11**). Gene ontology annotation suggested there was a strong signature of both pathways within HIF-2α but not HIF-1α binding sites. However, this signature did not change significantly with the hypoxia exposure time.

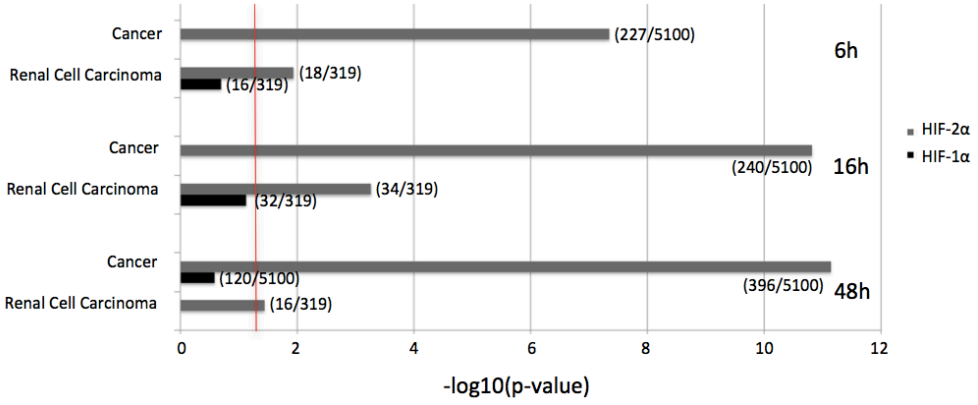

Figure 11. Gene ontology pathway analysis of the annotated HIF-α genes at each hypoxia time point. Annotation of gene outputs for HIF-1α and HIF-2α were used in analysis computed by Genomic Regions Enrichment of Annotations Tool (GREAT). The enrichment of genes in each pathway is shown by –log10(*p*-value). –log10(*p*-value)>1.3 indicates statistical significance and is highlighted in a red line. The number of observed genes and the total number of genes in that pathway are shown in the bracket.

Taken together, these results suggest that at qualitative level, the bindings of each of the HIF subunit had similar properties across the duration of hypoxia. However, HIF-1α and HIF-2α canonical binding sites clearly displayed different profiles to each other in

terms of the functional properties, i.e. the motif enrichment, distribution to TSS, downstream genes class and gene ontology pathways.

4.2.6 Quantitative analysis of canonical HIF-binding sites in response to timed hypoxia

Having shown that HIF bound different canonical sites at each hypoxia time point (**Figure 7**), next binding signals (i.e. RPKM) at those sites were examined to see whether this difference in more detail at a quantitative level.

There are a total of 926 HIF-1α canonical sites resulting from a combination of HIF-1α sites defined at 6h, 16h and 48h of hypoxia. Likewise, a total of 803 HIF-2α canonical sites were defined. For these HIF-1α (or HIF-2α) sites, the averaged RPKM from the two replicates of ChIP-seq experiments were compared across 0h, 6h, 16h and 48h of hypoxia (**Figure 12 A and B**). As expected, at the global level, binding at HIF-1α (or HIF-2α) canonical sites was strongly hypoxia inducible. The signal was strongest at 16h hypoxia, and a similar level of binding was observed between 6h and 48h hypoxia. Similar conclusions were obtained by a different analysis in **Figure 5**.

The averaged RPKM values at each HIF-1α (or HIF-2α) canonical site are also compared in a Heatmap format to show the distribution of signal around the binding sites (**Figure 12C and D**). For both isoforms, there was a strong hypoxia induced binding around the canonical sites. The binding signal intensity was maximal at 16h, and was similar between 6h and 48h. However, the binding patterns look remarkably similar across all hypoxia conditions.

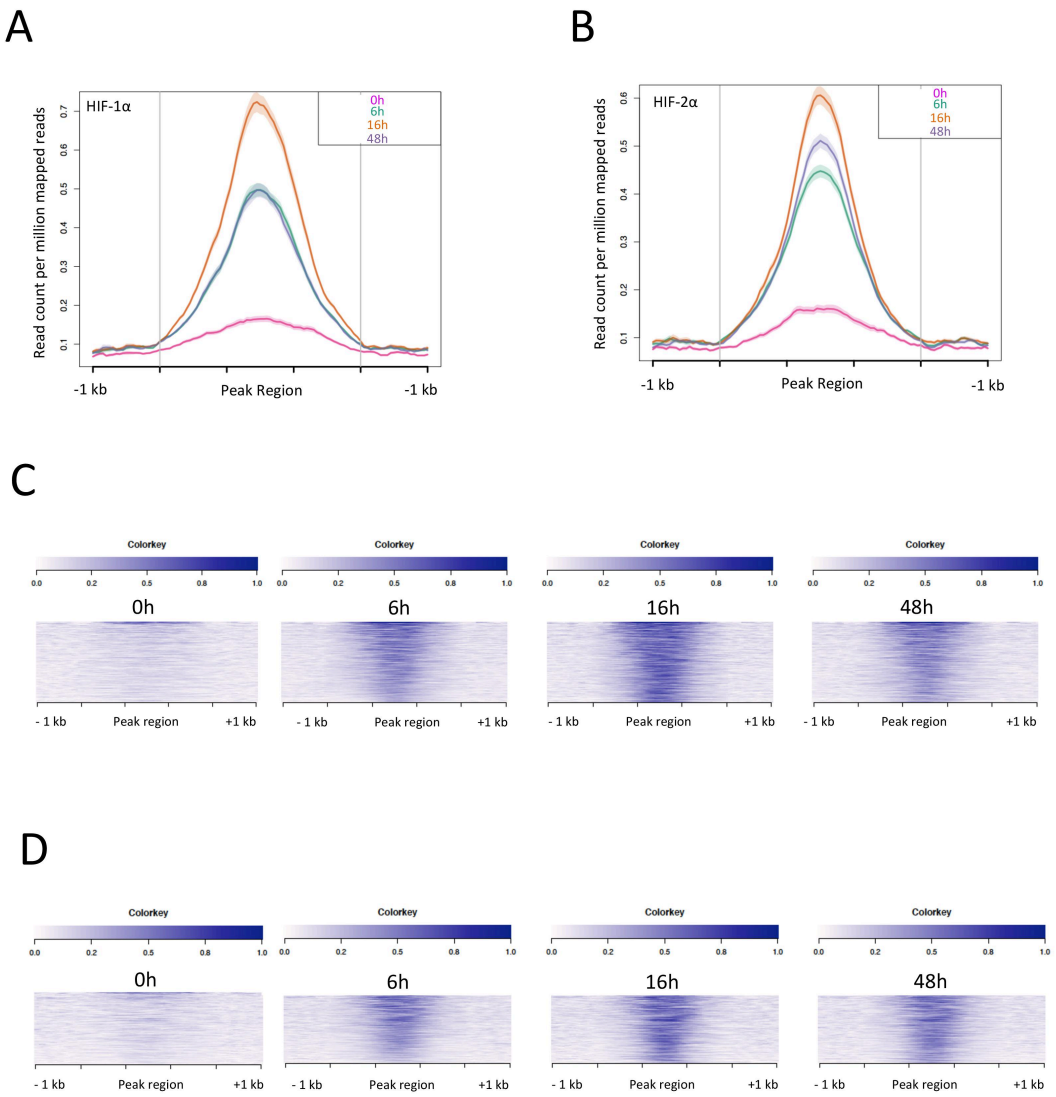

Figure 12. Comparing averaged RPKM around the HIF canonical binding sites at different hypoxia time points. HIF-1α (or HIF-2α) sites are a combination of canonical sites that appeared at 6h, 16h or 48h of hypoxia. RPKM from HIF ChIP experiments performed at 0h (pink), 6h (blue), 16h (orange) and 48h (purple) hypoxia are plotted for ±1 kb flanking regions around the (A) HIF-1α (n=926) and (B) HIF-2α (n=803) sites. Heatmap showing the distribution of RPKM signal -1 kb and +1 kb around the peak regions of (C) HIF-1α and (D) HIF-2α sites. Each row in the Heatmap represents a binding site. The sites were ranked by their enrichment of the ChIP signal intensity in the respective 6h ChIP dataset (2nd column), and were then plotted using the signal from each of the other ChIP dataset. Colour in the heatmap reflects the binding intensity at each site.

To further investigate whether some sites were uniquely or preferentially bound by HIF-α at certain hypoxia time point, the averaged RPKM values at individual HIF-1α

(or HIF-2α) sites between each two hypoxia time-points were compared in a scatter plot analysis (**Figure 13 and 14**). For each comparison of hypoxic conditions there was a strong correlation of binding as shown by the R_2 values. This indicated an overall similar binding signal intensity. This was true for both HIF-1α (**Figure 13**) and HIF-2α (**Figure 14**). The strongest binding was again observed at 16h of hypoxia as most sites were distributed closer to the axis of 16h, and the binding was similar between 6h and 48h of hypoxia. This was consistent with the observation at the genome-wide level (**Figure 12 A and B**).

Importantly, even though the sites displayed a spread in binding intensity values, there were no unique binding sites that appeared only at one hypoxia time point, i.e. no sites were found to appear on the axes. HIF-1α (and HIF-2α) essentially bound to all their respective canonical sites, and only the binding intensity varied over the duration of hypoxia, without creating any new sites or losing existing sites.

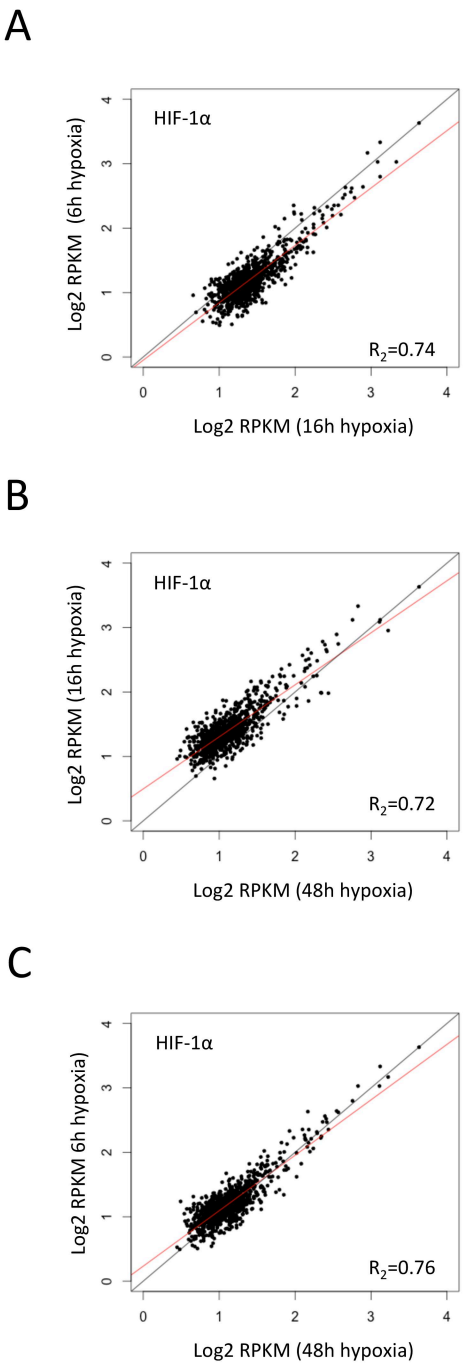

Figure 13. Quantitative analysis of signals at total HIF-1α canonical binding sites (n=926). Normalised reads (RPKM) at each HIF-1α site are compared between (A) 6h and 16h (B) 16h and 48h (C) 6h and 48h of hypoxia ChIP datasets. The correlation of binding intensity between HIF ChIP at two different conditions is shown by the red regression line and by the R-squared value.

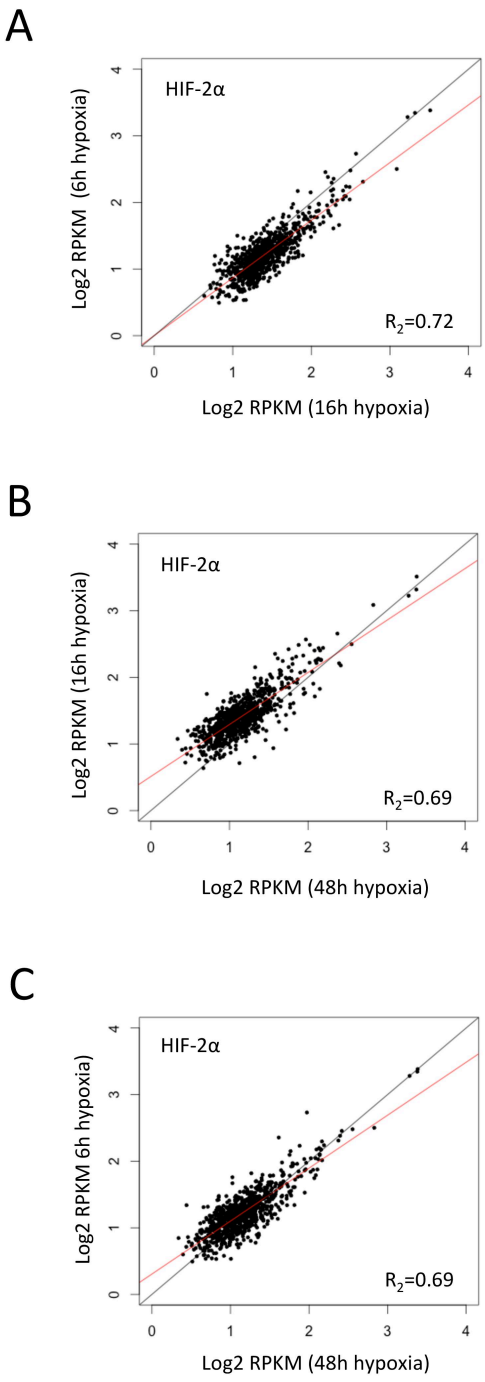

Figure 14. Quantitative analysis of signals at total HIF-2α canonical binding sites (n=803). Normalised reads (RPKM) at each HIF-1α site are compared between (A) 6h and 16h (B) 16h and 48h (C) 6h and 48h of hypoxia ChIP datasets. The correlation of binding intensity between HIF ChIP at two different conditions is shown by the red regression line and by the R-squared value.

4.3 Discussion

In this chapter, the effects of acute and chronic hypoxia on HIF protein abundance and genome-wide occupancy were examined. The key aim was to define the time dependence of both qualitative and quantitative changes in HIF binding and relate these to HIF expression levels, and to the characteristics of the binding sites.

4.3.1 Differential expression patterns of HIF subunits

The observation of dynamic and distinct protein expression patterns of HIF-1α and HIF-2α in response to timed hypoxia has been shown in multiple studies, and has been inherent in all cellular contexts tested so far (Lin et al., 2011; Ginouves et al., 2008; Moroz et al., 2009). This suggests a potential for a general adaptive response of HIF-α during chronic hypoxia. Consistent with the existing literature, our data showed a rapid increase of both HIF-1α and HIF-2α proteins under hypoxia, with the maximum protein level observed at earlier time points (3h or 6h). HIF-1α protein was then rapidly degraded by 16h, with the level further decreased at 48h. HIF-2α protein also decreased, but appeared to be more sustained over time (**Figure 1**).

At the protein level, induction of HIF-α may be modulated by multiple negative feedback loops in the pathway. First of all, a progressive accumulation of the PHDs as a result of increased transcription has been observed under prolonged hypoxia (Epstein et al., 2001; Stiehl et al., 2006; Metzen et al., 2005; reviewed in Berra et al., 2003). This could potentially compensate for the decrease of their activity in chronic hypoxia and bring HIF protein back to lower levels. In the HeLa cells that were cultured at 1% O_2 for up to 7 days, PHD1-3 showed a gradual activation due to the inhibition of mitochondrial respiration that resulted in increased intracellular oxygen availability (Ginouves et al., 2008). Furthermore, previous studies have also found that PHD1-3 isoforms have differential effects on the regulation of HIF-α proteins, with PHD2 appearing to have

more influence on HIF-1α than HIF-2α (Berra et al., 2003; Appelhoff et al., 2004). Another mechanism of feedback regulation may be through the product-inhibition effect of succinate, which interferes with the hydroxylation of HIF-1α by PHD2 (Selak et al., 2005). Additional mechanisms may operate through other pathways, e.g. HSP70 and the ubiquitin ligase CHIP (Carboxyl terminus of Hsc70-Interacting Protein). Using SILAC based proteomic screen, Luo et al., showed that hypoxia up-regulates HSP70, which then mediates the selective degradation of HIF-1α but not HIF-2α by recruiting the ubiquitin ligase CHIP (Luo et al., 2010).

The differential HIF-α expression pattern in response to timed hypoxia may also due to altered transcription of the HIF-α gene. In neuroblastoma cell lines, Lin et al., demonstrated that HIF-1α transcription was consistently repressed by acute and chronic hypoxia, whereas transcription of HIF-2α was up-regulated under the same hypoxic condition (Lin et al., 2011). The authors proposed that this could be due to the increased acetylation of histone H3 and H4 in HIF-2α promoter regions but not in HIF-1α. HIF-1α transcription can also be suppressed by binding of repressor element 1-silencing transcription factor REST (Cavadas et al., 2015), miRNA-155 (Bruning et al., 2011), and antisense HIF-1α (Uchida et al., 2004). In contrast, HIF-2α transcription either increased (Lin et al., 2011) or remained unchanged (Bruning et al., 2011). However, an analysis of HIF-α mRNAs in HeLa cells showed no variation in acute or chronic hypoxia (Ginouves et al., 2008). Overall, the majority of work supports a reduction in HIF-1α mRNA but not HIF-2α mRNA over the period of the current studies. However such findings are not universally observed and further work is required to address the mechanisms underlying such context specific effects.

Compared to HIF-α, the expression of the HIF-1β subunit was constitutive and not affected by the duration of hypoxia (**Figure 2**), or by the severity of hypoxia as shown in the previous chapter. This is consistent with multiple studies where hypoxia exposure did not affect total HIF-1β protein levels (Jerwell et al., 2001; Huang et al., 1996). However, it is worth noting that increased HIF-1β protein levels in hypoxia have previously been shown in certain cell lines (reviewed in Mandl and Depping 2014).

The results in this chapter confirmed the dynamic and differential expression patterns of HIF-α proteins in response to duration of hypoxia in the HKC-8 cells. However, since the main focus here was to make a new investigation of the effect of duration of hypoxia, on the genome-wide distribution of HIF-binding, the mechanism(s) responsible for time dependent changes in HIF-α protein levels have not been investigated further.

4.3.2 Potential explanations for the discrepancy between HIF protein and DNA-binding

Immunoblots of both whole cell extracts or chromatin fractions showed that there was more HIF-1α protein at 6h than at 16h hypoxia (**Figure 6A**). This observation was also confirmed by HIF-1α immunoprecipitation and immunoblot (**Figure 6B**). Overall, therefore, this time-course differs from that of DNA-binding as defined by ChIP-seq and ChIP-qPCR experiments, which showed a higher binding signal at 16h than 6h of hypoxia (**Figure 6C**). This indicates that HIF DNA-binding (as detected by ChIP-seq) is more efficient at 16h of hypoxia than at 6h.

Mechanisms such as post-translational modification of the HIF-α protein may affect HIF DNA-binding affinity. Liu et al., showed that Set7/9 methyltransferase could methylate HIF-1α at lysine32 and this methylation impaired HIF-α binding and reduced HIF target gene expression without affecting the HIF-1α protein level (Liu et al., 2015a).

However, this data was in conflict to another study where Set7/9 methylation increased HIF-1α protein level and target gene expression (Liu et al., 2015b). Hence, it remains unclear whether HIF-α DNA-binding affinity is affected by its methylation status. However, it does not rule out that other potential post-translational mechanisms may affect HIF and the DNA-binding.

FIH plays an important role in regulating the transcriptional activity of HIF-α via the hydroxylation of the asparagine residue (Asn-803 for HIF-1α, Asn-847 for HIF-2α), a post-translational modification that blocks recruitment of p300 to the C-terminal activation domain (Mahon et al., 2001; Lando et al., 2002a; Lando et al., 2002b). However when first identified, FIH was reported to bind to VHL in a transcriptional co-repressor complex that inhibited HIF-1α transactivation function by recruiting histone deacetylases (Mahon et al., 2001). It was previously shown in chapter 1 that the FIH protein is enzymatically active under 0.5% O_2, therefore one could speculate whether the level of FIH protein or its subcellular localisation may change in response to chronic hypoxia and consequently affect the HIF DNA-binding response. However, in our preliminary immunoblot comparing FIH protein level in both whole cell extracts and cell fractions under normoxia and hypoxia (0.5% O_2), we did not observe any significant differences in FIH protein level or distribution between 6h and 16h of hypoxia (**Supplementary Figure 2**).

Overall the data suggests that while HIF-α protein level is highest at 6h, HIF-α DNA-binding reached its maximal level later at 16h of hypoxia. The exact sequence of events leading from HIF-α stabilisation in hypoxia to dimerisation and DNA binding is still not fully understood, although these results are consistent with a time-dependent step in this process. At the moment the difference could not be explained, and more studies would be required to examine this.

4.3.3 HIF-1α shows distinct DNA-binding profiles to HIF-2α

The results from the Hierarchical Clustering Analysis and the Heatmap confirmed that HIF isoform specificity was the main determinant of the binding profile, i.e. hypoxia duration was not able to change the binding distribution of HIF-1α to resemble that of HIF-2α or vice-versa **(Figure 4)**. Overall the difference between ChIP experiments performed under different hypoxia time points is very subtle, indicating hypoxia duration may not be the main factor dictating HIF isoform binding. A covariation was seen again between HIF-1α and HIF-1β, suggesting a similar total binding signal between these two subunits. HIF-2α ChIP clustered separately. This could indicate less binding of HIF-2α at the canonical sites. Alternatively, this could be due to the higher noise level observed in HIF-2α ChIP datasets (**Figure 3**) and consequently a less accurate averaged read count at each site.

When HIF-1α and HIF-2α canonical binding sites were compared for differences in motif enrichment, distribution around TSS, and associated gene functions and ontology pathways, the two isoforms displayed distinct properties. Interestingly, HIF-2α sites were more likely to regulate pathways involved in cancer and RCC (**Figure 10**). This finding is consistent with a previous study where HIF-2α transcriptional targets overall confer a poor prognosis whereas HIF-1α targets favour a good prognosis in the setting of clear cell renal cancer (Salama et al., 2015). The new results suggest that HIF-2 may be more broadly pro-tumorigenic.

With respect to HIF-1β, the changes in HIF-1β DNA-binding profile at the canonical sites mirrored the profile of HIF-α, even though the total protein level did not change across the duration of hypoxia. This suggests that HIF-1β DNA-binding at the canonical sites is indeed hypoxia inducible and requires heterodimerisation with HIF-α.

4.3.4 The variation in HIF DNA-binding occurs at the same canonical sites

One of the major aims of this chapter is to assess how the canonical HIF DNA-binding response is affected by various durations of hypoxia at the quantitative level.

Detailed analysis of the distribution of isoform specific HIF binding thus provided new insights into the dynamics of HIF binding. Although some HIF-binding sites bound to both isoforms, at most sites the isoform-specific pattern of binding remained similar at each of the time points, despite different overall kinetics of protein induction (i.e. sites bound preferentially either to HIF-1α or HIF-2α at all the time points). This is consistent with work from another member of the laboratory who recently observed surprisingly little redistribution of HIF-1α or HIF-2α when the other isoform was ablated genetically.

However when the time-dependent binding of each isoform was considered independently there was little redistribution over the time studied. Thus temporal changes in the HIF response appear to arise more from the intrinsic specificity of HIF isoform restricted binding and differential kinetic of induction and maintenance rather than redistribution of binding over time. The isoform specific binding also largely matched with previous observations in the 786-O cells, indicating the divergent binding signatures of HIF-1α and HIF-2α may be robust across multiple cell types (Salama et al., 2015).

The lack of redistribution of HIF binding seems to contrast with the previous study in HUVEC cells, in which temporal differences in hypoxic gene expression was observed (Mimura et al., 2012). However, the caveat of that study was that mRNA level might be confounded by multiple factors such as indirect effects of other signalling pathway as well as mRNA stability. Therefore, it may not truly reflect the HIF binding. In addition, HIF response may be context-dependent.

ChIP-seq allows the genome-wide study of TF binding, however it can only detect the binding at the time of cross-linking. In this chapter, the kinetics of binding, such as

the binding rates or 'residence time' on the chromatin, has not been addressed. Some proteins can be temporarily immobilised due to their functional interactions with chromatin. Examples include the steroid receptors upon ligand stimulation (Stenoien et al., 2001), and RNA Pol2 upon transcription engagement (Becker et al., 2002). The binding kinetics of some TF may also vary across the genome. For instance, Max (myc-associated factor X) was predicted bound at weak binding sites with a residence time of ~5s, whereas it is ~14s for the strong binding sites (Phair et al., 2004). A recent study of the yeast TF Rap1 (Repressor/activator protein 1) suggests that transcriptional outcome is regulated by TF binding dynamics, rather than occupancy itself. The author showed that long residence of Rap1 was coupled to transcriptional activation, whereas rapid turnover ('treadmilling') was associated with transcriptional repression, although both gave a similar ChIP profile (Lickwar et al., 2012). It would therefore be of interest to examine the binding kinetics of HIF at the canonical sites in response to timed hypoxia, and the subsequent biological significance.

Finally it is also plausible that 48h hypoxia exposure examined here is not long enough to redistribute the genome-wide HIF DNA-binding profile. There is increasing evidence that HIF transcriptional activity is dependent on epigenetic modifications, which may occur at both histone and DNA level and dictate HIF binding to its targets. For instance, binding of HIF-1α to the 3' enhancer of the EPO gene in human neuroblastoma requires an unmethylated HRE (Rössler et al., 2004) and this likely true of all HIF binding sites. Gene specific DNA hypomethylation may reveal previously inaccessible HIF binding regions. On the other hand, hypoxia-induced gene specific DNA hypermethylation (Thienpont et al., 2016) may block previously active sites. The time course of such effects is not yet clear. Therefore, the interactions of epigenetics and

hypoxia over longer periods of time may influence and shape the HIF transcriptional response.

4.4 Conclusion

Overall, even though there were qualitative differences in HIF binding at canonical sites in response to different durations of hypoxia, quantitatively binding signals at those sites did not change significantly, at least up to 48 hours. Similar to the observations in response to graded hypoxia, HIF-α binds to the same canonical sites and hypoxia duration only alters the magnitude of binding intensity at these pre-existing sites.

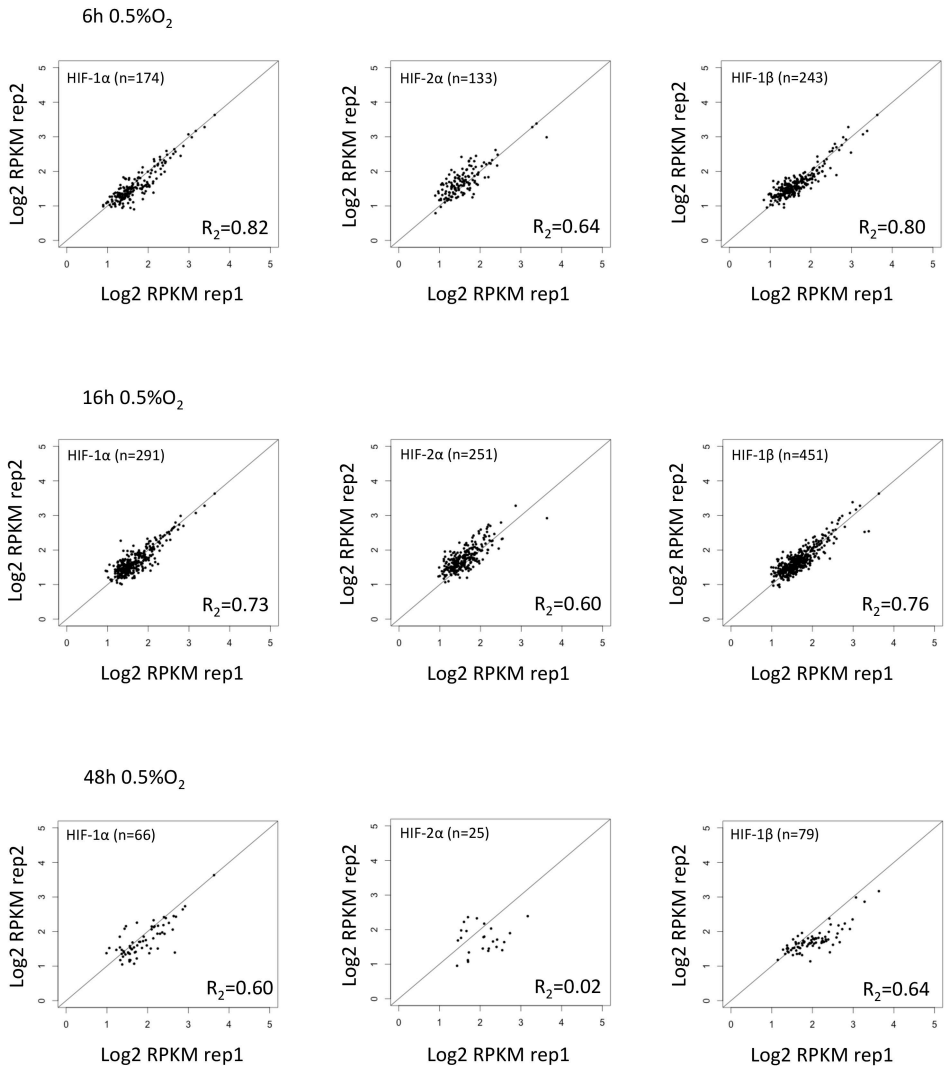

Supplementary Figure 1. Reproducibility between ChIP-seq replicates at the most stringently defined canonical HIF binding sites. HIF-α sites are defined at each condition by the presence of both HIF-1α (or HIF-2α) and HIF-1β with detection of each isoform in both replicates. HIF-1β sites are HIF-1α and HIF-2α sites combined. The number of binding sites is shown on each plot. For each binding site, the normalised binding signal (i.e. RPKM) from replicate 1 (horizontal axis) is plotted against the signal from replicate 2 (vertical axis) in a Log2 scale. The correlation of signal between two replicates is shown by R-squared values.

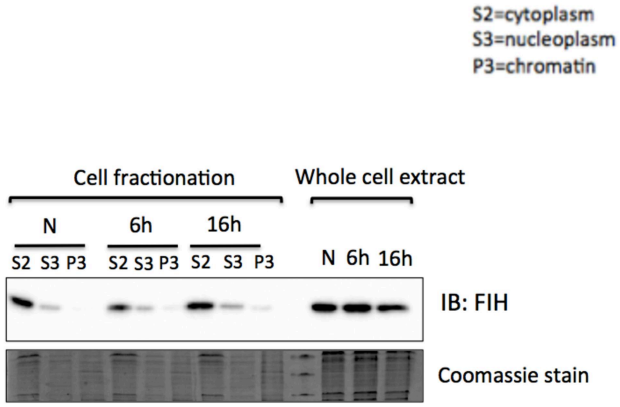

Supplementary Figure 2. Immunoblot of FIH protein was performed using extracts from different fractions of HKC-8 cells that were cultured under normoxia or hypoxia (0.5% O_2 for 6h or 16h). The extracts were separated into cytoplasm (S2), nucleoplasm (S3) and chromatin (P3) fractions. Immunoblot of FIH was also performed using the whole cell extracts that were prepared in parallel.

5

Loss of Tumour Suppressor or Oncogenic Proteins and the Consequences on Canonical HIF Binding Genome-wide

5.1 Introduction

Studies described in chapters 3 and 4 established that HIF binds to DNA at multiple sites broadly in accordance with the total level of binding across the genome under a particular experimental condition, at least as regards short term hypoxia of graded severity and duration. I found little evidence for re-association of either HIF isoform with different sites under these conditions.

In contrast with these studies, substantial evidence supports the existence of a high level of cell-type specificity in the HIF response, as defined either by cell-type specific binding of HIF to different sites or by cell-type specific HIF target gene expression. HIF binds to DNA at only a small fraction (i.e. less than 1%) of available sites that bear the consensus core binding and are in open chromatin regions (Mole et al., 2009; Xia et al., 2009). The reasons for this selectivity and its variation between different

cell types is unclear, and is not easy to analyse in that context as there are likely to be many contributors to somatic cell differentiation, which are not easy to isolate.

The question of whether and how HIF binding sites alter in different cellular contexts is of particular interest in cancer where HIF is commonly activated and commonly considered to contribute to the malignant phenotype. The most direct connection between activation of HIF and an oncogenic pathway is observed in VHL-associated kidney cancer, where inactivation of the pVHL ubiquitin E3 ligase prevents the destruction of HIF that normally occurs in oxygenated cells, thus at least in part mimicking the hypoxic state. This situation offers the possibility to test whether the inactivation of specific genes has effects on patterns of HIF binding across the genome. I chose to focus on two that are related to renal cancer; *VHL* itself and the gene encoding a component of the ATP-dependent chromatin-remodeling complex, *PBRM1*, which is also frequently mutated in VHL-associated kidney cancer. I also investigated the role of the HIF asparaginyl hydroxylase FIH, which is well known to regulate the HIF transcriptional output and which has also been associated with *VHL* function in some studies.

In each case I deployed CRISPR/Cas9 engineered mutant cells to examine the effects of relevant gene. Below I provide a brief background of each of the molecules to be studied and consider existing evidence for, and potential mechanisms by which the relevant gene product might affect HIF binding in chromatinised DNA.

In general, most of the pVHL functions in tumorigenesis are believed to be mediated through regulation of the HIF pathway (reviewed in Gossage et al., 2015; Kaelin 2007). Studies have shown that inactivating mutations, deletions or epigenetic silencing in VHL gene preferentially affect pVHL interactions with HIF (either by

disrupting binding of HIF to the beta-domain or preventing assembly of the E3 ligase complex that is required for ubiquitylation of HIF). This action generally results in constitutive stabilisation of both HIF-α isoforms and activation of HIF responsive genes (Clifford et al., 2001; Hoffman et al., 2001). Subsequent analysis of HIF DNA-binding sites and transcriptomic profiles across multiple pVHL-defective RCC cell lines and tumours revealed that many HIF targets are indeed overexpressed (Schödel et al., 2012; Schödel et al., 2013).

However, several studies have indicated that the rapidly inducible HIF-target gene repertoire observed when cells are exposed to hypoxia differs substantially from that associated with *VHL* inactivation. For instance, a study comparing VHL-/VHL+ RCC cells cultured under normoxia and hypoxia identified a number of differentially expressed genes that are VHL-independent but hypoxia-dependent, as well as VHL-dependent and hypoxia-independent genes (Leisz et al., 2015). Another study using proteome and phospho-proteomic approaches also found that in VHL± 786-O RCC cells, despite the high concordance of proteins expression in hypoxia and in a *VHL* negative condition, there are candidates that are sensitive to only parameter (Malec et al., 2015). However, it is possible that these reported differences might be due to clonal variation unrelated to pVHL status. In addition, it is unclear whether the differences are present at the level of HIF DNA-binding. It is also possible that changes appeared in HIF transcriptional response as a result of pVHL loss may be missed in experiments that utilise *VHL* re-expression in RCC cell lines (since binding changes that may have occurred due to pVHL loss are not necessarily reversible). Overall, these studies raise the possibility that long-term activation of the HIF pathway due to the loss of pVHL might have different effects to hypoxia on HIF DNA-binding profiles and subsequently target gene expression.

Accumulating evidence suggests that during RCC progression, cancer cells exploit diverse epigenetic alternations to drive tumorigenesis (reviewed in Morris and Latif 2016). Disturbances in epigenetic regulations may occur at multiple levels, such as nucleosome remodelling, histone modification, DNA methylation, and RNA-mediated targeting (reviewed in Sharma et al., 2010). Recent genome-wide exome-sequencing studies have identified frequent mutations in polybromo 1 (PBRM1), nuclear deubiquitinase BRCA1 associated protein-1 (BAP1), lysine (K)-specific demethylase 6A (UTX), lysine (K)-specific demethylase 5C (JARID1C) and SET domain containing 2 (SETD2) (Dalgliesh et al., 2010; van Haaften et al., 2009; Pena-Llopis et al., 2012; Varela et al., 2011). Most mutations in these genes are predicted to result in loss of function of the proteins, implying their roles as tumor suppressors (Hakimi et al., 2013). How loss of function of these chromatin-modifying enzymes contributes to RCC development, especially in the VHL-defective background is not fully understood, however it may involve cooperation with the HIF pathway.

The function of HIF is dependent on binding to DNA, which is in turn dependent on an open chromatin configuration. For example, normoxic chromatin accessibility (as shown by DNAse1 hypersensitivity) can predict hypoxic binding of HIF (Schödel et al., 2011). In addition, HIF binding is sensitive to CpG methylation (Wenger et al., 1998). Therefore, it is plausible that disturbances in chromatin accessibility may affect HIF DNA-binding and eventually leads to a tumorigenic phenotype. In the past, mutations in some of the chromatin regulators have been shown to have direct effects on HIF. For instance, it has been shown that DNMT3a can methylate and silence *EPAS1* (HIF-2α gene) and that loss of DNMT3a activates HIF-2α and facilitates tumour cell growth (Lachance et al., 2014). In addition, another study has shown that loss of PRC2 (Polycomb repressive complex 2) dependent H3K27 trimethylation led to activation of

HIF-dependent regulation of *CXCR4* (C-X-C motif receptor 4) and *CYTIP* (cytohesin 1 interacting protein), both of which are important pro-metastatic genes in RCC tumorigenesis (Vanharanta et al., 2013). However, so far there is little information about whether this is mediated through the altered HIF DNA-binding profiles.

Among these recently discovered mutations, *PBRM1* has the highest prevalence (~40%) in ccRCC samples (Pena-Llopis et al., 2012; Varela et al., 2011). *PBRM1* is the second most commonly mutated gene after *VHL* in ccRCC (reviewed in Brugarolas. 2014). The *PBRM1* gene product, BAF180 is a part of the multisubunit Polybromo- and BRG1-assiciated factors containing complex (PBAF) switch/sucrose nonfermentable (SWI/SNF) complexes. The bromodomain of PBRM1 (BAF180) reads histones with H3K4 acetylation (H3K4ac), a histone mark enriched at the promoter regions of actively transcribed genes (Wang et al., 2008). In this way, PBRM1 (BAF180) targets PBAF complex to specific genomic regions and alters the local accessibility of the chromatin.

It has been proposed that *VHL* and *PBRM1* mutations are likely to occur early in the development of RCC (reviewed in Brugarolas 2013). Interestingly, kidney-specific deletion of *VHL* and *PBRM1*, but not either gene alone, caused tumours, suggesting a stepwise progression may be required in the RCC development (Nargund et al., 2017). Overall, these findings point to the importance of interactions between *VHL* and *PBRM1* in the pathogenesis of RCC, although the mechanism is not fully understood. Given potential effects on chromatin, this led me to seek to analyse whether such interactions might affect patterns of binding of HIF to DNA.

In addition to PBRM1 (BAF180) protein, FIH has also been reported to regulate the HIF response via mechanisms such as modulation of the chromatin structure through the recruitment of histone modifiers such as CBP/p300 via their acetyl-transferase activity. This could add an additional (potential) action of FIH at regulating HIF DNA-

binding. As a key regulator of HIF-α, FIH catalyses the asparagine hydroxylation of HIF-α protein, which prevents its association with CBP/p300 transcriptional co-activators and consequently reduces its transcriptional activity. It has been shown that inhibition of FIH expression can augment the expression of HIF-1α targets and apoptosis in VHL-defective RCC cell lines (Khan et al., 2011). The negative effects of FIH on HIF target gene expression have also been reported in a range of other cell lines (e.g. HeLa, U2OS, and Hep3B) and across a wide range of oxygen tensions from 21 to 1% O_2 (Stolze et al., 2004). Overall, these findings suggest that FIH might be a candidate oncoprotein in the development of RCC, potentially through inhibition of anti-tumourigenic activity of HIF-1α and promotion of the survival of cancer cells. In line with this hypothesis, it has been shown that FIH may potentially be a prognostic marker in RCC. In normal kidney tissue, FIH is primarily located in the cytoplasm. In contrast, FIH staining is predominantly in the nuclear in the RCC samples, and low nuclear expression of FIH was associated with a poor overall survival (Kroeze et al., 2010). However, the functions of nuclear FIH and the reasons why low nuclear FIH levels have a worse overall survival are not clear.

In an *in vitro* study, FIH was shown to directly interact with pVHL that binds to HIF-1α. pVHL then acts as a transcriptional co-repressor and inhibits HIF-1α transcriptional activity by recruiting histone deacetylases (HDACs). A functional interaction between VHL and FIH was proposed to be essential for this transcriptional repression of HIF-1α (Mahon et al., 2001). An alternative but not mutually exclusive possibility is that FIH may interact with other co-repressors such as SMRT (silencing mediator for retinoid and thyroid receptors), which in turn recruits HDACs and inhibits HIF-1α activity (Kao et al., 2000).

Overall, in RCC evolution, the HIF pathway can be affected by the disturbances of tumour suppressor pathways mediated by pVHL and PBRM1 (BAF180), or by the

function of FIH. Inactivation of these proteins may alter chromatin structure and hence HIF DNA-binding patterns. In this chapter, I aimed to study the consequences of loss of function of these tumour suppressors or oncogenic proteins, on the HIF binding profile genome-wide by performing ChIP-seq experiments.

The laboratory had previously made CRISPR/Cas9 engineered *VHL* knockout sub-lines (VHL KO) of HKC-8 cells. In these cells, loss of *VHL* leads to constitutive expression of the HIF-α protein. This allowed me to directly compare the transcriptional consequences of long-term activation of the HIF pathway under normoxia with HIF response under hypoxia. In order to understand the effects of loss of *FIH* on the HIF transcriptional response, HIF DNA-binding profiles between VHLFIH double knockout (VHLFIH KO) cells and VHL KO cells were compared. In the last section, the effects of loss of *PBRM1* on the HIF transcriptional response are studied. The laboratory had generated VHLPBRM1 knockout (VHLPBRM1 KO) cells. By comparing these cells with VHL KO cells, the effects of *PBRM1* on the constitutively activated HIF pathway could be examined. In another approach, HIF DNA-binding was compared between the hypoxic PBRM1 knockout (PBRM1 KO) cells and wild-type (WT) cells. Overall, the aim of these experiments was to investigate whether the pan-genomic distribution of HIF binding sites was affected by inactivation of *VHL, FIH* or *PBRM1*.

5.2 Results

A series of CRISPR/Cas9 engineered HKC-8 knockout cell lines (VHL KO, VHLFIH KO, PBRM1 KO and PBRM1VHL KO) were previously generated in the laboratory (**Figure 1**). HIF ChIP-seq experiments were then undertaken to assess the effects that loss of either VHL, FIH or PBRM1 (BAF180) proteins has on HIF DNA-binding. The data are presented in sub-sections for each gene knockout.

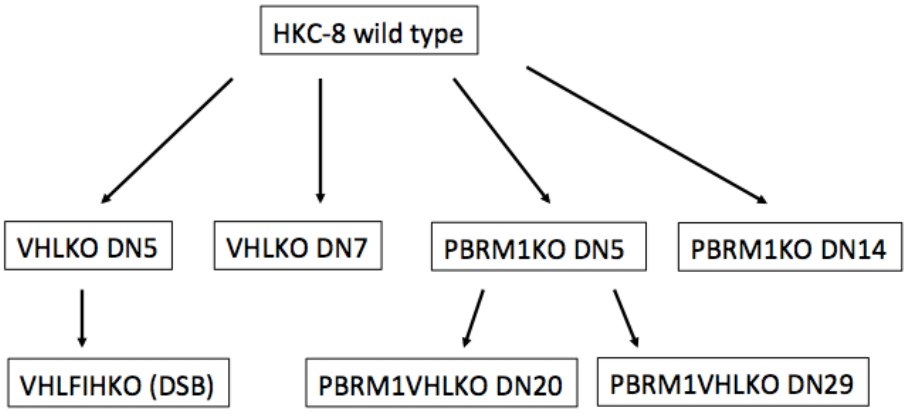

Figure 1. Schematic diagram indicating the derivation of the CRISPR/Cas9 engineered HKC-8 knockout cell lines used in this chapter. These cells were generated with either the Cas9 double nickase (DN) or double strand break (DSB) enzymes.

5.2.1 Comparing the consequences of *VHL* inactivation with hypoxia on HIF-DNA binding

5.2.1.1 The effect of *VHL* inactivation on HIF protein levels

The laboratory has previously made VHL KO clones in the HKC-8 background, i.e. VHLKO DN5 and VHLKO DN7. Although both were generated using the same CRISPR sgRNA, they harbour independent mutations of the genomic locus. Inactivation of *VHL* is anticipated to result in a pseudo-hypoxic environment with a constitutive stabilisation of HIF-α protein in normoxia. To examine the level of HIF-α protein in response to the loss

of pVHL in HKC-8 cells, VHL KO clones together with the WT cells were incubated at either normoxia (21% O_2) or hypoxia (0.5% O_2) for 16h and cell extracts were prepared. Immunoblots of HIF-1α and HIF-2α indicated that the loss of pVHL led to constitutive expression of both HIF-α subunits in the VHL KO cells **(Figure 2 left panel)**. The levels of HIF-α protein in VHL KO cells were also broadly comparable to the HIF-α levels induced by hypoxia in the WT cells **(Figure 2 right panel)**. Overall, the immunoblot results provided further confirmation of the VHL KO status of the cells, and confirmed that loss of pVHL did not alter the total HIF-α protein level.

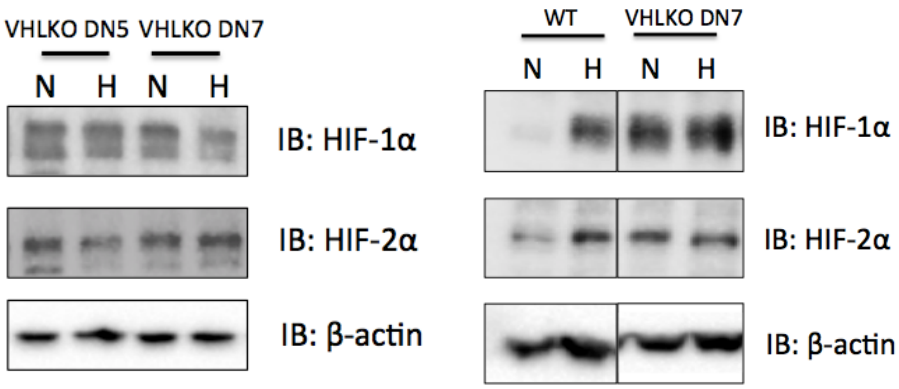

Figure 2. Immunoblot of HIF-1α and HIF-2α proteins in extracts from either VHL KO clones (DN5, DN7) or wild-type (WT) cells. The cells were exposed to either normoxia (N=21% O_2) or hypoxia (H=0.5% O_2) for 16h. Loss of pVHL leads to the constitutive expression of both HIF-1α and HIF-2α proteins in both clones of VHL KO cells. The HIF-α protein levels in the VHL KO cells are also comparable to the levels in the hypoxic WT cells. This suggests that loss of pVHL does not radically affect the total cellular capacity for HIF-α protein production.

5.2.1.2. Genome-wide HIF binding in VHL KO cells

Having confirmed the constitutive activation of the HIF pathway in the VHL mutant cells, HIF ChIP-seq experiments were then performed as shown in **Table 5.1**. HIF binding profiles in the VHL KO cells could then be compared with pre-existing HIF binding profiles obtained following induction of HIF binding by hypoxia in the WT cells.

Table 5.1 ChIP-seq experiments to study HIF binding in normoxic VHL KO cells versus hypoxic WT cells

cell line	condition	ChIP	clones/reps
VHL KO	Normoxia 21% O_2	HIF-1β	DN5 and DN7
VHL KO DN5	Normoxia 21% O_2	HIF-1α, HIF-2α, HIF-1β	2
WT*	6/16/48h 0.5% O_2	HIF-1α, HIF-2α, HIF-1β	2

* HIF ChIP data obtained from chapter 3 and 4

First of all, in order to assess clonal variation, a pilot HIF-1β ChIP-seq experiment was performed using the two VHL KO clones (DN5 and DN7) under normoxic conditions. In this analysis only the HIF-1β peaks that appeared in both clones were considered. This generated a total of 444 HIF-1β binding sites. The normalised binding signal intensity (RPKM) at each site was then plotted between the two clones **(Figure 3)**. R_2=0.73 suggests that there was a high concordance of ChIP signal, at least at these HIF-1β binding sites. In other words, 'strong sites' with high Log2 RPKM value are similarly strong across both clones, and the 'weak sites' are similarly weak.

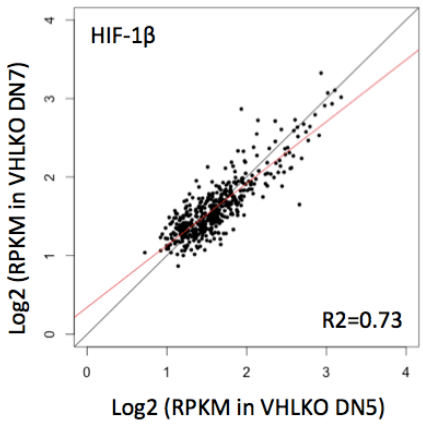

Figure 3. Reproducibility of HIF-1β ChIP signal (RPKM) in two independent VHL KO clones. HIF-1β binding sites (n= 444) detected in both clones are considered in this analysis. The normalised read counts (expressed as RPKM) at each binding site are plotted using data from VHLKO DN5 (horizontal axis) and VHLKO DN7 (vertical axis). The correlation of ChIP signal between two clones is indicated as the R-squared value, and by the regression line (highlighted in red).

Having established a strong concordance in HIF binding between the two VHL KO clones at these high confidence HIF-1β sites, this legitimises the use of multiple HIF ChIP-seq replicates in a single clone for the subsequent analysis (**Table 5.1**). Therefore, to investigate the potential effects of *VHL* inactivation on canonical HIF binding sites, VHLKO DN5 cells (hereafter known as VHL KO cells) were used for HIF-1α, HIF-2α and HIF-1β ChIP-seq, and the data was compared with the canonical HIF binding sites previously defined in the hypoxic WT cells (generated in chapter 3).

To be consistent and to enable comparison, HIF canonical sites in the VHL KO cells were defined using the same criteria as in chapter 3. HIF-1α (or HIF-2α) sites were defined as sites that appeared in either HIF-1α (or HIF-2α) replicate and that have HIF-1β binding in at least one HIF-1β replicate. This identified a total of 2291 HIF canonical sites, within which there were 2147 HIF-1α and 340 HIF-2α sites. The reproducibility of the ChIP-seq datasets was determined by comparing the RPKM at these canonical binding sites between each of the two replicates. A reasonable reproducibility of binding signal (R_2=0.54) in the HIF-1α datasets, and a high concordance of binding signal (R_2=0.70) in the HIF-1β datasets were observed (**Figure 4**). However for HIF-2α, the reproducibility between the ChIP-seq replicates was suboptimal (R_2=0.15).

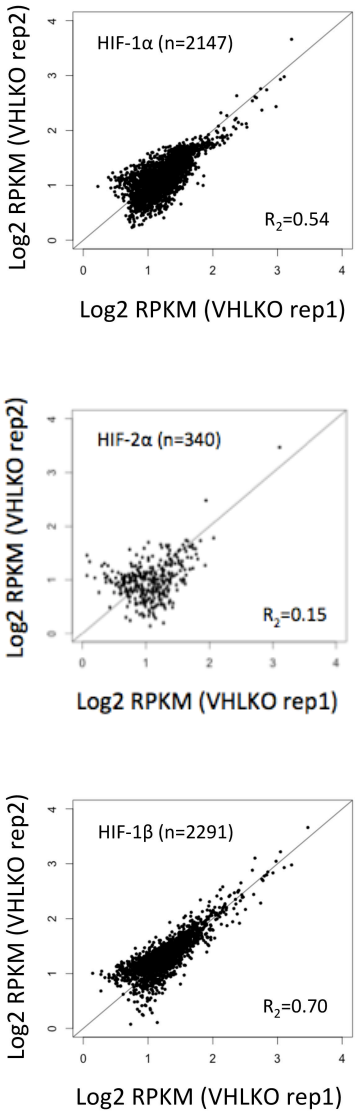

Figure 4. Reproducibility of ChIP signal at canonical HIF sites between the two replicates of HIF-1α, HIF-2α, or HIF-1β ChIP-seq from the VHL KO cells that were cultured under normoxia condition. Canonical HIF-1α (or HIF-2α) sites are defined by the presence of both HIF-1α (or HIF-2α) and HIF-1β with detection of each isoform in at least one replicate. HIF-1β sites are defined as a combination of HIF-1α and HIF-2α sites. (Note that some sites are bound both HIF-1 and HIF-2, hence the number of sites defined by HIF-1β is than the sum of those bound by HIF-1α plus HIF-2α). The number of binding sites is shown on each plot. The RPKM of each binding site from replicate 1 (horizontal axis) are plotted against the RPKM from replicate 2 (vertical axis) on a Log2 scale. The correlation of ChIP signal between replicates is shown as the R-squared value.

5.2.1.3. Qualitative and quantitative analyses comparing HIF DNA-binding in VHL KO cells and WT cells

In order to understand how VHL- and hypoxia-induced activation of the HIF pathways differ to each other, HIF-1α and HIF-2α binding sites that appeared in the normoxic VHL KO cells and in the hypoxic WT parental cells were compared, at both qualitative (i.e. based on the HIF sites identified in the ChIP-seq datasets) and quantitative (i.e. based on the binding intensity of each site) levels.

Analysis in chapter 3 showed that HIF bound to essentially the same canonical sites across a time-course of hypoxia (at least up to 48h), with only the magnitude of HIF binding varying with hypoxia exposure. Therefore, HIF-α canonical binding sites identified in the normoxic VHL KO cells were compared either with all HIF-1α sites that appeared in the WT cells under hypoxia, or with the sites that were specifically defined at each of the hypoxia time points (i.e. 6h, 16h or 48h) (**Figure 5 and Figure 10**).

5.2.1.3.1 Analyses of canonical HIF-1α sites

First of all, the analyses focused on the canonical HIF-1α sites. At the qualitative level, there were more sites defined in the VHL KO cells than in the WT cells. When sites identified in the WT cells are considered, 72.4% of them are found to overlap with sites in the VHL KO cells (**Figure 5A**). A similar result was observed when the canonical HIF-1α sites identified at each of the three hypoxia time points were intersected with the VHL KO sites (**Figure 5A**).

The analysis was also performed at a quantitative level. Firstly, HIF-1α canonical sites defined in the VHL KO cells were combined with the HIF-1α sites defined in the hypoxic WT cells to give a total of 2403 sites. The sites were then ranked according to their averaged signal intensity (averaged from the two replicates of ChIP experiments in the VHL KO cells), and displayed in a heatmap format showing binding ± 1kb around

each canonical HIF-1α binding site (**Figure 5B left panel**). A comparison was then made between the signal in the VHL KO cells and the averaged signal intensity for the same sites using the ChIP-seq data from the WT cells cultured under either 6, 16 or 48h of hypoxia **(Figure 5B right panel)**.

The heatmap indicated that the binding signals for HIF-1α are centered around the canonical binding sites, and that the majority of HIF-1α binding sites have stronger signal in the VHL KO cells. However, importantly, the pattern of signal intensity remains largely the same across all conditions, i.e. 'strong sites' in the VHL KO cells are also 'strong sites' in the hypoxic WT cells, and hypoxia duration did not seem to affect this binding pattern. VHL KO therefore did not result in any gross change in HIF DNA-binding patterns.

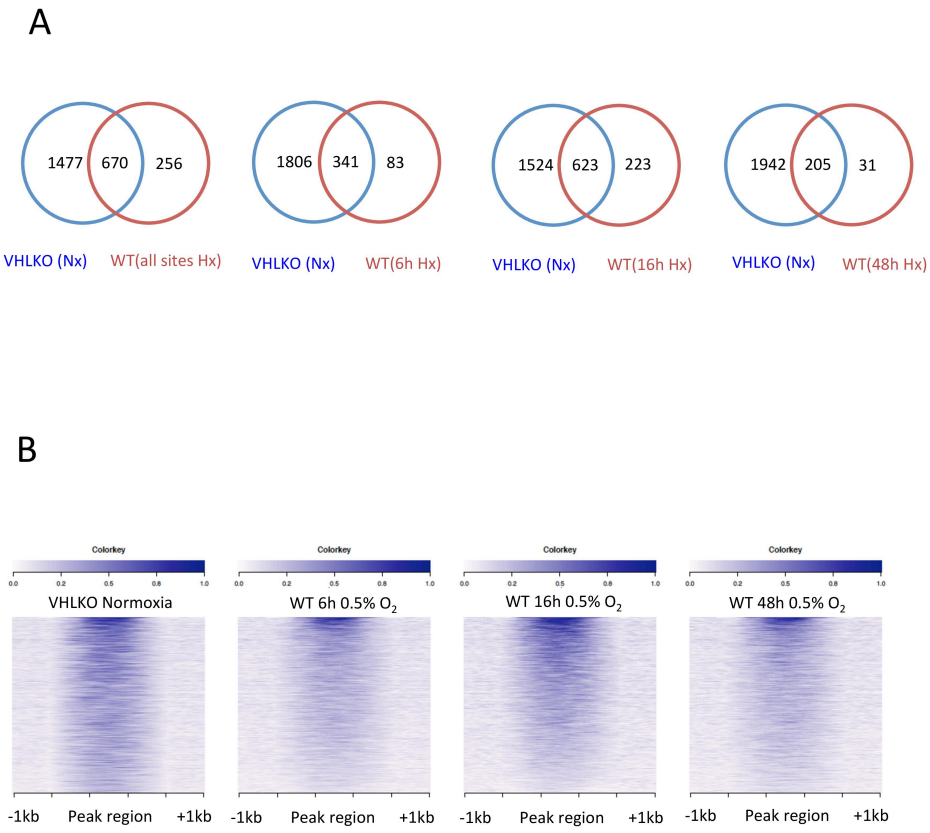

Figure 5. Qualitative and quantitative analyses of HIF-1α canonical binding sites. (A) Venn diagram comparing the HIF-1α sites defined in the normoxic VHL KO cell with those defined in the WT cells at different time-points of hypoxia (0.5% O_2). In total, there are 2147 HIF-1α canonical binding sites in the VHL KO cells. Canonical HIF-1α sites in the WT cells are defined in the previous chapter. There are 926 sites in total, within which 424 sites were detected at 6h, 846 sites at 16h and 236 sites at 48h of hypoxia. (B) Heatmap display showing HIF-1α ChIP signal enrichment by colour intensity around a ±1 kb region of the canonical HIF binding site. HIF-1α sites in the VHL KO cells and WT cells were combined to give a total of 2403 sites. The sites were ranked by their enrichment of the ChIP signal intensity in the VHL KO cells (1st column), and additional heatmaps were then plotted using the equivalent signal from each of the hypoxia datasets in the WT cells. Nx, normoxia. Hx, hypoxia.

Next, in order to examine whether there are any individual or small groups of sites that are specific for one condition (either VHL KO specific or hypoxia WT specific), a differential binding analysis was performed using two different approaches. In the first approach, a statistical analysis was undertaken to compare the RPKM at individual HIF-1α canonical sites in the VHL KO cells (y-axis) with those defined in the hypoxic WT cells at either 6h, 16h or 48h of hypoxia (x-axis) **(Figure 6)**. In this analysis, the large

majority of sites were above the identity line, indicating that their binding signal intensity was higher in the VHL KO cells. The Generalised Linear model (GLM) method was then applied to compare the difference between the read counts (RPKM) of each site in the VHL KO versus the WT cells, using a cut-off value of $p<0.05$ (Chen et al., 2008). This method identified 2 hypoxia-specific sites in the 6h hypoxia comparison, 1 hypoxia-specific site in the 16h comparison, and 1 in the 48h comparison (Appendix 8.9). However, overall there was only one site, *HGSNAT* (Heparan-Alpha-Glucosaminide N-Acetyltransferase), that appeared as hypoxia-specific in all comparisons between the VHL KO and each of the three hypoxia time points. On the other hand, there were no VHL KO-specific binding sites identified in this statistical analysis.

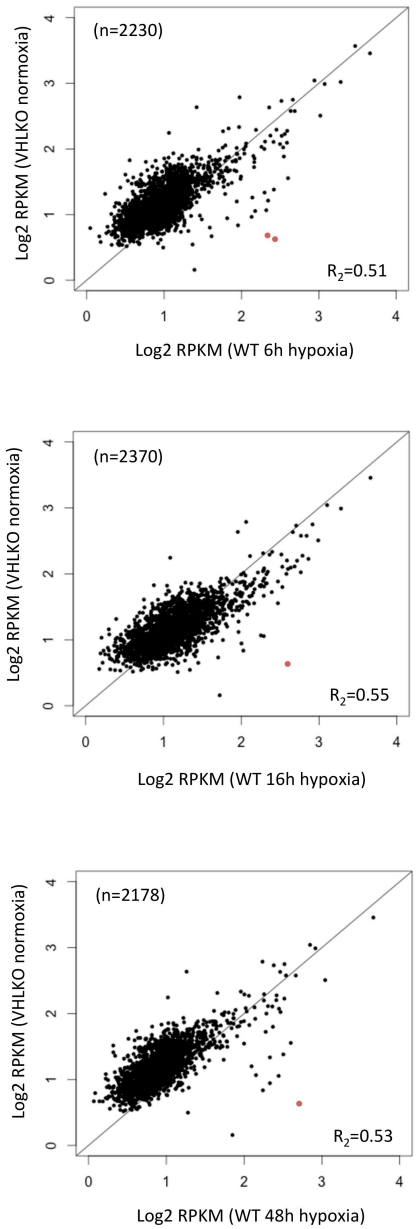

Figure 6. Statistical analysis to identify differential HIF-1α binding sites between normoxic VHL KO cells and WT cells that cultured at either 6h, 16h or 48h of hypoxia. Generalised Linear model (GLM) was used to compare the RPKM at each site between VHLKO (x-axis) and WT cells (y-axis), with a cut-off value of $p<0.05$. Overall, there are no statistically significant VHL KO specific sites in any comparison. There are a few hypoxia specific sites been identified in the WT cells and they are coloured in red. There is one hypoxia specific site, *HGSNAT*, that appeared in all three comparisons.

In the second approach, differential binding sites were manually selected based on the ratios of binding signal (RPKM) at each site, i.e. RPKM (VHL KO/WT) (**Figure 7)**. Within each comparison, the top 10 binding sites with the largest ratios were selected as VHL KO specific sites, and the 10 binding sites with smallest ratios were selected as WT hypoxia specific sites. Overall, there is only 1 site (*GPR61*) appeared as VHL KO-specific in all comparisons, and there are only 6 sites (4 sites associated with *HGSNAT,* 1 with *ATP9B,* and 1 with *LINC00910*) that appeared as hypoxia specific sites **(Figure 8)**. IGV tracks of these binding sites are shown in **Figure 9**. Within these ChIP-seq dataset analyses, they do indeed appear to be VHL KO specific or WT hypoxia specific. However, when looking across other ChIP-seq datasets (i.e. independent HIF-1β ChIP experiments performed in VHLKO DN5 and VHLKO DN7 cells), these sites do not remain as VHL KO specific or WT hypoxia specific sites. This indicates that although they appeared as 'hits' in the original analysis, they were likely generated as a result of low-level random noise in the datasets.

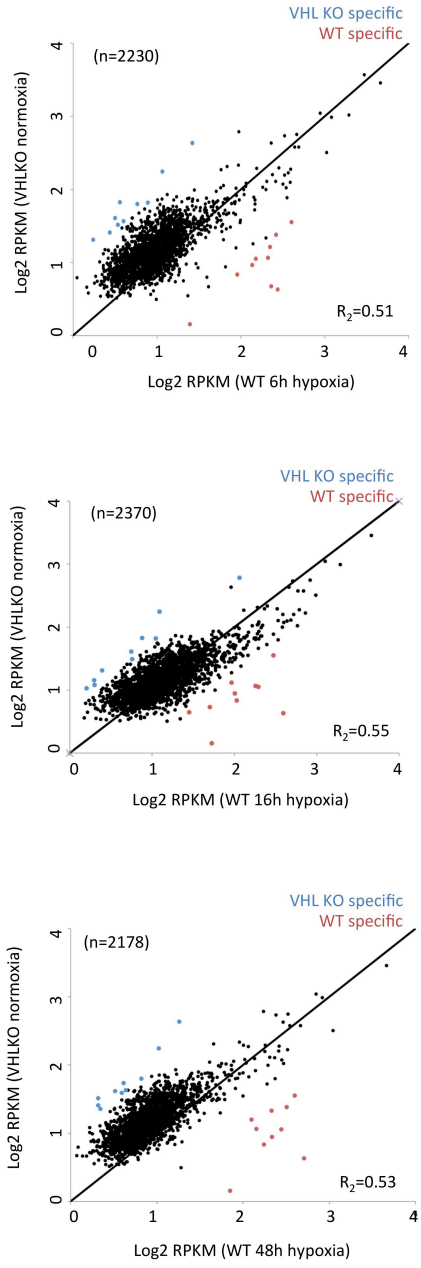

Figure 7. HIF-1α differential binding sites were manually selected based on their ratio of occupancy in VHL KO versus WT hypoxia. For each site, the ratio was calculated as RPKM in the VHL KO cells divided by the RPKM in the WT hypoxic cells, and then ranked. Top 10 sites with larger binding signal in the VHL KO cells were highlighted in blue (i.e. VHL KO specific sites), and top 10 sites with larger binding signal in the WT cells were highlighted in red (i.e. WT specific sites).

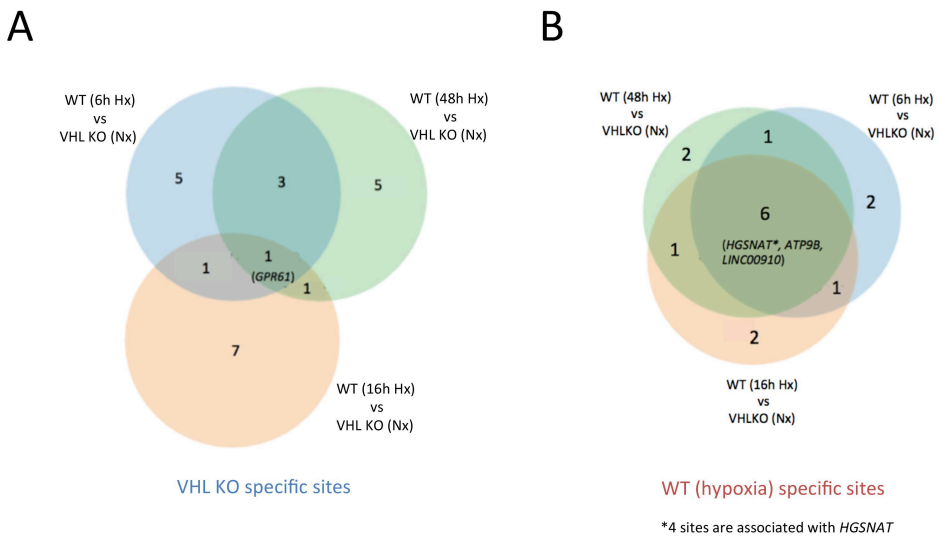

Figure 8. Venn diagrams summarising the (A) VHL KO specific sites and (B) WT (hypoxia) specific sites that were selected based on their RPKM ratio (VHL KO/WT) as shown in Figure.7.

A

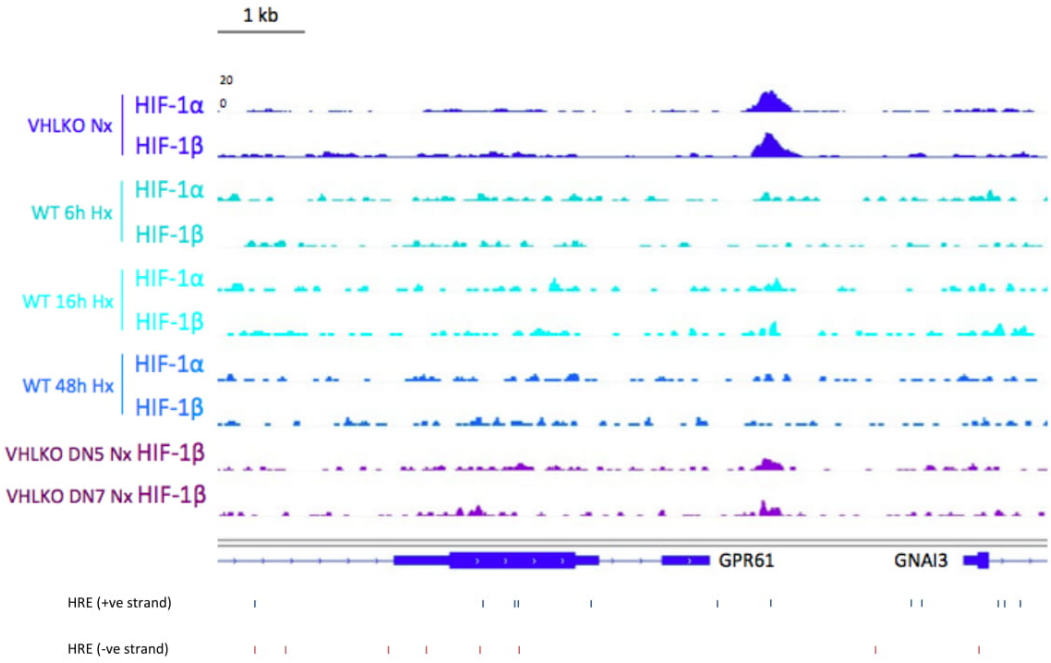
1 kb
20
0
VHLKO Nx
HIF-1α
HIF-1β
WT 6h Hx
HIF-1α
HIF-1β
WT 16h Hx
HIF-1α
HIF-1β
WT 48h Hx
HIF-1α
HIF-1β
VHLKO DN5 Nx HIF-1β
VHLKO DN7 Nx HIF-1β
GPR61
GNAI3
HRE (+ve strand)
HRE (-ve strand)

B

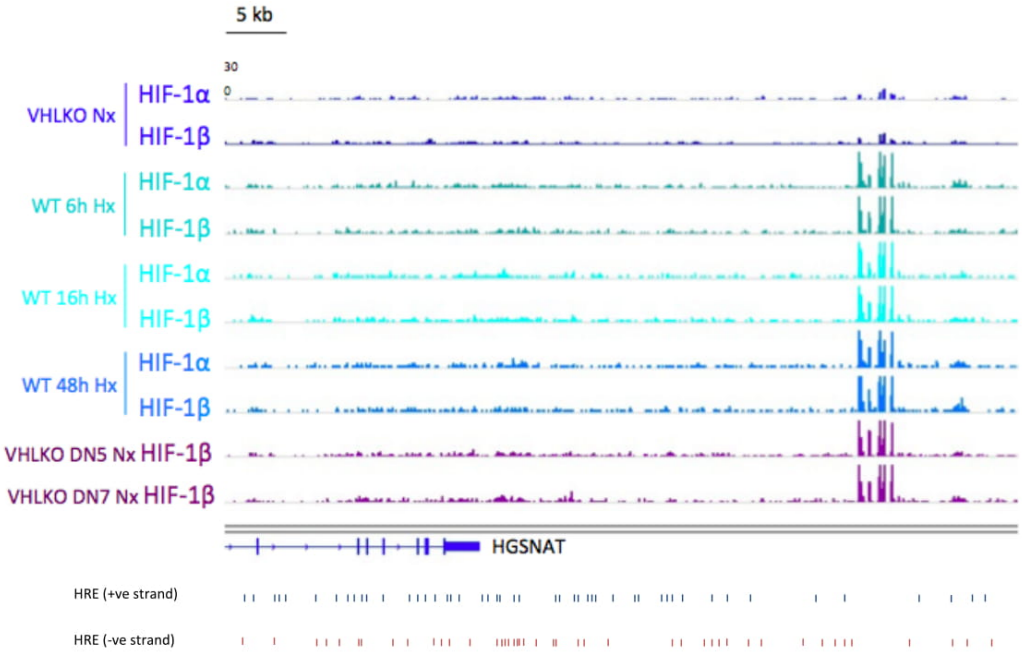
5 kb
30
0
VHLKO Nx
HIF-1α
HIF-1β
WT 6h Hx
HIF-1α
HIF-1β
WT 16h Hx
HIF-1α
HIF-1β
WT 48h Hx
HIF-1α
HIF-1β
VHLKO DN5 Nx HIF-1β
VHLKO DN7 Nx HIF-1β
HGSNAT
HRE (+ve strand)
HRE (-ve strand)

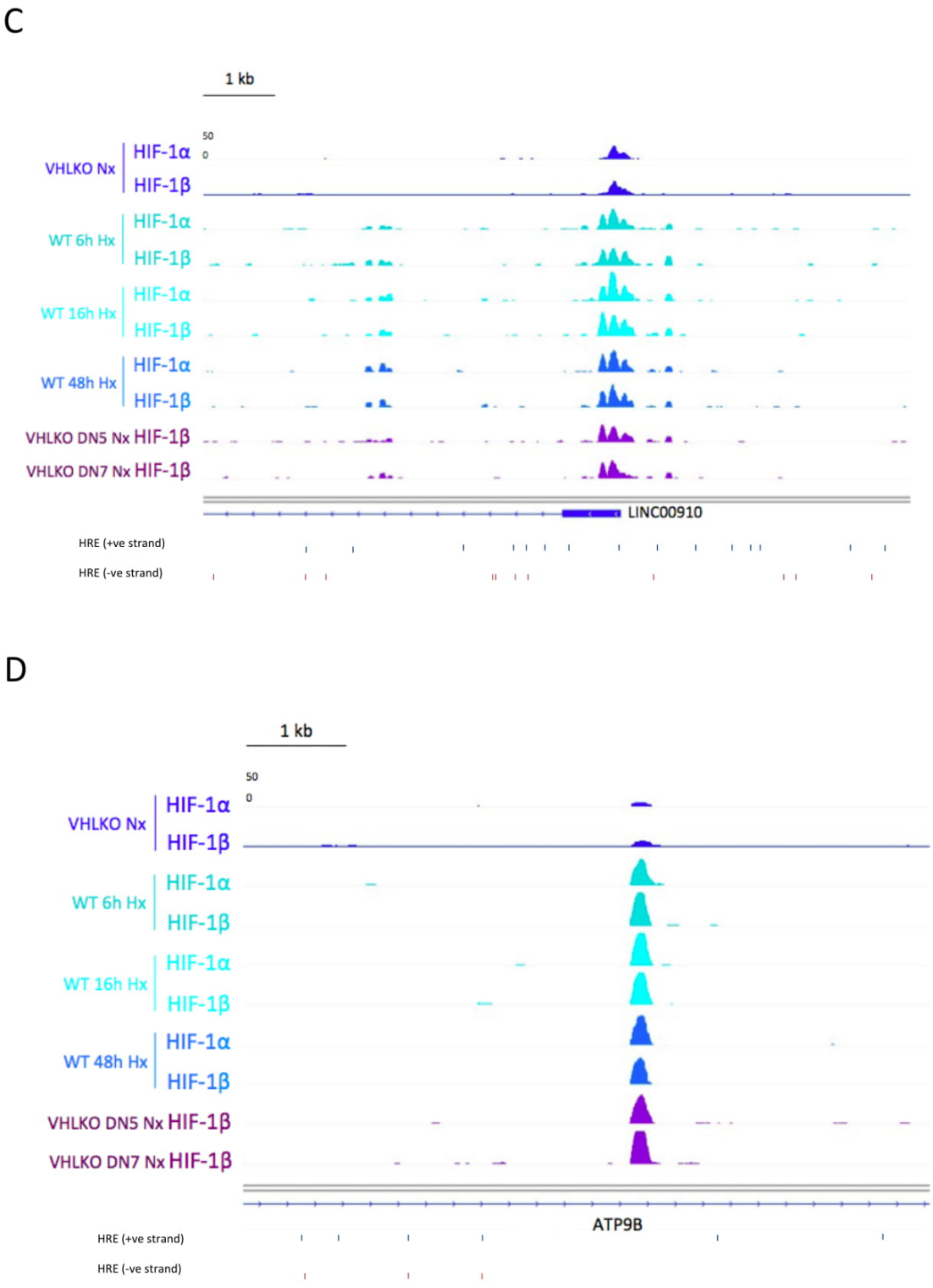

Figure 9. IGV tracks of VHL KO specific binding site *GPR61*, and WT hypoxia specific sites *HGSNAT*, *LIN00910* and *ATP9B* across multiple HIF ChIP-seq datasets.

5.2.1.3.2 Analyses of canonical HIF-2α sites

With the caveat that the HIF-2α ChIP-seq datasets may be less accurate, similar qualitative and quantitative analyses were also performed for HIF-2α canonical binding sites between the VHL KO background and the WT hypoxia background. Firstly, there were fewer HIF-2α sites in the VHL KO cells (n=339) compared to the 803 HIF-2α sites defined in the hypoxic WT cells. Of these 803 sites, only 19.3% overlapped with the HIF-2α sites identified in the VHL KO cells **(Figure 10A)**. When the HIF-2α sites identified at each of the three hypoxia time points were overlapped with the HIF-2α sites identified in the VHL KO cells, the best overlap was with 6h hypoxia dataset **(Figure 10A)**.

In the quantitative analysis, the sites that appeared in either the VHL KO or the hypoxic WT backgrounds were combined to give a total of 987 sites. The sites were then ranked based on their averaged RPKM (from the 2 ChIP-seq replicates in the VHL KO cells) as shown in the heatmap display (**Figure 10B left panel**). The corresponding RPKM of the same sites from the WT cells cultured under either 6, 16 or 48h of hypoxia are displayed on the right panels (**Figure 10B)**. Similar to the observations in the HIF-1α analysis, the pattern of canonical HIF-2α binding sites in the VHL KO remain very similar to that of the hypoxia WT background. The only difference lies in the signal intensity.

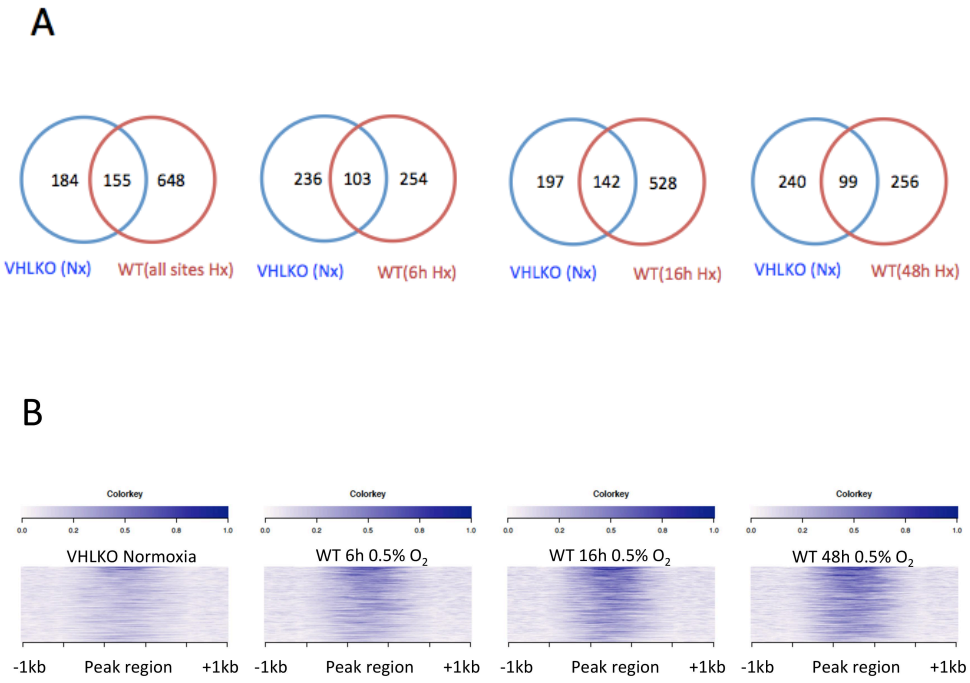

Figure 10. Qualitative and quantitative analyses of HIF-2α canonical binding sites. (A) Venn diagram comparing the HIF-2α sites that appeared in the normoxic VHL KO cell with those that appeared in the WT cells at different time-points of hypoxia (0.5% O_2). In total, there are 339 HIF-2α canonical binding sites in the VHL KO cells, and 803 sites in the hypoxic WT cells. Within the sites in the hypoxic WT cells, there are 357 sites at 6h, 670 sites at 16h and 355 sites at 48h of hypoxia. (B) Heatmap display showing the HIF-2α ChIP signal enrichment by colour intensity around a ±1 kb region of the canonical HIF binding site. HIF-2α sites in the VHL KO cells and WT cells were combined to give a total of 987 sites. The sites were ranked by their enrichment of the ChIP signal intensity (RPKM) in the VHL KO cells (1st panel), and the corresponding data from each of the WT hypoxic datasets was also displayed (right hand panels). Nx, normoxia. Hx, hypoxia.

In order to probe for individual or small groups of canonical HIF-2α sites that were specific to either the VHL KO or WT hypoxia condition, differential binding analyses were also performed by using statistical and manual-selection approaches (**Supplementary Figure 1 and 2).** Across all comparisons, there were no sites that appeared as VHL KO specific, and only 3 sites that appeared to be hypoxia specific (2 are associated with *HGSNAT,* 1 with *MIR1265*) (**Supplementary Figure 3)**. However, as previously when the IGV tracks of these sites were examined in the independent ChIP-seq experiments (**Supplementary Figure 4)**, they did not appear to be genuine hypoxia specific sites.

In summary, at the qualitative level, both HIF-1α and HIF-2α were found to bind to different canonical sites in the VHL KO cells and hypoxic WT cells, i.e. some sites appeared in only one condition but not the other. However, importantly when the HIF-α binding sites were examined at the quantitative level, loss of VHL and hypoxia were found to result in the same HIF DNA-binding patterns, with only differences in binding signal intensity being observed.

5.2.2 The effect of loss of *FIH* on HIF binding in VHL defective cells

Existing evidence has shown a positive effect of FIH knockdown on HIF-1α transcriptional activity across various cell lines (Stolze et al., 2004; Khan et al., 2011). Next, I aimed to examine whether loss of FIH protein could potentially influence the canonical HIF DNA-binding profile by a comparison of HIF DNA-binding in VHL KO versus VHLFIH KO cells. The use of VHL KO cells enables effects of FIH loss to be studied against the background of constitutive activation of the HIF pathway (thereby reducing any technical variation that might be introduced by having to additionally incubate cells under hypoxia conditions). In this analysis, VHL KO DN5 was compared with its subclone VHLFIH KO (DSB) (**Figure 1**).

First of all, whole cell extracts of these two cell lines were examined by immunoblot and the loss of FIH protein in the VHLFIH KO cells was confirmed **(Figure 11)**. Constitutive expression of HIF-α subunits was also observed in both cell lines, consistent with the loss of function of pVHL. HIF-1α level was slightly lower in the VHLFIH KO cells, which may be due to the variations in the immunoblot experiments since FIH inactivation did not alter HIF protein levels as shown in Chapter 1 Figure 5A. However, this could also be a true biological phenomenon since we have noted that following continuous culture of the VHLFIH KO cells, there is a reduction in both HIF-1α and HIF-2α protein level over a period of two months, data not shown.

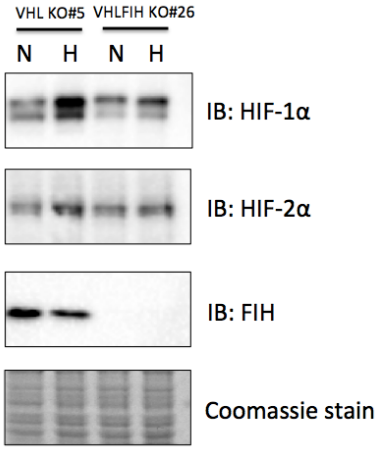

Figure 11. Immunoblots of HIF-α subunits and FIH protein in the VHL KO and VHLFIH KO cells. The cells were cultured under normoxia (N=21% O_2) or hypoxia (H=0.5% O_2) for 16h. Loss of FIH protein was confirmed in the VHLFIH KO cells. HIF-α protein levels were constitutively stabilised under normoxia in both cell lines, and were not affected by the loss of FIH protein.

HIF-α and HIF-1β ChIP-seq experiments were then performed in the VHLFIH KO cells (**Table 5.2**). The data was then compared with the respective HIF DNA-binding profiles identified in the parental VHL KO cells (as analysed in the earlier section of this chapter).

Table 5.2 ChIP-seq experiments to study the effect of loss of FIH protein

cell line	condition	ChIP	clones/reps
VHLFIH KO	Normoxia 21% O_2	HIF-1α, HIF-2α, HIF-1β	2
VHL KO	Normoxia 21% O_2	HIF-1α, HIF-2α, HIF-1β	2

Following ChIP-seq experiments, HIF canonical binding sites in VHLFIH KO cells were defined as previously described, i.e. HIF-1α (or HIF-2α) sites have to appear in either HIF-1α (or HIF-2α) replicate and have HIF-1β in at least one HIF-1β replicate. This approach identified a total of 1585 canonical HIF sites, within which there were 1363 HIF-1α and 442 HIF-2α sites. The reproducibility of binding signal at these sites

was compared between the two replicates and the R_2=0.55 for the HIF-1α and 0.66 for the HIF-1β datasets, indicated a reasonable correlation. However, again the HIF-2α datasets showed a low reproducibility (R_2=0.20) indicating the data to be noisy.

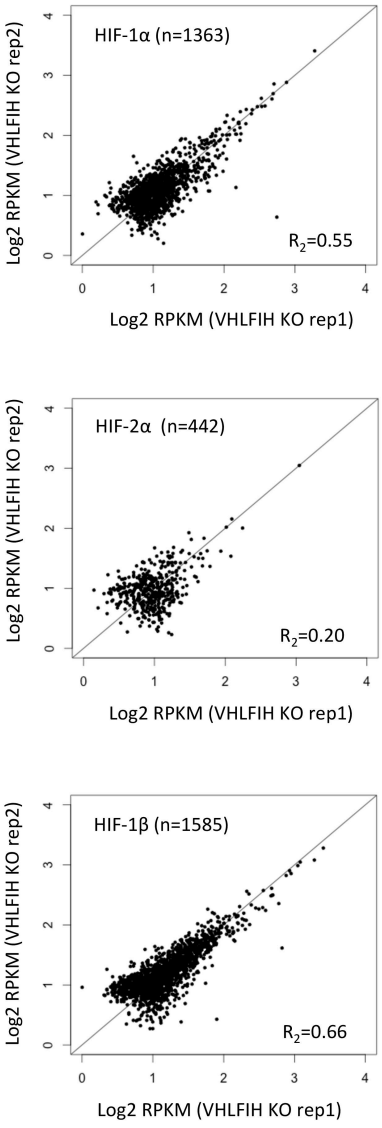

Figure 12. Assessment of the reproducibility at HIF canonical binding sites using the two replicates of HIF-1α, HIF-2α or HIF-1β ChIP-seq datasets from the VHLFIH KO cells cultured under normoxic conditions. HIF canonical binding sites were defined by the presence of both HIF-1α (or HIF-2α) and HIF-1β with detection of each isoform in at least one replicate. HIF-1β sites are defined as a combination of HIF-1α and HIF-2α sites. The number of canonical sites was shown on each plot. HIF ChIP signal intensity (RPKM) at each of the canonical binding site was plotted on a Log2 scale, using the data from replicate 1 (horizontal axis) and the data from replicate 2 (vertical axis). The correlation was shown as the R-squared value.

To examine whether the loss of FIH protein has any direct effects on the HIF-α DNA-binding patterns, both qualitative and quantitative analyses were performed to compare the canonical HIF-α binding profiles in the VHL KO and VHLFIH KO cells. The results of the qualitative analysis (displayed in a Venn diagram) suggest that for both HIF-α isoforms, the binding sites are different in these two cell lines (**Figure 13**). However, to fully interrogate this apparent difference, the sites were then analysed in a quantitative approach. The canonical HIF-1α (or HIF-2α) sites identified in the VHLFIH KO cells were combined with the sites that appeared in the VHL KO cells to result in a total of 2676 sites for HIF-1α and 678 sites for HIF-2α. Each binding site was then plotted according to its averaged RPKM value between the 2 replicates on a Log2 scale in the VHLFIH KO cells (horizontal axis) versus its RPKM value in the VHL KO cells (vertical axis) (**Figure 14**). A closer examination of this plot indicates that there is a higher binding signal in VHL KO cells for most of the canonical sites (i.e. most sites appear above the identity line). However, again there are no unique binding sites identified in either background, i.e. no sites appear on the axes (**Figure 14**). A GLM analysis also indicated that there were no differential HIF-1α (or HIF-2α) binding sites between these two cellular backgrounds (using a cut-off of $p<0.05$). Overall, there is no evidence indicating that loss of FIH can create new or block existing HIF-α binding sites.

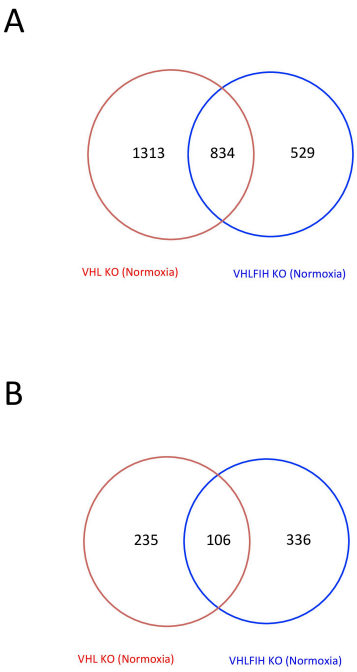

Figure 13. Qualitative analyses comparing canonical HIF-α binding sites that appeared in VHL KO cells and VHLFIH KO cells. The Venn diagrams suggest that both (A) HIF-1α and (B) HIF-2α sites that appeared in these two cell lines are overlapping but not identical.

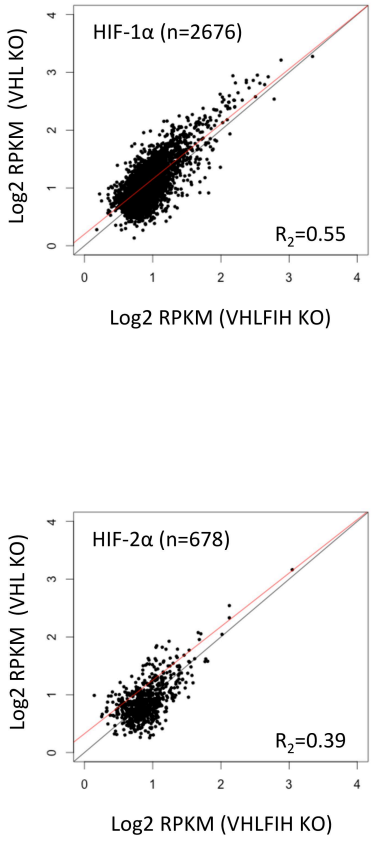

Figure 14. Quantitative analyses of the canonical HIF binding sites based on their RPKM values in VHL KO versus VHLFIH KO cells. HIF-1α (or HIF-2α) sites that appeared in the VHL KO cells and VHLFIH KO cells were combined. This gave a total of 2676 canonical HIF-1α and 678 HIF-2α sites. The RPKM values at each site were plotted on a Log2 scale, using the averaged signal from the two replicates of VHLFIH KO cells (horizontal axis) versus the averaged signal from the two replicates of VHL KO cells (vertical axis). The correlation of ChIP signals between the two cellular backgrounds is shown by the regression line (highlighted in red) and by the R-squared value. A GLM analysis was performed in order to identify binding sites that may be differentially bound between these two cell lines ($p<0.05$). However, for both isoforms there is no differential binding site (either VHL KO or VHLFIH KO specific) identified at this statistical level.

5.2.3 The effect of loss of *PBRM1* on HIF DNA-binding

Given the important role that loss of *PBRM1* plays in the development of RCC and the proposed role of its protein product BAF180 as a chromatin recognition subunit in the chromatin remodelling complex, next I examined the consequences of *PBRM1* inactivation on HIF DNA-binding genome-wide.

Two sets of ChIP-seq experiments were performed. In the first set, VHL KO cells were compared with PBRM1VHL double KO cells. This allows an assessment of the effect of PBRM1 KO against a background of constitutive activation of the HIF pathway (i.e. VHL KO) thereby eliminating the need for treatment of cells with hypoxia that may introduce additional variability due to the influence of duration of hypoxia. In the other comparison, HIF ChIP experiments were performed in PBRM1 KO cells and WT cells that were both cultured under hypoxia for the same duration of time.

Considering the better signal-to-noise obtained with HIF-1β ChIP and earlier evidence in previous chapters that both function and binding of HIF was mediated by canonical α/β binding it was considered that any change in HIF binding could properly be assayed by HIF-1β ChIP-seq. Accordingly in these experiments, HIF binding for the function and binding of HIF only HIF-1β ChIP-seq experiments were performed.

5.2.3.1 HIF-1β binding in the VHL KO versus PBRM1VHL KO cells that cultured under normoxia

Firstly, immunoblot of PBRM1 (BAF180) protein in the PBRM1 KO and PBRM1VHL KO cells (two independent clones for each cell line) confirmed that these knockout cells have lost PBRM1 (BAF180) protein **(Figure 15)**. Total HIF-1α protein level was also examined across the mutant cell lines. As shown in the immunoblot, the level of HIF-1α was similar in the VHL KO and PBRM1VHL KO cells that were cultured under normoxia (21% O_2). Therefore, loss of PBRM1 (BAF180) protein has no effects on the expression of HIF-1α protein, which allowed an analysis of HIF binding profiles by performing ChIP-seq experiments (**Table 5.3**).

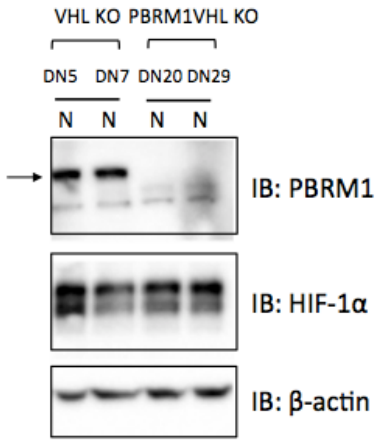

Figure 15. Inactivation of PBRM1 (BAF180) protein has no effects on total HIF-α protein level. The loss of PBRM1 (BAF180) protein was confirmed by immunoblotting the whole cell extracts from VHL KO cells (DN5 and DN7), and PBRM1VHL KO cells (DN20 and DN29). The cells were cultured under normoxia condition (N=21% O_2) for 16h. HIF-1α protein level in both clones of the PBRM1 KO cells was comparable to the level in the VHL KO and PRBM1VHL KO cells in which HIF-α was constitutively stabilised.

Table 5.3 ChIP-seq experiments to study the effect of loss of PBRM1 protein

cell line	condition	ChIP	clones/reps
VHL KO	Normoxia 21% O_2	HIF-1β	DN5 and DN7
PBRM1VHL KO	Normoxia 21% O_2	HIF-1β	DN20 and DN29

Since only one HIF-1β ChIP experiment was performed on each clone, in order to identify a high stringent set of sites for further analysis, HIF-1β sites in the PBRM1VHL KO cells were defined as sites that appeared in both clones (n=564). A high correlation of binding signal intensity at those sites was observed between the clones (R_2=0.75) **(Figure 16A**). These sites were then compared with the HIF-1β sites defined in the two clones of VHL KO cells (n=444) as shown earlier in this chapter (**Figure 3**).

Qualitative analysis again showed substantial but apparently incomplete overlap of HIF-1β binding profiles in the VHL KO and PBRM1VHL KO cells (**Figure 16B**). In the quantitative analysis, HIF-1β sites appeared in these two cell lines were combined (n=687). In this analysis it was clear that, despite apparent differences in the set of categorically defined binding sites, most sites distributed around the identity line

(R_2=0.71) i.e. binding in VHL KO and PBRM1VHL KO cells was similar. In keeping with this, formal GLM analysis detected no HIF-1β binding sites that manifest significant differential binding between VHL KO and PBRM1VHL KO cellular backgrounds at a level of p<0.05 (**Figure 16C**).

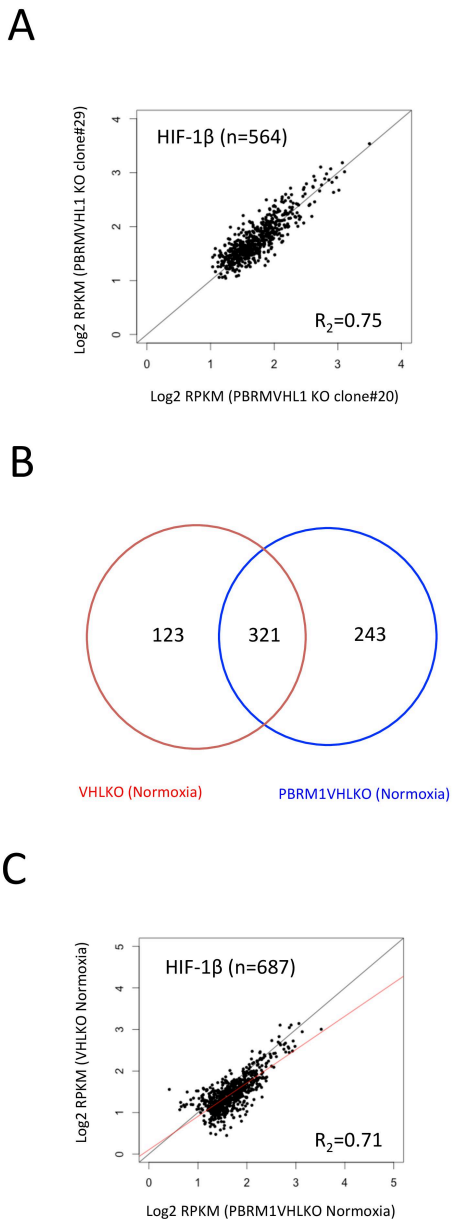

Figure 16. Qualitative and quantitative analyses comparing HIF-1β sites in the normoxic PBRM1VHL KO cells and VHL KO cells. HIF-α is constitutively stabilised in both cell lines due to the loss of pVHL. (A) A high reproducibility of ChIP signal intensity at HIF-1β sites was observed between the two clones of PBRM1VHL KO cells. HIF-1β sites were subsequently defined as sites that appeared in both clones (n=564). (B) The sites were then compared with HIF-1β sites in both clones of VHL KO cells (DN5 and DN7, n=444, see Figure 3) in the Venn diagram. (C) All HIF-1β sites that appeared in either PBRM1VHL KO cells or VHL KO cells are included in the analysis (n=687). ChIP signals at each of those sites were compared by plotting the average signal in the two PBRM1VHL KO clones (horizontal axis) versus the averaged signal in the two VHL KO clones (vertical axis). GLM analysis did not define any site in which differential HIF-1β binding in PBRM1VHL KO versus VHL KO reached a significance theshold of $p<0.05$.

5.2.3.2 HIF-1β binding in the WT versus PBRM1 KO cells under hypoxia (0.5% for 16h) condition

In the second set of experiments, immunoblotting confirmed the loss of PBRM1 (BAF180) protein in the two independent clones of PBRM1 KO cells **(Figure 17A)**. A very low level of expression was observed in one PBRM1 KO clone (DN14), indicating a potentially incomplete knockout of PBRM1 (BAF180) protein in this clone. Total HIF-1α protein level was examined in these cells. As shown in the immunoblot, the level of hypoxia induced HIF-1α was similar between the two clones of PBRM1 KO cells, and was comparable to the hypoxia induced HIF-α level in the WT cells (**Figure 17B**) (This experiment was performed by members of laboratory in the process of generating KO cell lines). This indicates that *PBRM1* inactivation does not alter the HIF-α protein level.

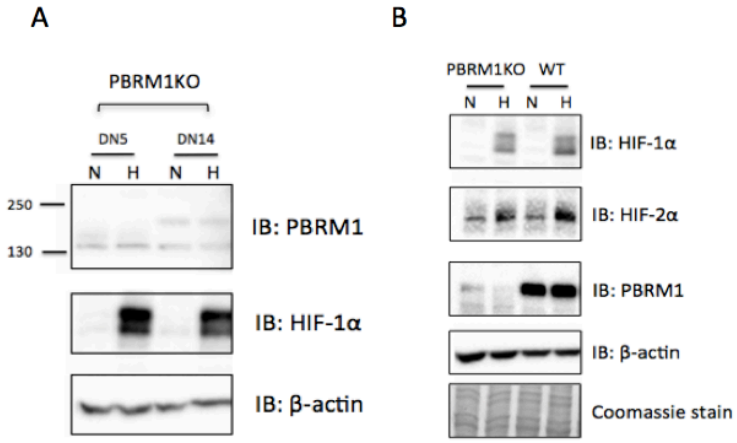

Figure 17. *PBRM1* inactivation does not alter total HIF-α protein level. (A) The loss of PBRM1 (BAF180) protein was confirmed by immunoblotting the whole cell extracts from two independent clones of PBRM1 KO cells (DN5 and DN14). The hypoxia induced HIF-1α level was similar in these two cell lines. (B) HIF-α level in the PBRM1KO DN5 was comparable to the hypoxia induced HIF-α level in the WT cells. The cells were cultured in normoxia (N=21% O_2) or hypoxia (H=0.5% O_2) for 16h.

Next, HIF-1β binding profiles were examined by performing ChIP-seq experiments (**Table 5.4**).

Table 5.4 ChIP-seq experiments to study the effect of loss of PBRM1 (BAF180) protein

cell line	condition	ChIP	clones/reps
PBRM1 KO	16h 0.5% O_2	HIF-1β	DN5 and DN14
HKC-8 WT*	16h 0.5% O_2	HIF-1β	2

* Data was obtained from chapter 4

As in the analyses performed earlier, HIF-1β sites in the PBRM1 KO cells were defined as sites that appeared in both clones of PBRM1 KO cells (n=399) (**Figure 18A)**. Binding signal intensity (RPKM) at those sites was compared between the two clones. R_2=0.70, indicating a high reproducibility of ChIP signal. In order to be directly comparable with these sites, HIF-1β sites in the hypoxic WT cells (0.5% O_2 for 16h, data from Chapter 4) were redefined as sites appeared in both replicates (n=1145). R_2=0.74 also indicated a high correlation of ChIP signals in the two hypoxic replicates of WT cells **(Figure 18B)**.

In order to investigate the effects of loss of PBRM1 (BAF180) protein on the HIF-1β DNA-binding profiles, HIF-1β sites were firstly compared at qualitative level, as illustrated in the Venn diagram in **Figure 18C.** This revealed an overlapping but non-identical binding profile between these two cellular backgrounds. The comparison was again also performed at quantitative level based on the RPKM at each site **(Figure 18D)**. HIF-1β sites which were defined in either the PBRM1 KO and WT cells were all considered in this quantitative analysis (n=1184). The binding intensity at the majority of sites distributed around the identity line, but was slightly higher in the hypoxic WT cells. However, no unique sites were observed in either cell line. GLM analysis identified 4

sites as WT specific sites based on a statistical threshold of $p<0.05$, i.e. sites that lost their binding when *PBRM1* is inactivated. On the other hand, 1 site were identified as *PBRM1* knockout specific sites, i.e. these sites gained binding in association with loss of PBRM1 (BAF180) protein (Appendix 8.10).

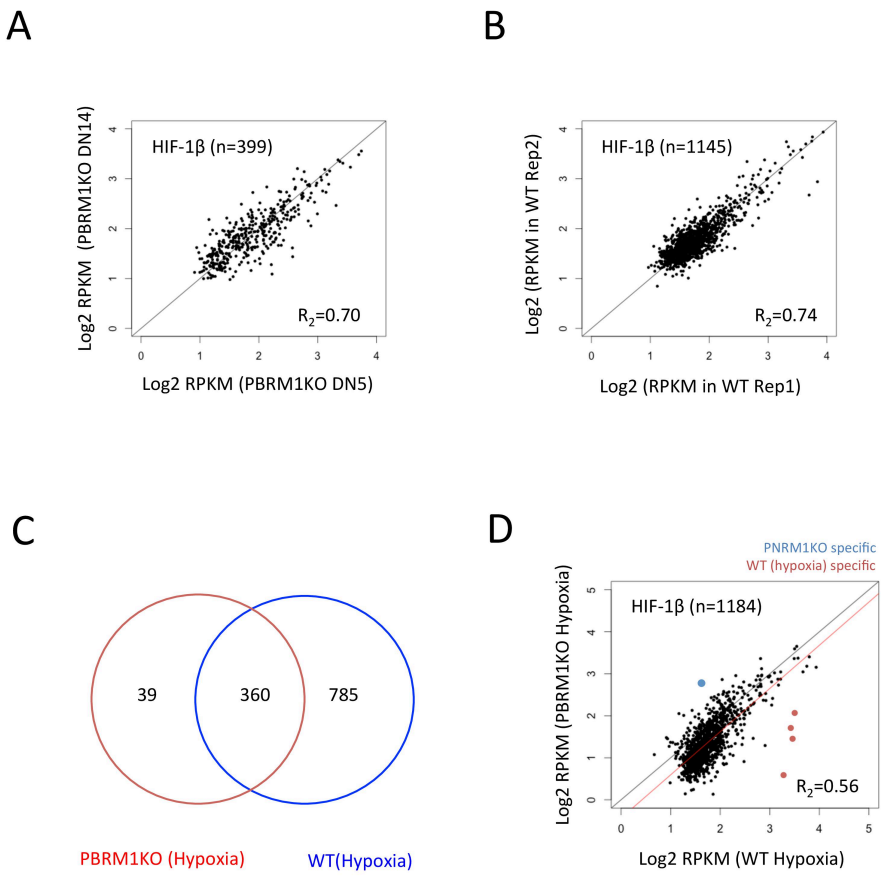

Figure 18. Comparison of HIF-1β sites in the hypoxic PBRM1 KO cells and WT cells. (A) Correlation of RPKM at HIF-1β sites that appeared in both clones of PBRM1 KO cells (n=399) indicates a high reproducibility of ChIP signal between the two clones. (B) Similarly, a high reproducibility of signal intensity at HIF-1β sites (n=1145) was observed between the two replicates of ChIP experiments in the WT cells. (C) Venn diagram suggests that at qualitative level, HIF-1β sites appeared in the PBRM1 KO cells and WT cells are not identical (D) HIF-1β sites appeared in both cell lines are included in the analysis (n=1184). ChIP signal at those sites was compared between the cells by plotting the averaged signal from the two WT replicates (horizontal axis) versus the averaged signal from two PBRM1 KO clones (vertical axis). GLM analysis was performed to detect differential binding sites in these two cellular backgrounds ($p<0.05$). Overall, there are 4 WT (hypoxia) specific sites which are highlighed in red, and 1 PBRM1 KO cells specific sites which are highlighted in blue.

However, when combining the results from the two sets of experiments (i.e. examining the PBRM1-dependent effects on HIF DNA-binding in VHL negative versus hypoxia backgrounds), even though a small number of HIF-1β sites gained or lost binding due to the loss of PBRM1 (BAF180) protein in the hypoxia background, no sites reached statistical significance in the VHL negative background in which HIF-α protein is constitutively stabilised. Overall, due to the inconsistent results, at least at quantitative level, loss of PBRM1 (BAF180) protein does not significantly redistribute HIF-1β binding sites.

5.3 Discussion

In this chapter, HIF canonical DNA-binding profiles in response to loss of VHL, FIH or PBRM1 (BAF180) proteins were examined. First of all, inactivation of these three proteins in the mutant cells has no discernable effects on total HIF-α protein level compared to that was induced by hypoxia in the WT cells.

For *VHL* inactivation this result was in line with expectations from previous work and from the well-established model whereby hypoxic suppression of prolyl hydroxylation prevents the action of pVHL in a common pathway that leads to the destruction of HIF in the presence of oxygen.

In the case of *FIH*, an oncoprotein action has been described in which loss of *FIH* has led to apoptosis of renal carcinoma cell lines, a result that has been attributed to negative effects on cell proliferation or viability from constitutive transcriptional activation of HIF-1α target genes. Although the laboratory has observed reductions in HIF-1α expression in *FIH* deficient cells in prolonged culture, this was not observed under the conditions of these experiments.

For *PBRM1*, effects on the level of HIF-α expression have been reported, but are inconsistent across different studies (Wang et al., 2017; Gao et al., 2017; Chowdhury et al., 2016). In the current work I observed no effect. This result appeared robust, at least in this cellular setting, and was observed irrespective of whether HIF was activated by hypoxia in *VHL* competent cells or activated in the presence of oxygen or by *VHL* loss.

The lack of effects on HIF-α protein levels simplified interpretation of HIF-α DNA-binding signals, since any change that was observed must be independent of HIF-α protein level. I applied two different strategies to the analysis of HIF DNA-binding signals; a qualitative analysis based on peak calling threshold and illustrated by Venn diagrams and quantitative analyses based on comparison of peak intensities between different conditions. The rationale for this was that each mode of analysis has strengths and weaknesses, but a true biological difference should be evident in both analyses, at least if it is above a certain threshold.

What I observed was that although categorical Venn diagrams suggested substantial alteration of canonical HIF-1α (and HIF-2α) binding sites between different conditions, such changes were much less evident when quantitative analyses were performed. Even though good correlation were observed in most of the replicate datasets, at any one site ChIP-seq signals exhibit some variability. The application of qualitative thresholds to intrinsically variable assays has the potential to exaggerate differences and therefore likely underlay the difference between qualitative and quantitative analyses.

In the quantitative analyses that were based on the RPKM of each binding site, the data in general revealed very few (sometimes no) canonical HIF-1α (and HIF-2α) sites at which differential binding reached a statistically significant threshold. For example, when the canonical HIF-1α (and HIF-2α) sites that appeared in the VHL KO cells were compared with the sites that appeared in the WT cells at 6h, 16h or 48h of hypoxia,

overall the VHL KO specific or WT (hypoxia) specific sites did not appear consistently in all the comparisons. Similarly, when the effect of loss of *PBRM1* on the HIF-1β binding was examined, paralleled analyses between PBRM1VHL KO cells and VHL KO cells, as well as between hypoxic WT cells and PBRM1 KO cells indicated that at the quantitative level, there were no unique HIF-1β sites that consistently appeared in the two sets of analyses (**Figure 16C and 17D**). In the case of inactivation of FIH, there were again no differential HIF-1α (or HIF-2α) binding sites between VHL KO and VHLFIH KO cells in the quantitative analyses, despite apparent differences in the Venn diagrams of qualitatively defined sites.

In summary, few statistically significant changes in the qualitative analyses of specific sites were observed, and when they were observed, they were not concordant across datasets where similar results might be have been expected (i.e. different durations of hypoxia, or hypoxia and VHL inactivation). Small numbers of statistically significant genes showing inconsistent patterns might have been the result of chance, or might represent clonal variations unrelated to the engineered genotype. It was therefore concluded that major effects of these genes on HIF-binding at specific sets of target loci are unlikely.

However, more subtle changes in HIF binding intensity were observed in some datasets. For instance, in the case of canonical HIF-1α sites, heatmaps showed that the stronger sites (i.e. top of the heatmap) appear to have similar binding intensity in the VHL KO cells or hypoxic WT cells, whereas the weaker sites (i.e. bottom of the heatmap) have more binding in the VHL KO cells (**Figure 5B**). This result also matched the observations in the scatter plots, which showed that most strong sites distribute around the identity line, whereas most of the weaker sites distribute above the line, i.e. larger signals in the VHL KO cells (**Figure 6**). Considering that the total HIF-α protein

level (as measured in the whole cell extract) was similar in these two cellular backgrounds, this suggests constitutive (long-term) activation of HIF may have some effect on its general binding distribution, even if changes at individual sites were not significant.

In summary, the current work revealed some subtle changes in binding intensity at sets of HIF binding sites that are common between different conditions and genotypes, but very little evidence for the redistribution of binding to new sites or large effects on specific categories of site when VHL, FIH or PBRM1 (BAF180) proteins were inactivated.

For FIH protein, this is consistent with the proposed action to recruit CBP-p300 co-activators to promote transcription, but suggests that the histone acetyltransferase activities associated with this protein do not substantially alter patterns of HIF binding to DNA.

For pVHL and PBRM1 (BAF180), the results were somewhat surprising, as a number of studies have reported their effects on HIF-dependent gene expression. Given potential effects of chromatin, it appeared likely that at least some of those differences might reflect changes in patterns of HIF binding. For example, loss of pVHL and hypoxia have been shown to result in different gene expression profiles in RCC cells lines (Leisz et al., 2015; Malec et al., 2015; Wykoff et al., 2000). The data on effects of *PBRM1* inactivation on gene expression is more complex. Analyses of the expression profiles in RCC showed that PBRM1-mutant tumours displayed a hypoxic transcriptional signature (Varela et al., 2011). This was taken to indicate that *PBRM1* co-operated with HIF pathway and that inactivation of the gene might modulate that pathway. At cellular level, suppression of *PBRM1* resulted in increased proliferation and migration of RCC ACHN cells (Wang et al., 2017). The restrains of *PBRM1* on HIF targets expression was also

observed in pVHL-defective RCC cell line A704 cells. By performing RNA-seq experiment in these cells with dox-inducible *PBRM1* expression, Gao et al., demonstrated that inactivation of *PBRM1* amplified the HIF transcriptional response (Gao et al., 2017). However, in contradiction to these findings, a recent study of re-expressing *PBRM1* in isogenic RCC cell lines showed an up-regulation of genes involved hypoxic response (Chowdhury et al., 2016). The reason for the discrepancy is not clear. Furthermore, in another study in Hep3B cells with shRNA-mediated knockdown of *PBRM1*, the authors showed that the induction of some of the HIF targets (*CA9* and *ENO2*) was reduced, whereas others (*GLUT1*, *LDHA*, *PDK1*, *PGK1*) were not affected.

Overall, the lack of changes in HIF DNA-binding patterns in this work suggests that any modulation of the HIF response (as reported) occurs mainly through post-DNA binding mechanisms. Nevertheless, our analyses does not rule out the possibility that the changes in HIF DNA-binding may occur for instance at the weak affinity sites, and that these are important in the genesis of RCC. For instance, small changes in DNA binding at specific sites have been demonstrated for GWAS-defined RCC-susceptibility polymorphisms. Changes of this magnitude would generally be missed by pan-genomic studies of this type.

The chromatin remodeller PBRM1 (BAF180) has been reported to have many functions in the regulation of gene expression and it is possible that its principal action is at the post-DNA binding level or on the binding or accessibility of other factors at HIF-binding loci. Further analyses using techniques such as DNaseI seq, ATAC-seq or NOMe-seq might be of interest in this respect (Buenrostro et al., 2015; Kelly et al., 2012).

Notable, in addition to the *PBRM1*, mutations in other chromatin-modifying enzymes have been reported to play an important role in RCC, such as *BAP1, UTX,*

JARID1C and SETD2. In particular, in a recent study with integration of HIF binding sites, Simon et al., demonstrated that RCC tumours with mutations in *SETD2* gene, which encodes for H3K36me3 (histone H3 lysine-36 trimethylation) methyltransferases, had widespread increases in chromatin accessibility as measured by formaldehyde-assisted isolation of regulatory elements followed by sequencing (FAIRE-seq) (Simon et al., 2014). This study demonstrates that chromatin accessibility is a factor in RCC biology. Importantly, it was the first study showing that tumour-associated changes in open chromatin were associated with changes in HIF binding sites and linked to genes involved in hypoxia response. Another example of epigenetic regulation of the HIF response in RCC is the *JARIDIC*, which encodes H3K4me3 (histone-3 lysine-4 trimethyl) demethylase. Suppression of this gene in 786-O RCC cell line restored H3K4me3 levels at the promoters of HIF targets (e.g. *IGFBP3*, *DNAJC12* and *COL6A1*) and augmented the expression levels of these genes (Niu et al., 2012). Therefore, the effects of these epigenetic modulations, or a combination of multiple modifications on HIF binding deserve further exploration.

5.4 Conclusion

In this chapter, the potential effects of loss of VHL, FIH and PBRM1 (BAF180) proteins on HIF canonical DNA-binding profiles were examined. Quantitative analysis suggests that HIF appears to bind largely similar canonical sites without a major redistribution of binding. The results suggest that effects of these proteins on the HIF transcriptome are largely mediated by post-DNA binding mechanisms, or through the regulation of the binding of other factors to DNA.

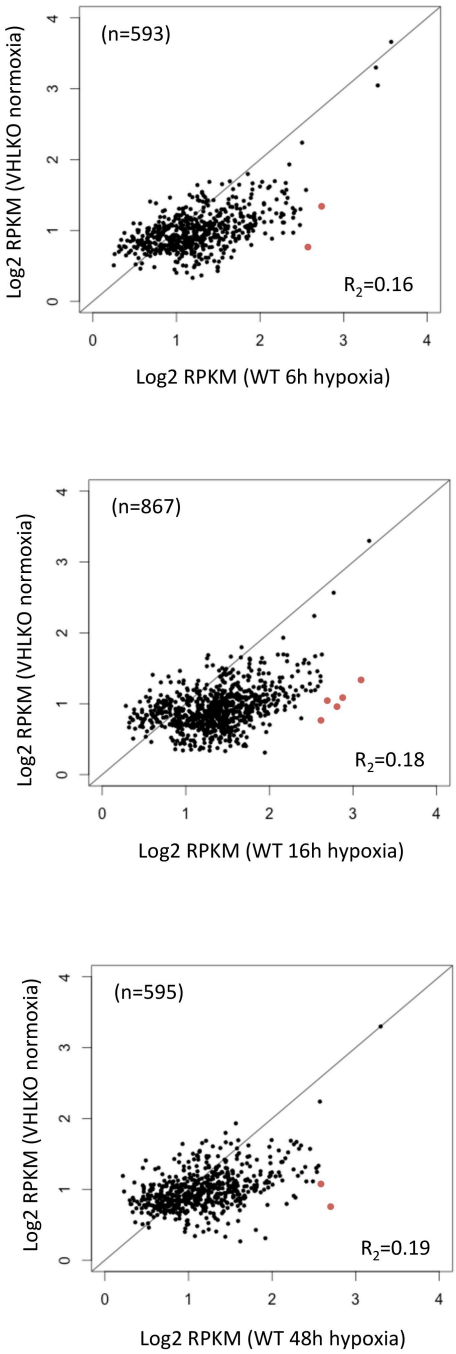

Supplementary Figure 1. Statistical analysis was performed to identify differential binding sites of HIF-2α between normoxic VHL KO cells and WT cells that cultured at either 6h, 16h or 48h of hypoxia. Generalised Linear model (GLM) was used with a cut-off value of $p<0.05$. Overall, there are no sites that were differentially bound in VHL KO cells within each comparison. Site that are differentially bound in the WT cells are coloured in red. There was one site, *HGSNAT*, that appeared in all three comparisons.

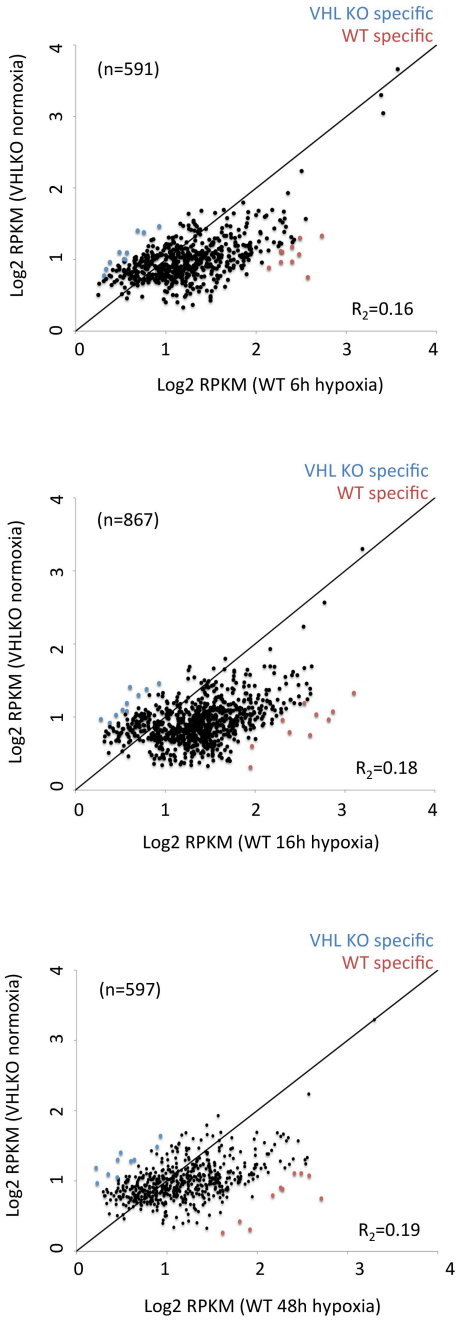

Supplementary Figure 2. HIF-2α differential binding sites were manually selected based on the fold change (FC) ratio. For each site, FC ratio was calculated as RPKM in the VHL KO cells divided by the RPKM in the WT cells, and then ranked. Top 10 sites with larger binding signal in the VHL KO cells were highlighted in blue (i.e. VHL KO specific sites), and top 10 sites with larger binding signal in the WT cells were highlighted in blue (i.e. WT specific sites).

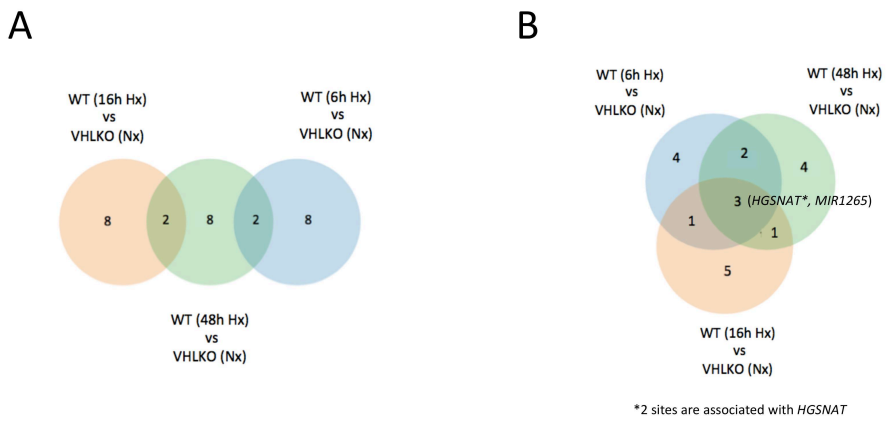

Supplementary Figure 3. Venn diagrams summarise the (A) VHL KO specific sites and (B) WT (hypoxia) specific sites that were selected based on the FC (VHL KO/WT) as shown in Supplementary Figure 2.

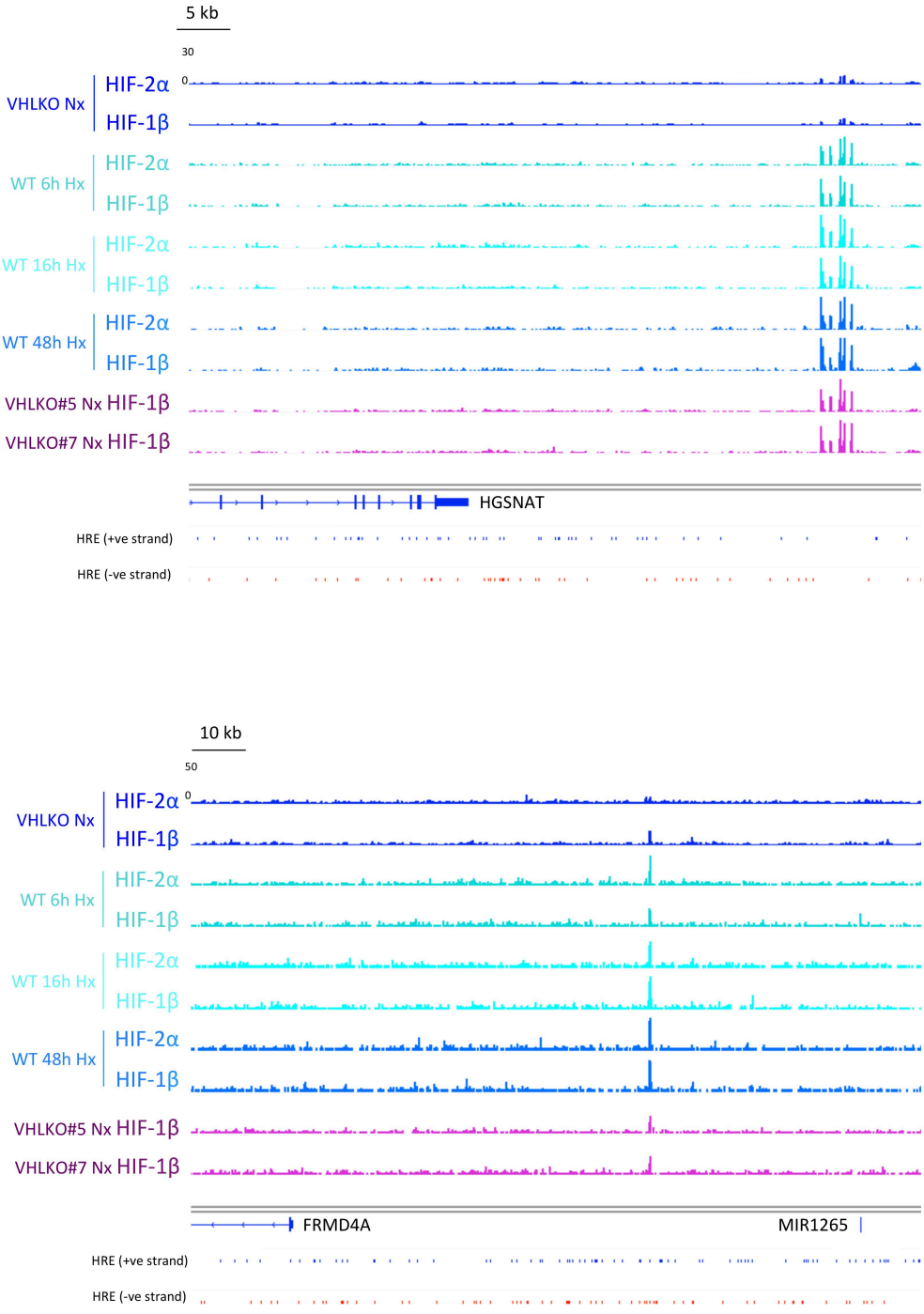

Supplementary Figure 4. IGV tracks of WT hypoxia specific sites *HGSNAT* and *MIR1265* across multiple HIF ChIP-seq datasets.

6

Discussion and Future Perspectives

In this study, the genome-wide responses of the HIF system to different conditions of hypoxia (both severity and duration), as well as to specific (and cancer-relevant) gene knockouts were investigated. By a comparison of RNA-seq data from HKC-8 wild type (WT) cells and cells engineered to either be HIF 'off' or constitutively HIF 'on', I was first able to demonstrate the extensive role of the canonical HIF pathway (i.e. via HIF-α/HIF-1β heterodimerisation) in hypoxia-regulated gene expression. Having established the critical role of the HIF DNA-binding heterodimer, I next examined the canonical HIF binding profiles in response to both physiologically relevant hypoxic stimuli (i.e. varying severity and duration of hypoxia), and to inactivation of genes linked to HIF pathway dysregulation in cancer (i.e. loss of *VHL*, *PBRM1* and *FIH*). Extensive analyses of HIF binding were performed using both quantitative and qualitative methods. The work revealed that in response to hypoxia of differing grade or duration, both major isoforms HIF-1α and HIF-2α bound a largely discrete set of sites across the genome, at levels that were increased broadly in proportion to the extent of activation of the relevant isoform, and independent of the absolute level of binding at a given site. These sites were also

largely unaltered after long-term constitutive induction of HIF following inactivation of *VHL*, by inactivation of *PBRM1* and by inactivation of the HIF asparaginyl hydroxylase, FIH. This suggests the existence of HIF-isoform specific mechanisms that tightly constrain HIF binding patterns across the genome independently of these conditions. In this final chapter, the implications and limitations of the current study, as well as suggestions for future experiments, will be discussed.

6.1 The contribution of the HIF system to hypoxia-regulated gene expression

Analyses of hypoxic gene expression profiles in the WT and CRISPR/Cas9 engineered mutant cells (in which one or more components of the HIF-VHL pathway are inactivated) demonstrated that hypoxia-dependent gene expression under the condition examined is mainly regulated through the canonical HIF pathway.

Overall, the work identified 893 hypoxia-regulated genes in the WT cells, of which 536 were activated and 357 were repressed by hypoxia. HIF is known as a transcriptional activator rather than repressor. Thus, the regulation of gene repression is likely through other factors with transcriptional repressive functions that are themselves induced by HIF. To date, at least ten transcriptional repressors have been reported to act under hypoxia, with REST (Repressor Element-1 Silencing Transcription factor) being the key player (reviewed in Ooi and Wood. 2007; Cavadas et al., 2016). In addition, epigenetic regulators such as the Sin3A histone deacetylase complex (including SIN3A, SAP30 and HDAC1/2) have also been shown to participate in the down-regulation of hypoxia repressed genes (Tiana et al., 2018). The level of REST gene expression did not change, and there was a small up-regulation of *SIN3A* (1.36-fold) in the hypoxic HKC-8 cells. Whether this small response contributes to gene down-regulation under hypoxia

remains unknown, but it appears likely that there are other, as yet undefined, repressor mechanisms that are induced in hypoxia. Nevertheless, ablation of HIF-α or HIF-1β, as well as constitutive activation of the HIF pathway all abolished the hypoxia-dependent repression of these genes, suggesting that the regulation is still ultimately controlled through the HIF pathway.

The panel of WT and HIF pathway mutant cell lines also enabled a comprehensive investigation of possible HIF-independent but hypoxia-dependent gene expression mechanisms, by analysing the genes that are regulated by hypoxia to a similar degree across all the cell lines. However, no convincing evidence for completely HIF-independent gene regulation in HKC-8 cells was found under the conditions studied. Given that many studies have proposed HIF-independent mechanisms of gene regulation and that there are multiple reported alternative substrates for the PHD enzymes, this study indicates that if indeed they operate in HKC-8 cells, they do not contribute substantially to adaptive gene expression in hypoxia. A small number of candidates were identified as potentially HIF-independent hypoxia-responsive genes by altering the stringency of selection criteria, however they showed only very small fold changes in the RNA-seq experiments and they could not be reproduced in the independent RT-qPCR assays. Either they represent false positives in the RNA-seq analysis or the lack of sensitivity of RT-qPCR assays prevents such small fold changes from being detected. More replicates of RNA-seq experiments, as well as more robust and independent validation assays would be required to investigate these genes further, but their regulation was at best of low amplitude.

A significant number of genes were observed to be up-regulated by hypoxia in the HIF-1β mutant cells, and the regulation appears to correlate (rather modestly) with the regulation in the WT cells. When the GO pathway analysis was performed, these genes

do not present a discrete physiological function. Since mutation of the targeted HIF-1β genomic locus, as well as the complete loss of HIF-1β protein and its function in these mutant cells was confirmed by a variety of assays, the residual hypoxic regulation observed might be due to a potential non-canonical function of the HIF-α subunit and consistent with this, no regulation of these genes was observed in the HIF-α DKO cells. HIF-α might form functional heterodimers with alternative bHLH-PAS dimerisation partners. Although there are multiple bHLH-PAS factors (Wu et al., 2016) and cross-talk with HIF-dependent gene expression is described in specific settings (e.g. BMAL1, Sumaya et al., 2016, Peek et al., 2017; NPAS4, Sabatini et al., 2018), only ARNT2 (a homologous to ARNT/HIF-1b) has been identified as an alternative heterodimerisation partner for HIF-α (Maltepe et al., 2000; Keith et al., 2001; Wu et al., 2016). ARNT2 is expressed at high levels in the mouse CNS and kidney (Jian et al., 1998) and although the transcript is barely detected in the HKC-8 cells compared to that of HIF-1β transcript, it is unclear how this might relate to its protein level. However it should be noted that the (limited) analyses of HIF DNA-binding (by ChIP-qPCR) and HIF transactivation function (by HRE-luciferase reporter readout) in the HIF-1β KO cells did not provide any evidence for alternative DNA-binding heterodimers. It may therefore be relevant that HIF-α has also been reported to interact with other TFs, such as NICD (Gustafsson et al., 2005), STAT3 (Pawlus et al., 2013), USF (Pawlus et al., 2012) and SP1 (Koizume et al., 2012) and that transcripts for these TFs are detected by RNA-seq in HKC-8 cells although the expression levels are much lower when compared with the level of HIF-1β.

The genes that are more regulated by hypoxia in the HIF-1β KO cells than in the WT cells were considered specifically, and a signature of lipid metabolism was observed. RT-qPCR experiments that were performed to validate the regulation confirmed a specific hypoxia regulation in HIF-1β KO cells (compared to the WT cells) but also

revealed that at least some of these genes were up-regulated by hypoxia in HIF-α DKO cells. This led me to re-examine the RNA-seq datasets for the HIF-α DKO cells. This revealed that in one replicate, but not the other, similar changes were observed. From these data, I inferred that the demonstration of the response (even if inconsistent) in HIF-α DKO cells was a dominating observation, which made it unlikely that this was truly a non-canonical function of HIF-α. More likely it appeared to be a response to hypoxia that was observed, albeit somewhat inconsistently, in HIF-deficient but not WT cells.

HIF has been implicated in several aspects of lipid metabolism including lipid uptake and lipid droplet biosynthesis, and some lipid metabolism genes are direct HIF targets (reviewed in Goda and Kanai. 2012). However, there are other studies that show hypoxia-dependent but HIF-independent effects on lipid metabolism. In some cases, lipids appeared to have a protective function. For instance, lipid droplets appear to have an antioxidant role in neural stem cells of *Drosophila* under hypoxia and oxidative stress, and in this case the induction was shown to be HIF-independent, as *Drosophila Sima* homozygotes (i.e. lacking HIF-1α activity) retained the ability to accumulate lipid droplets during hypoxia (Bailey et al., 2015). In another example, hypoxia and low serum were also found to alter lipid metabolism via the SREBP2-dependent expression of *ACSS2* in human cancer cells (Schug et al., 2015). Since ACSS2 converts acetate to acetyl-CoA, its upregulation was thought to provide a growth advantage under conditions of metabolic stress by enabling the use of acetate as an additional carbon source to sustain lipid production. These types of mechanism could also be operative in the HIF deficient HKC-8 cells giving rise to the up-regulation of lipid metabolism genes.

It has been reported that HIF-defective cells are less able to maintain ATP levels in hypoxia (Fukuda et al., 2007; reviewed in Semenza. 2010), but also less able to appropriately reduce mitochondrial metabolism resulting in excess production of radical

oxygen species and oxidant stress (Schipani et al., 2001). Whether either of these stresses underlies the observed effects in the HIF deficient HKC-8 cells will require further analysis.

To move forward in this study, first of all, a more comprehensive analysis of the hypoxia-inducible lipid gene signature (by both RT-qPCR and immunoblot) is required in the WT and HIF-1β KO/HIF-α DKO cells. The functional consequences then need to be considered, i.e. does the induction of these genes by hypoxia lead to any increased lipid droplet accumulation or is it simply a response of the cell to try to maintain lipid homeostasis under the stress conditions. In the first instance, a direct measurement of lipid molecules e.g. by Nile red staining (Greenspan et al., 1985) or LD540 dye (Spandl et al., 2009) might be considered.

6.2 Validation of HIF DNA-binding sites

Having established the critical role of the canonical HIF DNA-binding heterodimer in regulating hypoxic gene expression in the WT cells, it was then pertinent to focus directly on canonical HIF binding sites in the genome and access their occupancy in response to both different conditions of hypoxia (severity and duration) and to renal cancer relevant gene knockouts.

In order to generate a set of high confidence HIF canonical sites, I aimed to improve on the existing methods for identification of sites i.e. rather than using 'input' (i.e. genomic DNA without any immunoprecipitation), or mock IgG as controls to perform peak calling, I have used HIF ChIP-seq data generated from HIF-α DKO or HIF-1β KO cells. This approach should reduce false positive sites generated from experimental noise, such as cross-reactivity of the HIF antibodies, as well as stochastic amplification of genomic DNA. In addition, only sites with both HIF-1α (or HIF-2α) and

HIF-1β binding were considered as canonical. It was considered that this would help to filter out the erroneously identified peaks e.g. due to imperfections in the peak calling algorithm.

A number of approaches were then taken to ensure the quality of the input data (i.e. canonical HIF binding sites) by reference to expected (previously known) characteristics:

(1) Association with HIF target gene expression

First of all, in order to confirm the functional relevance of the canonical HIF binding sites, their nearest neighbour genes were compared with RNA-seq data from the WT cells that were cultured in normoxia versus 0.5% O_2 for 24h (this RNA-seq data pre-existed in the laboratory). In the gene set enrichment analyses (GSEA), canonical HIF-1β sites that appeared at each hypoxia time-point displayed a significant correlation with the genes that were up-regulated by hypoxia in the RNA-seq data (**Figure 1**). These findings confirmed that the high stringency canonical HIF binding sites defined in this study are indeed functionally correlated with hypoxia regulated gene expression.

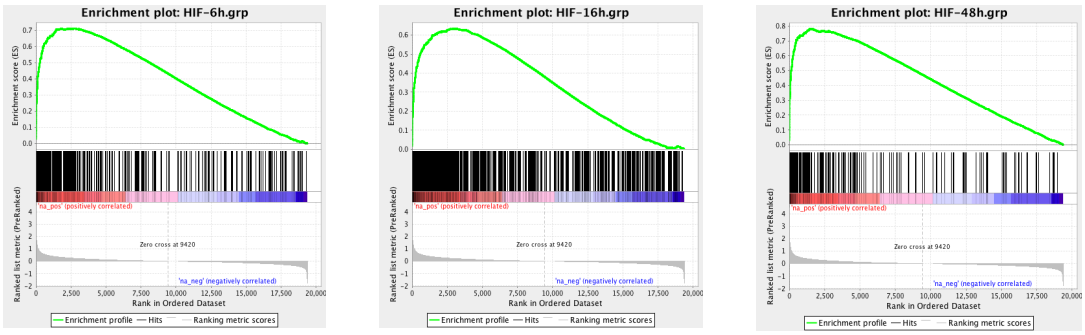

Figure 1. GSEA analysis comparing the nearest neighbour genes for the canonical HIF-1β binding sites defined in HKC-8 cells by ChIP-seq at each hypoxia time-point (i.e. 6h, 16h and 48h) with the hypoxic gene expression data (0.5% O_2 24h) from an RNA-seq study. Genes from the RNA-seq dataset were ranked according to their fold regulation by hypoxia (x-axis, red indicates up-regulation and blue indicates down-regulation. Canonical HIF-1β binding sites were annotated to the nearest genes. The cumulative enrichment score and the position of the ChIP-seq annotated genes among the genes ranked by their fold regulation in the RNA-seq dataset are shown. At each hypoxia condition, the ChIP-seq annotated genes clustered significantly with hypoxia up-regulated genes (*p* value=0 in each case).

(2) Differential distribution of HIF-α binding sites with regard to the TSS

Secondly, HIF-1α and HIF-2α displayed highly distinct binding patterns with regard to their distribution relative to the TSS. Consistent with the published data (Schödel et al., 2013; Salama et al., 2015), HIF-1α binding in HKC-8 cells is predominantly proximal to promoters, whereas HIF-2α binds to promoter-distal sites.

(3) The most enriched motifs within the HIF-α binding sites

Thirdly, close inspection of the HIF-α canonical sites identified at different time-points of hypoxia has revealed that HREs are the most enriched motifs within either HIF-1α or HIF-2α binding sites.

It was noted that the total read counts at canonical sites were similar for HIF-1α and HIF-1β, but this was not the case for HIF-2α and HIF-1β. This could be related to the relative ChIP-seq efficiencies of the HIF-1α versus the HIF-2α antibody. The HIF-1α antibody (PM14) was raised against residues 445-553 of mouse HIF-1α, while the HIF-2α antibody was raised against residues 357-439 of the mouse HIF-2α sequence (Lau et al. 2007). Additional experiments with independent ChIP-seq antibodies (raised against different HIF-1α and HIF-2α epitopes) would help to clarify this.

6.3 HIF DNA-binding in response to graded and timed hypoxia

Having validated the quality of canonical HIF binding sites, I then examined the HIF binding pattern in response to various hypoxia stimuli. Overall, the analyses showed a similar behaviour of HIF DNA-binding in respect of both graded and timed hypoxia across the genome.

Importantly, for both HIF-α isoforms, the binding signal at any one site was proportional to the total binding for that HIF protein. However, this deviated somewhat from measurement of the total quantity of HIF-α protein (at least in respect of time,

where HIF-α levels by IB were apparently higher at 6 hours than 16 hours). Although this suggests the possibility of other processing events occurring within that time interval, the data revealed that heterodimeric binding of HIF-α/β to DNA increases in a broadly similar manner across all sites in the genome as the DNA-binding complex is induced.

Specifically, I did not see evidence for redistribution of HIF binding within the time course or severity in hypoxia that was studied, despite substantial differences in the level of HIF induction. In addition, I did not see much evidence for saturation at those sites, which bound HIF strongly under weakly inducing conditions i.e. only very limited evidence for site-specific differential responses (i.e. sites being more or less loaded at 3% in relation to loading at 0.5% oxygen) were obtained.

6.3.1 Characteristics of HIF binding sites

Following analysis designed to investigate any sub-threshold signal, groups of progressive loading and early saturated sites were identified. Closer inspection of the sites showed that a small increase in the number of HREs was observed in those sites that were progressively loaded as the hypoxia severity increased. However, for both HIF-α isoforms, there was no difference in the contiguous sequences immediately flanking the core HRE motifs between the progressive loading and early-saturated sites, or between high and low affinity binding sites. This suggests that the binding properties of a particular site are not governed by the core consensus, but that there are intrinsic properties of a particular site, at least within that cellular context.

Previous work from the laboratory has highlighted differences in TF motifs in the vicinity of HIF-1α versus HIF-2α sites in RCC cell lines (**Figure 2**) (The figure was generated by other members of the laboratory). However, it is not clear whether/how these are causally related to isoform specific binding. Even though the current analyses identify HRE as the most enriched motif in the HIF-1α or HIF-2α binding sites in any

condition tested, nevertheless, it does not rule out the possibility that HIF may interact with cooperative partners, which then dictate the distinct HIF-1α versus HIF-2α binding patterns. A recently developed technique termed RIME (Rapid Immunoprecipitation Mass spectrometry of Endogenous proteins) may help to elucidate this question (Mohammed et al., 2013; Ji et al., 2014). In this technique, the protein complex is cross-linked on the chromatin, followed by digestion and subsequent mass spectrometry. Therefore, it can be considered to identify the interactome of DNA-bound HIF.

HIF-1 sites **HIF-2 sites**

Motif	Transcription factor	Database ID	Adjusted *p*-value	Motif	Transcription factor	Database ID	Adjusted *p*-value
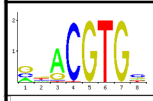	ARNT::HIF1A	MA0259.1	2.22E-45	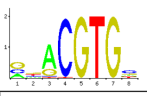	ARNT::HIF1A	MA0259.1	8.31E-26
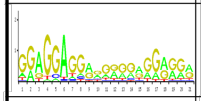	ZNF263	MA0528.1	2.85E-17	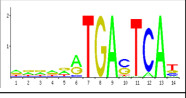	JUN(var.2)	MA0489.1	1.18E-08
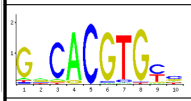	HEY2	MA0649.1	3.94E-17	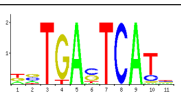	FOS	MA0476.1	6.29E-08
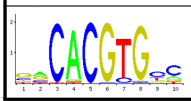	HEY1	MA0823.1	1.58E-14	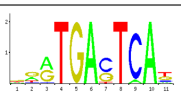	JUNB	MA0490.1	1.33E-07

Figure 2. Motif analysis of HIF-1α (or HIF-2α) binding sites in RCC4 cells. Peak summits were determined for each binding site and a 150bp window was subsequently generated around the summit coordinates. The sequences were then tested for enriched motifs using the JASPAR (2016) vertebrate library of known TF binding motifs. The top 4 motifs were listed, along with their JASPAR Database ID and adjusted *p*-value.

6.3.2 Physiological significance of HIF binding sites

As well as no difference in the consensus motifs, I was also unable to describe a difference in gene ontogeny based on the characteristics that I defined (either progressively loading versus early-saturated loading, or high versus low affinity binding sites, or sites that were defined at different hypoxia time points). It has been reported that genes induced at different time points of hypoxia are associated with different functions

(Mimura et al., 2012). However, this is not reflected in the HIF binding sites in this study. This suggests that the functional associations between HIF binding sites and the abundance of HIF target genes mRNA transcripts (if they exist) might not be mediated through HIF DNA binding.

There are other mechanisms by which physiologically distinct responses to hypoxia might be generated. Firstly, hypoxia induces global changes in modulation of translation, microRNA networks, and altered chromatin structure, asides from transcriptional activation. Due to the high complexity of the HIF transcriptional programme under hypoxia, many regulated transcripts may be secondary (or tertiary) effects that are independent of direct HIF DNA-binding control. Thus, any analysis would be limited by our ability to distinguish the genes that are directly regulated by HIF. Secondly, hypoxia may also affect the abundance of mRNA transcripts via regulating their stability (reviewed in Gorospe et al., 2011). As a result of that, the amount of mRNA present in cells may not always reflect the transcriptional changes. Techniques to identify nascent RNAs would better suit this purpose (Lopes et al., 2017; Gardini. 2017). Last but not the least, within the same population the majority of cells are 'non-equivalent' to each other, i.e. they exhibit cellular heterogeneity (reviewed in Lewis and Wolpert. 1976). As a result, the expression patterns of genes and the TF binding patterns may vary greatly between virtually every cell (even if they are the same cell type). This complexity cannot be captured with genome-wide analyses such as RNA-seq or ChIP-seq.

Nevertheless, differential activation of specific classes of HIF target genes might be obtained *in vivo*, where much more complex principles such as differential sensitivity of genes to transcriptional activation or (more likely) differential activation of HIF in different tissues or cell types, might arise from the pharmacokinetic properties of an agent

designed to activate or inactivate HIF. These considerations will likely be important in understanding the integrated physiology of the HIF responsive and/or pharmaceutical targeting of the HIF response (but are more complex to address experimentally).

6.3.3 Inferences on the kinetics of HIF binding sites

The behaviour during graded and timed hypoxia suggests that HIF-1α and HIF-2α behave largely independently. This was confirmed by other work in the laboratory, where HIF binding profiles were analysed in HIF-1α or HIF-2α single knockout cells (**Figure 3**) (The figure was generated by other members of the laboratory). The result revealed that ablation of one HIF-α isoform did not affect the binding distribution of the other.

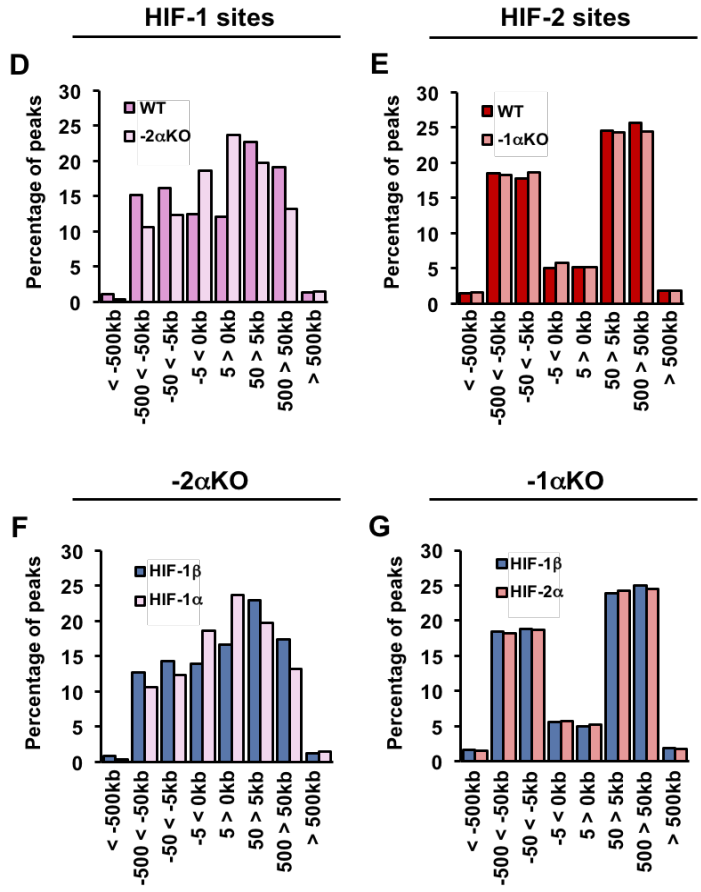

Figure 3. Assessment of the re-distribution of HIF binding sites in HKC-8 mutant cells relative to WT cells. Histograms showing the proportions of HIF-1α (or HIF-2α and HIF-1β) peak summits at canonical HIF-1α or HIF-2α sites in HKC-8 WT or HIF-α mutant cells, falling within the defined regions based on the distance from the TSS of the nearest gene.

Nevertheless, the binding dynamics at a given site was not measured in this study. Differences in binding profiles as assayed by ChIP-seq presumably reflect differences in duration of binding and hence differences in the number of cells binding at any one time. It is known that TFs exchange rapidly between bound and unbound states, with residence times on functional recognition sites often being only a few or tens of seconds (reviewed in Mueller et al., 2013; Hager et al., 2009; Bosisio et al., 2006; Karpova et al., 2008; Klokk et al., 2007). Thus, even though the DNA-binding profiles as shown by conventional ChIP-seq experiments can be identical, the underlying TF-DNA interactions may be quite different. Interestingly, a recent study suggests that the TF residence time

on the DNA, rather than occupancy itself, plays a key role in determining the functional consequences (Lickwar et al., 2012). Therefore, it is possible that the kinetics of HIF binding may respond differently to stimuli. Such transient binding can be detected by fluorescence microscopy approaches such as fluorescence recovery after photobleaching (FRAP) (van Royen et al., 2009), fluorescence correlation spectroscopy (FCS) (Zhao et al., 2017) and single molecule tracking (SMT) (Gebhardt et al., 2013). However, the throughput of these assays is low.

The apparently independent behaviour of HIF binding sites (i.e. similar characteristics under different oxygen concentrations and hypoxia durations; lack of evidence for saturation; lack of cross competition between HIF-1α and HIF-2α isoforms) suggests that the number of potential sites might be high in relation to the overall copy number of HIF heterodimers. It has been proposed that animal TFs are expressed at high abundance, typically at 10,000 to 300,000 molecules in a single cell (reviewed in Biggin. 2011). One study measured the ARNT protein level by immunoblot across 11 murine cell lines, and estimated that the concentrations of ARNT ranged between 14,000 and 33,000 molecules/cell (Holmes, JL and Pollenz, RS. 1997). The absolute copy number of HIF-α protein has not yet been fully characterised. Fluorescence intensity based assays, or newly emerged techniques such as SRM and high-resolution mass spectrometry and others (as mentioned in Chapter 3 Discussion) may be applied in order to accurately quantify the number of HIF protein molecules and to correlate this with the DNA-binding profile.

6.4 HIF DNA-binding in response to loss of VHL/PBRM1 (BAF180) /FIH proteins

Even though loss of function of these key tumour suppressor or potential oncogenic proteins has been reported to affect the HIF transcriptional programme, in this study little evidence suggests that this was through regulation of HIF DNA-binding (at least in HKC-8 cells).

Overall, HIF binding sites that were defined under hypoxia condition in the WT cells are essentially the same, with only minor differences in the read counts from those defined in the *VHL* mutant background where the HIF pathway is constitutively active. It has been reported that *VHL* inactivation and hypoxia result in different gene expression profiles in RCC cell lines (Leisz et al., 2015). The present study suggests this may not be through a direct regulation of HIF DNA-binding. This result also supports the findings from other work that is published by the laboratory, which showed that HIF acts mainly upon pre-existing chromatin-chromatin structures and that this is not affected by hypoxia or prolonged pVHL inactivation (Platt et al., 2016). However, a recent study showed that renal tubule cells and RCC tumours displayed different chromatin landscape, and loss of pVHL appeared to induce tumour-specific gains of histone binding at the enhancers of certain RCC hallmark genes (Yao et al., 2017). Nevertheless, it was not clear how those findings to the binding of HIF at different sites as a result of *VHL* inactivation as opposed to other differences between renal tubular and renal carcinoma cells. The present study is based on HKC-8 cells, therefore it is also possible that this may be a non-representative cellular model, and that HIF DNA-binding responds differently in other cellular settings. Therefore, it will be interesting to test whether this quantitatively continuous HIF binding profile is observed in other normal or transformed cell lines.

The effects of *PBRM1* (BAF180 protein) loss on HIF and its target gene expression have also been reported but appear to be inconsistent across different studies (Wang et al., 2017; Gao et al., 2016; Chowdhury et al., 2016). In this study, no discernable effects on total HIF protein levels was observed in the HKC-8 cells when *PBRM1* was inactivated, and the HIF DNA-binding profile remains unchanged. This result suggests that the effects of *PBRM1* on HIF target gene expression, if genuine, act through other mechanisms rather than altering the HIF binding distribution. Again, this could be a cell-line specific phenomenon, since the published studies mainly focused on RCC cell lines. Further studies, and potentially in other cell lines, are needed in order to dissect the potential mechanisms.

Similarly, the effect of the FIH protein on HIF target gene expression has been well-known through its regulation of the interaction between HIF and the histone modifiers CBP/p300, which possess acetyl-transferase activity and subsequently may alter the local chromatin structure. FIH may also interact with other co-factors, such as the transcriptional co-repressor SMRT, which represses basal transcription by recruiting histone deacetylase HDAC1 via the adaptor mSin3A (Kau et al., 2000) or directly with epigenetic modifiers such as the histone lysine methyltransferases G9a and GLP (Kang et al., 2018). However, our current study indicates that the effects of FIH on HIF target gene expression is unlikely to be due to any alteration of HIF DNA-binding profile.

In conclusion, this study demonstrates that the canonical HIF pathway plays a vital role in hypoxia-dependent gene expression. Despite widespread reports of alternative substrates and signalling pathways, the present study finds no evidence of any HIF-independent contribution for the PHD's or for other TF's to gene expression in hypoxia, at least under the conditions examined. Analyses of pan-genomic HIF DNA-

binding profiles in response to both physiologically relevant hypoxic stimuli (i.e. varying severities and durations of hypoxia), and to inactivation of genes linked to HIF pathway dysregulation in cancer, suggest that canonical HIF binding occurs continuously at the same sites (pre-determined by the underling cell type). The test conditions examined are only able to affect the magnitude of the binding rather than qualitatively generating new binding sites.

7

Materials and Methods

7.1 Cell lines

HKC-8 cells were kindly provided by L. Racusen (Baltimore, USA) (Racusen et al 1997). The wild-type parental cells used for this study were thawed from the cryostore collection of the laboratory.

All HKC-8 mutant sub-lines were generated by using CRISPR/Cas9 double nickase genome-editing technique. The HIF-1α/2α double knockout cells, VHL knockout cells, PBRM1 knockout cells, PBRM1VHL knockout cells and VHLFIH knockout cells already existed in the laboratory at the time of this study. The HIF-1β knockout cell line was generated as part of this thesis.

HEK293T cells were purchased European Collection of Authenticated Cell Cultures (ECACC) and were thawed from the cryo-stock collection from the laboratory.

7.2 Generation of HIF-1β knockout cells by CRISPR/Cas9 technique

7.2.1 The construction of single-guide RNA (sgRNA) expression vectors

A pair of guide RNAs was designed according to the algorithms provided by the Zhang lab (http://crispr.mit.edu/). Guide 1 corresponded to a 24-bp sequence (5'- CACCGCTCCTCCACCTTGAATTCC - 3') and guide 2 corresponded to a 25-bp sequence (5'- CACCGAGGGCTATTAAGCGGCGACC - 3') in the second exon of the *ARNT* (HIF-1β) gene.

Two complementary oligonucleotides representing each of these guide sequences and designed to create BbsI overhangs were generated (5'- AAACGGAATTCAAGGTGGAGGAGC-3' and 5'- AAACGGTCGCCGCTTAATAG CCCTC) and annealed by heating a 100 µM stock solution at 95°C for 5 min followed by cooling to room temperature. The oligonucleotides were then diluted 1:25 in water.

The annealed guide 1 oligonucleotides were ligated into the pX461 vector, and guide 2 oligonucleotides were ligated into the pX462 vector (**Figure M1**) using restriction enzyme BbsI (NEB, U.K.) (**Figure M2**).

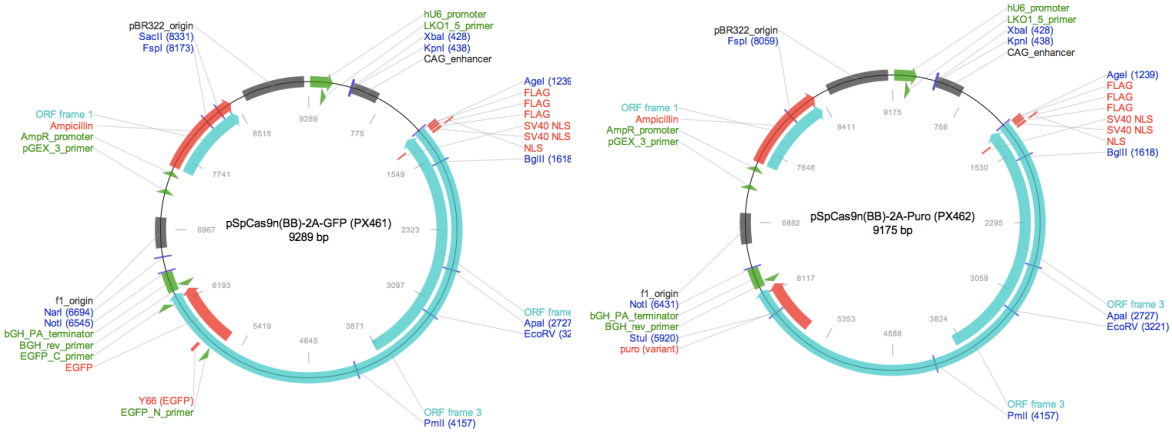

Figure M1: vector maps of the pX461 and pX462. Download from: https://www.addgene.org/crispr/nick/

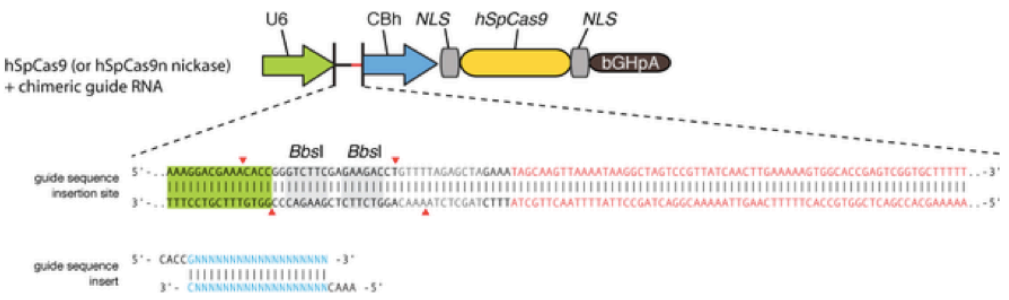

Figure M2: Each vector contains two expression cassettes, a human codon-optimised SpCas9n and the sgRNA. The vector can be digested using BbsI. Download from: https://www.addgene.org/crispr/zhang/

The vectors were cleaved in a 1.7 ml tube at 37°C for 90 min using the following protocol, and then purified using a PCR purification kit (Qiagen, U.K.).

Vector cleavage:

	Volume
BbsI	1 µl
10x NEB2 buffer	3 µl
Vector	3 µg
H_2O	
Total	30 µl

The ligation of the DNA fragments was performed in a 1.5ml tube using Quick Ligase (NEB, U.K.). The reagents are listed below:

Ligation	**Stock**	**Volume (µl)**
Ligation Reaction Buffer	10x	1.2
Quick Ligase	10 µM	1
H_2O		7.8
Vector DNA		1
Annealed insert DNA		1
Total		12

7.2.2 Transformation and isolation of the constructs

The ligation mixture was then transformed into chemically competent DH5α cells.

1. Cells were thawed on ice.
2. 7 µl ligation products was mixed with 100 µl cell suspension in a 1.5 ml tube.
3. The mixtures were kept on ice for 30 min followed by a 37°C heatshock for 3 min in a water bath.

4. 1 ml of LB was added and the mixtures were incubated at 37°C in a shaking incubator (200 rpm) for 1h.
5. Cells were pelleted by centrifuging at 2000 rpm for 5 min. 900 µl of the supernatant was removed. In general, centrifugations of 1.5 ml tubes were performed using an Eppendorf™ benchtop microcentrifuge (Model 5415R, Radius 83 mm).
6. Cells were resuspended in the remaining volume, plated onto LB agarose plates containing ampicillin (0.1 mg/ml) and grown overnight at 37°C.
7. Control ligations containing vector alone were prepared in parallel to estimate the background growth.
8. Colonies were picked from the agarose plates and transferred into 5 ml of LB medium containing ampicillin (0.1 mg/ml) in 30 ml universal centrifuge tubes for overnight growth at 37°C in a shaking incubator (200 rpm).
9. Cells were collected by centrifugation at 3750 rpm at 4°C for 10 min in a centrifuge (Beckman Coulter, Allegro X-12R, Rotor SX-4750).
10. Plasmid was then isolated by miniprep kit (Qiagen, U.K.) following manufacturer's instructions.

After the purification of plasmid DNA, minipreps were screened by restriction digest and the sequence of positive clones was verified by DNA sequencing performed by SourceBioscience, Oxford.

7.2.3 Testing efficiency of sgRNA's to introduce mutations

The efficiency of CRISPR/Cas9 sgRNAs activity was detected using a SURVEYOR® Mutation Detection Kit, which relies on Cel-1 nuclease to recognise and cleave both strands of DNA mismatches (i.e. heteroduplex DNA resulting from combination of wild-type and mutant sequences).

1. HEK293T cells in 6-well dishes were cultured to 50-60% confluence.
2. Cells were transfected with 2 µg *ARNT* sgRNA plasmid (i.e. 1 µg each of pX461 and pX462 plasmid) using polyethylenimine (PEI) reagent (100 mg/ml) following the protocol below.
3. 48h post-transfection, the cells were harvested and genomic DNA was extracted using the QuickExtract DNA extraction kit (Qiagen, U.K.). Genomic DNA was also harvested from the wild type cells, which were used as controls.
4. The Surveyor Assay was performed according to the manufacturer's protocol using the reagents listed below. Heteroduplex was formed in the PTC-200 PCT machine, using two steps: 95°C for 5 min, then 25°C for 60 min. Nuclease digestion was performed at 42°C for 60 min.
5. The products were run on a 2% agarose gel, which was then imaged using the BioRad ChemiDoc Imaging System.
6. Guides that successfully generated insertions/deletions were selected and transfected into the target HKC-8 cells.

Transfection protocol with PEI:

	Volume
DMEM	1 ml
PEI	16 µl
DNA	2 µg (i.e. 1 µg per sgRNA)

DNA-PEI complexes were then added directly to the cell culture medium.

Surveyor Assay – heteroduplex formation:

	Volume
Purified PCR product	450 ng
H_2O	
10x PFU buffer with Mg^{2+}	1.2 µl
Total	12 µl

Surveyor Assay – nuclease digestion:

	Volume (µl)
Heteroduplex DNA	12
150 mM $MgCl_2$	1.5
Enhancer	1
Surveyor Nuclease	1.5
Total	16

7.2.4 Transfection of target HKC-8 cells and cell sorting

HKC-8 parental cells were cultured in 6-well dishes to 70-80% confluence. Cells were transfected with 2 µg of each ARNT sgRNA plasmid (i.e. 1 µg each of pX461 and pX462 plasmid) using GeneJuice® transfection reagent (EMD Chemicals Inc, U.S.A.) and following manufacturer's instructions.

24h post-transfection, pX461-derived enhanced green fluorescent protein (eGFP) was used as a fluorescent marker to sort transfected cells. GFP-expressing cells were isolated by FACS (Fluorescence-activated cell sorting), and were then plated at limiting dilution to obtain individual clones.

7.2.5 Screening for HIF-1β knockout in HKC-8 clones

Genomic DNA of single-cell derived clones was isolated with QuickExtract DNA extraction kit (Qiagen, U.K.). The exon 2 region of the *ARNT* gene (encompassing the sgRNA-targeted region) was then amplified by genomic PCR using the following primers (Forward 5'- TGAGCATTTGGGATTTTTAGCAA- 3'; Reverse 5'- TGGTCAGGAATAGCGAAGTGAG– 3'). Products were resolved by agarose gel electrophoresis and imaged. The genomic PCR products were then purified using a PCR purification kit (Qiagen, U.K.) with elution in 50 µl H_2O.

The genomic PCR products were then sequenced to determine the exact mutation at each locus. Where mixed-sequence was obtained from the genomic PCR product, the genomic PCR product was cloned into a pcDNA3 vector (**Figure M3**),

transformed into *E.coli*, and DNA isolated from individual minipreps (10 in total) for sequencing (method below).

1. Restriction digest of the vector and the genomic PCR insert using the enzymes: EcoR1 F and Xba1 R, and was performed at 37°C for 2h.
2. 1 Unit of Alkaline Phosphatase was added to the vector digest, followed by incubation at 37°C for 25 min. The sample was run on a 1% gel and purified and eluted in 30 µl water.
3. The genomic PCR digests were purified from solution using PCR purification kit, and eluted in 30 µl water.
4. Ligation was performed using the reagents listed below, and the samples were incubated at room temperature for 2h. A vector alone sample was performed in parallel and used as a negative control.
5. The mixture was then transformed into 100 µl competent cells DH5α cells.
6. DNA was extracted from each colony and purified using Pasmid Miniprep kit (Qiagen, U.K.).
7. The cloned genomic PCR products were then subjected to sequencing performed by SourceBioscience, Oxford.

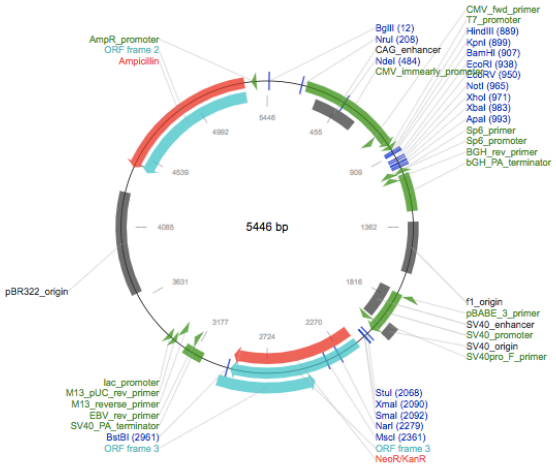

Figure M3: vector maps of the pcDNA3. Download from: https://www.addgene.org/vector-database/2092/

Restriction digest of the vector:

	Volume (µl)
pcDNA3 vector	2
EcoR1	1
Xba1	1
10x buffer 2	3
10x BSA (1 mg/ml)	3
H_2O	20
Total	30

Restriction digest of the insert:

	Volume (µl)
PCR product	50
EcoR1	2
Xba1	2
10x buffer 2	8
10x BSA (1 mg/ml)	8
H_2O	10
Total	80

Ligation:

	Volume (µl)
pcDNA3 vector	1
Insert	6
10x Ligase Reaction mix	1.5
T4 DNA ligase	0.75
H_2O	5.75
Total	15

7.3 Cell culture

HKC-8 wild type and mutant cell lines and HEK293T cells were grown in Dulbecco's modified Eagle's Medium, 100 U/ml penicillin and 100 µg /ml streptomycin and 10% fetal bovine serum (Sigma, U.K.) at 37°C, 5% CO_2 in a cell culture incubator. All experiments with reduced oxygen concentrations were conducted in a Ruskin Invivo2400 workstation equipped with a Gas Mixer Q (5% CO_2, 70% humidity).

7.4 DNA techniques

7.4.1 Isolation of DNA

Genomic DNA was prepared using DNA Extraction kit (Qiagen, U.K.), and plasmid DNA was purified using Plasmid Miniprep and Midiprep kits (Qiagen, U.K.), according to the manufacturer's protocol.

7.4.2 Quantification of DNA concentration

DNA concentrations were measured by NanoDrop ND-1000 spectrophotometer (Thermo Scientific, U.K.). The DNA absorbance was measured at 260nm, and was considered as pure at absorbance ratios 260/280 higher than 1.8.

7.4.3 DNA amplification by polymerase chain reaction (PCR)

PCR was performed using a PTC-200 thermal cycler (MJ Research, U.K.).

PCR reactions used the Phusion® High-Fidelity PCR Kit (NEB, U.K.).

Reagents	Stock	Volume (µl)
2x Phusion Mix		10
DMSO		0.6
Nuclease-free H_2O		6.4
Primer	5 µM	2
Genomic DNA	100 ng/ µl	1
Total		20

Typical PCR cycle conditions:

Step	Temperature (°C)	Time	Cycles
1	95	3 min	1
2	95	30 sec	30
	58	30 sec	
	72	1 min	
3	72	5 min	1
4	4		

7.4.4 Gel Electrophoresis

1-2% agarose gels were prepared by melting agarose in TRIS/Borate/EDTA (TBE) solution. 4 µl Ethidium bromide (10 mg/ml) was added to the mixture and the gel was

cast. DNA samples were mixed with 6x DNA Gel Loading Dye (Thermo scientific, U.K.) and electrophoresis was performed using a Biorad gel electrophoresis chamber (Biorad, U.K.) at 110V for 30 min. Bands were imaged by using the BioRad ChemiDoc Imaging System, and the size was compared to DNA marker (GeneRuler 1 kb ladder, Thermo scientific, U.K.). Bands of interest were excised under ultraviolet light.

7.4.5 Purification of DNA

PCR products or digested vectors were purified using the Qiagen PCR purification kit (Qiagen, U.K.) according to manufacturer's instructions.

7.5 Luciferase reporter assay

7.5.1 Reporter plasmids

The following reporter plasmids were used for the reporter assay in this study.

1. pGL3-basic control vector with a minimal SV40 promoter (**Figure M4**)
2. CA9-promoter luciferase vector was used in Wykoff et al., 2000. In this vector, a CA9 promoter sequence with ends corresponding to the 5' restriction cleavage sites of *Bgl*II and *Mlu*I was ligated into *Bgl*II/*Mlu*I-digested pGL3-basic vector. The HRE sequence corresponds to 5'-CGCGCTCCCCCACCC AGCTCTCGTTTCCAATGCACGTACAGCCCGTACACACCG-3'.
3. PGK luciferase vector (pGL3PGK6TKpLUC) was used in Vaux et al., 2001. In brief, the vector contained an optimised HRE enhancer/promoter (PGK6TKp) that consists of six copies of a 24-nt sequence of the *PGK1* HRE 5'-CGCGTCGTGCAGGACGTGACAAAT-3' linked to a minimal promoter consisting of nucleotides 107–194 from the herpes simplex virus thymidine kinase gene (GenBank™ accession number M80483).

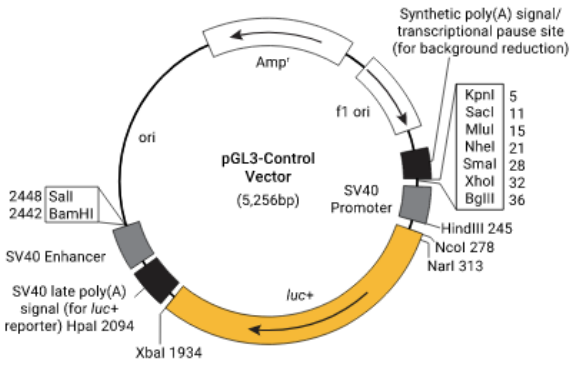

Figure M4: Vector maps of the pGL3-Promoter vector. Downloaded from: http://www.promega.com

7.5.2 Transient expression assays

Reporter assays were performed using the Luciferase Reporter assay (Promega, U.K.) or the Dual-Luciferase Reporter assay (Promega, U.K.) following manufacturer's instructions.

1. HKC-8 wild type cells, HIF-1β KO cells and HIF-α DKO cells were cultured in a 12-well plate.
2. Transfections of plasmids (1 µg total per well) were performed using GeneJuice transfection reagents (EMD Chemicals Inc, U.S.A.) at 30–50% cell density.
3. In addition to the luciferase plasmids, cells were co-transfected with a plasmid expressing β-galactosidase. This enabled luciferase activity to be normalised to the activity of β-galactosidase as an internal control for transfection efficiency.
4. Cells were then incubated at 21% O_2 for 8h, followed by 21% or 0.1% O_2 for 16h.
5. Cells were washed with PBS, lysed in 100 µl Passive lysis buffer (Promega, U.K.), frozen and stored for at least 2h at -80°C.
6. Cells were scraped and the lysed cells were transferred to a 1.7 ml tube.
7. Samples were centrifuged at 14,000 rpm for 5 min and 20 µl of the supernatant was pipetted into one well of a U-bottomed white 96-well plate.

8. 50 µl of Luciferase Assay Substrate (Promega, U.K.) was added to each well, and the firefly luciferase activity was determined using a Luminoskan Ascent luminometer (Labsystems, U.K.).
9. In Dual-Luciferase experiments, renilla luciferase activity was measured in parallel for transfection efficiency normalisation using the provided Stop&Glo® substrate (Promega, U.K.). Firefly luciferase activity readings were then corrected using their respective renilla luciferase activity readings.
10. In experiments where β-galactosidase was used for determining transfection efficiency, β-galactosidase activity was measured using 20 µl cell extract together with 80 µl Assay Buffer (Promega, U.K.) per well of a clear U-bottomed 96-well plate. This was followed by the addition of 20 µl of o-nitro-phenyl-beta-D-galactopyranoside (4 mg/ml) and incubation of the plate at 37°C with shaking at 200 rpm. On the appearance of a yellow colour, reactions were stopped by adding 50 µl NA_2CO_3 (1 M). Absorbance was then measured at 405 nm using a Vmax kinetic microplate reader (Molecular Devices, U.K.). Luciferase activity was corrected for transfection efficiency by dividing the luciferase activity reading by the respective β-galactosidase reading.
11. Single reporter assays were performed on triplicate biological samples and mean values and standard deviation were calculated.

7.6 Cellular fractionation

The protocol was modified from the method in Wysocka et al., 2001 (**Figure M5**).

1. Cells were cultured in 10 cm dishes to 70% confluence.
2. Ice-cold PBS was used to wash the cells twice, and the cells were transferred into a 1.7 ml tube.

3. Cells were centrifuged at 1,000 rpm for 1 min, and the supernatant was removed.
4. The cell pellet was resuspended in 200 µl Buffer A.
5. The sample was incubated on ice for 8 min, and then centrifuged at 3743 rpm for 5 min at 4°C.
6. The supernatant was collected as fraction S1. S1 was then centrifuged at 14,680 rpm for 5 min at 4°C. The supernatant was collected as fraction S2 (cytoplasm).
7. The pellet (nuclei, fraction P1) was washed once with Buffer A, and was lysed in 100 µl Buffer B for 30 min on ice.
8. Sample mixture containing P1 was centrifuged at 4280 rpm for 5 min at 4°C.
9. The supernatant was separated as fraction S3 (nucleoplasm).
10. The pellet was labeled as P3 (chromatin) and was washed once with Buffer B.
11. Fraction P3 was resuspended in 200 µl 1x Sample Buffer, and was heated at 95°C for 10 min.
12. Fraction S2 (cytoplasm) was resuspended in 33 µl 6x Sample Buffer.
13. Fraction S3 (nucleoplasm) was resuspended in a mixture of 67 µl Buffer B and 33 µl 6x Sample Buffer.

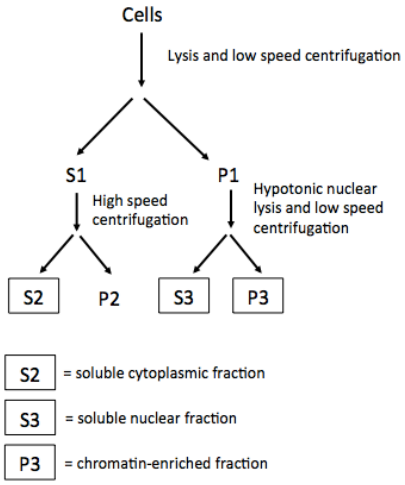

Figure. M5: Schematic of cellular fractionation. Modified from Wysocka et al., 2001.

7.7 Protein techniques

7.7.1 Protein lysates

1. Cells were cultured in either 6 cm or 10 cm dish for protein isolation.
2. Medium was removed and cells were washed twice with PBS, and transferred into 1.7 ml tubes.
3. Cells were pelleted by centrifugation at 2000 rpm for 5 min at 4°C.
4. Supernatant was removed and cells were lysed in 150 µl ILB (Igepal Lysis Buffer) per 6cm plate or 300 µl ILB per 10 cm plate.
5. 6x SDS-PAGE (sodium dodecyl sulphate polyacrylamide gel electrophoresis) buffer was added to the sample mixture.
6. The sample was heated at 95°C for 3 min.

7.7.2 Immunoblotting

SDS-PAGE was used to separate proteins of interest. 8% acrylamide gels and stacking gels were prepared using the reagents listed below.

1. SDS-PAGE was performed in a Mini-Protean apparatus (BioRad, U.K.).
2. Typically 10 µl of sample was loaded per well and a protein ladder – PageRuler (Fermentas, U.K.) was run on the same gel.
3. Electrophoresis was carried out in SDS-PAGE running buffer at a constant voltage of 120V for 1h.
4. Protein was then transferred onto Immobilon-P polyvinylindene fluoride (PVDF) membrane (Milipore, U.K.) using the Mini-Transblot apparatus (BioRad,U.K.). The membrane was pre-activated in 100% methanol for 1 min. Transfer was performed at a constant current of 180 mA for 25 min per gel.
5. Thereafter, the membrane was transferred into 4% milk blocking buffer for 1h.

6. Membrane was then incubated with specific primary antibody (diluted according to the manufacturers instruction in 4% milk blocking buffer) overnight at 4°C.
7. Membrane was then washed three times for 12 min in PBS-T before incubation with HRP (Horseradish peroxidase)-conjugated secondary antibody (anti-mouse IgG or anti-rabbit IgG, diluted 1:2000 in 4% milk blocking buffer, Dako, U.K.) for at least 1h.
8. Membrane was washed three times with PBS-T for 12 min.
9. Immunodetection was performed by visualising the HRP activity using the chemiluminescence reagents Dura (Pierce Biotechnology, U.K.) with detection and signal quantitation carried out using the BioRad ChemiDoc Imaging System.

Acrylamide gel (8%):

	Volume
30% acrylamide	3.2 ml
4x Lower buffer (pH 8.8)	3 ml
Distilled H_2O	5 ml
APS (10%)	120 µl
TEMED	12 µl
Total	11.2 ml

Stacking gel:

	Volume
30% acrylamide	1.3 ml
4x Upper buffer (pH 8.8)	2.5 ml
Distilled H_2O	6.2 ml
APS (10%)	120 µl
TEMED	16 µl
Total	10 ml

7.8 RNA techniques

7.8.1 RNA isolation from cultured cells

RNA isolation used phenol-chloroform based extraction methods (Trizol reagent, Sigma, U.K.).

1. Cells were grown in 6-well dishes to about 80-90% confluence.
2. During the harvest process, cells were washed twice with ice-cold PBS. 0.5 ml of Trizol reagent was added and the cell suspension was pipetted up and down for 5 times before transferring to 1.7 ml tubes.
3. Samples were kept at room temperature for 5 min.
4. 100 µl of chloroform was added to each sample and shaken by hand for 15 sec.
5. Samples were centrifuged at 14,000 rpm for 15 min at 4°C, after which the supernatants were transferred into a fresh 1.5 ml tube.
6. 250 µl of 100% isopropanol was added to each tube and the samples were kept on dry ice until completely frozen.
7. Samples were then centrifuged at 14,000 rpm at 4°C for 15 min.
8. Supernatant was removed and the pellet was washed with 1ml of 75% ethanol.
9. Samples were centrifuged at 14,000 rpm at 4°C for 15 min, supernatant was removed and the RNA pellet was air-dried.
10. RNA was then resuspended in 25 µl of RNase-free water.
11. The concentration and purity was determined by using a NanoDrop analyser (Thermo scientific, U.K.). Samples were kept at -80°C.

7.8.2 Generation of complementary DNA (cDNA)

cDNA was prepared using the High Capacity cDNA kit (Applied Biosystems, U.K.) according to the manufacturer's instructions. 1000 ng of RNA was reverse transcribed in the PTC-2000 Peltier Thermal cycler (MJ Research, U.K.) with reagents listed in the

table. For subsequent RT-PCR experiments, cDNA was diluted 1 in 10 with nuclease-free water.

cDNA reaction mix:

Reagents	Stock	Volume (µl)
10x RT Buffer	10x	2
25x dNTP Mix	100 mM	0.8
10x RT Random Primers	10x	2
MultiScribe® Reverse Transcriptase		1
RNase Inhibitor		1
RNA template	500 ng/µl	1
Nuclease-free H_2O		12.2
Total		20

cDNA reaction conditions:

Step	Temperature (°C)	Time (min)
1	25	10
2	37	120
3	85	5

7.8.3 Real-time quantitative PCR (RT-qPCR) experiment using SyBr Green® assay

Expression and enrichment analyses were performed using SyBr Green® (Applied Biosystems, U.K.). Primers were designed using the publically available web tool (https://www.ncbi.nlm.nih.gov/tools/primer-blast/). The product size was restricted to between 80-bp and 120-bp. Only primers spanning exon-exon junctions were considered in order to avoid amplification of any contaminating genomic DNA. The primer specificity was checked using the *in silico* PCR tool on the UCSC Genome Browser (http://genome.ucsc.edu/cgi-bin/hgPcr?command=start).

The qPCR reaction mixtures are listed in the table, and the experiments were performed using the StepOnePlus Real-Time PCR system (Applied Biosystems, U.K.) using the following settings.

SyBr Green® assay qPCR reaction mixture:

	Source	Stock	Volume (µl)
Fast SyBr Green® PCR buffer	AB	2x	5
Primer mix (Forward and Reverse)	Sigma	10 µM	0.5
H_2O			2.5
cDNA		Diluted 1:10	2

SyBr Green® method

Step	Temp in °C	Time
1	95	20 sec
2	95	3 sec
	60	30 sec
3	95	15 sec
4	60	1 min
5 Melting curve	Increase of +0.3 per step to 95	

7.8.4 Data analysis

Threshold cycles (CT) of the transcript of interest were compared to CT values of the housekeeping transcript *HPRT* (Hypoxanthine Phosphoribosyltransferase). The enrichment levels were calculated as fold change compared to *HPRT* control using delta-delta CT method. CT values higher than 35 cycles were excluded from the analysis. A melting curve analysis was performed to confirm only single products were enriched in the experiment.

7.9 Chromatin immunoprecipitation (ChIP)

7.9.1 ChIP protocol

The protocol was adapted from the method in Schödel et al., 2011.

1. Cells were grown in 15 cm dishes to sub-confluence (50-70%) and were exposed to normoxia (21% O_2), or hypoxia conditions. Oxygen concentrations and incubation times varied according to experiment conditions.
2. Cells were cross-linked with 1% formaldehyde (Sigma,U.K.) for 12 min on ice.

3. Cross-linking was stopped by adding freshly prepared 1M glycine solution to a final concentration of 125 mM for an additional 5 min on a rotator at room temperature.
4. Cells were then washed twice with ice-cold PBS, scraped in PBS and transferred into a 15 ml falcon tube.
5. Cells were pelleted at 500 rpm (Beckman Coulter centrifuge, Rotor SX-4750) for 10 min at 4°C. Supernatant was removed. The pellet was lysed in ChIP lysis buffer for 10 min on ice.
6. The cell lysate was transferred into a 15 ml tube (TPX tubes, Diagenode, U.K.) and sonicated using a water bath sonicator (Bioruptor, Diagenode, U.K.) filled with iced water for 4x4 min in pulses of 15 sec on and 15 sec off.
7. The lysate was transferred into a 1.5 ml tube and centrifuged at 13,000 rpm for 1 min to remove the cell debris.
8. The sonicated chromatin was then transferred into a 50 ml falcon tube and diluted 10 times with ChIP dilution buffer.
9. 120 µl of 50% Protein A agarose beads (Millipore, U.K.) slurry was added to the diluted chromatin for pre-clearing at 4°C for 1h on an end-over-end rotator.
10. Samples were centrifuged at 1000 rpm for 5 min at 4°C to remove the agarose beads.
11. 100 µl of the diluted chromatin was saved as input sample.
12. The rest of the diluted chromatin was aliquoted into 15 ml falcon tubes.
13. Antibodies were then added to the chromatin for immunoprecipitation overnight. 10 µl of in-house antibodies were used per ChIP (PM14 for HIF-1α; PM9 for HIF-2α). 15 µl was used for HIF-1β. During assays intended for ChIP-qPCR, rabbit serum was used for a negative control ChIP.

14. Samples were incubated overnight at 4°C on an end-over-end rotator.
15. 60 µl of 50% Protein A agarose beads slurry was added to each sample and the mixture was rotated for 3h at 4°C.
16. Thereafter the samples were centrifuged at 2000 rpm at 4°C for 10 min and supernatant was removed.
17. The beads were transferred into a 1.7 ml tube and washed with 1 ml of ice-cold low salt washing buffer by incubation on an rotator for 5 min at 4°C, followed by centrifugation at 2000 rpm for 1 min.
18. The samples were then washed with ice-cold high salt buffer then LiCl and TE buffer (twice) with exactly the same method.
19. After the last wash with TE buffer, the sample was centrifuged for 5 min, and supernatant was carefully removed.
20. Chromatin was eluted from the beads with 250 µl elution buffer by rotating on an end-to-end rotator at room temperature for 15 min.
21. Samples were centrifuged at 12000 rpm for 1 min, and the supernatant was transferred into a fresh 1.7 ml tube.
22. A further 250 µl elution buffer was added to the beads and the elution step was repeated.
23. 20 µl 5M NaCl and 2 µl Proteinase K (20 mg/ml, Roche, U.K.) was added to the 500 µl sample, and to the 100 µl input sample, which was diluted with 400 µl elution buffer.
24. Samples were incubated at 65°C overnight in an Eppendorf ThermoMixer F1.5 (Fisher Scientific, U.K.) at 1400 rpm to de-crosslink the chromatin.

25. The next day, samples were transferred into fresh 1.7 ml tubes and DNA was purified with the purification kit (Qiagen, U.K.) according to manufacture's protocol.
26. ChIP DNA samples were eluted with 30 µl nuclease-free water.
27. Aliquots of the DNA were further diluted 1 in 10 in nuclease-free water for ChIP qPCR analysis. Reagents and experimental conditions are listed below in **7.9.2.2**.
28. HIF binding enrichment levels were calculated using the delta-delta CT method. CT values were normalised to the internal negative control region (gamma actin) and related to the values from the negative control antiserum (pre-immune).

7.9.2 ChIP quality control

The quality of each ChIP sample was confirmed by measuring the average DNA fragment size and the enrichment of HIF binding at control HRE loci.

7.9.2.1 Confirmation of the DNA fragment size

ChIP DNA fragment size was verified by using the Agilent High Sensitivity D1000 ScreenTape kit and the 2200 TapeStation (Agilent Technologies). The average fragment size was between 250-300 bp.

1. All reagents and tape were equilibrated at room temperature for 30 min.
2. 3 µl D1000 sample buffer was added to 1 µl ChIP DNA sample and to 1 µl D1000 ladder.
3. The mixture was vortexed using the IKA vortexer and adaptor at 2000rpm for 1 min.
4. Samples were centrifuged and loaded into the 2200 TapeStation.

7.9.2.2 Confirmation of enrichment by ChIP qPCR

Enrichment of HIF binding at control HRE loci was confirmed by SyBr Green® based real-time qPCR using the StepOne thermocycler (Applied Bioscience, U.K.).

SyBr Green® assay ChIP qPCR reaction mixture

	Source	Stock	Volume (µl)
Fast SyBr Green® PCR buffer	AB	2x	5
Primer mix (Forward and Reverse)	Sigma	10 µM	0.5
H_2O			3.5
cDNA		Diluted 1:10	1
Total			10

The ChIP qPCR reaction conditions are described in **7.8.3**.

Usually the *NDRG1* and *EGLN3* HREs served as positive controls. The enrichment levels were calculated as fold change compared to the gamma actin negative control sequence using the delta-delta CT method. CT values higher than 35 cycles were excluded from the analysis.

In general, an enrichment of 5-fold or greater over the respective region in the control IgG ChIP was considered as appropriate for submission of samples for ChIP-seq.

7.9.3 High throughput sequencing of ChIP samples (ChIP-seq)

ChIP-seq was performed by the Core Genomic Facility at the Wellcome Trust Centre for Human Genetics (University of Oxford, U.K.). An aliquot of 20 µl of captured DNA fragments was submitted to the sequencing facility.

Libraries for sequencing were prepared using the Illumina ChIP-seq kit. 50 bp single end sequencing was performed on the platform. Sequences were mapped to the reference human genome (hg19).

7.10 Bioinformatic analysis of ChIP-seq data

ChIP-seq analysis pipelines were developed by Dr. Rafik Salama. The full method can be found in Salama et al., 2015. An outline of method is shown below.

7.10.1 Initial analysis

1. Adaptor sequences were trimmed using Trimgalore (0.3.3) and reads were aligned to the reference genome (hg19) using BWA (0.7.5a-r405).
2. Low quality mapping was removed (MapQ<15) using SAMtools (0.1.19). Reads mapping to Duke Encode black list regions (http://hgwdev.cse.ucsc.edu/cgi-bin/ hgFileUi?db = hg19&g = wgEncodeMapability) were excluded using BEDTools (2.17.0).
3. Duplicate reads were marked for exclusion using Picard tools (1.106) (http://picard. sourceforge.net/).
4. Read densities were normalised for sequencing depth and fragment length, and were expressed as RPKM (reads per kilobase per million mapped reads).

7.10.2 Peak calling

1. ChIP-seq peaks were identified using T-PIC (Tree shape Peak Identification for ChIP-Seq) (Hower et al., 2011), and MACS (Model-based analysis of ChIP-Seq) (Zhang et al., 2008b).
2. Peaks detected by both peak callers were filtered quantitatively using the total read counts under the peak to include regions that have significant enrichment ($p<0.0001$) over regions detected in the respective knockout cells.

7.10.3 Peak analysis tools

1. BEDTools intersect (Dale et al., 2011) was used to identify ChIP-seq peaks that overlapped between two peak files based on the peak coordinates.
2. SAMtools sort was used to sort the alignment by leftmost peak coordinates. SAMtools merge was used to merge sorted alignment .bam files into a single output file (Li et al., 2009). Full commands and options can be found at

http://www.htslib.org/doc/samtools-1.0.html

7.10.4 Hierarchical clustering analysis

Final RPKM values for all qualified binding sites were plotted as hierarchical clustering dendrograms (using *hclust* function) or in a clustering heatmap format (using *heatmap.2* function). Analyses were performed with the R package gplots version 3.0.1 (https://cran.r-project.org/web/packages/gplots/index.html).

7.10.5 Heatmap analysis and ngs.plot

Binding site heatmaps and average profile line plots were generated using ngsplot (2.08) (Shen et al., 2014) with the parameters: -GO none (No ranking algorithm was applied. Use order provided in the bed file), -FL = 50 (fragment length), -L 1000 (flanking regions size), SC = 0,1 (colour scale), MQ = 15 (read mapping quality cut-off according to Phred-scale), –SE 0 (standard error). A full list of parameters can be found here: https://github.com/shenlab-sinai/ngsplot/wiki/ProgramArguments101

7.10.6 *De novo* motif analysis

Sequences flanking each peak summit (±150 bp) were repeat-masked using RepeatMasker 4.0.3 (http://www.repeatmasker.org). *De novo* motifs were identified using Meme-chip (4.9.1) (Bailey et al., 2009) and matched, using the TomTom module, to known transcription factor motifs in the 2009 JASPAR core database (Portales-Casamar et al., 2010).

7.10.7 Differential binding analysis

Differential binding analysis of the ChIP-seq data was based on the normalised read counts (i.e. RPKM) using the R package, DiffBind (Ross-Innes et al., 2012). GLM analysis was performed by using package EdgeR (Robinson et al., 2010).

7.10.8 Other tools

The following software packages and web resources were also used in this study:

GREAT - http://great.stanford.edu/public/html/

WebLogo - http://weblogo.berkeley.edu/logo.cgi

AME (Analysis of Motif Enrichment) - http://meme-suite.org/tools/ame

UCSC Genome Browser - http://genome.ucsc.edu/

IGV - http://software.broadinstitute.org/software/igv/

IPA (Ingenuity Pathway Analysis): Version IPA 01-06

7.11 RNA-seq

Total RNA was prepared in duplicate using the RNeasy Mini Kit (Qiagen, U.K.) following manufacturer's instruction. RNA-seq libraries were prepared by the Genomic Core Facility in the Wellcome Trust Centre for Human Genetics (University of Oxford, U.K.). Sequencing was performed on the HiSeq 2000 platform (Illumina, San Diego, CA, USA).

7.12 Bioinformatic analysis of RNA-seq data

RNA-seq analysis pipelines were developed by Dr. Rafik Salama. The full method can be found in Salama et al., 2015. An outline of method is shown below.

1. Illumina adaptor sequences were trimmed using Trimgalore (0.3.3).
2. Raw reads were then aligned to GRCh37 using Tophat 2.0.8b (http://ccb.jhu.edu/software/tophat/index.shtml) and bowtie 1.0.0 (http://bowtie-bio.sourceforge.net/index.shtml) with non-uniquely mapping fragments excluded using SAMtools (0.1.19) (Li et al., 2009).
3. Total read counts for each UCSC defined gene were extracted using HTSeq

(0.5.4p3) (Anders et al., 2015) with 'intersection-strict' mode. Read densities were normalised and expressed as reads per kilobase per million reads (RPKM).

4. Differential gene expression between normoxia and hypoxia for each dataset was performed using EdgeR (Robinson et al., 2010) and DESeq2 (Love et al., 2014) packages with a FDR<0.01 used to call significant hits. The final gene list was comprised of overlapping genes that appeared in both EdgeR and DESeq2 analyses.

7.12.1 Gene set enrichment analysis (GSEA)

GSEA was performed using 10000 permutations, a weighted enrichment score and pre-ranked genes (Subramanian et al., 2005). Differential expression and significance according to DESeq2 and fold difference between expression of genes in normoxia and 0.5% O_2 (24h) were used to rank genes (Xiao et al., 2014). The equation is as follows:

$$x = -\log_{10}[\text{adjusted } p \text{ value}]*\log_2[\text{fold change}]$$

7.13 Antibodies

Name	Source	Host	Cat no	Application
HIF-1α	Laboratory	Rabbit polyclonal	PM14	ChIP
HIF-2α	Laboratory	Rabbit polyclonal	PM9	ChIP
Pre-immune	Laboratory	Rabbit polyclonal	PM14-pre	ChIP
Rabbit IgG	Millipore	Rabbit IgG	12-370	ChIP
HIF-1β	Novus Biological	Rabbit antiserum	NB100-110	ChIP, Immunoblot
HIF-1α	BD Bioscience	Mouse monoclonal	610959	Immunoblot
HIF-2α	Laboratory	Mouse monoclonal	190b	Immunoblot
Beta actin	Abcam	Mouse monoclonal	ab49900	Immunoblot
CA9	Abcam	Rabbit polyclonal	ab15086	Immunoblot
FIH	Novus Biological	Mouse monoclonal	162C	Immunoblot
PBRM1	Bethyl Laboratories	Rabbit polyclonal	A301-591A	Immunoblot
P564-OH	New England Biolabs	Rabbit monoclonal	D43B5	Immunoblot
N803-OH	Kind gift from MK Lee (Korea)			Immunoblot
Histone H3	Abcam	Rabbit polyclonal	ab1791	Immunoblot
HMGCS1	Bethyl Laboratories	Rabbit polyclonal	A304-590A-T	Immunoblot

7.14 Primers for SyBr Green® assay

Name	Forward	Reverse	Application
NDRG1	TCTTCCTCCCACATGGAGAC	CACGTGTTGCTGAGTCACCT	ChIP-qPCR
EGLN3	AGTGTCCGTTCCCAGCTCAG	TAGGCACAGTAAACAGGCC	ChIP-qPCR
ACTG	AGATGTGGATTAGCAAGCAGG	GCTTATTCCAGTTTCGTGGAGGC	ChIP-qPCR
HPRT	GAC CAG TCA ACA GGG GAC AT	AAC ACT TCG TGG GGT CCT TTT C	RT-qPCR
CA9	AGCACAGAAGGGGAACCAAAG	ATGAGCAGGACAGGACAGTTAC	RT-qPCR
BNIP3	CGTTCCAGCCTCGGTTTCTATT	GAGCGAGGTGGGCTGTCAC	RT-qPCR
S100A2	GCCAAGAGGGCGACAAGTTC	CTCATCCACTTTCTCCCCCAC	RT-qPCR
LOC100506548	AGGGCACGATTCCTCTGATT	CTCCTCACTCCTCACCTTTTGT	RT-qPCR
GRB10	GCTCTTGCCTTTTTCTGTG	ACAGCTCTCATCCTTGGAG	RT-qPCR
PSMC2	AGGGATGAGAGTGGGCGTGG	ACCTGCATCATGGTAACTGTTGGG	RT-qPCR
ACOX1	CTG AAG GCT TTC ACC TCC TG	CAT GCC ACACACCAACTT T	RT-qPCR
MRPL51	TTCGAGGTTGGAAAGGGAATG	GGATGCGTTTATTAAGGTTGTGC	RT-qPCR
ACSS2	AGC TTG TCT TCC TTG TCC TC	TAT TCC TAC AAC CAC AGG GC	RT-qPCR
INSIG1	CAG GTT TTG GTG GCA TTA	CAC TTC TGG AAC GAT CAA A	RT-qPCR
HMGCS1	CCGAAGGAGGAAACAGTGAC	GGCAACAATTCCCACATCTT	RT-qPCR

7.15 Solutions and buffers

7.15.1 Annealing buffer

Name	Final
Tris pH 7.5-8.0	10 mM
NaCl	50 mM
EDTA	1 mM

7.15.2 ILB (Igepal Lysis Buffer) for whole cell extraction

Name	Final
Tris pH 7.6	10 mM
NaCl	0.25 M
Igepal (NP-40)	0.5%

7.15.3 SDS-PAGE sample loading buffer (6x)

Name	Final
Tris/HCl pH 6.8	50 mM
Glycerol	10%
SDS	1%
DTT	0.5 M
Bromphenol Blue	0.1%

7.15.4 SDS-PAGE running buffer (10x)

Name	Final
Tris	0.25 M
Glycine	1.9 M
SDS	1%

7.15.5 Immunoblot transfer buffer (20x)

Name	Final
Tris	0.2 M
Glycine	2 M

7.15.6 Phosphate buffered saline (PBS)

Name	Final
NaCl	0.137 M
KCl	0.0027 M
Phosphate buffer	0.1 M

7.15.7 PBS-T

Name	Final
NaCl	0.137 M
KCl	0.0027 M
Phosphate buffer	0.1 M
Tween 20	0.05%

7.15.8 4% blocking buffer

Name	Volume (per 50 ml)	Final
Skim milk powder	2 g	4%
PBS-T	Fill to 50 ml	

7.15.9 ChIP lysis buffer

Name	Stock	Volume (per 50 ml)	Final
SDS	20%	1 ml	1%
EDTA	0.5 M	1 ml	10 mM
TRIS pH 8.1	1 M	5 ml	50 mM
H_2O		43 ml	

7.15.10 ChIP dilution buffer

Name	Stock	Volume (per 50 ml)	Final
SDS	10%	50 µl	0.01%
EDTA	0.5 M	120 µl	1.2 mM
TRIS pH 8.1	1 M	835 µl	16.7 mM
Triton X-100	20%	2.75 ml	1.1%
NaCl	5 M	1.67 ml	167 mM
H_2O		46.8 ml	

7.15.11 ChIP Low salt buffer

Name	Stock	Volume (per 50 ml)	Final
SDS	10%	500 µl	0.1%
Triton X-100	100%	500 µl	1%
EDTA	0.5M	200 µl	2 mM
TRIS pH 8.1	1M	1 ml	20 mM
NaCl	5M	1.5 ml	150 mM
H_2O		46.55 ml	

7.15.12 ChIP High salt buffer

Name	Stock	Volume (per 50 ml)	Final
SDS	10%	500 µl	0.1%
Triton X-100	100%	500 µl	1%
EDTA	0.5M	200 µl	2 mM
TRIS pH 8.1	1M	1 ml	20 mM
NaCl	5M	5 ml	500 mM
H_2O		43.05 ml	

7.15.13 ChIP Lithium chloride buffer

Name	Stock	Volume (per 50 ml)	Final
LiCl	8 M	1.6 ml	0.25 M
Igepal (NP-40)	100%	500 µl	1%
sodium deoxycholate	powder	500 mg	1%
EDTA	0.5 M	100 µl	1 mM
TRIS pH 8.1	1 M	500 µl	10 mM
H_2O		47.3 ml	

7.15.14 TE wash buffer

Name	Stock	Volume (per 50 ml)	Final
TRIS pH 8.0	1 M	500 µl	10 mM
EDTA	0.5 M	100 µl	1 mM
H_2O		49.4 ml	

7.15.15 ChIP Elution buffer

Name	Stock	Volume (per 10 ml)	Final
$NaHCO_3$		0.0841 g	0.1 M
SDS	10%	1 ml	1%
H_2O		9 ml	

7.15.16 Buffer A used in cellular fractionation experiment

Name	Stock	Final
HEPES	1 M	10 mM
KCl	1 M	10 mM
$MgCl_2$	1 M	1.5 mM
Sucrose	1 M	0.34 M
Glycerol	50%	10%
DTT	1 M	1 mM
DFO	10 mM	100 uM
H_2O		

7.15.17 Buffer B used in cellular fractionation experiment

Name	Stock	Final
EDTA	0.5 M	3 mM
EGTA	0.5 M	0.2 mM
DTT	1 M	1 mM
H_2O		

8

Appendix

8.1 Hypoxia up-regulated genes defined in the WT cells

The hypoxic regulations in each cell background are shown. The genes are ranked based on the hypoxia regulation in the WT cells (i.e. the 2nd column).

Gene	WT	DKO	1βKO	VHLFIHKO
NDRG1	28.60	1.46	1.89	0.88
ASNS	7.19	1.42	1.37	2.43
BNIP3	6.77	0.92	1.64	0.99
TMEM45A	6.44	0.99	0.96	0.65
VLDLR	6.02	1.71	1.70	1.15
PDK1	5.68	0.98	1.59	0.94
ARRDC3	5.32	1.01	1.21	0.81
PCK2	5.22	1.40	1.39	1.49
AK4	5.21	1.26	1.31	0.91
IGFBP3	4.94	1.11	1.19	1.23
MXI1	4.92	0.94	1.36	0.87
DDIT4	4.91	1.70	2.01	0.74
ASS1	4.66	0.96	1.07	1.21
NPPB	4.56	0.79	0.63	1.00
STC2	4.54	1.49	1.64	1.23
TRIB3	4.53	1.42	2.31	1.70
LIMCH1	4.34	1.13	1.02	1.15
BNIP3L	4.17	1.00	1.69	1.02
LOX	4.15	0.89	1.14	1.03
INSIG2	4.03	1.13	1.17	0.92
PGK1	4.02	1.03	1.20	1.09
SLC2A1	4.00	1.08	1.24	0.90
FAM107B	3.88	1.21	1.36	1.39
KDM3A	3.74	1.30	2.28	1.09
P4HA1	3.73	0.94	1.73	0.98
SLC1A4	3.67	1.58	1.21	1.37
PGM1	3.64	0.87	1.03	0.80
ZNF395	3.64	1.20	1.35	0.80
VEGFA	3.58	1.42	1.88	1.08
ERRFI1	3.57	1.11	1.31	1.79
ALDH1L2	3.46	1.17	1.09	1.14
EPPK1	3.41	1.19	1.11	1.29
HK2	3.41	1.17	1.21	1.06
PSAT1	3.37	1.73	1.25	2.09
FUT11	3.36	1.23	1.25	0.85
TXNIP	3.24	0.30	0.37	0.72
KDM4B	3.11	1.47	1.21	0.85
FAM162A	3.10	0.95	0.91	0.92
GPT2	3.09	1.68	1.21	1.27
LRP1	3.07	1.63	1.14	0.64
PHGDH	3.06	1.45	1.22	1.43
LDHA	3.04	1.14	1.53	0.96
P4HA2	3.01	1.07	1.23	0.86
ATF3	2.98	1.15	1.95	1.49
CBS	2.96	1.70	0.99	1.41
PFKFB3	2.95	1.54	1.38	0.93
SEMA5A	2.91	1.26	1.20	1.15
PFKL	2.85	1.14	1.16	0.94
C4orf3	2.78	0.96	1.16	0.63
GSN	2.74	1.77	1.29	0.79
AHNAK2	2.74	1.97	1.44	0.46
PAM	2.73	1.17	1.08	0.76
LOC730101	2.67	1.57	1.20	0.90
FLNB	2.61	1.52	1.20	0.97
CA12	2.61	1.02	0.88	0.87
LOXL2	2.60	1.18	1.49	0.96
COL5A1	2.59	1.40	1.28	0.84
CARS	2.48	1.26	0.95	1.36
CDCP1	2.48	1.13	1.15	1.31
SLC7A11	2.47	1.25	1.25	0.76
GBE1	2.45	0.80	0.98	0.67
NFIL3	2.43	1.34	1.25	1.19
BTBD2	2.43	1.43	1.12	1.10
KRT17	2.40	0.98	1.39	0.92
EGFR	2.39	1.19	1.04	0.95
LBH	2.37	1.40	1.69	1.00
SESN2	2.37	1.67	1.44	1.60
GARS	2.37	1.46	1.07	1.56
SORL1	2.35	1.40	0.90	0.88
DOCK2	2.35	1.13	1.45	1.05
SYTL2	2.34	0.75	1.34	0.93
ANXA4	2.33	1.30	1.40	0.88
ITGA5	2.33	1.14	1.27	0.85
WDR54	2.33	1.24	1.17	1.06
PKD1	2.31	1.67	1.21	0.76
PFKP	2.31	1.26	1.09	0.72
TNIP1	2.30	1.22	1.14	0.97
PKD1P1	2.29	1.36	1.19	0.99
PPP1R3B	2.29	0.85	1.20	1.19
RHOB	2.28	0.93	1.64	1.24
MTHFD2	2.26	1.14	1.14	1.31
LAMA5	2.25	1.95	1.13	0.71
KCNMA1	2.24	1.02	1.04	1.03

SFXN3	2.24	1.23	1.25	0.99
SERTAD2	2.22	1.28	1.05	1.05
FSTL3	2.21	1.21	1.00	0.85
THBS2	2.21	1.20	1.35	1.24
PLEKHA2	2.18	1.05	1.07	1.02
LONP1	2.18	1.43	0.98	1.25
SH3BP2	2.18	1.15	0.99	0.79
DENND2A	2.17	1.17	0.98	0.77
ALDOA	2.17	1.25	1.24	0.92
TGFBI	2.16	1.38	1.35	0.87
TANC2	2.15	1.02	0.91	0.80
MTUS1	2.15	1.09	0.98	0.92
RRAGA	2.13	1.27	1.01	0.88
ATF4	2.11	1.35	1.04	1.02
IDH2	2.11	1.19	1.40	1.04
HKDC1	2.09	1.06	1.26	2.08
GYS1	2.08	0.99	0.96	0.76
DEPTOR	2.08	1.13	1.29	1.36
AKAP12	2.06	1.40	1.12	1.20
ZNF185	2.04	1.41	1.04	0.75
ABCA1	2.03	0.77	0.95	0.96
ZNF292	2.03	0.95	1.33	0.90
DDIT3	2.03	0.98	1.22	1.26
SLC7A5	2.03	1.68	1.04	1.03
LTBP4	2.02	1.58	1.11	1.17
JDP2	2.01	1.74	1.45	1.22
PXK	2.01	1.25	1.52	1.20
SLC16A3	2.00	1.10	1.06	0.82
ERO1L	2.00	0.97	1.05	0.95
HILPDA	1.99	1.10	1.11	0.88
AARS	1.97	1.62	1.16	1.36
BTG1	1.97	1.26	1.47	0.96
FN1	1.97	1.10	1.02	0.89
HK1	1.96	1.49	1.12	1.14
GPI	1.96	1.26	1.17	0.85
SERPINE1	1.96	1.31	1.33	1.04
FKBP9	1.95	1.14	1.10	1.38
KALRN	1.94	0.88	1.11	1.02
PTK7	1.94	1.28	1.23	1.00
C3orf58	1.94	0.88	1.01	1.15
CMIP	1.94	1.68	1.33	0.95
GRN	1.91	1.39	1.13	0.94
TUBA1A	1.91	1.26	1.55	0.72
MARS	1.90	1.26	0.92	1.37
SLC4A5	1.90	1.15	1.31	1.56
PLOD1	1.90	1.18	1.04	0.76
CDCA7L	1.89	1.02	1.12	0.98
HMGCL	1.88	0.82	1.22	0.75
MYC	1.88	1.41	1.40	1.31
MRC2	1.87	1.21	1.27	1.18
OSMR	1.86	1.13	1.45	0.99
FOXN3	1.86	1.53	1.19	1.10
MPI	1.86	0.89	1.02	0.91
ZNF160	1.85	0.99	1.46	0.75
ARHGEF2	1.85	1.26	1.03	1.01
WARS	1.85	1.02	1.09	1.61
PXDN	1.85	1.51	1.08	0.87
SLC6A8	1.84	1.30	1.10	1.02
CEBPG	1.84	1.15	1.23	1.76
PLIN2	1.84	0.92	1.18	1.14
OBSCN	1.83	1.49	1.17	0.61
SLC25A36	1.83	1.15	1.16	0.98
FLNA	1.83	1.47	0.90	0.94
MTHFD1L	1.83	1.09	1.07	1.45
XPNPEP1	1.81	1.07	0.94	0.87
ZNF654	1.81	0.96	1.44	0.67
ELMSAN1	1.81	1.22	1.12	1.16
PSAP	1.80	1.47	1.18	0.98
NCOR2	1.80	1.35	1.00	0.88
PKM	1.79	1.16	1.06	0.94
ITPR3	1.79	1.60	1.20	1.10
PACS1	1.79	1.25	1.02	0.95
CD109	1.78	0.99	1.07	0.72
EPRS	1.78	1.09	0.92	1.15
ECE1	1.78	1.53	1.20	0.92
PLOD2	1.77	0.83	0.93	0.75
EIF4EBP1	1.77	1.07	1.08	1.36
CERCAM	1.77	1.03	1.04	0.80
WASF1	1.77	1.27	1.19	1.23
LONRF1	1.77	1.21	1.37	1.20
MYLK	1.77	1.34	1.15	0.74
RASAL1	1.77	1.16	0.71	0.57
RNF187	1.77	1.22	1.22	0.96
NUP210	1.76	1.37	1.12	1.09
INADL	1.75	1.14	0.99	0.80
GTPBP2	1.75	0.92	1.14	1.14
SARS	1.75	1.08	0.97	1.24
SLC7A1	1.75	1.23	1.05	0.99
RBCK1	1.74	1.09	1.11	1.14
LOC100506190	1.74	0.99	1.39	1.53
DNASE2	1.74	1.14	1.10	1.02
VKORC1	1.74	1.22	1.21	0.95
FBXO41	1.74	1.45	1.12	1.25
MYH9	1.74	1.48	1.05	1.03
DOCK7	1.74	1.09	0.84	0.78
JMY	1.73	1.20	1.22	1.17
LAMB3	1.73	1.31	1.19	0.62
ENO1	1.73	1.03	1.05	1.03
ANKRD11	1.73	1.62	1.07	0.99
GLG1	1.72	1.26	1.00	0.92
SEC63	1.72	1.09	1.11	1.30
TBL1X	1.71	1.40	1.00	1.10
TLN1	1.71	1.21	0.80	0.77
UACA	1.71	0.83	0.92	0.92
CABIN1	1.71	1.40	1.09	0.92
RIOK3	1.70	0.91	0.97	0.83
SNTA1	1.70	1.40	0.97	0.87
TBC1D22A	1.70	1.22	0.98	0.91
SLC6A6	1.70	0.97	1.88	1.31
MAN2C1	1.70	1.26	0.95	1.36
SFMBT2	1.70	0.87	1.13	1.12
IQGAP1	1.70	1.39	1.00	0.82
KIAA1715	1.70	0.97	1.09	1.06
MAFF	1.69	0.97	1.56	0.97
ZCCHC14	1.69	1.47	1.20	1.06
EGLN1	1.69	1.01	1.26	0.97
KLF10	1.69	0.91	1.31	0.97
PIAS2	1.69	1.13	1.11	1.02
PTPRG	1.69	1.55	1.12	0.91
FAM65A	1.69	1.36	1.06	1.07
MKI67	1.68	1.50	1.01	0.77
PAN2	1.68	1.18	1.30	1.16
SPINT2	1.68	0.91	0.96	0.86
RUNX1	1.68	1.10	1.06	0.98
DHX40	1.68	0.98	1.11	0.87
WDTC1	1.68	1.55	1.07	0.88
PLBD2	1.68	1.13	1.05	1.03
HSPG2	1.67	1.36	0.86	0.72
SPTBN1	1.67	1.23	1.08	0.93
SUMF1	1.67	1.07	0.99	0.96
CLSTN1	1.67	1.41	1.24	0.98
TNKS	1.67	1.21	1.10	0.90
FBLIM1	1.67	1.28	1.17	1.17
FYN	1.66	1.13	1.04	1.04
IL7R	1.66	1.04	0.98	0.94
FHL1	1.66	1.36	1.37	1.20
PSPH	1.65	1.45	1.02	1.23
YEATS2	1.65	1.36	1.17	0.96
RAI1	1.65	1.45	1.12	0.94
GPHN	1.65	1.07	0.98	1.01
SHMT2	1.65	0.90	0.98	1.47
IARS	1.65	1.03	1.01	1.48
RNMT	1.65	0.93	1.09	0.99
SMAD3	1.64	1.59	1.20	1.14
FBXO42	1.64	1.24	1.12	1.03
SREBF2	1.64	1.43	1.42	1.18
EPCAM	1.64	0.85	1.08	1.32
ZBTB10	1.64	1.15	1.26	1.21
KLF13	1.64	1.35	1.39	1.10
KRT80	1.64	1.61	0.97	1.94
NCKIPSD	1.63	1.09	1.10	0.98
AGRN	1.63	1.47	1.19	0.99
DGKD	1.63	1.39	1.14	1.20
CUL9	1.63	1.10	1.07	0.95
MYO6	1.63	1.35	0.99	0.77
ATXN2L	1.63	1.15	1.02	1.08
GRB10	1.62	1.41	1.51	1.27
HUWE1	1.62	1.40	0.91	0.81
DYNC1H1	1.62	1.14	0.93	0.73
TES	1.62	0.81	0.95	1.14
MAP4	1.62	1.35	1.06	0.84
CTSB	1.62	1.26	1.27	0.95

KLF11	1.62	1.32	1.47	1.26
SAP30	1.62	1.06	0.96	0.92
FOSL2	1.62	1.23	1.24	0.93
FAM84B	1.62	1.60	1.16	1.09
CITED2	1.62	1.25	1.12	1.04
EPS8L2	1.62	1.03	0.86	0.85
ATRN	1.62	1.19	1.03	1.03
EP400	1.62	1.23	0.95	0.88
VCL	1.62	1.20	1.00	0.99
CMTM4	1.61	1.27	0.99	1.00
E2F7	1.61	1.17	1.14	0.96
PKN1	1.61	1.42	1.01	1.12
COL4A2	1.61	1.32	1.25	0.98
RBL2	1.61	1.22	1.34	1.02
BRD3	1.61	1.53	1.29	1.07
TRAM2	1.60	1.17	0.86	0.74
NREP	1.60	1.00	1.05	0.72
EEF2	1.60	1.32	1.12	1.24
PHF10	1.60	1.07	0.97	1.09
TPI1	1.60	0.90	0.97	0.95
POGZ	1.59	1.30	1.07	0.84
DUSP1	1.59	1.08	1.61	1.50
WASF2	1.58	1.29	1.09	1.00
ITFG3	1.58	1.31	1.20	1.05
XPOT	1.58	1.06	0.98	1.21
PGLS	1.58	1.28	1.26	1.25
LAMB2	1.58	1.10	1.00	0.84
CTNNA1	1.58	1.20	1.10	0.94
COL7A1	1.58	1.21	1.06	1.03
COL4A1	1.58	1.14	1.25	0.96
ALPK3	1.58	1.37	1.01	0.96
CSRP2	1.57	0.93	1.32	0.92
KDM5B	1.57	1.19	1.13	0.70
ETS1	1.57	1.23	1.15	1.39
FNBP1L	1.57	1.14	1.13	0.92
CELSR1	1.57	1.58	1.02	0.94
IGF1R	1.57	1.46	1.32	0.88
ETS2	1.57	1.06	1.07	1.04
SH3BP4	1.57	1.43	1.09	1.12
GSE1	1.57	1.23	0.96	0.85
TBC1D16	1.56	1.30	1.27	1.15
IGF2R	1.56	1.64	1.13	1.01
YARS	1.56	1.36	0.89	1.40
NFKB2	1.56	1.13	0.81	0.87
EPN1	1.56	1.47	1.03	0.97
GAPDH	1.56	0.88	1.01	0.82
CRIP2	1.56	1.39	1.17	0.72
CEP250	1.56	1.42	1.04	0.68
WSB1	1.56	1.22	1.25	0.87
SLC3A2	1.56	1.08	1.05	1.11
BCKDK	1.56	1.29	0.94	0.87
EIF1	1.56	0.96	1.08	1.08
DHX32	1.56	0.91	1.11	1.00
NEK6	1.56	1.49	1.04	0.97
CNOT8	1.56	0.88	1.01	0.68
NCOA7	1.56	1.05	1.16	1.12
CYB5R3	1.55	1.33	1.09	0.86
PYCR1	1.55	1.08	1.03	1.49
MET	1.55	0.91	0.96	1.29
ZNF33B	1.55	1.00	1.27	1.06
MLLT4	1.55	1.39	1.08	1.08
THOC6	1.55	1.06	1.19	1.44
SLC1A5	1.54	1.53	0.95	0.94
PDLIM1	1.54	1.38	1.16	0.91
RPTOR	1.54	1.22	0.87	0.97
TUBE1	1.54	0.93	0.90	1.44
VPS39	1.54	1.23	1.02	0.97
PRKDC	1.54	1.14	0.91	0.92
CTDNEP1	1.54	1.13	1.01	1.02
SGSM2	1.54	1.20	1.08	1.04
KDM4C	1.54	0.94	1.05	0.77
TCTN2	1.54	1.26	1.15	0.79
ZC3HAV1L	1.54	0.94	1.08	0.89
SYNE2	1.53	1.08	1.00	0.42
SERPINB6	1.53	1.05	0.96	0.87
FAM219A	1.53	1.17	0.99	0.88
EEF1A2	1.53	1.36	0.91	0.92
ATP2B4	1.53	1.21	1.06	0.65
TPR	1.52	1.06	1.03	0.83
MYH10	1.52	1.51	1.11	0.95
NARS	1.52	1.01	0.90	1.31
SRC	1.52	1.27	1.09	0.94
HIVEP2	1.52	1.22	1.33	1.01
MICAL3	1.52	1.12	1.05	1.02
PRPF8	1.52	1.33	0.96	0.93
L1CAM	1.52	1.39	0.84	0.62
DARS	1.52	0.77	0.92	0.73
GANAB	1.51	1.19	0.97	0.94
TBC1D9B	1.51	1.31	1.09	1.13
FAM210A	1.51	0.98	1.08	1.13
VIM	1.51	1.09	1.07	0.84
UBR4	1.51	1.30	1.03	0.86
S100A2	1.51	1.60	2.09	2.02
SRRM2	1.51	1.37	1.02	0.90
CLIC4	1.51	1.03	1.07	1.06
C19orf21	1.51	1.28	1.35	0.79
ARHGEF10	1.51	1.28	1.21	1.20
UBE2O	1.51	1.24	0.94	0.91
DOPEY2	1.51	1.13	0.99	1.06
MLL3	1.50	1.21	0.93	0.79
PCBP2	1.50	0.92	0.98	1.06
HERPUD1	1.50	1.19	1.46	1.11
AMIGO2	1.50	1.01	1.16	1.86
APP	1.50	1.26	1.15	1.00
XPC	1.50	1.15	1.22	0.86
DSG2	1.50	1.11	1.05	0.91
CELSR3	1.50	1.23	0.94	0.90
P4HB	1.50	1.40	1.01	0.91
RNF213	1.50	1.38	1.04	0.78
PLXNB2	1.49	1.30	1.02	0.68
RLF	1.49	0.85	1.36	1.01
TCP11L1	1.49	1.13	0.88	0.81
MARCKS	1.49	1.10	1.05	0.79
JAG1	1.49	1.29	1.11	1.08
PGAM1	1.49	1.11	1.06	0.94
LPP	1.49	1.22	0.80	0.68
RERE	1.49	1.19	1.14	0.92
PALLD	1.49	1.09	1.05	1.11
YPEL5	1.49	1.11	1.41	0.79
SREBF1	1.49	1.31	1.23	1.12
SPTAN1	1.49	1.21	0.95	0.97
NCSTN	1.49	1.01	0.92	0.83
ATP9A	1.48	1.53	1.00	0.73
CASK	1.48	1.23	1.11	1.00
LARS	1.48	0.94	0.95	1.27
MLL	1.48	1.18	0.98	0.75
BCOR	1.48	1.62	1.14	1.01
AGAP1	1.48	1.30	1.13	0.99
EFHD2	1.48	1.09	1.13	0.98
MFHAS1	1.47	1.28	1.11	1.28
MFI2	1.47	1.33	1.44	0.97
CUL7	1.47	1.01	1.07	0.78
FLNC	1.47	1.35	0.89	0.90
FGFR1	1.47	1.45	1.19	1.15
ZXDC	1.47	1.25	1.12	1.03
AGTPBP1	1.46	0.93	1.15	1.22
AFAP1	1.46	1.32	1.31	0.93
PYGB	1.46	1.36	1.27	1.60
HEG1	1.46	1.47	1.32	1.04
CCSAP	1.46	1.03	0.89	0.98
TNNT1	1.46	1.03	1.24	0.77
SIPA1L1	1.46	1.16	1.08	0.94
SGPL1	1.46	1.16	1.16	1.17
SPG11	1.46	1.09	1.10	0.82
OBSL1	1.45	1.01	0.82	0.62
UHRF2	1.45	1.22	1.17	0.95
VAPB	1.45	1.04	1.00	1.04
PRKCA	1.45	1.56	1.05	0.74
AHNAK	1.45	1.56	0.96	0.69
CDK5RAP2	1.45	1.21	1.09	1.06
LOC100506548	1.45	1.30	1.38	1.36
CPOX	1.44	1.05	1.00	0.77
TSEN15	1.44	0.99	0.89	1.66
GNAS	1.44	1.64	1.11	1.00
LGALS3BP	1.44	1.15	1.02	1.12
HLTF	1.44	1.03	1.13	1.05
DLC1	1.44	1.50	1.01	1.04
ZBTB38	1.44	1.06	1.06	0.95
PIEZO1	1.43	1.27	1.01	0.95
SNRNP200	1.43	1.37	0.90	0.89
RSL24D1	1.43	0.90	1.06	1.25
CHTF8	1.43	0.98	1.02	0.76

PDCD4	1.43	1.17	1.09	0.87
C19orf48	1.43	1.09	1.11	1.22
CRYBG3	1.43	1.06	0.99	0.79
CBL	1.43	1.23	0.99	0.82
EIF4B	1.43	1.05	1.09	1.03
BAZ2A	1.43	1.30	1.09	0.85
ABL1	1.43	1.34	1.02	1.08
PABPC1	1.43	1.14	1.01	1.14
PTP4A1	1.43	0.95	0.99	1.31
ACTR1B	1.43	1.06	1.15	1.46
DIAPH1	1.42	1.33	1.07	1.18
LGALS1	1.42	1.21	0.99	0.74
VPS13A	1.42	1.01	1.00	0.97
NPEPPS	1.42	0.99	1.01	0.84
ZBTB44	1.42	1.16	1.18	1.10
KDM3B	1.42	1.13	1.13	1.02
GCN1L1	1.42	1.20	0.92	0.98
KDM2B	1.42	1.19	1.03	0.96
GALNT18	1.42	1.13	1.29	1.59
ERP29	1.42	1.03	1.16	1.17
KIAA1804	1.42	1.25	1.24	1.24
PAPD7	1.42	1.27	1.15	1.34
TRRAP	1.42	1.28	0.86	0.78
SMG1	1.42	1.16	0.95	0.89
KLF7	1.41	1.08	1.18	1.05
FAM115A	1.41	1.19	1.04	0.73
NFE2L1	1.41	1.20	1.06	1.06
NBAS	1.41	0.94	1.00	0.90
PTPRF	1.41	1.60	1.15	1.06
EDEM1	1.41	1.33	1.25	1.04
TBC1D5	1.41	1.10	1.14	0.94
POLA1	1.40	1.05	1.12	0.99
RBPJ	1.40	1.01	1.11	0.98
RB1	1.40	1.11	1.06	0.91
ACADVL	1.40	1.15	0.94	0.95
TRIM25	1.40	1.27	0.99	1.23
PKP2	1.40	1.15	0.71	1.19
TARS	1.40	0.87	0.97	1.25
MOCOS	1.40	1.09	0.77	1.38
FLOT2	1.40	1.45	1.04	1.03
NUAK1	1.40	1.43	0.84	1.39
LTA4H	1.40	1.20	1.00	0.98
PRKAA2	1.39	0.99	0.85	0.90
EIF2S2	1.39	0.99	1.01	1.39
COPA	1.39	1.13	0.99	0.87
SUN1	1.39	1.16	1.14	1.08
ARID1B	1.39	1.24	0.91	0.73
VPS13C	1.39	0.96	1.13	0.86
CEP120	1.39	1.02	1.10	0.96
MYOF	1.39	0.96	0.90	0.83
MAP1B	1.39	1.25	0.97	0.76
ZMYND8	1.39	1.64	1.20	1.10
CHD2	1.39	1.24	1.19	0.96
WNK1	1.38	1.36	0.98	0.96
DPYSL2	1.38	1.31	1.40	0.87
SND1	1.38	1.23	1.11	0.96
UGP2	1.38	0.91	1.05	0.93
DCTN1	1.38	1.31	1.01	1.07
MAP2K1	1.38	1.11	1.04	0.94
DYNC2H1	1.38	0.82	0.90	0.74
PTGFRN	1.38	1.31	1.08	0.95
RAD50	1.37	0.86	0.96	0.89
VPS13D	1.37	1.26	0.84	0.80
SEC61G	1.37	0.82	0.95	1.04
DOCK5	1.37	1.23	0.92	0.77
SDHA	1.37	1.38	1.16	1.14
COPE	1.37	1.19	1.05	1.05
MYO1E	1.37	1.00	1.13	1.12
KDM5C	1.37	1.18	1.04	1.08
TOP2B	1.37	1.10	0.99	0.98
COL12A1	1.37	0.97	0.95	0.99
FOXK1	1.37	1.32	1.17	1.03
NAMPT	1.37	0.94	1.40	1.08
SPEN	1.37	1.30	0.96	1.01
ANXA2	1.36	1.04	1.01	1.09
SIN3A	1.36	1.20	1.19	0.91
MGEA5	1.36	1.10	0.94	0.91
ABLIM1	1.36	1.24	0.90	1.02
NIPBL	1.36	1.06	0.94	0.82
ZMYM2	1.36	1.06	1.12	0.96
CCDC6	1.36	1.20	1.16	1.22
ESYT1	1.36	1.11	0.97	0.94
EIF3A	1.36	1.04	0.86	1.09
USP11	1.36	1.18	1.07	0.86
ALKBH5	1.36	1.16	1.09	0.93
HADHA	1.36	1.12	1.02	1.17
HELZ	1.36	1.00	0.81	0.65
JAK1	1.36	1.16	1.01	0.95
MTR	1.36	1.08	1.02	1.08
EIF4G3	1.36	1.19	1.03	1.07
PHF17	1.35	1.12	1.15	1.23
NDUFV1	1.35	1.15	0.97	1.08
LRRFIP1	1.35	1.46	1.01	1.04
FKBP8	1.35	1.25	1.03	0.99
PRRC2B	1.35	1.66	1.08	0.91
ZNF770	1.34	1.09	1.04	1.13
TRIO	1.34	1.17	0.98	0.88
QSER1	1.34	1.10	0.95	0.94
BCAT1	1.34	1.00	1.00	1.42
TJP1	1.34	1.16	0.99	1.10
DOCK1	1.34	1.24	1.10	0.94
NEDD4	1.33	0.72	0.87	0.82
CKAP5	1.33	1.08	0.99	0.88
SLC38A1	1.33	1.22	1.08	1.17
DENND5A	1.33	1.13	1.15	1.00
CHD6	1.33	1.18	1.24	0.84
MATR3	1.33	0.94	0.92	1.02
PDXK	1.33	1.22	1.35	1.00
NCAPG2	1.33	1.14	1.00	0.97
ESYT2	1.33	1.08	1.14	0.90
JMJD1C	1.32	1.04	1.02	0.90
TP53	1.32	1.20	1.06	1.19
MCM6	1.32	1.29	1.05	1.08
SF3B3	1.32	1.26	1.02	0.92
XPO5	1.32	1.20	0.93	1.58
VPS35	1.32	1.04	1.06	1.04
PJA2	1.32	1.21	1.04	0.92
RPN2	1.31	1.07	1.02	1.05
PCGF5	1.31	0.93	1.09	1.02
LRPPRC	1.31	1.12	1.08	1.14
POLR2A	1.31	1.36	1.07	0.94
NOTCH2	1.30	1.29	0.99	0.99
ADAM9	1.30	1.15	1.04	1.21
MCM3	1.30	1.19	1.09	1.07
HMGB2	1.30	1.09	1.08	0.79
CNOT1	1.29	1.13	1.02	0.91
IPO5	1.28	1.00	0.97	1.20
NONO	1.28	1.06	0.96	0.93
MTMR12	1.27	1.30	0.97	1.00

8.2 Hypoxia down-regulated genes defined in the WT cells

The hypoxic regulations in each cell background are shown. The genes are ranked based on their hypoxia regulation in the WT cells (i.e. the 2nd column).

Gene	WT	DKO	1βKO	VHLF1HKO
DKK1	0.22	0.67	0.87	0.88
PAGR1	0.37	0.29	0.88	0.87
FKRP	0.41	0.54	1.04	1.22
ID3	0.42	0.92	0.89	0.67
CCND1	0.42	0.77	0.99	2.50
IL32	0.43	0.31	0.98	1.10
MIR22HG	0.44	0.79	0.90	1.04
DLEU2L	0.44	0.78	0.68	0.67
OXTR	0.45	0.88	0.87	1.04
KITLG	0.46	0.67	0.85	0.91
TMEM50B	0.46	0.75	0.74	0.87
SEMA3C	0.46	0.59	0.78	0.86
KIAA1549	0.47	0.28	1.14	0.92
TRIM2	0.47	0.93	0.84	0.83
LRP8	0.48	0.96	1.14	0.98
GEM	0.48	0.66	0.81	1.35
ITGAE	0.49	0.78	0.79	1.12
RBM4	0.49	0.45	0.90	0.98
TRIM56	0.50	0.52	1.02	0.78
NCEH1	0.50	0.87	0.93	1.24
PIK3R3	0.50	0.90	1.12	1.00
FAM46B	0.51	1.15	0.81	0.74
LINC00472	0.51	0.76	0.95	1.40
EIF5A2	0.52	0.80	0.89	1.32
AP1M2	0.52	1.10	1.47	1.51
TRUB2	0.52	0.38	0.85	0.85
ATP10D	0.52	0.77	0.88	0.58
ARMCX1	0.52	0.83	0.99	0.56
GATA2	0.53	1.21	1.12	1.31
MEST	0.53	1.11	0.66	0.56
TOMM6	0.54	1.06	0.89	0.94
NXPE3	0.54	0.99	0.74	0.64
GCLM	0.54	0.72	0.67	0.62
ASF1A	0.54	0.86	0.74	0.61
ARSJ	0.54	0.75	0.61	1.00
TAF13	0.54	0.97	0.90	1.02
CYB5R1	0.55	0.83	0.73	0.73
TOMM40L	0.55	0.81	0.84	0.88
ISOC2	0.55	0.88	0.81	0.85
SLC35G1	0.55	1.02	0.89	1.90
GPATCH4	0.55	0.93	0.78	1.56
MON1A	0.55	0.89	0.88	1.46
HSPB8	0.56	1.08	0.78	0.86
TIMM17A	0.56	0.87	0.82	1.13
C17orf89	0.56	0.95	0.89	1.10
RAB27B	0.56	0.73	1.09	0.79
UNKL	0.57	1.14	0.76	0.82
CCNYL1	0.57	0.47	1.04	1.20
CTU2	0.57	0.93	0.65	1.09
GEMIN6	0.58	0.75	0.73	1.11
DOLPP1	0.58	0.97	0.86	0.94
HSPE1	0.58	1.21	0.96	0.97
CHPF2	0.58	1.06	0.74	0.64
POLR3K	0.58	1.11	0.88	1.46
ARHGAP18	0.58	0.70	0.69	0.63
RNF145	0.58	0.88	0.56	0.55
HIF1A	0.58	1.06	1.31	1.14
PPM1K	0.58	0.90	1.24	0.81
ELL2	0.59	1.14	1.18	1.26
PLK2	0.59	0.84	0.83	1.22
MAP2K3	0.59	1.29	0.85	0.85
SMTN	0.59	0.84	0.90	0.56
AAED1	0.59	0.74	0.89	1.06
CUTC	0.59	0.89	0.79	1.37
CCND3	0.59	1.07	0.97	1.22
SBDSP1	0.59	0.85	0.75	1.44
HOXC11	0.59	1.19	1.14	1.02
PSMB10	0.60	0.87	0.82	1.13
PKNOX1	0.60	0.37	1.07	0.77
LSM1	0.60	0.77	0.84	1.03
HTATSF1P2	0.60	0.77	0.68	0.60
MALAT1	0.60	1.02	1.07	1.11
ENTPD7	0.60	0.68	0.78	0.72
AP4B1	0.60	0.83	0.75	0.91
TMEM5	0.60	0.74	0.78	1.44
SLC25A33	0.60	0.90	0.94	1.69
RNF144B	0.60	0.90	0.85	1.07
ARL4A	0.61	0.66	1.06	1.27
GPAM	0.61	0.86	0.57	0.75
LIN28B	0.61	0.91	0.95	1.46
SELRC1	0.61	0.82	0.86	1.37
CCDC86	0.61	1.12	0.76	1.27
IDI1	0.61	0.99	2.22	1.23
MFSD1	0.62	0.77	0.85	1.01
SRPRB	0.62	0.92	0.86	1.35
SAT1	0.62	0.63	1.05	0.90
FAM217B	0.62	1.03	0.84	1.13
LOC100506305	0.62	0.59	0.53	0.73
DERL2	0.62	0.72	0.84	0.90
RDH10	0.62	1.01	1.05	1.77
COA6	0.62	0.81	0.83	0.96
NOL6	0.62	0.98	0.67	1.41
PTS	0.62	0.79	0.82	0.96
NOP16	0.62	1.19	0.73	1.38
ZMPSTE24	0.62	0.64	0.82	1.24
SLC5A6	0.62	0.96	0.79	1.12
TMEM126B	0.62	0.76	0.77	1.17
PTCD3	0.62	0.58	0.88	0.92
LAYN	0.62	0.82	0.93	1.22
CHAC2	0.62	0.73	0.71	1.67
ISCU	0.63	0.83	0.92	1.17
ID1	0.63	1.18	1.46	0.65
IL18	0.63	0.71	0.96	0.75
NABP1	0.63	0.72	0.95	1.05
NEK7	0.63	0.83	1.08	0.98
JKAMP	0.63	0.73	0.90	0.93
HECW2	0.63	1.01	0.89	0.57
BRMS1	0.63	0.91	0.71	1.16
MTRNR2L8	0.64	0.88	1.16	1.34
SLC30A7	0.64	0.83	0.84	1.00
RRP9	0.64	0.84	0.71	1.40
LYAR	0.64	0.85	0.95	1.57
BAG2	0.64	0.77	0.85	0.96
LTV1	0.64	0.79	0.77	1.30
CDC26	0.64	1.03	0.90	1.07
RFK	0.64	0.91	0.96	1.81
FAM136A	0.64	0.89	0.88	1.34
DNAJB4	0.65	0.86	0.87	0.58
PCYT1A	0.65	0.81	0.79	0.67
AEN	0.65	0.82	0.94	1.82
SPRTN	0.65	0.80	0.89	1.15
PMP22	0.65	0.92	0.83	0.60
APOL2	0.65	0.78	0.89	0.73
RPP40	0.65	0.59	0.72	1.19
SMURF2	0.65	0.81	0.89	0.85
POP1	0.65	0.70	0.63	1.11
ADAM19	0.65	1.35	1.04	0.78
ATP6V0B	0.65	0.96	0.90	1.11
EEF1E1	0.65	0.80	0.89	1.25
C12orf75	0.66	0.82	0.94	1.17
TYW3	0.66	0.91	0.95	1.15
TACSTD2	0.66	1.35	1.61	0.96
DHCR24	0.66	1.18	1.01	0.80
CLMP	0.66	1.09	0.93	0.99
DIMT1	0.66	0.85	0.90	1.30
SRSF2	0.66	1.03	0.83	0.94
STRA13	0.66	0.90	1.06	1.20
GTF3C6	0.66	0.80	0.84	1.21
MRPL20	0.66	0.85	0.78	0.91

TMA7	0.66	0.82	0.88	0.97
SEC22B	0.66	0.85	0.81	0.78
PNO1	0.66	0.94	0.76	1.44
SELT	0.66	1.01	0.99	1.13
RRS1	0.66	0.96	0.72	2.03
PSMD3	0.66	1.03	0.83	0.90
SLC25A25	0.66	0.88	0.83	1.37
TRMT61A	0.66	1.01	0.69	1.20
SPR	0.66	1.00	1.12	0.98
FABP5	0.67	0.79	0.85	1.18
TNFRSF12A	0.67	0.86	0.81	1.24
DNAJB11	0.67	0.84	0.78	0.86
PRMT3	0.67	0.77	0.81	1.68
DCDC2	0.67	0.78	0.77	0.64
SOAT1	0.67	0.77	1.00	0.97
TIPIN	0.67	0.68	0.78	1.08
TMEM9B	0.67	0.87	0.96	1.04
LPCAT1	0.67	1.08	0.69	0.56
NIP7	0.67	0.87	0.74	1.28
KIAA0930	0.67	0.94	0.85	0.71
FASTKD1	0.67	0.83	0.85	0.85
NAA38	0.67	0.98	1.01	0.95
LOC401397	0.67	0.65	0.76	0.78
TRMT5	0.67	0.44	0.89	1.05
SLC35D1	0.67	0.95	0.83	0.82
MSRB1	0.67	0.88	0.71	0.54
RRP36	0.67	0.76	0.88	1.08
TLE4	0.67	1.16	1.03	0.85
NOC3L	0.67	0.75	0.78	1.22
TMEM87A	0.68	0.73	0.94	1.01
BLOC1S2	0.68	0.85	0.79	1.11
TMEM126A	0.68	0.68	0.81	1.01
C11orf48	0.68	1.07	0.95	1.14
ANKRD13C	0.68	0.85	0.86	0.94
EIF5	0.68	0.80	0.75	1.11
PLXND1	0.68	1.19	0.89	0.75
NCBP2	0.68	0.58	0.83	1.06
CISD1	0.68	0.86	0.83	0.89
LRR1	0.68	0.79	0.86	1.05
PSMD11	0.68	1.09	0.84	0.95
EIF2B3	0.68	0.88	0.75	1.03
ORMDL1	0.68	0.76	0.96	1.30
AASS	0.68	0.88	0.84	0.64
SVIP	0.68	0.76	0.72	0.92
DPH2	0.68	1.04	0.80	1.39
HMGCS1	0.68	1.00	3.58	1.25
USF1	0.68	0.86	0.85	1.01
HNRNPAB	0.68	1.18	0.85	1.27
PSME3	0.68	0.91	0.74	1.23
SAR1B	0.68	0.99	0.83	0.87
ARL2BP	0.68	0.75	0.76	1.02
PSMA5	0.68	0.85	0.89	0.95
NQO1	0.68	0.68	0.75	0.64
POLR2L	0.68	1.37	0.93	0.89
EPHA2	0.68	1.04	0.94	1.43
SPCS3	0.69	1.00	1.01	1.15
TFPI2	0.69	0.79	0.85	1.08
YRDC	0.69	0.74	0.83	1.37
PSMD12	0.69	0.98	0.72	0.91
CYB5A	0.69	0.98	0.78	0.87
ACOX1	0.69	0.75	0.76	0.71
UTP15	0.69	0.85	0.76	1.42
WSB2	0.69	0.98	0.90	0.78
BPNT1	0.69	0.83	0.87	0.81
ATAD3B	0.69	1.23	0.89	1.27
ABHD2	0.69	1.03	0.71	0.82
WDR77	0.69	1.17	0.88	1.42
RWDD4	0.69	0.84	0.89	1.21
MANF	0.69	0.96	0.86	0.79
OLR1	0.69	0.67	0.78	0.95
ANKRD13A	0.69	0.85	0.90	1.19
LSM7	0.69	1.01	1.01	1.10
FGF2	0.69	0.71	1.22	1.38
IDH1	0.69	0.93	1.21	0.93
FASTKD2	0.69	0.76	0.76	0.94
MAPK6	0.69	0.88	0.94	1.04
YOD1	0.69	0.71	0.79	0.94
GNG11	0.69	0.64	0.88	0.60
NOP10	0.69	0.87	1.00	0.88
TAF9B	0.69	0.91	0.86	1.11
FAM3C	0.69	1.13	0.86	1.20
PSMC6	0.70	0.83	0.79	0.80
GLMN	0.70	0.67	0.87	0.97
CYB561	0.70	1.07	0.91	1.23
GRWD1	0.70	0.97	0.82	1.13
UGDH	0.70	0.82	0.87	0.81
MIS12	0.70	0.77	1.02	1.19
HEXIM1	0.70	1.05	1.04	1.38
NECAP1	0.70	0.89	0.88	0.97
PAK1IP1	0.70	0.85	0.82	1.37
C12orf49	0.70	0.98	0.99	1.24
IDH3A	0.70	0.96	0.87	1.23
KIAA1586	0.70	0.65	0.75	0.72
PRPS1	0.70	0.84	0.93	1.26
SEC61B	0.70	0.93	0.88	1.01
TMCO1	0.70	0.77	0.80	0.87
MSMO1	0.70	1.03	2.56	1.15
PSMD1	0.70	0.97	0.87	0.91
TMEM167A	0.70	0.89	0.84	0.86
FASTKD3	0.70	0.74	0.79	1.34
QTRTD1	0.70	0.99	0.84	1.26
HMGCR	0.70	0.85	1.57	1.05
CD55	0.70	0.84	0.69	0.97
MRPL27	0.70	0.88	0.89	0.96
LIMA1	0.71	0.99	0.93	1.25
TPMT	0.71	0.92	0.80	0.80
CDKN2C	0.71	0.85	0.85	0.60
TOMM5	0.71	0.97	0.99	1.19
POMP	0.71	0.98	0.93	0.98
IMP4	0.71	1.16	0.85	1.34
ARF6	0.71	0.99	0.97	0.75
RPS26	0.71	1.14	0.90	0.93
CD47	0.71	0.84	0.95	0.90
DNAJB1	0.71	1.11	1.02	0.99
CDC25A	0.71	0.98	0.92	1.27
PHF5A	0.71	0.84	0.87	1.17
C12orf5	0.71	0.99	0.94	1.60
CHORDC1	0.71	1.29	0.98	1.24
BDNF	0.71	0.95	0.98	1.03
POLR2K	0.71	0.77	0.88	1.13
LRRC59	0.71	1.01	0.88	1.10
TPM3	0.71	0.45	1.04	1.11
SHC1	0.71	1.04	0.79	0.50
GTF2A2	0.71	1.12	0.90	1.13
MPDU1	0.71	0.84	0.89	1.25
SUMO3	0.71	0.99	0.88	0.89
MPHOSPH10	0.72	0.92	0.81	0.90
SKP2	0.72	0.93	0.73	0.80
GPX8	0.72	0.83	0.89	0.87
HRSP12	0.72	0.84	0.82	0.85
DCP2	0.72	1.03	1.02	0.74
RWDD1	0.72	0.83	0.84	1.11
CBFB	0.72	0.94	0.98	1.02
MRPL49	0.72	0.99	1.12	1.03
MED30	0.72	0.68	0.83	0.83
SNRPG	0.72	0.81	0.99	1.07
NAA50	0.72	0.97	0.99	1.33
SERP1	0.72	0.90	0.94	1.06
MRPL18	0.72	1.08	0.90	1.07
ATP1B1	0.72	1.05	1.13	1.29
EIF2B1	0.72	1.21	0.83	1.00
DYNLL1	0.72	0.83	0.91	1.03
FAM96A	0.72	0.85	0.96	1.05
SNHG3	0.72	0.86	0.88	0.80
CDC42EP3	0.72	1.09	0.95	1.85
CMTM6	0.72	0.86	0.94	0.95
CHUK	0.73	0.82	0.87	1.04
HSPH1	0.73	1.06	1.02	1.00
SRXN1	0.73	0.92	0.86	1.29
ARL6IP5	0.73	1.13	0.80	0.74
METTL21A	0.73	0.92	0.92	1.05
ATP6V0E1	0.73	1.08	0.95	0.92
B4GALT5	0.73	1.07	0.92	0.86
MAK16	0.73	0.97	0.83	1.19

PSMB2	0.73	1.09	0.81	0.94
UTP20	0.73	0.86	0.78	1.01
RPL17	0.73	0.58	0.96	1.15
BCCIP	0.73	0.93	0.90	1.22
PHACTR2	0.73	1.00	0.99	0.99
FAM98A	0.73	1.10	0.92	1.11
PSMC2	0.73	0.81	0.81	0.83
PUS7L	0.73	0.68	0.85	1.02
SNTB2	0.73	1.14	0.99	0.86
SOCS6	0.73	0.89	0.93	1.09
ZFAND5	0.73	1.01	0.99	1.07
IMPA1	0.73	0.79	0.91	0.91
KNSTRN	0.73	0.81	0.91	0.85
NFATC2IP	0.73	0.46	1.08	1.03
SRSF6	0.73	1.16	0.85	1.03
SPARC	0.74	1.11	0.87	0.63
TMEM64	0.74	0.99	1.03	1.15
NAA15	0.74	0.95	0.82	1.11
PTRF	0.74	1.18	0.97	0.88
RARS	0.74	0.78	0.87	0.89
TTL	0.74	0.95	0.94	1.17
POLR3G	0.74	0.91	0.87	1.48
PTPN1	0.74	0.94	0.88	0.98
USMG5	0.74	0.65	0.91	1.07
TCEB1	0.74	0.85	0.96	1.10
HSPA8	0.74	0.78	0.98	0.96
DDX47	0.74	0.81	0.83	0.93
EPT1	0.74	0.82	0.87	0.96
TRMT112	0.74	0.90	0.86	0.95
H3F3B	0.74	0.84	0.90	0.88
FRMD6	0.75	0.81	1.07	0.80
DSE	0.75	0.96	1.02	0.88
USP16	0.75	0.70	0.81	0.96
EIF4E	0.75	0.88	0.96	1.24
SAR1A	0.75	0.93	1.07	0.90
TMEM184C	0.75	0.91	0.82	0.90
MRPL51	0.75	0.81	0.85	0.85
SDHD	0.75	0.81	0.94	0.84
SNRPD1	0.75	0.91	0.92	1.06
CRCP	0.75	0.96	0.96	1.06
NPLOC4	0.75	1.03	0.89	1.11
ADRM1	0.75	0.92	0.88	1.15
CDK2AP1	0.75	0.95	0.98	1.07
PPP2R1B	0.75	0.98	0.80	0.86
UBB	0.75	0.83	0.91	0.90
PPP2CA	0.75	0.88	0.84	0.96
PSMB5	0.75	1.02	0.86	0.83
CFL2	0.76	0.80	0.82	0.88
WWTR1	0.76	1.00	0.82	1.03
SRSF1	0.76	0.90	0.81	0.86
CTC1	0.76	0.46	1.02	1.10
NBN	0.76	0.70	0.87	1.00
SSR3	0.76	0.86	1.03	1.04
SKA2	0.77	0.98	0.97	0.92
PGAM5	0.77	1.03	0.92	1.45
CYB5B	0.77	0.91	1.09	0.93
GLS	0.77	1.09	1.04	1.03
TAOK1	0.78	0.61	0.89	0.78
DNAJA1	0.78	1.00	0.95	1.16
CAPZA1	0.78	1.05	0.97	0.98
CALM2	0.78	0.81	1.00	1.02
SUB1	0.78	0.92	1.03	1.18
HSPA4	0.79	0.97	0.94	1.07
YWHAB	0.79	0.78	1.02	1.16

8.3 Hypoxia up-regulated genes defined in the HIF-1β KO cells

8.3.1 Genes that were more up-regulated by hypoxia in WT than in HIF-1β KO cells.

The ratios of hypoxic fold regulations (fold change, FC) between WT cells and HIF-1β KO cells, i.e. FC(WT)/FC(1βKO)>1.2, are shown in the 2nd column. The hypoxia regulations in each cell background are shown in the 3rd-6th columns. The genes are ranked based on their hypoxia regulation in the HIF-1β mutant cells (i.e. the 3rd column).

Gene	WT/1βKO	1βKO	WT	DKO	VHLFIH KO
TRIB3	1.97	2.31	4.53	1.42	1.70
KDM3A	1.64	2.28	3.74	1.30	1.09
DDIT4	2.44	2.01	4.91	1.70	0.74
ATF3	1.53	1.95	2.98	1.15	1.49
NDRG1	15.16	1.89	28.60	1.46	0.88
VEGFA	1.90	1.88	3.58	1.42	1.08
P4HA1	2.16	1.73	3.73	0.94	0.98
VLDLR	3.55	1.70	6.02	1.71	1.15
BNIP3L	2.46	1.69	4.17	1.00	1.02
LBH	1.40	1.69	2.37	1.40	1.00
RHOB	1.39	1.64	2.28	0.93	1.24
BNIP3	4.14	1.64	6.77	0.92	0.99
LDHA	1.98	1.53	3.04	1.14	0.96
LOXL2	1.75	1.49	2.60	1.18	0.96
BTG1	1.34	1.47	1.97	1.26	0.96
JDP2	1.38	1.45	2.01	1.74	1.22
OSMR	1.29	1.45	1.86	1.13	0.99
SESN2	1.65	1.44	2.37	1.67	1.60
AHNAK2	1.91	1.44	2.74	1.97	0.46
IDH2	1.51	1.40	2.11	1.19	1.04
ANXA4	1.67	1.40	2.33	1.30	0.88
MYC	1.35	1.40	1.88	1.41	1.31
CDKN1A	1.21	1.38	1.68	1.17	0.72
PFKFB3	2.15	1.38	2.95	1.54	0.93
FHL1	1.21	1.37	1.66	1.36	1.20
ITGB8	1.23	1.37	1.69	1.03	0.70
ZNF395	2.68	1.35	3.64	1.20	0.80
THBS2	1.64	1.35	2.21	1.20	1.24
TGFBI	1.61	1.35	2.16	1.38	0.87
RBL2	1.20	1.34	1.61	1.22	1.02
ZNF292	1.53	1.33	2.03	0.95	0.90
SERPINE1	1.47	1.33	1.96	1.31	1.04
CMIP	1.46	1.33	1.94	1.68	0.95
AK4	3.99	1.31	5.21	1.26	0.91
PAN2	1.29	1.30	1.68	1.18	1.16
COL5A1	2.03	1.28	2.59	1.40	0.84
ITGA5	1.83	1.27	2.33	1.14	0.85
CTSB	1.28	1.27	1.62	1.26	0.95
HKDC1	1.65	1.26	2.09	1.06	2.08
EGLN1	1.35	1.26	1.69	1.01	0.97
WSB1	1.25	1.25	1.56	1.22	0.87
COL4A2	1.29	1.25	1.61	1.32	0.98
COL4A1	1.26	1.25	1.58	1.14	0.96
CLSTN1	1.34	1.24	1.67	1.41	0.98
ALDOA	1.75	1.24	2.17	1.25	0.92
FOSL2	1.31	1.24	1.62	1.23	0.93
SREBF1	1.21	1.23	1.49	1.31	1.12
RNF187	1.44	1.22	1.77	1.22	0.96
PGK1	3.35	1.20	4.02	1.03	1.09

8.3.2 Genes that were up-regulated similarly by hypoxia in WT and in HIF-1β KO cells.

The ratios of hypoxic fold regulations (fold change, FC) between WT cells and HIF-1β KO cells, i.e. FC(WT)/FC(1βKO) is between 0.8 and 1.2, are shown in the 2nd column. The hypoxia regulations in each cell background are shown in the 3rd-6th columns. The genes are ranked based on their hypoxia regulation in the HIF-1β mutant cells (i.e. the 3rd column).

Gene	WT/1βKO	1βKO	WT	DKO	VHLFIH KO
KLHL24	0.84	2.11	1.77	1.05	0.95
SLC6A6	0.91	1.88	1.70	0.97	1.31
DUSP1	0.99	1.61	1.59	1.08	1.50
PROSER2	0.87	1.56	1.35	1.43	1.53
MAFF	1.09	1.56	1.69	0.97	0.97
THEM6	0.85	1.54	1.30	1.04	1.23
PNRC1	0.87	1.53	1.33	1.01	0.96
HIP1R	0.93	1.53	1.43	1.23	1.24
GRB10	1.08	1.51	1.62	1.41	1.27
ZFP62	0.90	1.50	1.36	0.98	1.09
PINK1	0.91	1.50	1.36	1.12	1.00
NPC1	0.84	1.48	1.24	1.06	1.05
HECA	0.82	1.47	1.21	1.26	0.93
KLF11	1.10	1.47	1.62	1.32	1.26
HERPUD1	1.03	1.46	1.50	1.19	1.11
ITPRIP	0.93	1.46	1.36	1.47	1.26
MFI2	1.02	1.44	1.47	1.33	0.97
DVL2	0.87	1.44	1.24	1.30	1.08
KRT19	0.92	1.43	1.31	0.94	0.80
SREBF2	1.16	1.42	1.64	1.43	1.18
SMAD7	0.81	1.42	1.15	1.33	1.15
SIRT5	1.00	1.42	1.41	0.99	1.30
GPR56	0.98	1.41	1.39	1.46	1.51
YPEL5	1.06	1.41	1.49	1.11	0.79
DPYSL2	0.99	1.40	1.38	1.31	0.87
NAMPT	0.97	1.40	1.37	0.94	1.08
CARHSP1	0.86	1.39	1.19	1.21	1.02
LRP4	0.96	1.39	1.33	1.46	1.22
KLF13	1.18	1.39	1.64	1.35	1.10
LOC100506548	1.04	1.38	1.45	1.30	1.36
CEBPB	0.92	1.38	1.28	1.19	1.21
IRF2BP2	0.97	1.38	1.34	1.04	1.09
LATS2	0.88	1.37	1.21	1.43	1.34
PACS2	0.93	1.37	1.28	1.44	1.46
SLC25A1	0.84	1.37	1.15	1.18	0.85
FOXO3	0.98	1.37	1.34	1.12	0.92
RLF	1.10	1.36	1.49	0.85	1.01
PDXK	0.98	1.35	1.33	1.22	1.00
C19orf21	1.12	1.35	1.51	1.28	0.79
ABHD14B	0.89	1.34	1.19	1.14	1.57
GPRC5A	1.00	1.34	1.33	1.12	1.32
PTBP3	0.94	1.34	1.26	1.19	1.08
SH3GLB2	0.92	1.33	1.22	1.16	0.99
HIVEP2	1.14	1.33	1.52	1.22	1.01
IGF1R	1.19	1.32	1.57	1.46	0.88
HEG1	1.11	1.32	1.46	1.47	1.04
ZBTB1	0.87	1.32	1.15	1.02	1.28
TEX264	0.96	1.31	1.26	1.12	1.36
PMAIP1	0.86	1.31	1.13	1.05	1.39
PDIA5	0.99	1.31	1.30	1.01	1.11
AFAP1	1.12	1.31	1.46	1.32	0.93
PLCG1	0.99	1.30	1.29	1.31	1.31
NCS1	0.80	1.30	1.04	1.16	1.28
MINK1	1.01	1.29	1.30	1.50	1.10
QPRT	0.82	1.29	1.06	1.17	0.69
PTPRS	1.02	1.28	1.31	1.59	1.07
DAPK1	0.93	1.28	1.19	1.53	1.29
PYGB	1.15	1.27	1.46	1.36	1.60
PTPN12	1.01	1.27	1.29	1.12	1.09
RHOQ	0.89	1.26	1.12	0.99	1.26
MASTL	0.81	1.25	1.02	0.90	0.97
CHD6	1.08	1.24	1.33	1.18	0.84
GGA2	0.94	1.23	1.16	1.37	0.95
TMEM123	0.92	1.23	1.13	1.14	1.18
CD9	0.92	1.23	1.12	0.91	0.89
LITAF	0.86	1.23	1.06	1.30	1.13
CTDSP2	1.01	1.22	1.24	1.76	0.87
RHOBTB3	0.84	1.21	1.02	1.28	0.95

8.3.3 Genes that were more up-regulated by hypoxia in HIF-1β mutant than in the WT cells.

The ratios of hypoxic fold regulations (fold change, FC) between WT cells and HIF-1β KO cells, i.e. FC(WT)/FC(1βKO)<0.8, are shown in the 2nd column. The hypoxia regulations in each cell background are shown in the 3rd-6th columns. The genes are ranked based on their hypoxia regulation in the HIF-1β mutant cells (i.e. the 3rd column).

Gene	WT/1βKO	1βKO	WT	DKO	VHLFIH KO
INSIG1	0.28	3.92	1.09	1.28	1.02
HMGCS1	0.19	3.58	0.68	1.00	1.25
ACSS2	0.43	2.89	1.24	1.30	1.38
MSMO1	0.27	2.56	0.70	1.03	1.15
SCD	0.57	2.26	1.30	1.40	1.50
LPIN1	0.43	2.25	0.96	1.30	1.82
TNFSF9	0.34	2.24	0.77	0.85	0.82
IDI1	0.28	2.22	0.61	0.99	1.23
ZC3H6	0.62	2.13	1.32	1.28	0.79
LDLR	0.49	2.11	1.04	1.27	1.19
S100A2	0.72	2.09	1.51	1.60	2.02
MVD	0.40	2.07	0.82	1.30	1.08
DHCR7	0.40	2.04	0.81	1.18	1.27
CYP51A1	0.42	1.99	0.84	0.90	1.33
LSS	0.48	1.98	0.94	1.52	1.30
SQLE	0.42	1.98	0.83	0.93	1.24
SPP1	0.31	1.96	0.61	0.69	0.60
FADS2	0.62	1.85	1.15	1.17	1.35
FDFT1	0.46	1.83	0.83	1.04	1.24
MVK	0.40	1.78	0.72	1.15	1.09
STARD4	0.58	1.72	1.01	0.90	1.17
JUND	0.64	1.72	1.10	1.17	1.48
ITM2B	0.72	1.69	1.22	1.12	0.87
FASN	0.72	1.66	1.19	1.42	1.12
ACSL1	0.58	1.65	0.96	0.99	1.50
TFRC	0.68	1.64	1.12	1.23	0.94
TACSTD2	0.41	1.61	0.66	1.35	0.96
HMGCR	0.45	1.57	0.70	0.85	1.05
CREBRF	0.72	1.56	1.13	1.05	1.13
ACSL3	0.71	1.56	1.10	1.07	1.44
PROSAPIP1	0.60	1.54	0.92	1.36	1.37
RPRD1A	0.75	1.52	1.15	1.12	1.31
FADS1	0.73	1.52	1.11	0.92	1.35
GPC1	0.64	1.51	0.97	1.46	0.92
PLCB4	0.71	1.51	1.08	1.37	1.07
DUSP5	0.62	1.50	0.93	1.25	1.55
SNX25	0.57	1.50	0.86	1.23	1.16
NSDHL	0.53	1.49	0.79	1.30	0.93
TUB	0.74	1.49	1.10	1.44	1.46
SOCS3	0.51	1.48	0.76	1.19	0.82
IRF2BPL	0.71	1.47	1.05	1.10	1.07

AP1M2	0.35	1.47	0.52	1.10	1.51
SC5DL	0.58	1.46	0.85	1.01	1.25
ID1	0.43	1.46	0.63	1.18	0.65
ACLY	0.77	1.46	1.12	1.01	0.98
MMAB	0.78	1.45	1.13	0.96	1.14
ID2	0.66	1.44	0.95	1.08	1.62
RNF168	0.64	1.44	0.92	1.02	1.11
ALAS1	0.73	1.43	1.04	0.97	2.32
SOD2	0.62	1.43	0.88	0.90	1.39
ARHGEF18	0.72	1.42	1.02	1.28	0.90
FLCN	0.64	1.42	0.91	1.09	1.32
ETV5	0.71	1.42	1.01	1.16	1.61
UBASH3B	0.78	1.42	1.10	1.15	1.07
TGIF1	0.59	1.40	0.83	0.99	0.89
KLF6	0.77	1.39	1.08	1.09	0.84
TMEM135	0.74	1.39	1.03	0.96	1.01
EBP	0.56	1.39	0.78	0.80	0.98
CHST15	0.77	1.39	1.07	1.18	1.21
CD276	0.73	1.38	1.01	1.28	1.03
FDPS	0.71	1.38	0.98	1.05	1.01
RRAGC	0.66	1.38	0.91	0.93	1.31

CCSER2	0.70	1.37	0.96	1.02	1.08
ACAT2	0.57	1.35	0.77	0.97	1.17
FBXL18	0.59	1.32	0.78	1.15	0.97
RNF149	0.72	1.32	0.94	1.03	1.32
HIF1A	0.44	1.31	0.58	1.06	1.14
SLC2A6	0.58	1.31	0.76	0.88	1.21
HIAT1	0.63	1.30	0.81	0.87	1.14
INPPL1	0.79	1.30	1.03	1.38	1.02
FAM213A	0.75	1.30	0.97	1.04	1.08
MAP3K3	0.73	1.29	0.95	1.36	1.21
DBI	0.62	1.28	0.79	1.10	1.10
ZFP36L2	0.71	1.28	0.91	1.02	1.22
TMEM97	0.63	1.27	0.80	1.20	1.22
TIMP2	0.74	1.26	0.94	1.51	0.87
GJC1	0.74	1.25	0.93	0.99	1.00
CACUL1	0.77	1.25	0.97	1.18	1.07
CYBRD1	0.69	1.25	0.86	1.19	0.85
PGRMC1	0.76	1.24	0.95	1.00	0.97
CD44	0.64	1.21	0.77	1.11	0.94

8.4 Hypoxia down-regulated genes defined in the HIF-1β KO cells

8.4.1 Genes that showed greater suppression by hypoxia in WT cells than mutant cells

The ratios of hypoxic fold regulations (fold change, FC) between WT cells and HIF-1β KO cells, i.e. FC(WT)/FC(1βKO)<0.8, are shown in the 2nd column. The hypoxia regulations in each cell background are shown in the 3rd-6th columns. The genes are ranked based on their hypoxia regulation in the HIF-1β mutant cells (i.e. the 3rd column).

Gene	WT/1βKO	1βKO	WT	DKO	VHLFIH KO
CHPF2	0.79	0.74	0.58	1.06	0.64
ASF1A	0.73	0.74	0.54	0.86	0.61
NXPE3	0.72	0.74	0.54	0.99	0.64
SLC5A6	0.79	0.79	0.62	0.96	1.12
SRSF2	0.80	0.83	0.66	1.03	0.94
PLK2	0.71	0.83	0.59	0.84	1.22

8.4.2 Genes that were down-regulated similarly by hypoxia in WT and in HIF-1β KO cells.

The ratios of hypoxic fold regulations (fold change, FC) between WT cells and HIF-1β KO cells, i.e. FC(WT)/FC(1βKO) is between 0.8 and 1.2, are shown in the 2nd column. The hypoxia regulations in each cell background are shown in the 3rd-6th columns. The genes are ranked based on their hypoxia regulation in the HIF-1β mutant cells (i.e. the 3rd column).

Gene	WT/1βKO	1βKO	WT	DKO	VHLFIH KO
LOC100506305	1.18	0.53	0.62	0.59	0.73
RNF145	1.05	0.56	0.58	0.88	0.55
GPAM	1.07	0.57	0.61	0.86	0.75
ARSJ	0.89	0.61	0.54	0.75	1.00
PTK2B	1.04	0.62	0.64	0.97	0.54
TRPC4	1.18	0.62	0.73	0.99	0.93
POP1	1.03	0.63	0.65	0.70	1.11
CTU2	0.88	0.65	0.57	0.93	1.09
MEST	0.81	0.66	0.53	1.11	0.56
GCLM	0.81	0.67	0.54	0.72	0.62
NOL6	0.93	0.67	0.62	0.98	1.41
RABL3	1.11	0.67	0.74	0.72	0.69
RCN2	1.15	0.67	0.77	0.88	0.79
DDX56	1.15	0.68	0.78	0.86	0.98
ARHGAP18	0.85	0.69	0.58	0.70	0.63
TRMT61A	0.96	0.69	0.66	1.01	1.20
LPCAT1	0.97	0.69	0.67	1.08	0.56

CD55	1.02	0.69	0.70	0.84	0.97
POGLUT1	1.15	0.69	0.79	0.84	1.13
MTMR10	0.89	0.70	0.62	0.91	0.64
GULP1	0.95	0.70	0.66	0.74	0.65
NEXN	1.10	0.70	0.77	1.10	1.02
POLR1E	1.19	0.70	0.83	0.97	0.88
BRMS1	0.90	0.71	0.63	0.91	1.16
RRP9	0.90	0.71	0.64	0.84	1.40
MSRB1	0.95	0.71	0.67	0.88	0.54
ABHD2	0.97	0.71	0.69	1.03	0.82
DHDDS	1.13	0.71	0.80	0.99	0.91
RRS1	0.92	0.72	0.66	0.96	2.03
CDCA3	0.95	0.72	0.68	0.85	0.68
PSMD12	0.95	0.72	0.69	0.98	0.91
NOP16	0.86	0.73	0.62	1.19	1.38
SLC25A12	0.97	0.73	0.72	0.87	0.75
SKP2	0.97	0.73	0.72	0.93	0.80
PNPO	1.05	0.73	0.76	1.00	1.24

DHX29	1.08	0.73	0.79	0.84	0.90
PDE12	1.08	0.73	0.79	0.95	1.15
SDPR	1.09	0.73	0.80	1.26	0.92
STXBP5	1.10	0.73	0.80	0.95	0.91
NIP7	0.91	0.74	0.67	0.87	1.28
PSME3	0.92	0.74	0.68	0.91	1.23
RABGGTB	1.07	0.74	0.79	0.90	1.05
GEMIN5	1.18	0.74	0.87	0.98	1.13
ODC1	0.84	0.75	0.63	0.97	1.64
NQO1	0.91	0.75	0.68	0.68	0.64
EIF5	0.91	0.75	0.68	0.80	1.11
WDR46	1.00	0.75	0.75	0.82	1.18
DNAJC2	1.01	0.75	0.76	0.76	1.14
ANXA1	1.07	0.75	0.80	0.77	0.78
CSTF2	1.08	0.75	0.81	0.82	0.91
NSMAF	1.08	0.75	0.81	0.92	1.04
FECH	1.18	0.75	0.89	1.02	0.79
CCDC86	0.81	0.76	0.61	1.12	1.27
PNO1	0.88	0.76	0.66	0.94	1.44
ARL2BP	0.90	0.76	0.68	0.75	1.02
FASTKD2	0.91	0.76	0.69	0.76	0.94
ZFHX4	1.04	0.76	0.80	0.86	0.65
L3MBTL2	1.15	0.76	0.87	1.05	0.99
LTV1	0.84	0.77	0.64	0.79	1.30
DCDC2	0.87	0.77	0.67	0.78	0.64
VPS13B	1.04	0.77	0.80	0.84	0.48
TDG	1.08	0.77	0.83	0.86	1.06
MRPS34	1.09	0.77	0.84	0.85	0.98
SRM	1.11	0.77	0.85	1.20	1.39
FUBP1	1.12	0.77	0.87	0.87	0.79
DNAJB11	0.86	0.78	0.67	0.84	0.86
NOC3L	0.87	0.78	0.67	0.75	1.22
OLR1	0.88	0.78	0.69	0.67	0.95
UTP20	0.93	0.78	0.73	0.86	1.01
RRP12	1.02	0.78	0.79	0.99	1.21
PLS1	1.09	0.78	0.84	0.78	0.95
CAP2	1.14	0.78	0.89	1.06	0.78
PSMC6	0.88	0.79	0.70	0.83	0.80
SHC1	0.91	0.79	0.71	1.04	0.50

CDCA8	0.94	0.79	0.75	1.20	0.75
PPIL1	0.96	0.79	0.75	0.75	1.11
MRPL4	1.00	0.79	0.79	0.96	1.17
IGFN1	1.00	0.79	0.79	0.67	0.61
DCAF13	1.01	0.79	0.80	0.92	1.25
PRMT5	1.02	0.79	0.81	0.96	1.09
IVD	1.02	0.79	0.81	1.12	0.87
PSMD6	1.04	0.79	0.82	0.87	0.99
ABCF2	1.10	0.79	0.87	0.95	1.24
ABCE1	1.12	0.79	0.88	0.88	1.26
PHLDB1	1.16	0.79	0.91	1.29	0.75
EHD1	0.96	0.80	0.77	1.05	0.76
POLE3	0.97	0.80	0.78	0.89	0.87
MBNL1	0.99	0.80	0.79	0.95	0.92
EIF2AK4	1.04	0.80	0.84	1.15	0.93
ZC3H7B	1.13	0.80	0.90	1.12	0.94
ASPM	1.17	0.80	0.93	0.74	0.49
SEC22B	0.82	0.81	0.66	0.85	0.78
PSMB2	0.90	0.81	0.73	1.09	0.94
PSMC2	0.91	0.81	0.73	0.81	0.83
NOP2	0.92	0.81	0.74	1.03	1.64
SRSF1	0.93	0.81	0.76	0.90	0.86
SAMHD1	0.94	0.81	0.76	0.95	0.92
ZNF512B	0.98	0.81	0.80	1.23	1.15
TROAP	1.02	0.81	0.82	0.78	0.81
SPAG5	1.06	0.81	0.86	0.94	0.70
MYBBP1A	1.12	0.81	0.90	1.32	1.40
ZFR	1.12	0.81	0.91	0.92	0.99
ZFP106	1.16	0.81	0.94	0.95	0.87
NAA15	0.90	0.82	0.74	0.95	1.11
CFL2	0.92	0.82	0.76	0.80	0.88
AURKA	1.00	0.82	0.82	0.90	0.71
ARHGDIA	1.03	0.82	0.84	1.21	1.10
SFPQ	1.17	0.82	0.96	0.99	0.98
CDC25B	1.19	0.82	0.97	1.08	0.72
PHB2	1.19	0.82	0.97	0.98	1.13
PSMD3	0.80	0.83	0.66	1.03	0.90

8.4.3 Genes that showed greater suppression by hypoxia in HIF-1β mutant than in the WT cells.

The ratios of hypoxic fold regulations (fold change, FC) between WT cells and HIF-1β KO cells, i.e. FC(WT)/FC(1βKO)>1.2, are shown in the 2nd column. The hypoxia regulations in each cell background are shown in the 3rd-6th columns. The genes are ranked based on their hypoxia regulation in the HIF-1β mutant cells (i.e. the 3rd column).

Gene	WT/1βKO	1βKO	WT	DKO	VHLFIH KO
GLIPR1	1.33	0.43	0.57	0.49	0.78
TFPI	1.75	0.52	0.92	0.70	0.75
ATF7IP	1.39	0.56	0.78	0.69	0.41
DIS3L	1.28	0.68	0.87	0.95	1.45
FERMT1	1.34	0.69	0.92	0.96	1.46
FHOD1	1.32	0.70	0.92	1.09	0.71
RMDN3	1.27	0.72	0.92	1.04	1.00
UROD	1.28	0.72	0.92	0.81	1.03
PDCD11	1.36	0.73	0.99	0.99	1.09

CARD10	1.36	0.73	0.99	1.08	0.59
POLR2G	1.22	0.74	0.91	0.90	0.90
ARHGAP23	1.21	0.75	0.90	1.37	0.84
AXL	1.25	0.75	0.93	1.06	0.93
COL4A3BP	1.21	0.76	0.93	1.00	0.72
CCNH	1.22	0.76	0.92	0.63	1.16
FZD6	1.25	0.76	0.95	0.87	0.81
TGFBRAP1	1.27	0.76	0.96	1.07	1.19
SPPL2A	1.29	0.76	0.98	0.93	0.81
ZNF532	1.31	0.76	0.99	0.94	1.05

UBR1	1.24	0.77	0.95	0.83	0.82
SEC24A	1.28	0.77	0.98	0.78	0.77
POLR1A	1.28	0.78	1.00	1.26	1.00
EIF6	1.21	0.80	0.96	0.99	0.99

CIRH1A	1.24	0.80	0.99	1.01	1.35
DKC1	1.20	0.81	0.97	1.01	1.49
DDX3X	1.20	0.82	0.99	1.13	1.13

8.5 Hypoxia up-regulated genes defined in the HIF-α DKO cells

The ratios of hypoxic fold regulations (fold change, FC) between WT cells and HIF-α DKO cells, i.e. FC(WT)/FC(DKO), are shown in the 2nd column. The hypoxia regulations in each cell background are shown in the 3rd-5th columns. The genes are ranked based on their hypoxia regulation in the HIF-α mutant cells (i.e. the 3rd column).

FC(WT)/FC(DKO)>1.2					
Gene	**WT/DKO**	DKO	WT	1βKO	VHLFIH KO
AHNAK2	1.39	1.97	2.74	1.44	0.46
PSAT1	1.95	1.73	3.37	1.25	2.09
FC(WT)/FC(DKO) between 0.8 and 1.2					
Gene	**WT/DKO**	DKO	WT	1βKO	VHLFIH KO
LAMA5	1.16	1.95	2.25	1.13	0.71
GNAS	0.88	1.64	1.44	1.11	1.00
FAM84B	1.01	1.60	1.62	1.16	1.09
FC(WT)/FC(DKO)<0.8					
Gene	**WT/DKO**	DKO	WT	1βKO	VHLFIH KO
PRMT7	0.51	2.36	1.21	0.81	0.95
TRAPPC2	0.68	1.75	1.19	0.78	0.79
ANKRD33B	0.72	1.70	1.22	1.16	1.39

8.6 Hypoxia down-regulated genes defined in the HIF-α DKO cells

The ratios of hypoxic fold regulations (fold change, FC) between WT cells and HIF-α DKO cells, i.e. FC(WT)/FC(DKO), are shown in the 2nd column. The hypoxia regulations in each cell background are shown in the 3rd-5th columns. The genes are ranked based on their hypoxia regulation in the HIF-α mutant cells (i.e. the 3rd column).

FC(WT)/FC(DKO)<0.8					
Gene	**WT/DKO**	DKO	WT	1βKO	VHLFIH KO
SEMA3C	0.79	0.59	0.46	0.78	0.86
FC(WT)/FC(DKO) between 0.8 and 1.2					
Gene	**WT/DKO**	DKO	WT	1βKO	VHLFIH KO
RBM4	1.10	0.45	0.49	0.90	0.98
CCNYL1	1.20	0.47	0.57	1.04	1.20
GLIPR1	1.16	0.49	0.57	0.43	0.78
TRIM56	0.97	0.52	0.50	1.02	0.78
NCBP2	1.17	0.58	0.68	0.83	1.06
PTCD3	1.07	0.58	0.62	0.88	0.92
FC(WT)/FC(DKO)>1.2					
Gene	**WT/DKO**	DKO	WT	1βKO	VHLFIH KO
KIAA1549	1.68	0.28	0.47	1.14	0.92
PAGR1	1.25	0.29	0.37	0.88	0.87
TXNIP	10.62	0.30	3.24	0.37	0.72
FGD6	2.54	0.33	0.83	0.85	0.66
PKNOX1	1.59	0.37	0.60	1.07	0.77
TRUB2	1.37	0.38	0.52	0.85	0.85
GLUD1	1.79	0.43	0.77	1.01	1.24
UHRF1BP1	1.91	0.43	0.81	0.99	1.17
TPM3	1.59	0.45	0.71	1.04	1.11
NFATC2IP	1.59	0.46	0.73	1.08	1.03
COMMD2	1.52	0.52	0.80	0.90	1.12
HCG11	1.53	0.54	0.82	1.07	0.68
RPL17	1.25	0.58	0.73	0.96	1.15
AFAP1L1	1.45	0.62	0.89	0.96	1.80

8.7 Hypoxia up-regulated genes defined in the VHLFIH KO cells

The hypoxic regulations in each cell background are shown. The genes are ranked based on their hypoxia regulation in the VHLFIH KO cells (i.e. the 2nd column).

Gene	VHLFIHKO	WT	DKO	1β KO
MARS2	2.33	0.73	1.14	0.80
ALAS1	2.32	1.04	0.97	1.43
ST3GAL1	2.18	1.36	1.05	1.27
STEAP3	2.14	0.86	1.35	0.95
HKDC1	2.08	2.09	1.06	1.26
SDCCAG3	2.05	0.94	0.98	1.03
LIF	2.05	0.98	1.01	1.06
RRS1	2.03	0.66	0.96	0.72
S100A2	2.02	1.51	1.60	2.09
TMEM158	1.96	1.13	1.33	0.85
KRT80	1.94	1.64	1.61	0.97
AMIGO2	1.86	1.50	1.01	1.16
CDC42EP3	1.85	0.72	1.09	0.95
C15orf52	1.83	1.30	1.04	0.91
URB2	1.82	0.83	1.05	0.84
NANP	1.82	0.93	0.98	1.13
AEN	1.82	0.65	0.82	0.94
LPIN1	1.82	0.96	1.30	2.25
ERRFI1	1.79	3.57	1.11	1.31
SLC7A2	1.76	0.81	1.02	0.91
CEBPG	1.76	1.84	1.15	1.23
DEAF1	1.76	1.18	1.28	1.30
PPRC1	1.64	0.97	1.20	0.91
CTPS1	1.62	0.98	1.16	1.00
COTL1	1.61	0.96	1.20	1.10
CDC42EP1	1.60	1.10	1.07	0.90
PYGB	1.60	1.46	1.36	1.27

8.8 Hypoxia down-regulated genes defined in the VHLFIH KO cells

The hypoxic regulations in each cell background are shown. The genes are ranked based on their hypoxia regulation in the VHLFIH KO cells (i.e. the 2nd column).

Gene	VHLFIHKO	WT	DKO	1bKO
SPARC	0.63	0.74	1.11	0.87
HSP90B1	0.63	1.12	0.99	0.87
CARD10	0.59	0.99	1.08	0.73
RASAL1	0.57	1.77	1.16	0.71
LPCAT1	0.56	0.67	1.08	0.69
TENM3	0.56	1.12	1.18	0.91
CDC25C	0.56	1.21	0.97	0.97
RNF145	0.55	0.58	0.88	0.56
MVP	0.55	1.32	1.00	0.96
TUG1	0.54	1.17	1.11	0.93
TNS1	0.53	1.56	1.24	0.87
MORC2	0.52	0.99	1.23	1.05
CD24	0.51	2.19	0.90	1.33
SHC1	0.50	0.71	1.04	0.79
CSPG4	0.50	1.34	1.10	1.10
ASPM	0.49	0.93	0.74	0.80
VPS13B	0.48	0.80	0.84	0.77
NBEAL1	0.48	1.04	0.88	0.89
AHNAK2	0.46	2.74	1.97	1.44
SYNE2	0.42	1.53	1.08	1.00
ATF7IP	0.41	0.78	0.69	0.56
CEP41	0.37	0.88	0.83	0.78
SAMD9	0.32	0.92	0.55	0.78

8.9 HIF-1α (and HIF-2α) differential binding sites

HIF sites in the hypoxic WT cells (under either 6h, 16h or 48h hypoxia) and normoxic VHLKO cells were compared using the GLM method with a cut-off of $p<0.05$. There were no VHL KO-specific binding sites identified in this statistical analysis.

HIF-1α differential binding sites	chromosome	start	end	nearest gene	Adjusted *p*-value
6h hypoxia	chr12	1683339	1683850	FBXL14	0.040
	chr8	43092677	43093448	HGSNAT	0.027
16h hypoxia	chr8	43092677	43093448	HGSNAT	0.014
48h hypoxia	chr8	43092677	43093448	HGSNAT	0.011

HIF-2α differential binding sites	chromosome	start	end	nearest gene	Adjusted *p*-value
6h hypoxia	chr8	23202587	23203284	LOXL2	0.050
	chr8	43092677	43093448	HGSNAT	0.024
16h hypoxia	chr1	8271792	8272575	SLC45A1	0.031
	chr10	14438914	14439685	MIR1265	0.014
	chr22	18543721	18544386	PEX26	0.014
	chr8	23202587	23203284	LOXL2	0.009
	chr8	43092677	43093448	HGSNAT	0.021
48h hypoxia	chr10	14438914	14439685	MIR1265	0.043
	chr8	43092677	43093448	HGSNAT	0.011

8.10 HIF-1β differential binding sites

The sites in the hypoxic WT cells and PBRM1 KO cells were compared using the GLM method with a cut-off of $p<0.05$.

HIF- 1β differential binding sites	chromosome	start	end	nearest gene	Adjusted *p*-value
WT	chr10	6243172	6244034	PFKFB3	0.037
	chr10	133794925	133796071	BNIP3	0.006
	chr11	568342	569249	MIR210HG	0.001
	chr8	28269073	28270099	FBXO16	0.015
PBRM1 KO	chr5	3392202	3393008	LOC285577	0.035

8.11 RNA-seq mapped read counts

Cell line	Condition	Mapped reads
HKC-8 HIF-1β KO	21% O_2 Rep 1	52,352,960
HKC-8 HIF-1β KO	21% O_2 Rep 2	48,746,479
HKC-8 HIF-1β KO	0.5% O_2 (24h) Rep 1	50,771,082
HKC-8 HIF-1β KO	0.5% O_2 (24h) Rep 2	52,578,671
HKC-8 VHLFIH KO	21% O_2 Rep 1	54,122,790
HKC-8 VHLFIH KO	21% O_2 Rep 2	58,269,864
HKC-8 VHLFIH KO	0.5% O_2 (24h) Rep 1	49,932,089
HKC-8 VHLFIH KO	0.5% O_2 (24h) Rep 2	53,297,078

8.12 ChIP-seq mapped read counts

Cell line	ChIP-seq	Condition	Mapped reads
HKC-8 WT	HIF-1α	21% O_2	13,595,336
HKC-8 WT	HIF-2α	21% O_2	13,266,606
HKC-8 WT	HIF-1β	21% O_2	14,074,326
HKC-8 WT	HIF-1α	0.5% O_2 (6h) Rep 1	20,821,458
HKC-8 WT	HIF-2α	0.5% O_2 (6h) Rep 1	18,634,757
HKC-8 WT	HIF-1β	0.5% O_2 (6h) Rep 1	17,037,703
HKC-8 WT	HIF-1α	0.5% O_2 (6h) Rep 2	15,571,657
HKC-8 WT	HIF-2α	0.5% O_2 (6h) Rep 2	16,716,870
HKC-8 WT	HIF-1β	0.5% O_2 (6h) Rep 2	12,544,961
HKC-8 WT	HIF-1α	3% O_2 (6h) Rep 1	17,799,251
HKC-8 WT	HIF-2α	3% O_2 (6h) Rep 1	18,592,234
HKC-8 WT	HIF-1β	3% O_2 (6h) Rep 1	18,405,322
HKC-8 WT	HIF-1α	3% O_2 (6h) Rep 2	13,169,642
HKC-8 WT	HIF-2α	3% O_2 (6h) Rep 2	13,282,788
HKC-8 WT	HIF-1β	3% O_2 (6h) Rep 2	13,645,185
HKC-8 WT	HIF-1α	0.5% O_2 (16h) Rep 1	14,397,829
HKC-8 WT	HIF-2α	0.5% O_2 (16h) Rep 1	13,049,427
HKC-8 WT	HIF-1β	0.5% O_2 (16h) Rep 1	15,299,803
HKC-8 WT	HIF-1α	0.5% O_2 (16h) Rep 2	10,265,623
HKC-8 WT	HIF-2α	0.5% O_2 (16h) Rep 2	17,964,698
HKC-8 WT	HIF-1β	0.5% O_2 (16h) Rep 2	13,049,427
HKC-8 WT	HIF-1α	0.5% O_2 (48h) Rep 1	13,507,819
HKC-8 WT	HIF-2α	0.5% O_2 (48h) Rep 1	13,826,582
HKC-8 WT	HIF-1β	0.5% O_2 (48h) Rep 1	13,304,101
HKC-8 WT	HIF-1α	0.5% O_2 (48h) Rep 2	13,102,871
HKC-8 WT	HIF-2α	0.5% O_2 (48h) Rep 2	12,643,629
HKC-8 WT	HIF-1β	0.5% O_2 (48h) Rep 2	13,777,633
HKC-8 HIF1/2α KO	HIF-1α	21% O_2	61,180,386
HKC-8 HIF1/2α KO	HIF-2α	21% O_2	63,389,949
HKC-8 HIF1/2α KO	HIF-1β	21% O_2	48,636,427
HKC-8 HIF-1β KO	HIF-1α	21% O_2	62,349,537
HKC-8 HIF-1β KO	HIF-2α	21% O_2	52,191,795

HKC-8 HIF-1β KO	HIF-1β	21% O_2	56,508,234
HKC-8 VHL KO DN5	HIF-1β	21% O_2	21,958,811
HKC-8 VHL KO DN7	HIF-1β	21% O_2	18,019,774
HKC-8 VHL KO DN5	HIF-1α	21% O_2 Rep 1	38,198,106
HKC-8 VHL KO DN5	HIF-2α	21% O_2 Rep 1	28,257,555
HKC-8 VHL KO DN5	HIF-1β	21% O_2 Rep 1	34,040,913
HKC-8 VHL KO DN5	HIF-1α	21% O_2 Rep 2	33,507,845
HKC-8 VHL KO DN5	HIF-2α	21% O_2 Rep 2	30,132,951
HKC-8 VHL KO DN5	HIF-1β	21% O_2 Rep 2	30,881,835
HKC-8 VHLFIH KO	HIF-1α	21% O_2 Rep 1	30,857,681
HKC-8 VHLFIH KO	HIF-2α	21% O_2 Rep 1	30,618,286
HKC-8 VHLFIH KO	HIF-1β	21% O_2 Rep 1	30,690,076
HKC-8 VHLFIH KO	HIF-1α	21% O_2 Rep 2	34,649,879
HKC-8 VHLFIH KO	HIF-2α	21% O_2 Rep 2	15,703,657
HKC-8 VHLFIH KO	HIF-1β	21% O_2 Rep 2	49,030,723
HKC-8 PBRM1VHL KO DN20	HIF-1β	21% O_2	20,009,834
HKC-8 PBRM1VHL KO DN29	HIF-1β	21% O_2	19,170,925
HKC-8 PBRM1 KO DN5	HIF-1β	0.5% O_2 (16h)	15,409,566
HKC-8 PBRM1 KO DN14	HIF-1β	0.5% O_2 (16h)	20,317,306

8.13 List of abbreviations

2-OG	2-Oxoglutarate
3C	Chromatin Conformation Capture assay
ACSS2	Acyl-CoA Synthetase Short Chain Family Member 2
ACTG	Gamma actin
aHIF	Antisense HIF-1α
ACOX1	Acyl-CoA Oxidase 1
AHR	Aryl Hydrocarbon Receptor
AKT1	Serine/Threonine Kinase 1
ALDOA	Aldolase A
ANG-2	Angiopoietin 2
AP-1	Activator Protein 1
ARNT	Aryl hydrocarbon Receptor Nuclear Translocator
ATAC-seq	Assay for Transposase-Accessible Chromatin using sequencing
ATF-4	Activating Transcription Factor-4
ATP	Adenosine Triphosphate
ATP9B	ATPase Phospholipid Transporting 9B (Putative)
BCL2	Apoptosis regulator
bHLH	Basic helix-loop-helix
BNIP3	BCL2 Interacting Protein 3
BNIP3L	BCL2 Interacting Protein 3 Like
bp	base pair
CA9	Carbonic Anhydrase 9
CBP	CREB-binding protein
CCND1	Cyclin D1
ccRCC	Clear-cell Renal Cell Carcinoma
CDK2	Cyclin Dependent Kinase 2
cDNA	Complementary DNA
CEBPB	CCAAT-enhancer binding protein
CHIP	Carboxyl terminus of Hsc70-interacting protein
ChIP	Chromatin Immunoprecipitation
ChIP-seq	Chromatin Immunoprecipitation-sequencing
CK1	Casein Kinase 1
CREB	CAMP Responsive Element Binding Protein

CRISPR	Clustered Regularly Interspaced Short Palindromic Repeats
CT	Cycle Threshold
C-TAD	C-terminal Activation Domain
CXCR4	C-X-C motif Receptor 4
CYTIP	Cytohesin 1 Interacting Protein
DDIT4	DNA Damage Inducible Transcript 4
DEC	Differentiated Embryo Chondrocyte
DKO	Double Knockout
DMOG	Dimethyloxallyl Glycine
DNA	Deoxyribonucleic Acid
DNAse1	Deoxyribonuclease 1
DNMT3a	DNA Methyltransferase 3 Alpha
dNTP	Deoxyribonucleotide Triphosphate
E2F1	E2F Transcription Factor 1
E-box	Enhancer box
EDTA	Ethylendiamine Tetraacetic Acid disodium salt
EGFP	Enhanced Green Fluorescent Protein
EGR1	Early Growth Response 1
EGLN3	Egl-9 Family Hypoxia Inducible Factor 3
eIF4E2	Eukaryotic Translation Initiation Factor 4E Family Member 2
EMSA	Electrophoretic Mobility Shift Assay
ENO2	Enolase 2
EPAS1	Endothelial PAS domain protein 1
EPO	Erythropoetin
ESCs	Embryonic Stem Cells
FAIRE	Formaldehyde Assisted Isolation of Regulatory Elements
Fe2+	Iron (II)
FIH	Factor Inhibiting HIF
FNR	Fumarate and Nitrate Reduction Regulators
FH	Fumarate Hydratase
FOXO3a	Forkhead Box O3
FAS	Fas Cell Surface Death Receptor
FLT1	Fms Related Tyrosine Kinase 1
GADD45A	Growth Arrest And DNA Damage Inducible Alpha
GLM	Generalised Linear Model
GLUT1	Glucose Transporter 1
GPR61	G Protein-Coupled Receptor 61
GRB10	Growth Factor Receptor Bound Protein 10
GSEA	Gene Set Enrichment Analysis
GWAS	Genome-wide Association Study
GYS1	Glycogen Synthase 1
H3	Histone 3
H3K27me3	Histone 3 lysine 27 trimethylation
H3K27ac	Histone 3 lysine 27 acetylation
HAP1	Heme Activator Protein 1
HARS	histidyl-tRNA synthase
HDAC	Histone Deacetylase
HEPES	4-(2-hydroxyethyl)-1-piperazineethanesulfonic acid
HES	Hes Family BHLH Transcription Factor
HEY2	Hes Related Family BHLH Transcription Factor With YRPW Motif 2
HGSNAT	Heparin-Alpha-Glucosaminide N-Acetyletransferase
HIF	Hypoxia Inducible Factor
HK1	Hexokinase 1
HMGCS1	3-Hydroxy-3-Methylglutaryl-CoA Synthase 1

HRE	Hypoxia Responsive Element
HRP	Horse-radish Peroxidase
HPRT	Hypoxanthine-guanine Phosphoribosyltransferase
HSP70	Heat Shock Protein
IB	Immunoblot
ILB	Igepal Lysis Buffer
IKKB	IκB kinase beta
INSIG1	Insulin Induced Gene 1
JARID1C	Jumonji, AT rich interactive domain 1C
JmjC-KDMs	JmjC-domain containing histone lysine demethylases
kb	kilo base
KCl	Potassium chloride
kPa	Kilopascal
KO	Knockout
LB	Lysogeny Broth
LDHA	Lactate Dehydrogenase A
LiCl	Lithium Chloride
lincRNA	Long intergenic noncoding RNA
LOX	Lysyl Oxidase
LZIP	Lucine Zipper
MACS	Model-based Analysis of ChIP-Seq
MART1	Melan-A
Max	Myc-associated factor X
MgCl	Magnesium Chloride
MITF	microphthalmia-associated transcription factor
miRNA	microRNA
mM	milli molar
mmHg	millimeter of mercury
MMP1	Matrix Metallopeptidase 1
mRNA	messenger RNA
MRPL51	Mitochondrial Ribosomal Protein L51
Msn2	stress-responsive transcription factor
mTOR	mammalian target of rapamycin
myc	Myc Proto-Oncogene
NaCl	Sodium Chloride
$NaHCO_3$	Sodium Bicarbonate
NDRG1	N-myc Down-regulated Gene 1
NF-κB	Nuclear factor kappa-light-chain-enhancer of activated B cells
NFY	Nuclear transcription factor Y
NICD	Notch intracellular domain
NOXA	Phorbol-12-Myristate-13-Acetate-Induced Protein 1
NOMe-seq	Nucleosome Occupancy and Methylome Sequencing
NPAS	Neuronal PAS Domain Protein
N-TAD	N-terminal Transactivation Domain
ODDD	Oxygen Dependent Degradation Domain
Oct-4	Octamer-binding Transcription Factor 4
p53	Tumor protein p53
PAI-1	Plasminogen Activator Inhibitor-1
PBAF	Polybromo- and BRG1-associated factors containing complex
PBRM1	Polybromo 1
PBS	Phosphate Buffered Saline
PBS-T	Phosphate Buffered Saline Tween
PCR	Polymerase Chain Reaction
PDGF	Platelet Derived Growth Factor Subunit

PDK1	Pyruvate Dehydrogenase Kinase 1
PER	Period circadian protein
PGK1	Phosphoglycerate Kinase 1
PHD	Prolyl Hydroxylase Domain-containing protein
PI3K	Phosphatidylinositol-4,5-bisphosphate 3-kinase
PPAR-γ	Peroxisome Proliferator-activated Receptor gamma
PRC2	Polycomb Repressive Complex2
pVHL	von Hippel-Lindau protein
PVT1	PVT1 Oncogene (Non-Protein Coding)
PSMC2	Proteasome 26S Subunit, ATPase 2
qPCR	quantitative PCR
Rap1	Repressor/activator Protein 1
RBM4	RNA Binding Motif Protein 4
RCC	Renal Cell Carcinoma
REST	RE1 Silencing Transcription Factor
RNA	Eibonucleic acid
RNA pol2	RNA polymerase II
RXRα	Retinoid X Receptor Alpha
ROS	Reactive Oxygen Species
ROX1	RNA on the X
rpm	revolutions per minute
RPKM	Reads Per Kilobase per Million mapped reads
RT-qPCR	Quantitative Reverse Transcription PCR
S100A2	S100 Calcium Binding Protein A2
SDS	Sodium Dodecyl Sulphate
SDS-PAGE	Sodium Dodecyl Sulphate Polyacrylamide Gel Electrophoresis
SEM	Standard Error of the Mean
SETD2	SET domain containing 2
sgRNA	Single guide RNA
SILAC	Stable isotope labeling with amino acids in cell culture
SIM	Single-minded
siRNA	Silencing RNA
SP1	Specificity protein 1
SREBP	Sterol regulatory element-binding protein
SRM	Selected Reaction Monitoring
STAT3	Signal Transducer and Activator of Transcription 3
SWI/SNF	Switch/sucrose nonfermentable chromatin remodelling proteins
Set7/9	SET domain containing lysine methyltransferase SETD7
SMRT	Silencing mediator for retinoid and thyroid receptors
SDF1	Stromal cell-derived factor 1
TE	Tris-EDTA
TF	Transcription Factor
TPIC	Tree shape Peak Identification for ChIP-seq
TRIS	Tris(hydroxymethyl)aminomethane
TSS	Transcriptional start site
TXNIP	Thioredoxin-interacting Protein
TYR	Tyrosinase
USF	Upstream stimulatory factor
USP9x	Ubiquitin Specific Peptidase 9, X-Linked
UTX	Ubiquitously transcribed X chromosome tetratricopeptide repeat protein
VEGF	Vascular Endothelial Growth Factor
WT	Wild type
XRE	Xenobiotic Responsive Element
Yap4	Yeast activator protein

8.14 Publication arising from this thesis

A manuscript related to my thesis work has been submitted in May 2018.

Smythies, J., Sun, M., Masson, N., Salama, R., Simpson, P., Murray, E., Neumann, V., Cockman, M.E., Choudhry, H., Ratcliffe, P.J., Mole, D.R. (2018). Inherent DNA binding specificities of the HIF-1α and HIF-2α transcription factors in chromatin.

9

Bibliography

Adam, J., Hatipoglu, E., O'Flaherty, L., Ternette, N., Sahgal, N., Lockstone, H., et al. (2011). Renal Cyst Formation in Fh1-Deficient Mice Is Independent of the Hif/Phd Pathway: Roles for Fumarate in KEAP1 Succination and Nrf2 Signaling. *Cancer Cell*, 20(4), 524–537.

Ameri, K1., Lewis, CE., Raida, M., Sowter, H., Hai, T., Harris, AL. (2004). Anoxic induction of ATF-4 through HIF-1-independent pathways of protein stabilization in humancancer cells. *Blood*, 103(5):1876-82.

Angel, P., Imagawa, M., Chiu, R., Stein, B., et al. (1987). Phorbol ester-inducible genes contain a common cis element recognized by a TPA-modulated trans-acting factor. *Cell*, 49(6):729-39.

Appelhoff, RJ., Tian, YM., Raval, RR., Turley, H., Harris, AL., Pugh, CW., Ratcliffe, PJ., Gleadle, JM. (2014). Differential function of the prolyl hydroxylases PHD1, PHD2, and PHD3 in the regulation of hypoxia-inducible factor. *J Biol Chem*, 279(37):38458-65.

Audenet, F., Cancel-Tassin, G., Pierre, B., et al. (2014). Germline genetic variations at 11q13 and 12p11 locus modulate age at onset for renal cell carcinoma. *J Urol*, 191:487–92.

Bagnall, J., Leedale, J., Taylor, SE., Spiller, DG., White, MR., Sharkey, KJ., Bearon, RN., Sée V. (2014). Tight control of hypoxia-inducible factor-α transient dynamics is essential for cell survival in hypoxia. *J Biol Chem*, 289(9):5549-64.

Bailey, T., Krajewski, P., Ladunga, I., Lefebvre, C., et al. (2013). Practical guidelines for the comprehensive analysis of ChIP-seq data. *PLoS Comput Biol*, 9(11):e1003326.

Bailey, TL., Boden, M., Buske, FA., Frith, M., et al. (2009). MEME SUITE: tools for motif discovery and searching. *Nucleic Acids Res.* 37(Web Server issue):W202-8.

Baranova, O., Miranda, LF., Pichiule, P., Dragatsis, I., Johnson, RS., Chavez, JC. (2007). Neuron-specific inactivation of the hypoxia inducible factor 1 alpha increases brain injury in a mouse model of transient focal cerebral ischemia. *J Neurosci*, 27(23):6320-32.

Bayer, C., Shi, K., Astner, ST., Maftei, CA., Vaupel, P. (2011). Acute versus chronic hypoxia: why a simplified classification is simply not enough. *Int J Radiat Oncol Biol Phys*, 80(4):965-8.

Becerra, M., Lombardía-Ferreira, LJ., Hauser, NC., Hoheisel, JD., Tizon, B., Cerdán, ME. (2002). The yeast transcriptome in aerobic and hypoxic conditions: effects of hap1, rox1, rox3 and srb10 deletions. *Mol Microbiol*, 43(3):545-55.

Becker, M., Baumann, C., John, S., Walker, DA., Vigneron, M., McNally, JG., Hager, GL. (2002). Dynamic behavior of transcription factors on a natural promoter in living cells. *EMBO Rep*, 3(12):1188-94.

Bedford, DC., Kasper, LH., Fukuyama, T., Brindle, PK. (2010). Target gene context influences the transcriptional requirement for the KAT3 family of CBP and p300 histone acetyltransferases. *Epigenetics*, 5(1):9-15.

Bellot, G., Garcia-Medina, R., Gounon, P., Chiche, J., Roux, D., Pouysségur, J., Mazure, NM. (2009). Hypoxia-induced autophagy is mediated through hypoxia-inducible factor induction of BNIP3 and BNIP3L via their BH3 domains. *Mol Cell Biol*, 29(10):2570-81.

Benita, Y., Kikuchi, H., Smith, AD., Zhang, MQ., Chung, DC., Xavier, RJ. (2009). An integrative genomics approach identifies Hypoxia Inducible Factor-1 (HIF-1)-target genes that form the core response to hypoxia. *Nucleic Acids Res*, 37(14):4587-602.

Berra, E., Benizri, E., Ginouvès, A., Volmat, V., Roux, D., Pouysségur, J. (2003). HIF prolyl-hydroxylase 2 is the key oxygen sensor setting low steady-state levels of HIF-1alpha in normoxia. *EMBO J*, 22(16):4082-90.

Berry, DB., Gasch, AP. (2008). Stress-activated genomic expression changes serve a preparative role for impending stress in yeast. *Mol Biol Cell*, 19(11):4580-7.

Bertout, JA., Patel, SA., Simon, MC. (2008). The impact of O2 availability on human cancer. Nat Rev *Cancer*, 8(12):967-75.

Bertout, JA., Majmundar, AJ., Gordan, JD., et al. (2009). HIF2alpha inhibition promotes p53 pathway activity, tumor cell death, and radiation responses. *Proc Natl Acad Sci U S A*, 106:14391–6.

Bieda, M., Xu, X., Singer, MA., Green, R., Farnham, PJ. (2006). Unbiased location analysis of E2F1-binding sites suggests a widespread role for E2F1 in the human genome. *Genome Res*, 16(5):595-605.

Biggin, MD. (2011). Animal Transcription Networks as Highly Connected, Quantitative Continua. Dev *Cell*, 21(4):611-26.

Blouw, B1., Song, H., Tihan, T., Bosze, J., Ferrara, N., Gerber, HP., Johnson, RS., Bergers, G. (2003). The hypoxic response of tumors is dependent on their microenvironment. *Cancer Cell*, 4(2):133-46.

Bordji, K., Grandval, A., Cuhna-Alves, L., Lechapt-Zalcman, E., Bernaudin, M. (2014). Hypoxia-inducible factor-2α (HIF-2α), but not HIF-1α, is essential for hypoxic induction of class III β-tubulin expression in human glioblastoma cells. *FEBS J*, 281(23):5220-36.

Bosisio, D., Marazzi, I., Agresti, A., Shimizu, N., Bianchi, ME., Natoli, G. (2006). A hyper-dynamic equilibrium between promoter-bound and nucleoplasmic dimers controls NF-kappaB-dependent gene activity. *EMBO J,* 25(4):798-810.

Bracken, CP., Fedele, AO., Linke, S., Balrak, W., Lisy, K., Whitelaw, ML., Peet, DJ.(2006). Cell-specific regulation of hypoxia-inducible factor (HIF)-1alpha and HIF-2alphastabilization and transactivation in a graded oxygen environment. *J Biol Chem*, 281(32):22575-85.

Brahimi-Horn, MC., Chiche, J., Pouysségur, J. (2007). Hypoxia and cancer. *J Mol Med (Berl*), 85(12):1301-7.

Brewster, RC., Weinert, FM., Garcia, HG., Song, D., Rydenfelt, M., Phillips, R. (2014). The transcription factor titration effect dictates level of gene expression. *Cell*, 156(6):1312-1323.

Brizel, DM., Scully, SP., Harrelson, JM., Layfield, LJ., Bean, JM., Prosnitz, LR., Dewhirst, MW. (1996). Tumor oxygenation predicts for the likelihood of distant metastases in human soft tissue sarcoma. *Cancer Res*, 56(5):941-3.

Brown, JM., Wilson, WR. (2004). Exploiting tumour hypoxia in cancer treatment. *Nat Rev Cancer*, 4(6):437-47.

Brugarolas, J., Kaelin, WG Jr. (2004). Dysregulation of HIF and VEGF is a unifying feature of the familial hamartoma syndromes. *Cancer Cell*, 6(1):7-10.

Brugarolas, J. (2013). PBRM1 and BAP1 as novel targets for renal cell carcinoma. *Cancer J*, 19(4):324-32.

Brugarolas, J. (2014). Molecular genetics of clear-cell renal cell carcinoma. *J Clin Oncol*, 32(18):1968-76.

Bruning, U., Cerone, L., Neufeld, Z., Fitzpatrick, SF., Cheong, A., Scholz, CC., Simpson, DA., Leonard, MO., Tambuwala, MM., Cummins, EP., Taylor, CT. (2011). MicroRNA-155 promotes resolution of hypoxia-inducible factor 1alpha activity during prolongedhypoxia. *Mol Cell Biol*, 31(19):4087-96.

Buenrostro, JD., Wu, B., Chang, HY., Greenleaf, WJ. (2015). ATAC-seq: A Method for Assaying Chromatin Accessibility Genome-Wide. *Curr Protoc Mol Biol*, 109:21.29.1-9.

Burgin, E., Salehi-Reyhani, A., Barclay, M., Brown, A., Kaplinsky, J., Novakova, M., Neil, MA., Ces, O., Willison, KR., Klug, DR. (2014). Absolute quantification of protein copy number using a single-molecule-sensitive microarray. *Analyst*, 139(13):3235-44.

Burroughs, SK., Kaluz, S., Wang, D., Wang, K., Van Meir, EG., Wang, B. (2013). Hypoxia inducible factor pathway inhibitors as anticancer therapeutics. *Future Med Chem*, 5(5):553-72.

Cancer Genome Atlas Research Network. Comprehensive molecular characterization of clear cell renal cell carcinoma. (2013). *Nature*, 499(7456):43-9.

Carmeliet, P., Dor, Y., Herbert, JM., Fukumura, D., et al. (1998). Role of HIF-1alpha in hypoxia-mediated apoptosis, cell proliferation and tumour angiogenesis. *Nature*, 394(6692):485-90.

Carroll, JS., Meyer, CA., Song, J., Li, W., et al. (2006). Genome-wide analysis of estrogen receptor binding sites. *Nat Genet*, 38(11):1289-97.

Cavadas, MA., Mesnieres, M., Crifo, B., Manresa, MC., et al. (2015). REST mediates resolution of HIF-dependent gene expression in prolonged hypoxia. *Sci Rep*, 5:17851.

Chen, W., Hill, H., Christie, A., Kim, MS., Holloman, E., et al. (2016). Targeting renal cell carcinoma with a HIF-2 antagonist. *Nature*, 539(7627):112-117.

Chi, JT., Wang, Z., Nuyten, DS., Rodriguez, EH., Schaner, ME., Salim Aet al. (2006). Gene expression programs in response to hypoxia: cell type specificity and prognosticsignificance in human cancers. *PLoS Med*, 3(3):e47.

Cho, H., Du, X., Rizzi, JP., Liberzon, E., Chakraborty, AA., Gao, W., Carvo, I., et al. (2016). On-target efficacy of a HIF-2α antagonist in preclinical kidney cancer models. *Nature*, 539(7627):107-111.

Choi, SM., Cho, HJ., Cho, H., Kim, KH., Kim, JB., Park, H. (2008). Stra13/DEC1 and DEC2 inhibit sterol regulatory element binding protein-1c in a hypoxia-inducible factor-dependent mechanism. *Nucleic Acids Res*. 36(20):6372-85.

Choudhry, H., Schödel, J., Oikonomopoulos, S., Camps, C., Grampp, S., Harris, AL., Ratcliffe, PJ., Ragoussis, J., Mole, DR. (2014). Extensive regulation of the non-coding transcriptome by hypoxia: role of HIF in releasing pausedRNApol2. *EMBO Rep*, 15(1):70-6.

Chowdhury, B., Porter, EG., Stewart, JC., Ferreira, CR., Schipma, MJ., Dykhuizen, EC. (2016). PBRM1 Regulates the Expression of Genes Involved in Metabolism and Cell Adhesion in Renal Clear Cell Carcinoma. *PLoS One*, 11(4):e0153718.

Clifford, SC., Cockman, ME., Smallwood, AC., Mole, DR., Woodward, ER., Maxwell, PH., Ratcliffe, PJ., Maher, ER. (2001). Contrasting effects on HIF-1alpha regulation by disease-causing pVHL mutations correlate with patterns of tumourigenesis in von Hippel-Lindau disease. *Hum Mol Genet*, 10(10):1029-38.

Cockman, ME., Masson, N., Mole, DR., Jaakkola, P., Chang, GW., Clifford, SC., Maher, ER., Pugh, CW., Ratcliffe, PJ., Maxwell, PH. (2000). Hypoxia inducible factor-alpha binding and ubiquitylation by the von Hippel-Lindau tumor suppressor protein. *J Biol Chem*, 275(33):25733-41.

Coleman, ML., McDonough, MA., Hewitson, KS., Coles, C., Mecinovic, J,. et al. (2007). Asparaginyl hydroxylation of the Notch ankyrin repeat domain by factor inhibiting hypoxia-inducible factor. *J Biol Chem*. 282(33):24027-38.

Compernolle, V., Brusselmans, K., Acker, T., Hoet, P., et al. (2002). Loss of HIF-2alpha and inhibition of VEGF impair fetal lung maturation, whereas treatment with VEGF prevents fatal respiratory distress in premature mice. *Nat Med*, 8(7):702-10.

Covello, KL., Kehler, J., Yu, H., Gordan, JD., Arsham, AM., Hu, CJ., Labosky, PA., Simon, MC., Keith, B. (2006). HIF-2alpha regulates Oct-4: effects of hypoxia on stem cell function, embryonic development, and tumor growth. *Genes Dev*, 20(5):557-70.

Cummins, EP., Berra, E., Comerford, KM., Ginouves, A., et al. (2006). Prolyl hydroxylase-1 negatively regulates IkappaB kinase-beta, giving insight into hypoxia-induced NFkappaB activity. *Proc Natl Acad Sci U S A*, 103(48):18154-9.

Cummins, EP., Taylor, CT. (2005). Hypoxia-responsive transcription factors. *Pflugers Arch*, 450(6):363-71.

Dale, RK., Pedersen, BS., Quinlan, AR. (2011). Pybedtools: a flexible Python library for manipulating genomic datasets and annotations. *Bioinformatics*, 27(24):3423-4.

Dalgliesh, GL., Furge, K., Greenman, C., Chen, L,. et al. (2010). Systematic sequencing of renal carcinoma reveals inactivation of histone modifying genes. *Nature*, 463(7279):360-3.

Dames, SA., Martinez-Yamout, M., De Guzman, RN., Dyson, HJ., Wright, PE. (2002). Structural basis for Hif-1 alpha /CBP recognition in the cellular hypoxic response. *Proc Natl Acad Sci U S A*, 99(8):5271-6.

Davidson, EH. (2010). Emerging properties of animal gene regulatory networks. *Nature*, 468(7326):911-20.

Davies, JO., Telenius, JM., McGowan, SJ., Roberts, NA., Taylor, S., Higgs, DR., Hughes, JR. (2016). Multiplexed analysis of chromosome conformation at vastly improved sensitivity. *Nat Methods*, 13(1):74-80.

Dayan, F., Roux, D., Brahimi-Horn, MC., Pouyssegur, J., Mazure, NM. (2006). The oxygen sensor factor-inhibiting hypoxia-inducible factor-1 controls expression of distinct genes through the bifunctional transcriptional character of hypoxia-inducible factor-1alpha. *Cancer Res*, 66(7):3688-98.

Dekker, J., Marti-Renom, MA., Mirny, LA. (2013). Exploring the three-dimensional organization of genomes: interpreting chromatin interactiondata. *Nat Rev Genet*, 14(6):390-403.

del Peso, L., Castellanos, MC., Temes, E., Martin-Puig, S., Cuevas, Y., Olmos, G., Landazuri, MO. (2003). The von Hippel Lindau/hypoxia-inducible factor (HIF) pathway regulates the transcription of the HIF-proline hydroxylase genes in response to low oxygen. *J Biol Chem*, 278(49):48690-5.

Dengler, VL., Galbraith, M., Espinosa, JM. (2014). Transcriptional regulation by hypoxia inducible factors. *Crit Rev Biochem Mol Biol*, 49(1):1-15.

Denko, NC., Giaccia, AJ. (2001). Tumor hypoxia, the physiological link between Trousseau's syndrome (carcinoma-induced coagulopathy) and metastasis. *Cancer Res*, 61(3):795-8.

Denko, NC., Fontana, LA., Hudson, KM., Sutphin, PD., Raychaudhuri, S., Altman, R., Giaccia, AJ. (2003). Investigating hypoxic tumor physiology through gene expression patterns. *Oncogene*, 22(37):5907-14.

De Santis, V., Singer, M. (2015). Tissue oxygen tension monitoring of organ perfusion: rationale, methodologies, and literature review. *Br J Anaesth*, 115(3):357-65.

Deschoemaeker, S., Di Conza, G., Lilla, S., Martín-Pérez, R., et al. (2015). PHD1 regulates p53-mediated colorectal cancer chemoresistance. *EMBO Mol Med*, 7(10):1350-65.

Dewhirst, MW., Cao, Y., Moeller, B. (2008). Cycling hypoxia and free radicals regulate angiogenesis and radiotherapy response. *Nat Rev Cancer*, 8(6):425-37.

Drutel, G., Kathmann ,M., Heron, A., Schwartz, JC., Arrang, JM. (1996). Cloning and selective expression in brain and kidney of ARNT2 homologous to the Ah receptor nuclear translocator (ARNT). *Biochem Biophys Res Commun*, 225(2):333-9.

Drutel, G., Kathmann, M., Héron, A., Gros, C., Macé, S., Schwartz, JC., Arrang, JM. (2000). Two splice variants of the hypoxia-inducible factor HIF-1alpha as potential dimerization partners of ARNT2 in neurons. *Eur J Neurosci*, 12(10):3701-8.

Duan, DR., Pause, A., Burgess, WH., et al. (1995). Inhibition of transcription elongation by the VHL tumor suppressor protein. *Science,* 269(5229):1402-6.

Dvorak, HF. (1986). Tumors: wounds that do not heal. Similarities between tumor stroma generation and wound healing. *N Engl J Med*, 315(26):1650-9.

Ebert, BL., Bunn, HF. (1998). Regulation of transcription by hypoxia requires a multiprotein complex that includes hypoxia-inducible factor 1, an adjacent transcription factor, and p300/CREB binding protein. *Mol Cell Biol*, 18(7):4089-96.

Ellis, LM., Hicklin, DJ. (2008). VEGF-targeted therapy: mechanisms of anti-tumour activity. *Nat Rev Cancer*, 8(8):579-91.

Elson, DA., Ryan, HE., Snow, JW., Johnson, R., Arbeit, JM. (2000). Coordinate up-regulation of hypoxia inducible factor (HIF)-1alpha and HIF-1 target genes during multi-stage epidermal carcinogenesis and wound healing. *Cancer Res*, 60(21):6189-95.

Elvidge, GP., Glenny, L., Appelhoff, RJ., Ratcliffe, PJ., Ragoussis, J., Gleadle, JM. (2006). Concordant regulation of gene expression by hypoxia and 2-oxoglutarate-dependent dioxygenase inhibition: the role of HIF-1alpha, HIF-2alpha, and other pathways. *J Biol Chem*, 281(22):15215-26.

Ema, M., Taya, S., Yokotani, N., Sogawa, K., Matsuda, Y., Fujii-Kuriyama, Y. (1997). A novel bHLH-PAS factor with close sequence similarity to hypoxia-inducible factor 1alpha regulates the VEGF expression and is potentially involved in lung and vascular development. *Proc Natl Acad Sci U S A*, 94(9):4273-8.

Epstein, AC., Gleadle, JM., McNeill, LA., Hewitson, KS., et al. (2001). C. elegans EGL-9 and mammalian homologs define a family of dioxygenases that regulate HIF by prolyl hydroxylation. *Cell*, 107(1):43-54.

Ezer, D., Zabet, NR., Adryan, B. (2014). Physical constraints determine the logic of bacterial promoter architectures. *Nucleic Acids Res*, 42(7):4196-207.

Fandrey, J., Bunn, HF. (1993). In vivo and in vitro regulation of erythropoietin mRNA: measurement by competitive polymerase chain reaction. *Blood*, 81(3):617-23.

Fandrey, J., Gorr, TA., Gassmann, M. (2006). Regulating cellular oxygen sensing by hydroxylation. *Cardiovasc Res*, 71(4):642-51.

Feng, J., Liu, T., Qin, B., Zhang, Y., Liu, XS. (2012). Identifying ChIP-seq enrichment using MACS. *Nat Protoc*, 7(9):1728-40.

Ferlay, J., Shin, HR., Bray, F., Forman, D., Mathers, C., Parkin, DM. (2010). Estimates of worldwide burden of cancer in 2008: GLOBOCAN 2008. *Int J Cancer*, 127(12):2893-917.

Firth, JD., Ebert, BL., Ratcliffe, PJ. (1995). Hypoxic regulation of lactate dehydrogenase A. Interaction between hypoxia-inducible factor 1 and cAMP response elements. *J Biol Chem*, 270(36):21021-7.

Flamme, I., Fröhlich, T., von Reutern, M., Kappel, A., Damert, A., Risau, W. (1997). HRF, a putative basic helix-loop-helix-PAS-domain transcription factor is closely related to hypoxia-inducible factor-1 alpha and developmentally expressed in blood vessels. *Mech Dev*, 63(1):51-60.

Fliedner, SM., Shankavaram, U., Marzouca, G., Elkahloun, A., et al. (2016). Hypoxia-Inducible Factor 2α Mutation-Related Paragangliomas Classify as DiscretePseudohypoxic Subcluster. *Neoplasia*, 18(9):567-76.

Fullwood, MJ., Liu, MH., Pan, YF., Liu, J., et al. (2009). An oestrogen-receptor-alpha-bound human chromatin interactome. *Nature*, 462(7269):58-64.

Freedman, SJ., Sun, ZY., Kung, AL., France, DS., Wagner, G., Eck, MJ. (2003). Structural basis for negative regulation of hypoxia-inducible factor-1alpha by CITED2. *Nat Struct Biol*, 10(7):504-12.

Fu, J., Taubman, MB. (2013). EGLN3 inhibition of NF-κB is mediated by prolyl hydroxylase-independent inhibition of IκB kinaseγ ubiquitination. *Mol Cell Biol*, 33(15):3050-61.

Fukuda, R., Zhang, H., Kim, JW., Shimoda, L., Dang, CV., Semenza, GL. (2007). HIF-1 regulates cytochrome oxidase subunits to optimize efficiency of respiration in hypoxic cells. *Cell*, 129(1):111-22.

Furuta, E., Pai, SK., Zhan, R., Bandyopadhyay, S., et al. (2008). Fatty acid synthase gene is up-regulated by hypoxia via activation of Akt and sterol regulatory element binding protein-1. *Cancer Res*, 68(4):1003-11.

Galbraith, MD., Allen, MA., Bensard, CL., Wang, X., et al. (2013). HIF1A employs CDK8-mediator to stimulate RNAPII elongation in response to hypoxia. *Cell*, 153(6):1327-39.

Gao, W., Li, W., Xiao, T., Liu, XS., Kaelin, WG Jr. (2017). Inactivation of the PBRM1 tumor suppressor gene amplifies the HIF-response in VHL-/- clear cell renal carcinoma. *Proc Natl Acad Sci U S A*, 114(5):1027-1032.

Gardini, A. (2017). Global Run-On Sequencing (GRO-Seq). *Methods Mol Biol,* 1468:111-20.

Gebhardt, JC., Suter, DM., Roy, R., Zhao, ZW., et al. (2013). Single-molecule imaging of transcription factor binding to DNA in live mammalian cells. *Nat Methods,* 10(5):421-6.

Geng, H., Liu, Q., Xue, C., David, LL., Beer, TM., Thomas, GV., Dai, MS., Qian, DZ. (2012). HIF1α protein stability is increased by acetylation at lysine 709. *J Biol Chem*, 287(42):35496-505.

Gerald, D., Berra, E., Frapart, YM., Chan, DA., et al. (2004). JunD reduces tumor angiogenesis by protecting cells from oxidative stress. *Cell*, 118(6):781-94.

Ginouvès, A., Ilc, K., Macías, N., Pouysségur, J., Berra, E. (2008). PHDs overactivation during chronic hypoxia "desensitizes" HIFalpha and protects cells from necrosis. *Proc Natl Acad Sci U S A*, 105(12):4745-50.

Giordano, FJ. (2005). Oxygen, oxidative stress, hypoxia, and heart failure. *J Clin Invest*. 115(3):500-8.

Gnarra, JR., Tory, K., Weng, Y., Schmidt, L,. et al. (1994). Mutations of the VHL tumour suppressor gene in renal carcinoma. *Nat Genet*, 7(1):85-90.

Goda, N., Kanai, M. (2012). Hypoxia-inducible factors and their roles in energy metabolism. *Int J Hematol,* 95(5):457-63.

Gordan, JD., Lal, P., Dondeti, VR., et al. (2008). HIF-alpha effects on c-Myc distinguish two subtypes of sporadic VHL-deficient clear cell renal carcinoma. *Cancer Cell*, 14:435–46.

Gordan, JD., Bertout, JA., Hu, CJ., Diehl, JA., Simon, MC. (2007a). HIF-2alpha promotes hypoxic cell proliferation by enhancing c-myc transcriptional activity. *Cancer Cell*, 11:335–47.

Gordan, JD., Thompson, CB., Simon, MC. (2007b). HIF and c-Myc: sibling rivals for control of cancer cell metabolism and proliferation. *Cancer Cell*, 12:108–13.

Gorospe, M., Tominaga, K., Wu ,X., Fähling, M., Ivan, M. (2011). Post-Transcriptional Control of the Hypoxic Response by RNA-Binding Proteins and MicroRNAs. *Front Mol Neurosci*, 4:7.

Gossage, L., Eisen, T., Maher, ER. (2015). VHL, the story of a tumour suppressor gene. *Nat Rev Cancer*, 15(1):55-64.

Grampp, S., Platt, JL, Lauer, V., Salama, R., et al. (2016). Genetic variation at the 8q24.21 renal cancer susceptibility locus affects HIF binding to a MYC enhancer. *Nat Commun*, 7:13183.

Green, J., Scott, C., Guest, JR. (2001). Functional versatility in the CRP-FNR superfamily of transcription factors: FNR and FLP. *Adv Microb Physiol*. 44:1-34.

Greijer, AE., van der Groep, P., Kemming, D., Shvarts, A., et al. (2005). Up-regulation of gene expression by hypoxia is mediated predominantly by hypoxia-inducible factor 1 (HIF-1). *J Pathol*, 206(3):291-304.

Gu, J., Milligan, J., Huang, LE. (2001). Molecular mechanism of hypoxia-inducible factor 1alpha -p300 interaction. A leucine-richinterface regulated by a single cysteine. *J Biol Chem*, 276(5):3550-4.

Gu, YZ., Moran, SM., Hogenesch, JB., Wartman, L., Bradfield, CA. (1998). Molecular characterization and chromosomal localization of a third alpha-class hypoxia inducible factor subunit, HIF3alpha. *Gene Expr*, 7(3):205-13.

Guo, J., Chakraborty, AA., Liu, P., Gan, W., et al. (2016). pVHL suppresses kinase activity of Akt in a proline-hydroxylation-dependent manner. *Science*, 353(6302):929-32.

Gustafsson, MV., Zheng, X., Pereira, T., et al. (2005). Hypoxia requires notch signaling to maintain the undifferentiated cell state. *Dev Cell*, 9(5):617-28.

Hager, GL., McNally, JG., Misteli, T. (2009). Transcription dynamics. *Mol Cell*. 35(6):741-53.

Hahne, M., Schumann, P., Mursell, M., Strehl, C., Hoff, P., Buttgereit, F., Gaber, T. (2018). Unraveling the role of hypoxia-inducible factor (HIF)-1α and HIF-2α in the adaption

process of human microvascular endothelial cells (HMEC-1) to hypoxia: Redundant HIF-dependent regulation of macrophage migration inhibitory factor. *Microvasc Res*, 116:34-44.

Hakimi, AA., Chen, YB., Wren, J., Gonen, M., Abdel-Wahab, O., et al. (2013). Clinical and pathologic impact of select chromatin-modulating tumor suppressors in clear cell renal cell carcinoma. *Eur Urol*, 63(5):848-54.

Hamatani, T., Carter, MG., Sharov, AA. (2004). Dynamics of global gene expression changes during mouse preimplantation development. *Dev Cell*, 6(1):117-31.

Hamidian, A., von Stedingk, K., Munksgaard Thorén, M., Mohlin, S., Påhlman, S. (2015). Differential regulation of HIF-1α and HIF-2α in neuroblastoma: Estrogen-related receptor alpha (ERRα) regulates HIF2A transcription and correlates to poor outcome. *Biochem Biophys Res Commun*, 461(3):560-7.

Han, SS., Yeager, M., Moore, LE., et al. (2012). The chromosome 2p21 region harbors a complex genetic architecture for association with risk for renal cell carcinoma. *Hum Mol Genet*, 21:1190–200.

Hancock, RL., Dunne, K., Walport, LJ., Flashman, E., Kawamura, A. (2015). Epigenetic regulation by histone demethylases in hypoxia. *Epigenomics*, 7(5):791-811.

Hao, N., O'Shea, EK. (2011). Signal-dependent dynamics of transcription factor translocation controls gene expression. *Nat Struct Mol Biol*, 19(1):31-9.

Hara, S., Hamada, J., Kobayashi, C., Kondo, Y., Imura, N. (2001). Expression and characterization of hypoxia-inducible factor (HIF)-3alpha in human kidney: suppression of HIF-mediated gene expression by HIF-3alpha. *Biochem Biophys Res Commun*, 287(4):808-13.

Hardy, AP., Prokes, I., Kelly, L., Campbell, ID., Schofield, CJ. (2009). Asparaginyl beta-hydroxylation of proteins containing ankyrin repeat domains influences their stability and function. *J Mol Biol*, 392(4):994-1006.

Hashimoto, T., Shibasaki, F. (2015). Hypoxia-inducible factor as an angiogenic master switch. *Front Pediatr*. 3:33.

Hébert, SS., De Strooper, B. (2007). Molecular biology. miRNAs in neurodegeneration. *Science*, 317(5842):1179-80.

Herman, JG., Latif, F., Weng, Y., Lerman, MI., et al. (1994). Silencing of the VHL tumor-suppressor gene by DNA methylation in renal carcinoma. *Proc Natl Acad Sci U S A*, 91(21):9700-4.

Hewitson, KS., McNeill, LA., Riordan, MV., et al. (2002). Hypoxia-inducible factor (HIF) asparagine hydroxylase is identical to factor inhibiting HIF (FIH) and is related to the cupin structural family. *J Biol Chem*, 277(29):26351-5.

Hewitson, KS., Liénard, BM., McDonough, MA., Clifton, IJ., et al. (2007). Structural and mechanistic studies on the inhibition of the hypoxia-inducible transcription factor hydroxylases by tricarboxylic acid cycle intermediates. *J Biol Chem*, 282(5):3293-301.

Hirose, K., Morita, M., Ema, M., Mimura, J., et al. (1996). cDNA cloning and tissue-specific expression of a novel basic helix-loop-helix/PAS factor (Arnt2) with close sequence similarity to the aryl hydrocarbon receptor nuclear translocator (Arnt). *Mol Cell Biol*, 16(4):1706-13.

Hochachka, PW., Buck, LT., Doll, CJ., Land, SC. (1996). Unifying theory of hypoxia tolerance: molecular/metabolic defense and rescue mechanisms for surviving oxygen lack. *Proc Natl Acad Sci U S A*, 93(18):9493-8.

Hoek, KS., Goding, CR. (2010). Cancer stem cells versus phenotype-switching in melanoma. *Pigment Cell Melanoma Res*, 23(6):746-59.

Höckel, M., Schlenger, K., Knoop, C., Vaupel, P. (1991). Oxygenation of carcinomas of the uterine cervix: evaluation by computerized O2 tension measurements. *Cancer Res*, 51(22):6098-102.

Höckel, M., Vaupe,l P. (2001). Tumor hypoxia: definitions and current clinical, biologic, and molecular aspects. *J Natl Cancer Inst*, 93(4):266-76.

Hoffmann, A., Gloe, T., Pohl, U. (2001). Hypoxia-induced upregulation of eNOS gene expression is redox-sensitive: a comparison between hypoxia and inhibitors of cell metabolism. *J Cell Physiol,* 188(1):33-44.

Holmes, JL., Pollenz RS. (1997). Determination of aryl hydrocarbon receptor nuclear translocator protein concentration and subcellular localization in hepatic and nonhepatic cell culture lines: development of quantitative Western blotting protocols for calculation of aryl hydrocarbon receptor and aryl hydrocarbon receptor nuclear translocator protein in total cell lysates. *Mol Pharmacol,* 52(2):202-11.

Holmquist-Mengelbier, L., Fredlund, E., Löfstedt, T., Noguera, R., et al. (2006). Recruitment of HIF-1alpha and HIF-2alpha to common target genes is differentially regulated in neuroblastoma: HIF-2alpha promotes an aggressive phenotype. *Cancer Cell*, 10(5):413-23.

Hong, WX., Hu, MS., Esquivel, M., et al. (2014). The Role of Hypoxia-Inducible Factor in Wound Healing. *Adv Wound Care (New Rochelle)*, 3(5):390-399.

Hower, V., Evans, SN., Pachter, L. (2011). Shape-based peak identification for ChIP-Seq. *BMC Bioinformatics*, 12:15.

Hu, CJ., Wang, LY., Chodosh, LA., Keith, B., Simon, MC. (2003). Differential roles of hypoxia-inducible factor 1alpha (HIF-1alpha) and HIF-2alpha in hypoxic gene regulation. *Mol Cell Biol*, 23(24):9361-74.

Hu, CJ., Iyer, S., Sataur, S., Covello, KL., Chodosh, LA., Simon, MC. (2006). Differential regulation of the transcriptional activities of hypoxia-inducible factor 1 α (HIF-1α) and HIF-2α in stem cells. *Molecular Cell Biology*, 26:3514–3526.

Huang, CY., Bredemeyer, AL., Walker, LM., Bassing, CH., Sleckman, BP. (2008). Dynamic regulation of c-Myc proto-oncogene expression during lymphocyte development revealed by a GFP-c-Myc knock-in mouse. *Eur J Immunol*, 8(2):342-9.

Huang, LE., Gu, J., Schau, M., Bunn, HF. (1998). Regulation of hypoxia-inducible factor 1alpha is mediated by an O2-dependent degradation domain via the ubiquitin-proteasome pathway. *Proc Natl Acad Sci U S A*, 95(14):7987-92.

Huang, LE., Arany, Z., Livingston, DM., Bunn, HF. (1996). Activation of hypoxia-inducible transcrip- tion factor depends primarily upon redox- sensitive stabilization of its alpha subunit. *J Biol Chem*, 271:32253–9.

Hughes, JR., Roberts, N., McGowan, S., Hay, D., et al. (2014). Analysis of hundreds of cis-regulatory landscapes at high resolution in a single, high-throughput experiment. *Nat Genet*, 46(2):205-12.

Ikeda, E., Achen, MG., Breier, G., Risau, W. (1995). Hypoxia-induced transcriptional activation and increased mRNA stability of vascular endothelial growth factor in C6 glioma cells. *J Biol Chem*, 270(34):19761-6.

Iliopoulos, O., Kibel, A., Gray, S., Kaelin, WG Jr. (1995). Tumour suppression by the human von Hippel-Lindau gene product. *Nat Med*, 1(8):822-6.

Ivan, M., Kondo, K., Yang, H., Kim, W., et al. (2001). HIFalpha targeted for VHL-mediated destruction by proline hydroxylation: implications for O2 sensing. *Science*, 292(5516):464-8.

Iyer, NV., Kotch, LE., Agani, F., Leung, SW., et al. (1998a). Cellular and developmental control of O2 homeostasis by hypoxia-inducible factor 1 alpha. *Genes Dev*, 12(2):149-62.

Iyer, NV., Leung, SW., Semenza, GL. (1998b). The human hypoxia-inducible factor 1alpha gene: HIF1A structure and evolutionary conservation. *Genomics*, 52(2):159-65.

Jaakkola, P., Mole, DR., Tian, YM., Wilson, MI., et al. (2001). Targeting of HIF-alpha to the von Hippel-Lindau ubiquitylation complex by O2-regulated prolyl hydroxylation. *Science*, 292(5516):468-72.

Jain, S., Maltepe, E., Lu, MM., Simon, C., Bradfield, CA. (1998). Expression of ARNT, ARNT2, HIF1 alpha, HIF2 alpha and Ah receptor mRNAs in the developing mouse. *Mech Dev,* 73(1):117-23.

Jeong, JW., Bae, MK., Ahn, MY., Kim, SH., et al. (2002). Regulation and destabilization of HIF-1alpha by ARD1-mediated acetylation. *Cell*, 111(5):709-20.

Jewell, UR., Kvietikova, I., Scheid, A., Bauer, C., Wenger, RH., Gassmann, M. (2001). Induction of HIF-1alpha in response to hypoxia is instantaneous. *FASEB J*, 15(7):1312-4.

Jiang, BH., Semenza, GL., Bauer, C., Marti, HH. (1996). Hypoxia-inducible factor 1 levels vary exponentially over a physiologically relevant range of O2 tension. *Am J Physiol*, 271(4 Pt 1):C1172-80.

Kaelin, WG Jr., Ratcliffe, PJ. (2008). Oxygen sensing by metazoans: the central role of the HIF hydroxylase pathway. *Mol Cell*, 30(4):393-402.

Kaelin, WG. (2007). Von Hippel-Lindau disease. *Annu Rev Pathol*, 2:145-73.

Kalousi, A., Mylonis, I., Politou, AS., Chachami, G., Paraskeva, E., Simos, G. (2010). Casein kinase 1 regulates human hypoxia-inducible factor HIF-1. *J Cell Sci*, 123(Pt 17):2976-86.

Kang, J., Shin, SH., Yoon, H., Huh, J4., et al, (2018). FIH Is an Oxygen Sensor in Ovarian Cancer for G9a/GLP-Driven Epigenetic Regulation of Metastasis-Related Genes. *Cancer Res,* 78(5):1184-1199.

Kao, H-Y., Downes, M., Ordentlich, P., Evans, RM. (2000). Isolation of a novel histone deacetylase reveals that class I and class II deacetylases promote SMRT-mediated repression. *Genes & Dev*, 14:55–66.

Karpova, TS., Kim, MJ., Spriet, C., Nalley, K., et al. (2008). Concurrent fast and slow cycling of a transcriptional activator at an endogenous promoter. *Science*, 319(5862):466-9.

Karuppagounder, SS., Ratan, RR. (2012). Hypoxia-inducible factor prolyl hydroxylase inhibition: robust new target or another big bust for stroke therapeutics? *J Cereb Blood Flow Metab*, 32(7):1347-61.

Kasper, LH., Boussouar, F., Boyd, K., Xu, W., et al. (2005). Two transactivation mechanisms cooperate for the bulk of HIF-1-responsive gene expression. *EMBO J*, 24(22):3846-58.

Keith, B., Adelman, DM., Simon, MC. (2001). Targeted mutation of the murine arylhydrocarbon receptor nuclear translocator 2 (Arnt2) gene reveals partial redundancy with Arnt. *Proc Natl Acad Sci U S A,* 98(12):6692-7.

Keith, B., Simon, MC. (2007). Hypoxia-inducible factors, stem cells, and cancer. *Cell*, 129(3):465-72.

Kelly, TK., Liu, Y., Lay, FD., Liang, G., Berman, BP., Jones, PA. (2012). Genome-wide mapping of nucleosome positioning and DNA methylation within individual DNA molecules. *Genome Res*, 22(12):2497-506.

Kenneth, NS., Rocha, S. (2008). Regulation of gene expression by hypoxia. *Biochem J*, 414(1):19-29.

Khan, MN., Bhattacharyya, T., Andrikopoulos, P., et al. (2011). Factor inhibiting HIF (FIH-1) promotes renal cancer cell survival by protecting cells from HIF-1α-mediated apoptosis. *Br J Cancer*, 104(7):1151-9.

Kibel, A., Iliopoulos, O., DeCaprio, JA., Kaelin, WG Jr. (1995). Binding of the von Hippel-Lindau tumor suppressor protein to Elongin B and C. *Science*, 269(5229):1444-6.

Kim, SY., Yang, EG. (2015). Recent Advances in Developing Inhibitors for Hypoxia-Inducible Factor Prolyl Hydroxylases and Their Therapeutic Implications. *Molecules*, 20(11):20551-68.

Kim, JW., Tchernyshyov, I., Semenza, GL., Dang, CV. (2006). HIF-1-mediated expression of pyruvate dehydrogenase kinase: a metabolic switch required for cellular adaptation to hypoxia. *Cell Metab*, 3(3):177-85.

Kishida, T., Stackhouse, TM., Chen, F., Lerman, MI., Zbar, B. (1995). Cellular proteins that bind the von Hippel-Lindau disease gene product: mapping of binding domains and the effect of missense mutations. *Cancer Res*, 55(20):4544-8.

Klokk, TI., Kurys, P., Elbi, C., Nagaich, AK., et al. (2007). Ligand-specific dynamics of the androgen receptor at its response element in living cells. *Mol Cell Biol,* 27(5):1823-43.

Knippschild, U., Gocht, A., Wolff, S., Huber, N., Löhler, J., Stöter, M. (2005). The casein kinase 1 family: participation in multiple cellular processes in eukaryotes. *Cell Signal*, 17(6):675-89.

Köditz, J., Nesper, J., Wottawa, M., Stiehl, DP., et al. (2007). Oxygen-dependent ATF-4 stability is mediated by the PHD3 oxygen sensor. *Blood*, 110(10):3610-7.

Koivunen, P., Tiainen, P., Hyvärinen, J., et al. (2007). An endoplasmic reticulum transmembrane prolyl 4-hydroxylase is induced by hypoxia and acts on hypoxia-inducible factor alpha. *J Biol Chem*, 282(42):30544-52.

Koivunen, P., Hirsilä, M., Günzler, V., Kivirikko, KI., Myllyharju, J. (2004). Catalytic properties of the asparaginyl hydroxylase (FIH) in the oxygen sensing pathway are distinct from those of its prolyl 4-hydroxylases. *J Biol Chem*, 279(11):9899-904.

Koizume, S., Ito, S., Miyagi, E., et al. (2012). HIF2α-Sp1 interaction mediates a deacetylation-dependent FVII-gene activation under hypoxicconditions in ovarian cancer cells. *Nucleic Acids Res*, 40(12):5389-401.

Kondo, K., Klco, J., Nakamura, E., Lechpammer, M., Kaelin, Jr WG. (2002). Inhibition of HIF is necessary for tumor suppression by the von Hippel-Lindau protein. *Cancer Cell*, 1:237–46.

Kondo, K., Kim, WY., Lechpammer, M., Kaelin, Jr WG. (2003). Inhibition of HIF2alpha is sufficient to suppress pVHL-defective tumor growth. *PLoS Biol*, 1:E83.

Koong, AC., Chen, EY., Giaccia, AJ. (1994). Hypoxia causes the activation of nuclear factor kappa B through the phosphorylation of I kappa B alpha on tyrosine residues. *Cancer Res*, 54(6):1425-30.

Kroeze, SG., Vermaat, JS., van Brussel, A., van Melick, HH., Voest, EE., Jonges, TG., et al. (2010). Expression of nuclear FIH independently predicts overall survival of clear cell renal cell carcinoma patients. *Eur J Cancer*, 46(18):3375-82.

Kulshreshtha, R., Ferracin, M., Wojcik, SE., et al. (2007). A microRNA signature of hypoxia. *Mol Cell Biol*, 27(5):1859-67.

Kung, AL., Wang, S., Klco, JM., Kaelin, WG., Livingston, DM. (2000). Suppression of tumor growth through disruption of hypoxia-inducible transcription. *Nat Med*, 6(12):1335-40.

Kuschel, A., Simon, P., Tug, S. (2012). Functional regulation of HIF-1α under normoxia--is there more than post-translational regulation*? J Cell Physiol*, 227(2):514-24.

Lachance, G., Uniacke, J., Audas, TE., et al. (2014). DNMT3a epigenetic program regulates the HIF-2α oxygen-sensing pathway and the cellularresponse to hypoxia. *Proc Natl Acad Sci U S A*, 111(21):7783-8.

Laderoute, KR. (2005). The interaction between HIF-1 and AP-1 transcription factors in response to low oxygen. *Semin Cell Dev Biol*, 16(4-5):502-13.

Landázuri, MO., Vara-Vega, A., Vitón, M., Cuevas, Y., del Peso, L. Analysis of HIF-prolyl hydroxylases binding to substrates. *Biochem Biophys Res Commun*, 351(2):313-20.

Lando, D., Peet, DJ., Gorman, JJ., et al. (2002a). FIH-1 is an asparaginyl hydroxylase enzyme that regulates the transcriptional activity of hypoxia-inducible factor. *Genes Dev*, 16:1466–1471.

Lando, D., Peet, DJ., Whelan, DA., et al. (2002b). Asparagine Hydroxylation of the HIF Transactivation Domain: A Hypoxic Switch. *Science Signaling*, 295:858.

Lane, N., Martin, W. (2010). The energetics of genome complexity. *Nature*, 467:929–934.

Lau, KW., Tian, YM., Raval, RR., Ratcliffe, PJ., Pugh, CW. (2007). Target gene selectivity of hypoxia-inducible factor-alpha in renal cancer cells is conveyed by post-DNA-binding mechanisms. *Br J Cancer*, 96(8):1284-92.

Lendahl, U., Lee, KL., Yang, H., Poellinger, L. (2009). Generating specificity and diversity in the transcriptional response to hypoxia. *Nat Rev Genet*, 10(12):821-32.

Ledaki, I., McIntyre, A., Wigfield, S., Buffa, F., McGowan, S., Baban, D., Li, JL., Harris, AL. (2015). Carbonic anhydrase IX induction defines a heterogeneous cancer cell response to hypoxia and mediates stem cell-like properties and sensitivity to HDAC inhibition. *Oncotarget*, 6(23):19413-27.

Lee, MC., Huang, HJ., Chang, TH., et al. (2016). Genome-wide analysis of HIF-2α chromatin binding sites under normoxia in human bronchialepithelial cells (BEAS-2B) suggests its diverse functions. *Sci Rep*, 6:29311.

Lee, DC, Sohn, HA., Park, ZY., Oh, S., et al. (2015). A lactate-induced response to hypoxia. *Cell*, 161(3):595-609.

Leisz, S., Schulz, K., Erb, S., Oefner, P., et al. (2015). Distinct von Hippel-Lindau gene and hypoxia-regulated alterations in gene and protein expression patterns of renal cell carcinoma and their effects on metabolism. *Oncotarget*, 6(13):11395-406.

Lewis, JH., Wolpert, L. (1976). The principle of non-equivalence in development. *J Theor Biol,* 62(2):479-90.

Li, H., Handsaker, B., Wysoker, A., et al. (2009). The Sequence Alignment/Map format and SAMtools. *Bioinformatics*, 25(16):2078-9.

Lickwar, CR., Mueller, F., Hanlon, SE., McNally, JG., Lieb, JD. (2012). Genome-wide protein-DNA binding dynamics suggest a molecular clutch for transcription factor function. *Nature*, 484(7393):251-5.

Lim, JH., Lee, YM., Chun, YS., Chen, J., Kim, JE., Park, JW. (2010). Sirtuin 1 modulates cellular responses to hypoxia by deacetylating hypoxia-inducible factor 1alpha. *Mol Cell*, 38(6):864-78.

Lin, TY., Chou, CF., Chung, HY., Chiang, CY., et al. (2014). Hypoxia-inducible factor 2 alpha is essential for hepatic outgrowth and functions via the regulation of leg1 transcription in the zebrafish embryo. *PLoS One*, 9(7):e101980.

Lin, Q., Cong, X., Yun, Z. (2011). Differential hypoxic regulation of hypoxia-inducible factors 1alpha and 2alpha. *Mol Cancer Res*, 9(6):757-65.

Liu, X., Chen, Z., Xu, C., Leng, X., et al. (2015a). Repression of hypoxia-inducible factor α signaling by Set7-mediated methylation. *Nucleic Acids Res*, 43(10):5081-98

Liu, Q., Geng, H., Xue, C., Beer, TM., Qian, DZ. (2015b). Functional regulation of hypoxia inducible factor-1α by SET9 lysine methyltransferase. *Biochim Biophys Acta*,1853(5):881-91.

Ljungberg, B., Campbell, SC., Choi, HY., Jacqmin, D., et al. (2011). The epidemiology of renal cell carcinoma. *Eur Urol*, 60(4):615-21.

Lopes, R., Agami, R., Korkmaz, G. (2017). GRO-seq, A Tool for Identification of Transcripts Regulating Gene Expression. *Methods Mol Biol,* 1543:45-55

Love, MI., Huber, W., Anders, S. (2014). Moderated estimation of fold change and dispersion for RNA-seq data with DESeq2. *Genome Biol*, 15(12):550.

Luo, W., Lin, B., Wang, Y., et al. (2014). PHD3-mediated prolyl hydroxylation of nonmuscle actin impairs polymerization and cell motility. *Mol Biol Cell*, 25(18):2788-96.

Luo, W1., Zhong, J., Chang, R., et al. (2010). Hsp70 and CHIP selectively mediate ubiquitination and degradation of hypoxia-inducible factor (HIF)-1alpha but Not HIF-2alpha. *J Biol Chem*, 285(6):3651-63.

MacArthur, S., Li, XY., Li, J., et al. (2009). Developmental roles of 21 Drosophila transcription factors are determined by quantitative differences in binding to an overlapping set of thousands of genomic regions. *Genome Biol*, 10(7):R80.

Mahon, PC., Hirota, K., Semenza, GL. (2001). FIH-1: a novel protein that interacts with HIF-1alpha and VHL to mediate repression of HIF-1 transcriptional activity. *Genes Dev*, (20):2675-86.

Makino, Y., Cao, R., Svensson, K., et al. (2001). Inhibitory PAS domain protein is a negative regulator of hypoxia-inducible gene expression. *Nature*, 414(6863):550-4.

Makino, Y., Kanopka, A., Wilson, WJ., Tanaka, H., Poellinger, L. (2002). Inhibitory PAS domain protein (IPAS) is a hypoxia-inducible splicing variant of the hypoxia-inducible factor-3alpha locus. *J Biol Chem*, 277(36):32405-8.

Malec, V., Coulson, JM., Urbé, S., Clague, MJ. (2015). Combined Analyses of the VHL and Hypoxia Signaling Axes in an Isogenic Pairing of Renal Clear Cell Carcinoma Cells. *J Proteome Res*, 14(12):5263-72.

Maltepe, E., Keith, B., Arsham, AM., Brorson, JR,. Simon, MC. (2000). The role of ARNT2 in tumor angiogenesis and the neural response to hypoxia. *Biochem Biophys Res Commun,* 273(1):231-8.

Mandl, M., Depping, R. (2014). Hypoxia-inducible aryl hydrocarbon receptor nuclear translocator (ARNT) (HIF-1β): is it a rare exception? *Mol Med*, 20:215-20.

Mandriota, SJ., Turner, KJ., Davies, DR., Murray, PG., Morgan, NV., Sowter, HM., Wykoff, CC., Maher, ER., Harris, AL., Ratcliffe, PJ., Maxwell, PH. (2002). HIF activation

identifies early lesions in VHL kidneys: evidence for site-specific tumor suppressor function in the nephron. *Cancer Cell*, 1(5):459-68.

Martínez-Sáez, O., Gajate Borau, P., Alonso-Gordoa, T., Molina-Cerrillo, J., Grande, E. (2017). Targeting HIF-2 α in clear cell renal cell carcinoma: A promising therapeutic strategy. *Crit Rev Oncol Hematol*, 111:117-123.

Masoud, GN., Li, W. (2015). HIF-1α pathway: role, regulation and intervention for cancer therapy. *Acta Pharm Sin B*, 5(5):378-89.

Massari, ME., Murre, C. (2000). Helix-loop-helix proteins: regulators of transcription in eucaryotic organisms. *Mol Cell Biol*, 20(2):429-40.

Masson, N., Willam, C., Maxwell, PH., Pugh, CW., Ratcliffe, PJ. (2001). Independent function of two destruction domains in hypoxia-inducible factor-alpha chains activated by prolyl hydroxylation. *EMBO J*, 20(18):5197-206.

Masson, N., Singleton, RS., Sekirnik, R., Trudgian, DC., Ambrose, LJ., Miranda, MX., Tian, YM., Kessler, BM., Schofield, CJ., Ratcliffe, PJ. (2012). The FIH hydroxylase is a cellular peroxide sensor that modulates HIF transcriptional activity. *EMBO Rep*, 13(3):251-7.

Masson, N., Ratcliffe, PJ. (2014). Hypoxia signaling pathways in cancer metabolism: the importance of co-selecting interconnected physiological pathways. *Cancer Metab*, 2(1):3.

Maxwell, PH., Dachs, GU., Gleadle, JM., Nicholls, LG., et al. (1997). Hypoxia-inducible factor-1 modulates gene expression in solid tumors and influences both angiogenesis and tumor growth. *Proc Natl Acad Sci U S A*, 94(15):8104-9.

Maxwell, PH., Wiesener, MS., Chang, GW., Clifford, SC., et al. (1999). The tumour suppressor protein VHL targets hypoxia-inducible factors for oxygen-dependent proteolysis. *Nature*, 399(6733):271-5.

Maynard, MA., Qi, H., Chung, J., Lee, EH., et al. (2003). Multiple splice variants of the human HIF-3 alpha locus are targets of the von Hippel-Lindau E3 ubiquitin ligase complex. *J Biol Chem*, 278(13):11032-40.

Maynard, MA., Evans, AJ., Hosomi, T., Hara, S., Jewett, MA., Ohh, M., et al. (2005). Human HIF-3alpha4 is a dominant-negative regulator of HIF-1 and is down-regulated in renal cell carcinoma. *FASEB J*, 19(11):1396-406.

Melvin, A., Rocha, S. (2012). Chromatin as an oxygen sensor and active player in the hypoxia response. *Cell Signal*, 24(1):35-43.

Metzen, E., Stiehl, DP., Doege, K., Marxsen, JH., Hellwig-Bürgel, T., Jelkmann, W. (2005). Regulation of the prolyl hydroxylase domain protein 2 (phd2/egln-1) gene: identification of a functional hypoxia-responsive element. *Biochem J*, 387(Pt 3):711-7.

Michiels, C. (2004). Physiological and pathological responses to hypoxia. *Am J Pathol*, 164(6):1875-82.

Mikhaylova, O., Ignacak, ML., Barankiewicz, TJ., Harbaugh, SV., et al. (2008). The von Hippel-Lindau tumor suppressor protein and Egl-9-Type proline hydroxylases regulate the large subunit of RNA polymerase II in response to oxidative stress. *Mol Cell Biol*, 28(8):2701-17.

Mimura, I., Nangaku, M., Kanki, Y., Tsutsumi, S., et al. (2012). Dynamic change of chromatin conformation in response to hypoxia enhances the expression of GLUT3 (SLC2A3) by cooperative interaction of hypoxia-inducible factor 1 and KDM3A. *Mol Cell Biol*, 32(15):3018-32.

Miranda, E., Nordgren, IK., Male, AL., Lawrence, CE., et al. (2013). A cyclic peptide inhibitor of HIF-1 heterodimerization that inhibits hypoxia signaling in cancercells. *J Am Chem Soc*, 135(28):10418-25.

Miyoshi, A., Kitajima, Y., Ide, T., Ohtaka, K., Nagasawa, H., Uto, Y., Hori, H., Miyazaki, K. (2006). Hypoxia accelerates cancer invasion of hepatoma cells by upregulating MMP expression in an HIF-1alpha-independent manner. *Int J Oncol*, 29(6):1533-9.

Mole, DR., Blancher, C., Copley, RR., Pollard, PJ., Gleadle, JM., Ragoussis, J., Ratcliffe, PJ. (2009). Genome-wide association of hypoxia-inducible factor (HIF)-1alpha and HIF-2alpha DNA binding with expression profiling of hypoxia-inducible transcripts. *J Biol Chem*, 284(25):16767-75.

Monzon, FA., Alvarez, K., Peterson, L., et al. (2011). Chromosome 14q loss defines a molecular subtype of clear-cell renal cell carcinoma associated with poor prognosis. *Mod Pathol*, 24:1470–9.

Morais, C., Gobe, G., Johnson, DW., Healy, H. (2011). The emerging role of nuclear factor kappa B in renal cell carcinoma. *Int J Biochem Cell Biol*, 43(11):1537-49.

Morris, MR., Hughes, DJ., Tian, YM., Ricketts, CJ., et al. (2009). Mutation analysis of hypoxia-inducible factors HIF1A and HIF2A in renal cell carcinoma. *Anticancer Res*, 29(11):4337-43.

Morris, MR., Latif, F. (2017). The epigenetic landscape of renal cancer. *Nat Rev Nephrol*, 13(1):47-60.

Moroz, E., Carlin, S., Dyomina, K., Burke, S., Thaler, HT., Blasberg ,R., Serganova, I. (2009). Real-time imaging of HIF-1alpha stabilization and degradation. *PLoS One*, 4(4):e5077.

Motzer, RJ., Bander, NH., Nanus, DM. (1996). Renal-cell carcinoma. *N Engl J Med*, 335(12):865-75.

Mueller, F., Stasevich, TJ., Mazza, D., McNally, JG. (2013). Quantifying transcription factor kinetics: at work or at play? *Crit Rev Biochem Mol Biol,* 48(5):492-514.

Myllyharju, J., Koivunen, P. (2013). Hypoxia-inducible factor prolyl 4-hydroxylases: common and specific roles. *Biol Chem*, 394(4):435-48.

Nargund, AM., Pham, CG., Dong, Y., Wang, PI., et al. (2017). The SWI/SNF Protein PBRM1 Restrains VHL-Loss-Driven Clear Cell Renal Cell Carcinoma. *Cell Rep*, 18(12):2893-2906.

Nguyen, AD., McDonald, JG., Bruick, RK., DeBose-Boyd, RA. (2007). Hypoxia stimulates degradation of 3-hydroxy-3-methylglutaryl-coenzyme A reductase through accumulation of lanosterol and hypoxia-inducible factor-mediated induction of insigs. *J Biol Chem*, 282(37):27436-46.

Nguyen, LK., Cavadas, MA., Scholz, CC., Fitzpatrick, SF., et al. (2013). A dynamic model of the hypoxia-inducible factor 1α (HIF-1α) network. *J Cell Sci,* 126(Pt 6):1454-63.

Ni, L., Bruce, C., Hart, C., Leigh-Bell, J., Gelperin, D., Umansky, L., Gerstein, MB., Snyder, M. (2009). Dynamic and complex transcription factor binding during an inducible response in yeast. *Genes Dev*, 23(11):1351-63.

Nishiyama, Y1., Goda, N., Kanai, M., Niwa, D., et al. (2012). HIF-1α induction suppresses excessive lipid accumulation in alcoholic fatty liver in mice. *J Hepatol*, 56(2):441-7.

Niu, X., Zhang, T., Liao, L., Zhou, L, et al. (2012). The von Hippel-Lindau tumor suppressor protein regulates gene expression and tumor growththrough histone demethylase JARID1C. *Oncogene*, 31(6):776-86.

Nizet, V., Johnson, RS. (2009). Interdependence of hypoxic and innate immune responses. *Nat Rev Immunol*, 9(9):609-17.

Norouzirad, R., González-Muniesa, P., Ghasemi, A. (2017). Hypoxia in Obesity and Diabetes: Potential Therapeutic Effects of Hyperoxia and Nitrate. *Oxid Med Cell Longev*, 2017:5350267.

Oehme, F., Ellinghaus, P., Kolkhof, P., Smith, TJ., et al. (2002). Overexpression of PH-4, a novel putative proline 4-hydroxylase, modulates activity of hypoxia-inducible transcription factors. *Biochem Biophys Res Commun*, 296(2):343-9.

O'Flaherty, L., Adam, J., Heather, LC., et al. (2010). Dysregulation of hypoxia pathways in fumarate hydratase-deficient cells is independent of defective mitochondrial metabolism. *Hum Mol Genet*, 19(19):3844-51

Ohh, M., Park, CW., Ivan, M., Hoffman, MA., et al. (2000). Ubiquitination of hypoxia-inducible factor requires direct binding to the beta-domain of the von Hippel-Lindau protein. *Nat Cell Biol*, 2(7):423-7.

Ooi, L., Wood, IC. (2007). Chromatin crosstalk in development and disease: lessons from REST. *Nat Rev Genet*, 8(7):544-54.

O'Rourke, JF., Tian, YM., Ratcliffe, PJ., Pugh, CW. (1999). Oxygen-regulated and transactivating domains in endothelial PAS protein 1: comparison with hypoxia-inducible factor-1alpha. *J Biol Chem*, 274(4):2060-71.

Ortiz-Barahona, A., Villar, D., Pescador, N., Amigo, J., del Peso, L. (2010). Genome-wide identification of hypoxia-inducible factor binding sites and target genes by a probabilistic model integrating transcription-profiling data and in silico binding site prediction. *Nucleic Acids Res*, 38(7):2332-45.

Osborne, TF., Espenshade, PJ. (2009). Evolutionary conservation and adaptation in the mechanism that regulates SREBP action: what a long, strange tRIP it's been. *Genes Dev*, 23(22):2578-91.

Papandreou, I., Cairns, RA., Fontana, L., Lim, AL., Denko, NC. (2006). HIF-1 mediates adaptation to hypoxia by actively downregulating mitochondrial oxygen consumption. *Cell Metab*, 3(3):187-97.

Pasanen, A., Heikkilä, M., Rautavuoma, K., Hirsilä, M., Kivirikko, KI., Myllyharju, J. (2010). Hypoxia-inducible factor (HIF)-3alpha is subject to extensive alternative splicing in human tissues and cancer cells and is regulated by HIF-1 but not HIF-2. *Int J Biochem Cell Biol*, 42(7):1189-200.

Pawlus, MR., Wang, L., Murakami, A., Dai, G., Hu, CJ. (2013). STAT3 or USF2 contributes to HIF target gene specificity. *PLoS One*, 8(8):e72358.

Pawlus, MR., Wang, L., Ware, K., Hu, CJ. (2012). Upstream stimulatory factor 2 and hypoxia-inducible factor 2α (HIF2α) cooperatively activate HIF2target genes during hypoxia. *Mol Cell Biol*, 32(22):4595-610.

Peña-Llopis, S., Vega-Rubín-de-Celis, S., Liao, A., et al. (2012). BAP1 loss defines a new class of renal cell carcinoma. *Nat Genet*, 44(7):751-9.

Perez-Perri, JI., Acevedo, JM., Wappner, P. (2011). Epigenetics: New Questions on the Response to Hypoxia. *Int J Mol Sci*, 12(7): 4705–4721.

Phair, RD., Gorski, SA., Misteli, T. (2004). Measurement of dynamic protein binding to chromatin in vivo, using photobleaching microscopy. *Methods Enzymol*, 375:393-414.

Peek, CB., Levine, DC., Cedernaes, J., Taguchi, A., et al. (2017). Circadian Clock Interaction with HIF1α Mediates Oxygenic Metabolism and Anaerobic Glycolysis in Skeletal Muscle. *Cell Metab,* 25(1):86-92.

Peng, J., Zhang, L., Drysdale, L., Fong, GH. (2000). The transcription factor EPAS-1/hypoxia-inducible factor 2alpha plays an important role in vascular remodeling. *Proc Natl Acad Sci U S A*, 97(15):8386-91.

Pettersen, EO., Juul, NO., Rønning, OW. (1986). Regulation of protein metabolism of human cells during and after acute hypoxia. *Cancer Res*, 46(9):4346-51.

Platt, JL., Salama, R., Smythies, J., Choudhry, H., et al. (2016). Capture-C reveals preformed chromatin interactions between HIF-binding sites and distant promoters. *EMBO Rep*, 17(10):1410-1421.

Portales-Casamar, E., Thongjuea, S., Kwon, AT., Arenillas, D., et al. (2010). JASPAR 2010: the greatly expanded open-access database of transcription factor binding profiles. *Nucleic Acids Res*, 38(Database issue):D105-10.

Purdue, MP., Johansson, M., Zelenika, D., et al. (2011). Genome-wide association study of renal cell carcinoma identifies two susceptibility loci on 2p21 and 11q13.3. *Nat Genet*, 43:60–5.

Purvis, JE., Karhohs, KW., Mock, C., Batchelor, E., Loewer, A., Lahav, G. (2012). p53 dynamics control cell fate. *Science*, 336(6087):1440-4.

Racusen, LC., Monteil, C., Sgrignoli, A., Lucskay, M., Marouillat, S., Rhim, JG., Morin, JP. (1997). Cell lines with extended in vitro growth potential from human renal proximal tubule: characterization, response to inducers, and comparison with established cell lines. *J Lab Clin Med*, 129(3):318-29.

Ramos, AI., Barolo, S. (2013). Low-affinity transcription factor binding sites shape morphogen responses and enhancer evolution. *Philos Trans R Soc Lond B Biol Sci*, 368(1632):20130018.

Rankin, EB., Giaccia, AJ. (2008). The role of hypoxia-inducible factors in tumorigenesis. *Cell Death Differ*, 15(4):678-85.

Rankin, EB., Higgins, DF., Walisser, JA., Johnson, RS., Bradfield, CA., Haase, VH. (2005). Inactivation of the arylhydrocarbon receptor nuclear translocator (Arnt) suppresses von Hippel-Lindau disease-associated vascular tumors in mice. *Mol Cell Biol*, 25(8):3163-72.

Rankin, EB., Rha, J., Selak, MA., Unger, TL., Keith, B., Liu, Q., Haase, VH. (2009). Hypoxia-inducible factor 2 regulates hepatic lipid metabolism. *Mol Cell Biol*, 29(16):4527-38.

Ratcliffe, PJ. (2013). Oxygen sensing and hypoxia signalling pathways in animals: the implications of physiology for cancer. *J Physiol,* 591(8):2027-42.

Raval, RR., Lau, KW., Tran, MG., Sowter, HM., et al. (2005). Contrasting properties of hypoxia-inducible factor 1 (HIF-1) and HIF-2 in von Hippel-Lindau-associated renal cell carcinoma. *Mol Cell Biol*, 25(13):5675-86.

Ravenna, L., Salvatori, L., Russo, MA. (2016). HIF3α: the little we know. *FEBS J,* 283(6):993-1003.

Reyes, H., Reisz-Porszasz, S., Hankinson, O. (1992). Identification of the Ah receptor nuclear translocator protein (Arnt) as a component of the DNA binding form of the Ah receptor. *Science*, 256(5060):1193-5.

Richard, DE., Berra, E., Gothié, E., Roux, D., Pouysségur, J. (1999). p42/p44 mitogen-activated protein kinases phosphorylate hypoxia-inducible factor 1alpha (HIF-1alpha) and enhance the transcriptional activity of HIF-1. *J Biol Chem,* 274(46):32631-7.

Robinson, MD., McCarthy, DJ., Smyth, GK. (2010). edgeR: a Bioconductor package for differential expression analysis of digital gene expression data. *Bioinformatics*, 26(1):139-40.

Rocha, S. (2007). Gene regulation under low oxygen: holding your breath for transcription. *Trends Biochem Sci*, 32(8):389-97.

Rong, Y., Hu, F., Huang, R., Mackman, N., et al. (2006). Early growth response gene-1 regulates hypoxia-induced expression of tissue factor in glioblastoma multiforme through hypoxia-inducible factor-1-independent mechanisms. *Cancer Res*, 66(14):7067-74.

Romero-Ruiz, A., Bautista, L., Navarro, V., et al. (2012). Prolyl hydroxylase-dependent modulation of eukaryotic elongation factor 2 activity and protein translation under acute hypoxia. *J Biol Chem*, 287(12):9651-8.

Rosenberger, C., Mandriota, S., Jürgensen, JS., Wiesener, MS. (2002). Expression of hypoxia-inducible factor-1alpha and -2alpha in hypoxic and ischemic rat kidneys. *J Am Soc Nephrol*, 13(7):1721-32.

Ross-Innes, CS., Stark, R., Teschendorff, AE., et al. (2012). Differential oestrogen receptor binding is associated with clinical outcome in breast cancer. *Nature*, 481(7381):389-93.

Rössler, J., Stolze, I., Frede, S., et al. (2004). Hypoxia-induced erythropoietin expression in human neuroblastoma requires a methylation free HIF-1 binding site. *J Cell Biochem*, 93(1):153-61.

Rowan, S., Siggers, T., Lachke, SA., Yue, Y., Bulyk, ML., Maas, RL. (2010). Precise temporal control of the eye regulatory gene Pax6 via enhancer-binding site affinity. *Genes Dev*, 24(10):980-5.

Ruthenborg, RJ., Ban, JJ., Wazir, A., Takeda, N., Kim, JW. (2014). Regulation of wound healing and fibrosis by hypoxia and hypoxia-inducible factor-1. *Mol Cells*, 37(9):637-43.

Ryan, HE., Poloni, M., McNulty, W., Elson, D., et al. (2000). Hypoxia-inducible factor-1alpha is a positive factor in solid tumor growth. *Cancer Res*, 60(15):4010-5.

Sabatini, PV., Speckmann, T., Nian, C., Glavas, MM., et al. (2018). Neuronal PAS Domain Protein 4 Suppression of Oxygen Sensing Optimizes Metabolism during Excitation of Neuroendocrine Cells. *Cell Rep,* 22(1):163-174.

Salama, R., Masson, N., Simpson, P., et al. (2015). Heterogeneous Effects of Direct Hypoxia Pathway Activation in Kidney Cancer. *PLoS One*, 10(8):e0134645.

Sánchez-Fernández, EM., Tarhonskaya, H., Al-Qahtani ,K., et al. (2013). Investigations on the oxygen dependence of a 2-oxoglutarate histone demethylase. *Biochem J*, 449(2):491-6.

Schietke, RE., Hackenbeck, T., Tran, M., et al. (2012). Renal tubular HIF-2α expression requires VHL inactivation and causes fibrosis and cysts. *PLoS One*, 7(1):e31034.

Schipani, E., Ryan, HE., Didrickson, S., Kobayashi, T., Knight, M., Johnson, RS. (2001). Hypoxia in cartilage: HIF-1alpha is essential for chondrocyte growth arrest and survival. *Genes Dev*, 15(21):2865-76.

Schödel, J., Oikonomopoulos, S., Ragoussis, J., Pugh, CW., Ratcliffe, PJ., Mole, DR. (2011). High-resolution genome-wide mapping of HIF-binding sites by ChIP-seq. *Blood*, 117(23):e207-17.

Schödel, J., Bardella, C., Sciesielski, LK., Brown, JM., et al. (2012). Common genetic variants at the 11q13.3 renal cancer susceptibility locus influence binding of HIF to an enhancer of cyclin D1 expression. *Nat Genet*, 44(4):420-5, S1-2.

Schödel, J., Mole, DR., Ratcliffe, PJ. (2013). Pan-genomic binding of hypoxia-inducible transcription factors. *Biol Chem*. Apr;394(4):507-17.

Schödel, J., Grampp, S., Maher, ER., Moch, H., Ratcliffe, PJ., Russo, P., Mole, DR. (2016). Hypoxia, Hypoxia-inducible Transcription Factors, and Renal Cancer. *Eur Urol*, 69(4):646-57.

Schofield, CJ., Ratcliffe, PJ. (2004). Oxygen sensing by HIF hydroxylases. *Nat Rev Mol Cell Biol*, 5(5):343-54.

Schug, ZT., Peck, B., Jones, DT., Zhang, Q., et al. (2015). Acetyl-CoA synthetase 2 promotes acetate utilization and maintains cancer cell growth under metabolic stress. *Cancer Cell*, 27(1):57-71.

Selak, MA., Armour, SM., MacKenzie, ED., et al. (2005). Succinate links TCA cycle dysfunction to oncogenesis by inhibiting HIF-alpha prolyl hydroxylase. *Cancer Cell*, 7(1):77-85.

Semenza, GL. (2003). Targeting HIF-1 for cancer therapy. *Nat Rev Cancer*, 3(10):721-32.

Semenza, GL. (2010). Defining the role of hypoxia-inducible factor 1 in cancer biology and therapeutics. *Oncogene*, 29(5):625-34.

Semenza, GL., Wang, GL. (1992). A nuclear factor induced by hypoxia via de novo protein synthesis binds to the human erythropoietin gene enhancer at a site required for transcriptional activation. *Mol Cell Biol*, 12(12):5447-54.

Sermeus, A., Michiels, C. (2011). Reciprocal influence of the p53 and the hypoxic pathways. *Cell Death Dis*, 2:e164

Shen, C., Beroukhim, R., Schumacher, SE., et al. (2011). Genetic and functional studies implicate HIF1α as a 14q kidney cancer suppressor gene. *Cancer Discov*, 1(3):222-35.

Shen, L., Shao, N., Liu, X., Nestler, E. (2014). ngs.plot: Quick mining and visualization of next-generation sequencing data by integrating genomic databases. *BMC Genomics*, 15:284.

Shilatifard, A. (2006). Chromatin modifications by methylation and ubiquitination: implications in the regulation of gene expression. *Annu Rev Biochem*, 75:243-69.

Shuch, B., Amin, A., Armstrong, AJ., et al. (2015). Understanding pathologic variants of renal cell carcinoma: distilling therapeutic opportunities from biologic complexity. *Eur Urol*, 67(1):85-97.

Simicevic, J., Schmid, AW., Gilardoni, PA., et al. (2013). Absolute quantification of transcription factors during cellular differentiation using multiplexed targeted proteomics. *Nat Methods*, 10(6):570-6.

Simon, JM., Hacker, KE., Singh, D., Brannon, ARet al. (2014). Variation in chromatin accessibility in human kidney cancer links H3K36 methyltransferase losswith widespread RNA processing defects. *Genome Res*, 24(2):241-50.

Sogawa, K., Nakano, R., Kobayashi, A., et al. (1995). Possible function of Ah receptor nuclear translocator (Arnt) homodimer in transcriptional regulation. *Proc Natl Acad Sci U S A,* 92(6):1936-40.

Sowter, HM, Raval, RR., Moore, JW., Ratcliffe, PJ., Harris, AL.(2003). Predominant role of hypoxia-inducible transcription factor (Hif)-1alpha versus Hif-2alpha in regulation of the transcriptional response to hypoxia. *Cancer Res*, 63(19):6130-4.

Spandl, J., White, DJ., Peychl, J., Thiele, C. (2009). Live cell multicolor imaging of lipid droplets with a new dye, LD540. *Traffic,* 10(11):1579-84.

Stenoien, DL., Nye, AC., Mancini, MG., Patel, K., et al. (2001). Ligand-mediated assembly and real-time cellular dynamics of estrogen receptor alpha-coactivator complexes in living cells. *Mol Cell Biol*, 21(13):4404-12.

Stiehl, DP., Wirthner, R., Köditz, J., Spielmann, P., Camenisch, G., Wenger, RH. (2006). Increased prolyl 4-hydroxylase domain proteins compensate for decreased oxygen levels. Evidence for an autoregulatory oxygen-sensing system. *J Biol Chem*, 281(33):23482-91.

Stolze, IP., Tian, YM., Appelhoff, RJ., Turley, H., Wykoff, CC., Gleadle, JM., Ratcliffe, PJ. (2004). Genetic analysis of the role of the asparaginyl hydroxylase factor inhibiting hypoxia-inducible factor (FIH) in regulating hypoxia-inducible factor (HIF) transcriptional target genes [corrected]. *J Biol Chem*, 279(41):42719-25.

Stroka, DM., Burkhardt, T., Desbaillets, I., Wenger, RH., et al. (2001). HIF-1 is expressed in normoxic tissue and displays an organ-specific regulation under systemic hypoxia. *FASEB J*, 15(13):2445-53.

Su, T., Han, YF., Yu, YW., et al. (2013). A GWAS-identified susceptibility locus on chromosome 11q13.3 and its putative molecular target for prediction of postoperative prognosis of human renal cell carcinoma. *Oncol Lett*, 6:421–6.

Subramanian, A., Tamayo, P., Mootha, VK., et al. (2005). Gene set enrichment analysis: a knowledge-based approach for interpreting genome-wide expression profiles. *Proc Natl Acad Sci U S A*, 102(43):15545-50.

Suyama, K., Silagi, ES., Choi, H., Sakabe, K., et al. (2016). Circadian factors BMAL1 and RORα control HIF-1α transcriptional activity in nucleus pulposus cells: implications in maintenance of intervertebral disc health. *Oncotarget*, 7(17):23056-71.

Swanson, HI. (2002). DNA binding and protein interactions of the AHR/ARNT heterodimer that facilitategene activation. *Chem Biol Interact*, 141(1-2):63-76.

Taghibiglou, C., Martin, HG., Rose, JK., et al. (2009). Essential role of SBP-1 activation in oxygen deprivation induced lipid accumulation and increase in body width/length ratio in Caenorhabditis elegans. *FEBS Lett*, 583(4):831-4.

Takeda, K., Aguila, HL., Parikh, NS., Li, X., et al. (2008). Regulation of adult erythropoiesis by prolyl hydroxylase domain proteins. *Blood*, 111(6):3229-35.

Takeda, K., Ho, VC., Takeda, H., Duan, LJ., Nagy, A., Fong, GH. (2006). Placental but not heart defects are associated with elevated hypoxia-inducible factor alpha levels in mice lacking prolyl hydroxylase domain protein 2. *Mol Cell Biol*, 26(22):8336-46.

Takeda, N., O'Dea, EL., Doedens, A., et al. (2010). Differential activation and antagonistic function of HIF-{alpha} isoforms in macrophages are essential for NO homeostasis. *Genes Dev*, 24(5):491-501.

Tanaka, T., Wiesener, M., Bernhardt, W., Eckardt, KU., Warnecke, C. (2009). The human HIF (hypoxia-inducible factor)-3alpha gene is a HIF-1 target gene and may modulate hypoxic gene induction. *Biochem J*, 424(1):143-51.

Tanimoto, K., Makino, Y., Pereira, T., Poellinger, L. (2000). Mechanism of regulation of the hypoxia-inducible factor-1 alpha by the von Hippel-Lindau tumor suppressor protein. *EMBO J*, 19(16):4298-309.

Tanimoto, K., Tsuchihara, K., Kanai, A., et al. (2010). Genome-wide identification and annotation of HIF-1α binding sites in two cell lines using massively parallel sequencing. *Hugo J*, 4(1-4):35-48.

Taylor, CT., Cummins, EP. (2009). The role of NF-kappaB in hypoxia-induced gene expression. *Ann N Y Acad Sci*, 1177:178-84.

Thienpont, B., Steinbacher, J., Zhao, H., et al. (2016). Tumour hypoxia causes DNA hypermethylation by reducing TET activity. *Nature*, 537(7618):63-68.

Tian, H., McKnight, SL., Russell, DW. (1997). Endothelial PAS domain protein 1 (EPAS1), a transcription factor selectively expressed in endothelial cells. *Genes Dev*, 11(1):72-82.

Tiana, M., Acosta-Iborra, B., Puente-Santamaría, L., Hernansanz-Agustin, P., et al. (2018). The SIN3A histone deacetylase complex is required for a complete transcriptional response to hypoxia. *Nucleic Acids Res,* 46(1):120-133.

Todd, BL., Stewart, EV., Burg, JS., Hughes, AL., Espenshade, PJ. (2006). Sterol regulatory element binding protein is a principal regulator of anaerobic gene expression in fission yeast. *Mol Cell Biol*, 26(7):2817-31.

Tsai, YP., Wu, KJ. (2012). Hypoxia-regulated target genes implicated in tumor metastasis. *J Biomed Sci*, 19:102.

Tsai, YP., Wu, KJ. (2014). Epigenetic regulation of hypoxia-responsive gene expression: focusing on chromatin and DNA modifications. *Int J Cancer*, 134(2):249-56.

Tsankov, AM., Gu, H., Akopian, V., et al. (2015). Transcription factor binding dynamics during human ES cell differentiation. *Nature*, 518(7539):344-9.

Uchida, T., Rossigno,l F., Matthay, MA., et al. (2004). Prolonged hypoxia differentially regulates hypoxia-inducible factor (HIF)-1alpha and HIF-2alpha expression in lung epithelial cells: implication of natural antisense HIF-1alpha. *J Biol Chem*, 279(15):14871-8.

Unden, G., Schirawski, J. (1997). The oxygen-responsive transcriptional regulator FNR of Escherichia coli: the search for signals and reactions. *Mol Microbiol*, 25(2):205-10.

Uniacke, J., Holterman, CE., Lachance, G., et al. (2012). An oxygen-regulated switch in the protein synthesis machinery. *Nature*, 486(7401):126-9.

van Haaften, G., Dalgliesh, GL., Davies, H., et al. (2009). Somatic mutations of the histone H3K27 demethylase gene UTX in human cancer. *Nat Genet*, 41(5):521-3.

Vanharanta, S., Shu, W., Brenet, F., Hakimi, AA., et al. (2013). Epigenetic expansion of VHL-HIF signal output drives multiorgan metastasis in renal cancer. *Nat Med*, 19(1):50-6.

van Royen, ME., Farla, P., Mattern, KA., Geverts, B., Trapman, J., Houtsmuller, AB. (2009). Fluorescence recovery after photobleaching (FRAP) to study nuclear protein dynamics in living cells. *Methods Mol Biol,* 464:363-85.

Varela, I., Tarpey, P., Raine, K., Huang, D., et al. (2011). Exome sequencing identifies frequent mutation of the SWI/SNF complex gene PBRM1 in renalcarcinoma. *Nature*, 469(7331):539-42.

Vaux, EC., Metzen, E., Yeates, KM., Ratcliffe, PJ. (2001). Regulation of hypoxia-inducible factor is preserved in the absence of a functioning mitochondrial respiratory chain. *Blood*, 98(2):296-302.

Villar, D., Ortiz-Barahona, A., Gómez-Maldonado, L., et al. (2012). Cooperativity of stress-responsive transcription factors in core hypoxia-inducible factor bindingregions. *PLoS One*, 7(9):e45708.

Wallace, EM., Rizzi, JP., Han, G., et al. (2016). A Small-Molecule Antagonist of HIF2α Is Efficacious in Preclinical Models of Renal Cell Carcinoma. *Cancer Res*, 76(18):5491-500.

Wang, GL., Semenza, GL.(1995). Purification and characterization of hypoxia-inducible factor 1. *J Biol Chem*, 270(3):1230-7.

Wang, V., Davis, DA., Haque, M., Huang, LE., Yarchoan, R. (2005). Differential gene up-regulation by hypoxia-inducible factor-1alpha and hypoxia-inducible factor-2alpha in HEK293T cells. *Cancer Res*, 65(8):3299-306.

Wang, Y., Wan, C., Deng, L., Liu, X., et al. (2007). The hypoxia-inducible factor alpha pathway couples angiogenesis to osteogenesis during skeletal development. *J Clin Invest*, 117(6):1616-26.

Wang, H., Qu, Y., Dai, B., et al. (2017). PBRM1 regulates proliferation and the cell cycle in renal cell carcinoma through a chemokine/chemokine receptor interaction pathway. *PLoS One*, 12(8):e0180862.

Wang, GL., Fu, YC., Xu, WC., et al. (2009). Resveratrol inhibits the expression of SREBP1 in cell model of steatosis via Sirt1-FOXO1 signaling pathway. *Biochem Biophys Res Commun*, 380(3):644-9.

Wang, Z., Zang, C., Rosenfeld, JA., et al (2008). Combinatorial patterns of histone acetylations and methylations in the human genome. *Nat Genet*, 40(7):897-903.

Warnecke, C., Zaborowska, Z., Kurreck, J., et al. (2004). Differentiating the functional role of hypoxia-inducible factor (HIF)-1alpha and HIF-2alpha(EPAS-1) by the use of RNA interference: erythropoietin is a HIF-2alpha target gene in Hep3B and Kelly cells. *FASEB J*, 18(12):1462-4.

Watson, JA., Watson, CJ., McCrohan, AM., et al. (2009). Generation of an epigenetic signature by chronic hypoxia in prostate cells. *Hum Mol Genet*, 18(19):3594-604.

Weake, VM., Workman, JL. (2010). Inducible gene expression: diverse regulatory mechanisms. *Nat Rev Genet*, 11(6):426-37.

Wellmann, S., Bührer, C., Moderegger, E., et al. (2004). Oxygen-regulated expression of the RNA-binding proteins RBM3 and CIRP by a HIF-1-independent mechanism. *J Cell Sci*, 117(Pt 9):1785-94.

Wenger, RH., Stiehl, DP., Camenisch, G. (2005). Integration of oxygen signaling at the consensus HRE. *Sci STKE*, 2005(306):re12.

Wenger, RH., Kvietikova, I., Rolfs, A., Camenisch, G., Gassmann, M. (1998). Oxygen-regulated erythropoietin gene expression is dependent on a CpG methylation-free hypoxia-inducible factor-1 DNA-binding site. *Eur J Biochem*, 253(3):771-7.

Wiesener, MS., Turley, H., Allen, WE., et al. (1998). Induction of endothelial PAS domain protein-1 by hypoxia: characterization and comparison with hypoxia-inducible factor-1alpha. *Blood*, 92(7):2260-8.

Wigerup, C., Påhlman, S., Bexell, D. (2016). Therapeutic targeting of hypoxia and hypoxia-inducible factors in cancer. *Pharmacol Ther*, 164:152-69.

Wood, SM., Gleadle, JM., Pugh, CW., Hankinson, O., Ratcliffe, PJ. (1996). The role of the aryl hydrocarbon receptor nuclear translocator (ARNT) in hypoxic induction of gene expression. Studies in ARNT-deficient cells. *J Biol Chem*, 271(25):15117-23.

Wu, X., Scelo, G., Purdue, MP., et al. (2012). A genome-wide association study identifies a novel susceptibility locus for renal cell carcinoma on 12p11.23. *Hum Mol Genet*, 21:456–62.

Wu, D., Su, X., Potluri, N., Kim, Y., Rastinejad, F. (2016). NPAS1-ARNT and NPAS3-ARNT crystal structures implicate the bHLH-PAS family as multi-ligand binding transcription factors. *Elife*, 5. pii: e18790.

Wykoff, CC., Pugh, CW., Maxwell, PH., Harris, AL., Ratcliffe, PJ. (2000). Identification of novel hypoxia dependent and independent target genes of the von Hippel-Lindau (VHL) tumour suppressor by mRNA differential expression profiling. *Oncogene*, 19(54):6297-305.

Wysocka, J., Reilly, PT., Herr, W. (2001). Loss of HCF-1-chromatin association precedes temperature-induced growth arrest of tsBN67 cells. *Mol Cell Biol*, 21(11):3820-9

Xia, X., Kung, AL. (2009). Preferential binding of HIF-1 to transcriptionally active loci determines cell-type specific response to hypoxia. *Genome Biol*, 10(10):R113.

Xiao, Y., Hsiao, TH., Suresh, U., et al. (2014). A novel significance score for gene selection and ranking. *Bioinformatics*, 30(6):801-7.

Yang, M., Su, H., Soga, T., Kranc, KR., Pollard, PJ. (2014). Prolyl hydroxylase domain enzymes: important regulators of cancer metabolism. *Hypoxia (Auckl),* 2:127-142.

Yeh, TL., Leissing, TM., Abboud, MI., et al. (2017). Molecular and cellular mechanisms of HIF prolyl hydroxylase inhibitors in clinical trials. *Chem Sci,* 8(11):7651-7668.

Yi, Y., Mikhaylova, O., Mamedova, A., et al. (2010). von Hippel-Lindau-dependent patterns of RNA polymerase II hydroxylation in human renal clear cell carcinomas. *Clin Cancer Res*, 16(21):5142-52.

Yoon, H., Lim, JH., Cho, CH., et al. (2011). CITED2 controls the hypoxic signaling by snatching p300 from the two distinct activation domains of HIF-1α. *Biochim Biophys Acta*, 1813(12):2008-16.

Yu, T., Tang, B., Sun, X. (2017). Development of Inhibitors Targeting Hypoxia-Inducible Factor 1 and 2 for Cancer Therapy. *Yonsei Med J*, 58(3):489-496.

Yun, Z., Maecker, HL., Johnson, RS., Giaccia, AJ. (2002). Inhibition of PPAR gamma 2 gene expression by the HIF-1-regulated gene DEC1/Stra13: a mechanism for regulation of adipogenesis by hypoxia. *Dev Cell*, 2(3):331-41.

Zabet, NR., Adryan, B. (2015). Estimating binding properties of transcription factors from genome-wide binding profiles. *Nucleic Acids Res*, 43(1):84-94.

Zhang, H., Bosch-Marce, M., Shimoda, LA., et al. (2008). Mitochondrial autophagy is an HIF-1-dependent adaptive metabolic response to hypoxia. *J Biol Chem*, 283(16):10892-903.

Zhang, Y., Liu, T., Meyer, CA., et al. (2008b). Model-based analysis of ChIP-Seq (MACS). *Genome Biol*, 9(9):R137.

Zhao, ZW., White, MD., Alvarez, YD., Zenker, J., et al. (2017). Quantifying transcription factor-DNA binding in single cells in vivo with photoactivatable fluorescence correlation spectroscopy. *Nat Protoc,* 12(7):1458-1471.

Zheng, X., Linke, S., Dias, JM., Zheng, X., et al. (2008). Interaction with factor inhibiting HIF-1 defines an additional mode of cross-coupling between the Notch and hypoxia signaling pathways. *Proc Natl Acad Sci U S A*, 105(9):3368-73.

Zheng, X., Zhai, B., Koivunen, P., Shin, SJ., et al. (2014). Prolyl hydroxylation by EglN2 destabilizes FOXO3a by blocking its interaction with the USP9x deubiquitinase. *Genes Dev*, 28(13):1429-44.

Zhong, H., Chiles, K., Feldser, D., Laughner, E., et al. (2000). Modulation of hypoxia-inducible factor 1alpha expression by the epidermal growth factor/phosphatidylinositol 3-kinase/PTEN/AKT/FRAP pathway in human prostate cancer cells: implications for tumor angiogenesis and therapeutics. *Cancer Res*, 60(6):1541-5.

Zitomer, RS., Limbach, MP., Rodriguez-Torres, AM., et al. (1997). Approaches to the study of Rox1 repression of the hypoxic genes in the yeast Saccharomyces cerevisiae. *Methods*, 11(3):279-88.